# Preface

One of the most challenging problems in atmospheric science is to develop an adequate understanding of the variability of the Indian monsoon on various time-scales: subseasonal, interannual and decadal, that could be translated into a predictive capability. The monsoon is strongly coupled to the warm oceans surrounding the subcontinent. Most of the monsoon rainfall occurs in association with synoptic systems, such as lows and depressions, generated over the warm oceans and their subsequent propagation over the Indian landmass. The Bay of Bengal is exceptionally fertile generating these systems and plays an important role in monsoon variability.

Studies of satellite data over the past two decades have revealed the nature of convection/precipitation over the oceans and their relationship with monsoon variability. These is turn, have led to various hypotheses to explain the propagation of these systems in the atmosphere, their impact on the ocean and the recovery of the atmosphere and ocean to the predisturbance state. These hypotheses need to be tested and refined by detailed observations of the air-sea coupling during the monsoon.

The BOBMEX field experiment, an acronym for the 'Bay of Bengal and the Monsoon Experiment' is aimed at accomplishing this objective by generating critical data on the subseasonal variation of important variables of the atmosphere, the ocean and their interface processes. This is the first major national effort at designing experiments to gain critical insights into the structure of monsoon variability. The earlier international observational programmes in 1977 and 1979 provided some insights into the heat and moisture budgets of the Bay. Under the first national observational programme of the monsoon trough (MONTBLEX), some observations of the variation of winds, surface fluxes and other parameters were made in the head Bay. The BOBMEX envisaged the use of state-of-the-art instrumentation to obtain time series data at two critical locations over the Bay during the months of July – August 1999. Prior to this, a pilot experiment was undertaken over the Bay in October – November of 1998 to test the instruments and obtain a first order picture of the nature of the variability. Results of this pilot experiment are presented in this volume.

BOBMEX is an important component of the Indian Climate Research Programme (ICRP), made possible by the development of adequate expertise in the country for the use of state-of-the-art instrumentation, and availability of scientific infrastructure notably research vessels and buoys. The main observational programme, successfully carried out in July – August 1999, has already yielded exciting results and has set the stage for making a concerted effort to profitably involve scientists from different institutions in addressing other observational experiments planned under the ICRP.

**Sulochana Gadgil**
Centre for Atmospheric and Oceanic Sciences,
Indian Institute of Science, Bangalore.

**U C Mohanty**
Centre for Atmospheric Sciences,
Indian Institute of Technology, New Delhi.

# Bay of Bengal Monsoon Experiment (BOBMEX) – A component of the Indian Climate Research Programme (ICRP)

D R SIKKA[1] and P SANJEEVA RAO[2]

[1]40 Mausam Vihar, New Delhi 110 051, India
[2]Department of Science and Technology, New Delhi 110 016, India.

The Indian Climate Research Programme (ICRP) focuses on the study of climate variability and its impact on agriculture. To address the role of the Bay of Bengal in monsoon variability, a process study was organised during July–August 1999, deploying research ships, buoys, INSAT, coastal radar and conventional observational systems to collect information about the coupled ocean-atmosphere system over the warm waters of the Bay of Bengal. The paper gives the background of the ICRP and the organisation and implementation of the Bay of Bengal Monsoon Experiment (BOBMEX) in its field phase.

## 1. Introduction

Climate variability has become an important topic of scientific pursuit during the last two decades or so. The economy of a nation is intimately linked with its climate-resource. Any short-term (within a season) or long-term (inter-annual and decadal scales) fluctuations in the climate have important impacts on the progress of a nation, particularly so in a developing economy. India's economy has been traditionally known to be a gamble on the monsoon. Therefore a deeper understanding of the monsoon variability on different time-scales is expected to pave the way for better predictions on the performance of rains over India during the summer monsoon season. The Indian Climate Research Programme (ICRP), as formulated in its Science Plan (DST, 1996), is a multi-agency programme which is focussed on the following major objectives:

- Understanding the physical processes responsible for climate variability on sub-seasonal, seasonal, interannual and decadal time-scales of the monsoon, the oceans (especially the Indian seas and the equatorial Indian Ocean) and the coupled atmosphere-ocean-land system.

- Study of the space-time variation of the monsoon from sub-seasonal, interannual to decadal scales for assessing the feasibility for climate prediction and development of methods for prediction.
- Study of change in climate and its variability on centennial and longer time scales generated by natural and anthropogenic factors.
- Investigation of the links between climate variability and critical resources such as agricultural productivity to provide a basis for deriving agricultural strategies for maximising the sustainable yield in the face of climate variability, and for realistic assessment of impact of climate change.

ICRP addresses the above foci in three components viz.,

- Monsoon Variability (MONVAR),
- Past Climates and Climate Change (PCCC) and
- Climate and Agriculture (CLIMAG).

Several departments of the Government of India (Department of Science and Technology (DST), Department of Ocean Development (DOD), Defence Research and Development Organisation (DRDO), Department of Space (DOS), India Meteorological Department (IMD), Council of Scientific and Industrial

Keywords. Monsoon; climate variability; Bay of Bengal; ocean-atmosphere coupling.

Forests (MoEF), Indian Council of Agricultural Research (ICAR) and their agencies and autonomous research organisations under their control as well as universities and institutions like Indian Institute of Science (IISc), Indian Institute of Technology (IIT), Delhi are participating in the promotion and implementation of the ICRP.

The programme MONVAR addresses questions relating to variability of monsoon, oceans and the coupled system. It has four process-oriented sub-programmes viz. Bay of Bengal Monsoon (BOBMON), Arabian Sea Monsoon (ARMON), Continental Tropical Convergence Zone (CTCZ) and Circulation, Hydrology and Thermodynamics of North Indian Ocean (CHATNI). These sub-programmes are to be carried out in stages over the next several years to obtain detailed data for better understanding of the coupled processes involved in monsoon variability within the ambit of the coupled land-ocean-atmosphere system. Within the BOBMON sub-programme the processes to be studied include:

- Heat and freshwater balance of the Bay of Bengal,
- Coupling between the mixed layers of the atmosphere and the ocean,
- Convective cloud systems over the Bay on different space-time scales,
- Structure of meso-scale convection,
- Role of low-frequency waves in the circulation over the Bay of Bengal.

## 2. Bay of Bengal Monsoon Experiment (BOBMEX)

To address the problems linked with the fluctuations of the Bay of Bengal Monsoon during the summer monsoon season (June-September), a multi-pronged approach (viz., monitoring by conventional atmospheric networks with relevant enhancement, recently installed Met-Ocean Buoy network of DOD, weather satellites, etc.) is necessary. The intensive field phase observational component known as Bay of Bengal Monsoon Experiment (BOBMEX) was formulated for better understanding of monsoon-related processes with the following broad objectives.

- Study of the vertical stability of the atmosphere during different phases of organised convection,
- Study of variability of upper ocean currents in relation to changing wind and thermohaline circulation,
- Study of the surface fluxes and atmospheric and oceanic boundary layer characteristics during different phases of convection, and
- Air-sea coupling.

BOBMEX is planned to be carried out as a well coordinated multi-agency project with the nodal agency

Committee for ICRP, Standing Committee on Earth System Sciences of DST, Project Advisory and Monitoring Committee for Monsoon and Tropical Climate (MONTCLIM) and Indian Climate Research Programme (ICRP), Working Group on Atmosphere-Ocean Field Experiments under ICRP, Committee on Atmospheric and Oceanographic Instruments etc.) held science meetings during 1997–1999 to plan and implement the BOBMEX. It had been decided in early 1998 that prior to the full field operation of BOBMEX, to be undertaken in July-August 1999, a short duration Pilot experiment (BOBMEX-Pilot) be carried out in 1998. This was required to test the field readiness of different facilities (research ships, met-ocean buoy, conventional systems, specially acquired physical oceanography and meteorological instruments to be used on board research ship, etc.). BOBMEX was designed exclusively for the first time jointly by the ocean-atmosphere science community in India. This was considered to be very relevant as BOBMEX was focussed on the study of the coupled ocean-atmosphere system, which is important for the variability of the Indian monsoon.

## 3. Implementation of BOBMEX-Pilot

The special observing systems deployed for the BOBMEX-Pilot experiment were the oceanographic research vessel Sagar Kanya (ORV-SK) and the Met-ocean buoys in the Bay of Bengal and the India Meteorological Department (IMD) conventional observing systems over the Bay of Bengal islands and east coast of India. Measurements on board ORV-SK included deployment of several advanced sensors and instruments. The main objectives of the BOBMEX Pilot were:

- To try out the objectives of the BOBMEX on a smaller scale, in order to test the equipment/systems required for meeting the objectives of BOBMEX, develop modalities for archiving the data and their dissemination and also identify problem areas.
- To obtain high quality data during the experiment so as to be useful in understanding inter-annual variability when combined with data from the past and future field studies and also to help in the design and proper implementation of the main BOBMEX in 1999.

The BOBMEX-Pilot was successfully carried out during October-November 1998. ORV Sagar Kanya sailed from its base in Goa on October 23rd and reached Tuticorin on November 12th, thus, providing nearly three weeks of observations. The first stationary position was taken by the vessel near 7°N 87°E for two days on October 30th and 31st, 1998. The second and third stationary positions were taken by the vessel

on 2nd–3rd November 1998 near 10°N 87°E and on 5th November near 13°N 87°E. Thus, the three stationary positions were along a meridional direction along 87°E beginning in near-equatorial warm waters at 7°N and ending at 13°N. This was the zone where organised convection associated with the withdrawing southwest monsoon was located. Fluctuations in its intensity were observed with the formation/passage of cyclonic disturbances.

The atmospheric component of the observations on ORV Sagar Kanya was managed by the Centre for Atmospheric and Ocean Studies of the Indian Institute of Science, Bangalore while the oceanic component was managed by the National Institute of Oceanography, Goa. Data were collected on various atmospheric, ocean-atmosphere coupled and oceanic parameters. Some of the observations such as the air-sea (fast and slow response) fluxes parameters, sea surface temperature (SST) using infra-red thermometer, outgoing longwave radiation (OLR) and incoming solar radiation and high resolution temperature and humidity soundings of the atmosphere were done for the first time. Besides, oceanographic observations on CTD and currents using VM-ADC probe were also collected.

The period of the experiment witnessed two active weather disturbances in the area of the experiment – a cyclonic storm and a low pressure area. The data collected were distributed among participating scientists and agencies. A workshop was organised by the DST to discuss the results of the BOBMEX-Pilot at the IIT, New Delhi on 23rd April 1999 during which 12 papers containing the preliminary results utilising the data collected during the pilot experiment were presented. The major results which emerged from these studies were:

- Significant fluctuations in SST ($> 1.0°C$) during the experiment as a consequence of active synoptic weather activity.
- Fluctuations of the atmospheric boundary layer (ABL) in response to synoptic weather disturbances and simulation of the ABL.
- Spatial distribution of ocean mixed layer from near-equatorial to central Bay of Bengal.
- Role of northward advective processes on the upper ocean thermodynamics of the south Bay of Bengal.
- Net heat loss over the Bay of Bengal.
- Air-sea exchange processes including exchange of Dimethyl Sulphide (DMS).

The results of the detailed analysis of the observations during the pilot experiment are presented by different authors in this issue.

1999 for a period of nearly 45 days. Two research Vessels, (ORV Sagar Kanya of Antarctica Study Centre, DOD, Goa and R V Sagar Dhwani of Naval Physical Oceanographic Laboratory, Cochin) and 2 deep ocean buoys in the Bay of Bengal deployed by the National Institute of Ocean Technology (NIOT) were used as special observing platforms. The IMD provided the requisite observational support from the coastal network (Calcutta, Bhubaneswar, Vishakapatnam, Machilipatnam, Chennai, Karaikal and Portblair) of conventional meteorological observations such as radiosonde, radar and INSAT imageries, during the experimental period. The IMD and National Centre for Medium Range Weather Forecasting (NCMRWF), New Delhi provided the synoptic weather and model output products to the ships as weather advisories. The BOBMEX Operations Science Team (BOST) provided the necessary guidance in identifying the intensive observational periods. All these activities during the BOBMEX main experiment were co-ordinated by the BOBMEX Operations Centre at IMD, Mausam Bhawan, New Delhi. About 80 scientists working in multi-disciplinary subjects from 15 organisations participated in the observational campaign. Several interesting results have emerged which will be published by scientists of participating agencies in the near future.

## Acknowledgement

## 4. Implementation of BOBMEX-Main

## References

# Synoptic weather conditions during the pilot study of Bay of Bengal and Monsoon Experiment (BOBMEX)

S R KALSI

*India Meteorological Department, New Delhi, India*

BOBMEX-Pilot was organised from 23rd October – 11th November, 1998 when the seasonal trough had already shifted to south Bay of Bengal. The activity during this period was marked by the development of a monsoon depression from 26th–29th October that weakened over the sea; onset of northeast monsoon along the east coast of India on 29th October; a low pressure area that formed on 2nd November over southwest Bay off Sri Lanka – southTamilnadu coast; and another cyclonic circulation that formed towards the end of the BOBMEX-Pilot period. This paper describes the development of these synoptic systems through synoptic charts and satellite data.

## 1. Bay of Bengal and Monsoon pilot experiment (BOBMEX-Pilot)

The main aim of the experiment was to study air-sea coupling and its high frequency variability over the Bay in the summer monsoon season. It had specific objectives relating to the influence of the ocean on convection, and changes in the upper ocean driven by the air-sea fluxes and fresh water discharge. DOD committed its ship Sagar Kanya in this connection. Intensive observations for the Bay of Bengal convection and the marine boundary layer were conducted. The track of the ship is given in figure 1. The position of the ship is also shown in charts included in this study wherever required. It cruised mostly in the central parts of south Bay of Bengal where the seasonal trough had shifted as discussed in the following paragraphs.

## 2. Deep depression from 26th – 28th October 1998

The seasonal shear line in the lower troposphere during the initial phase of the pilot experiment was located over the south Bay of Bengal along and south of 10°N latitude with light winds on either side of the trough on 23rd October. A huge convection lay over Malay peninsula and adjacent areas of the Andaman Sea as seen in the INSAT imagery included in figure 2. The initial disturbance at this stage discerned at about 8°N/101.5°E was highly innocuous as seen in the satellite imagery . The wind strength as seen from the scanty data available from the shear zone was just 10–15 knots. Outgoing longwave radiation (OLR) minima of 160 watts per square meter associated with this pocket indicated strong convection which shifted westwards and became more compact with time. Figure 3 indicates that even on 25th October OLR minima of 180 watts per square meter was seen over southern parts of the Bay of Bengal. Along with the convection associated with the northern hemispheric equatorial trough (NHET) another band of low OLR was seen due to the southern hemispheric equatorial trough (SHET) (see figure 11). Surface meteorological observations collected on board ORV Sagar Kanya during the pilot phase of the BOBMEX indicate that the equatorial westerlies seem to have strengthened to some extent between these two troughs. The persistent diabetic heating associated with the intense convection in the south Bay of Bengal where scanty ship reports and buoy data reveal warm sea with sea surface temperature more than 29°C gave rise to the formation of a low pressure on 25th October that concentrated into a depression on 26th October over
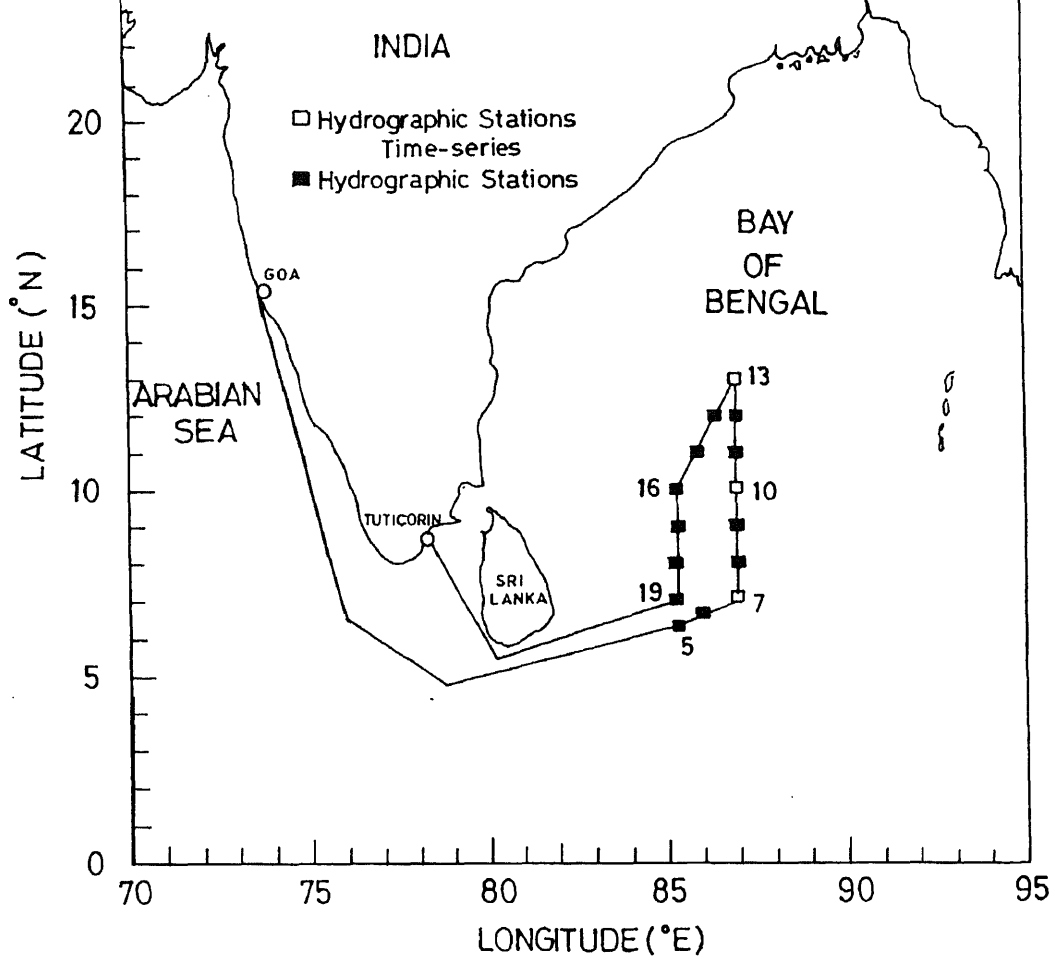
Figure 1. Pilot BOBMEX cruise track, Sagar Kanya Cruise No: SK 138C. Period: 23-10-98 to 11-11-98 (Goa – Tuticorin).

southeast Bay. The average daily OLR again reached a low of 160 watts per square meter on 27th October though it was seen in an earlier study (Kalsi *et al* 1995) that the OLR value may reach as low as 100 watts per square meter during the formation of a depression. Cloud organisation in the satellite imagery is seen on the basis of which it was declared and accepted as a depression, though no characteristic organisation of depression (Kanti Prasad *et al* 1990; Srinivasan *et al* 1971) is seen in the visible satellite images of 26th October. It moved initially northwestwards and intensified into a deep depression at 12 UTC of 27th October when it was located near latitude $13.0°N$/long. $87.0°E$. Figure 4 shows the track of this depression. The global analysis charts of the National Centre for Medium Range Weather Forecasting (NCMRWF) indicate that there was virtually no slope of this system between 850 and 500 hPa levels (figure 5) at 00 UTC of 27th October 1998. This is in conformity with results of Kanti Prasad *et al* (1990) wherein it has been seen that during the intense stages of monsoon depression, the associated cyclonic circulation becomes

vertical. Thereafter as seen through the subsequent satellite images the depression moved first westward up to 12 UTC of 28th October and again took a northwest course. ORV Sagar Kanya came under the influence of the depression only on 28th October when it cruised towards the Bay of Bengal. It reported strengthening of the wind speed to about 34 knots at 00 UTC of 28th October. The winds weakened in the vicinity of this ship around noon of 28th October. Under the influence of a strong mid and upper troposphere westerly/southwesterly current seen over central and northwest India ahead of a westerly trough observed over Pakistan on 29th October far to the northwest of the depression, it apparently weakened over the sea itself and its convection got sheared off northeastwards along and off east coast of India.

## 3. Onset of northeast monsoon

Though the depression discussed above weakened on 29th October, relatively strong ITCZ conditions

INSAT1 ASIA MER    23-OCT-98 03:00Z    IR BAND        INSAT1D    IR WINTER ENH
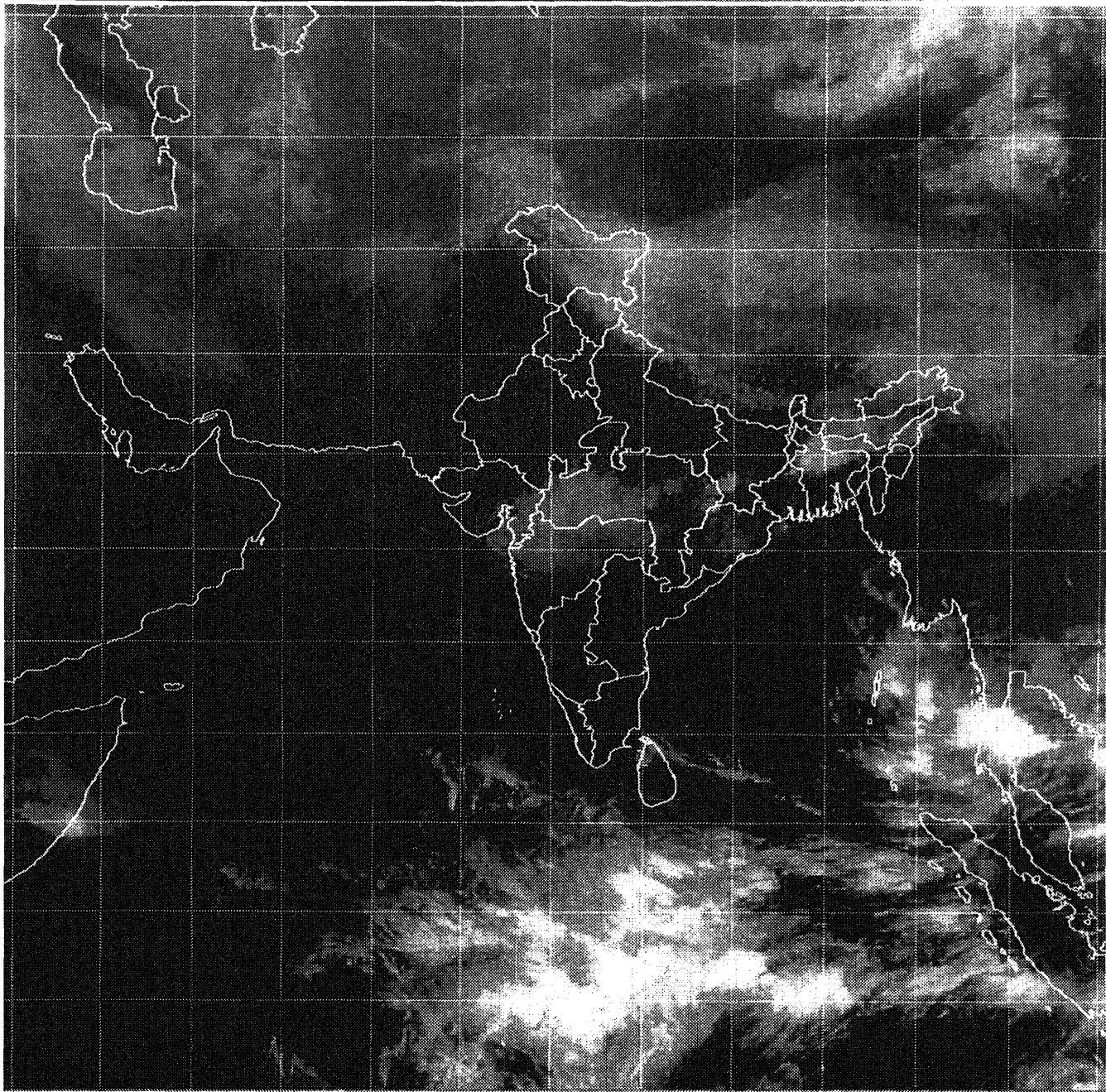IMDPS IMD NEW DELHI

Figure 2.   INSAT picture of 23rd October 1998 showing a cloud cluster over Malay Peninsula and neighbourhood.
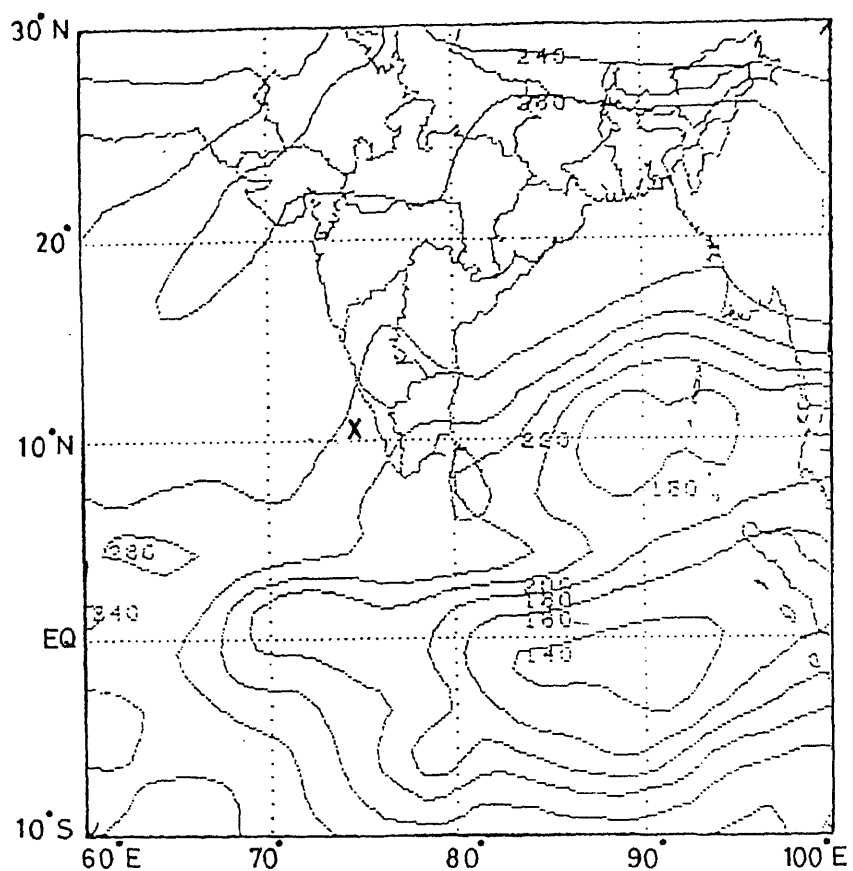
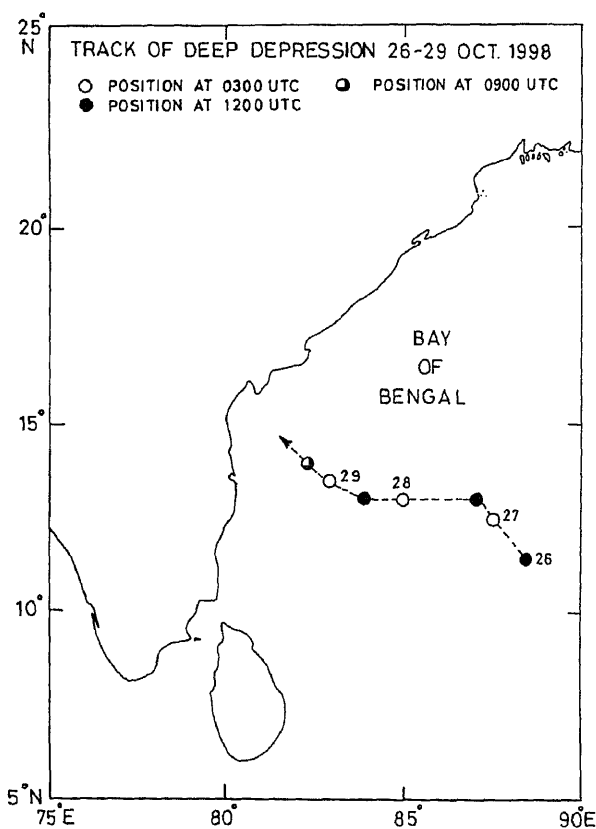Figure 3.   INSAT derived OLR. Units: watts/mtr.sq; Date: 25-10-1998; X – position of Sagar Kanya ship.



Figure 4.

continued over the south Bay. The northeast cu[...] strengthened on 28th October itself in assoc[...] with the deep depression along and off the east[...] of India as seen in figure 6 that shows deepening [...] low at 850 hPa level. After the shearing off proc[...] the depression discussed above, the seasonal t[...] got somewhat elongated northeastwards. Th[...] supported by the backing of the winds report[...] Sagar Kanya from a direction of 280° at 00 UT[...] 28th October to 240° at 06 UTC of 29th Oc[...] when the wind speed also decreased from abo[...] knots to 14 knots. Figure 7 shows the sequen[...] satellite pictures indicating weakening of the d[...] sion and the advance of northeast monsoon. Th[...] the tropical circulations are in general insulated [...] mid-latitude flows by sub-tropical highs, the pe[...] tion of troughs in westerlies into tropics impac[...] tropical vortices by shearing them off northeastw[...] The depression in the west central Bay als[...] sheared off under similar circumstances. The rem[...] of the depression came close to the north Tami[...] and south coastal Andhra Pradesh on 30th Oc[...] and became unimportant on 31st October [...] crossing the coast. The weekly rainfall chart [...] week ending 4th November 1998 showed [...] rainfall in Tamilnadu, coastal Andhra Prades[...] Rayalaseema in association with the arrival [...] northeast monsoon.
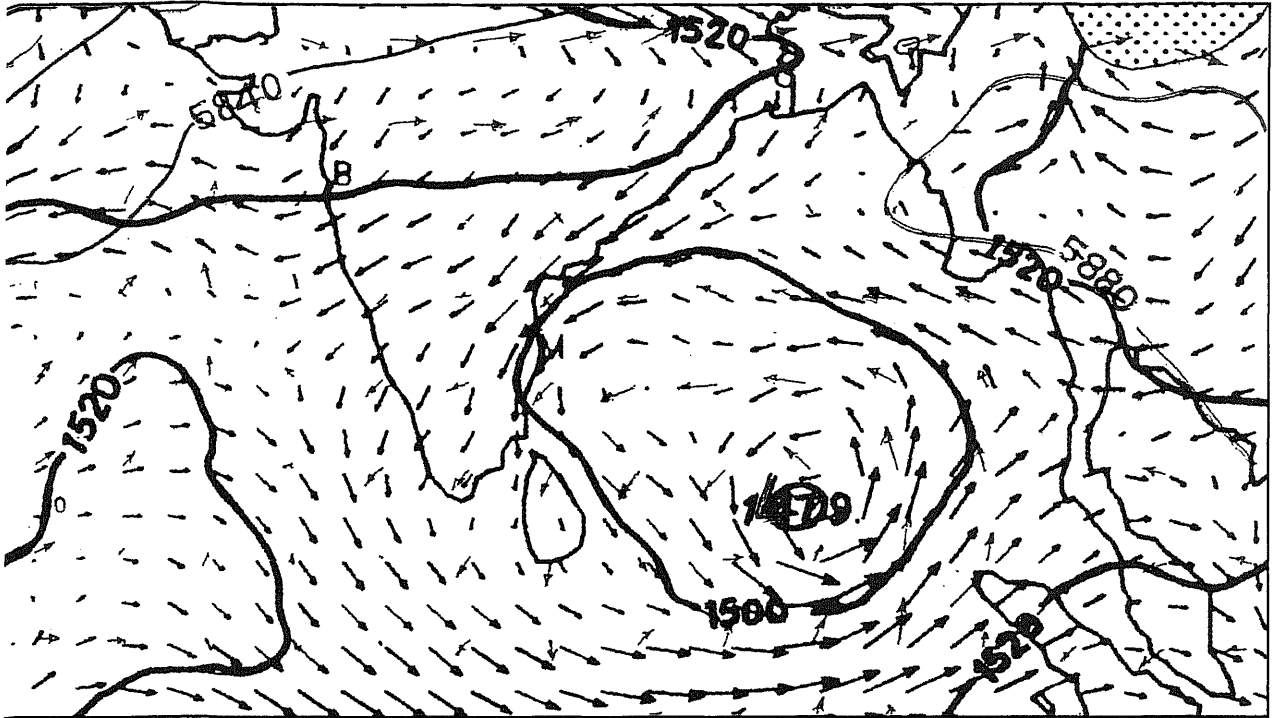
Figure 5. NCMRWF analysis of 27.10.98 – 850hPa – 500hPa.
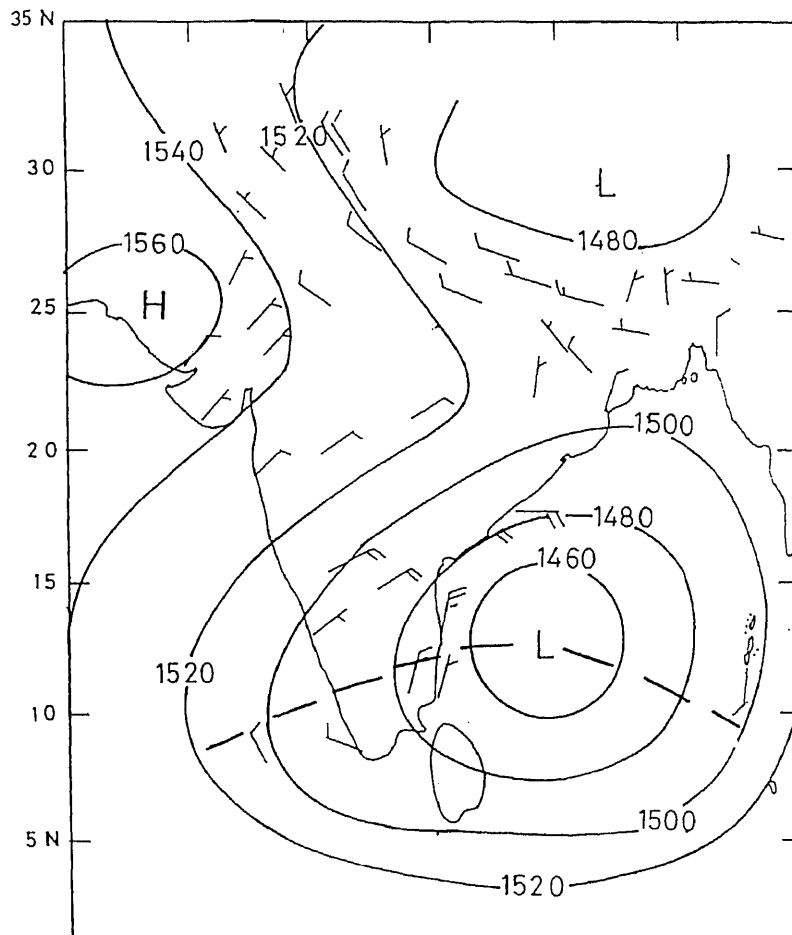
## 28 OCT 1998
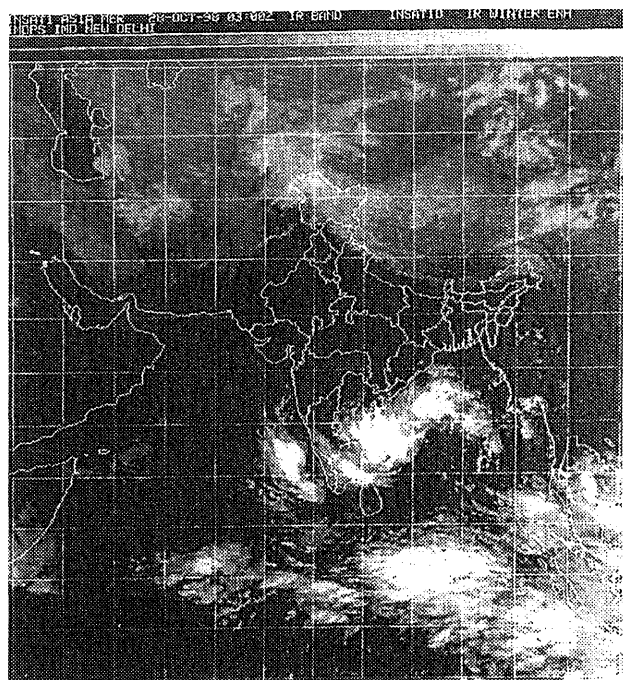
## 29 OCT 1998
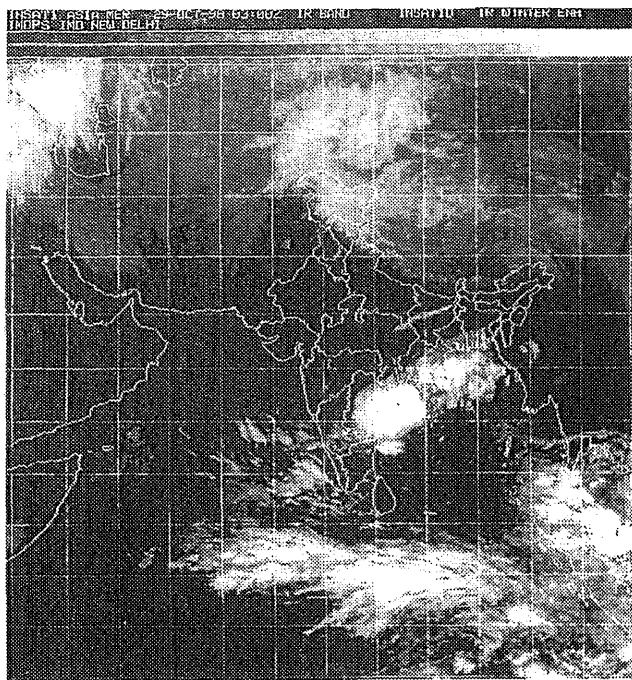
## 30 OCT 1998
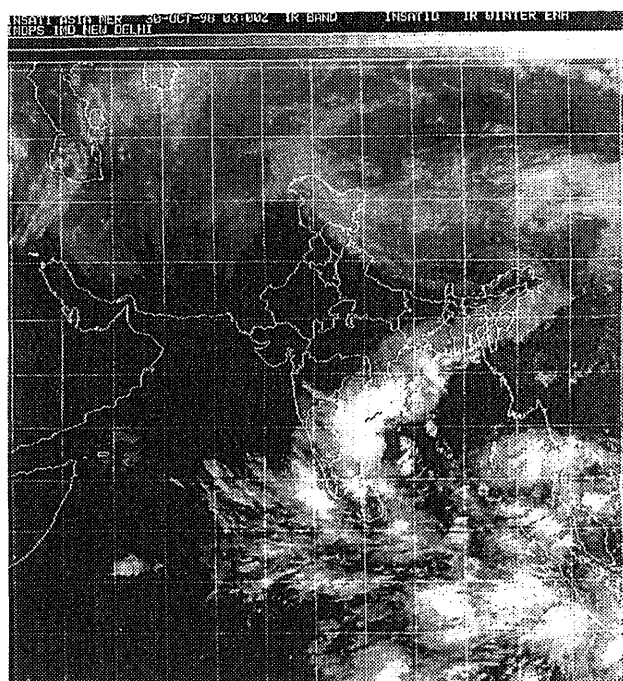
## 31 OCT 1998
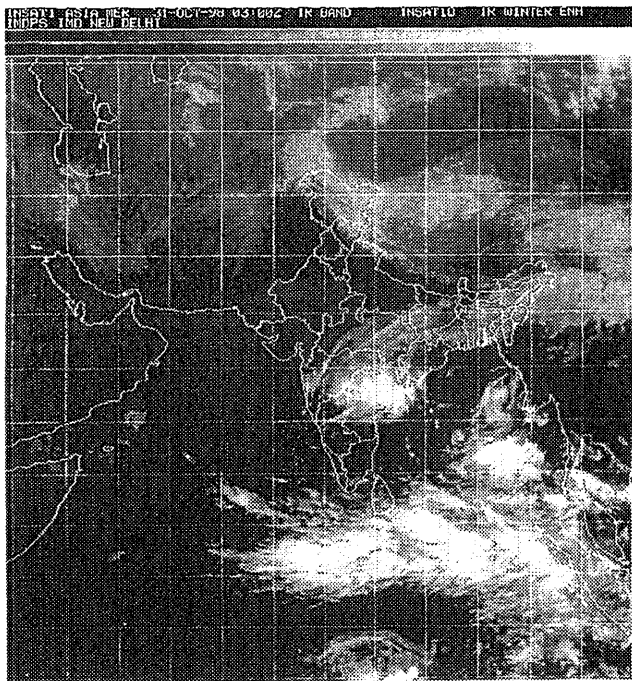
Figure 7. Sequence of INSAT pictures (IR) showing weakening of depression and advancement of NE monsoon.
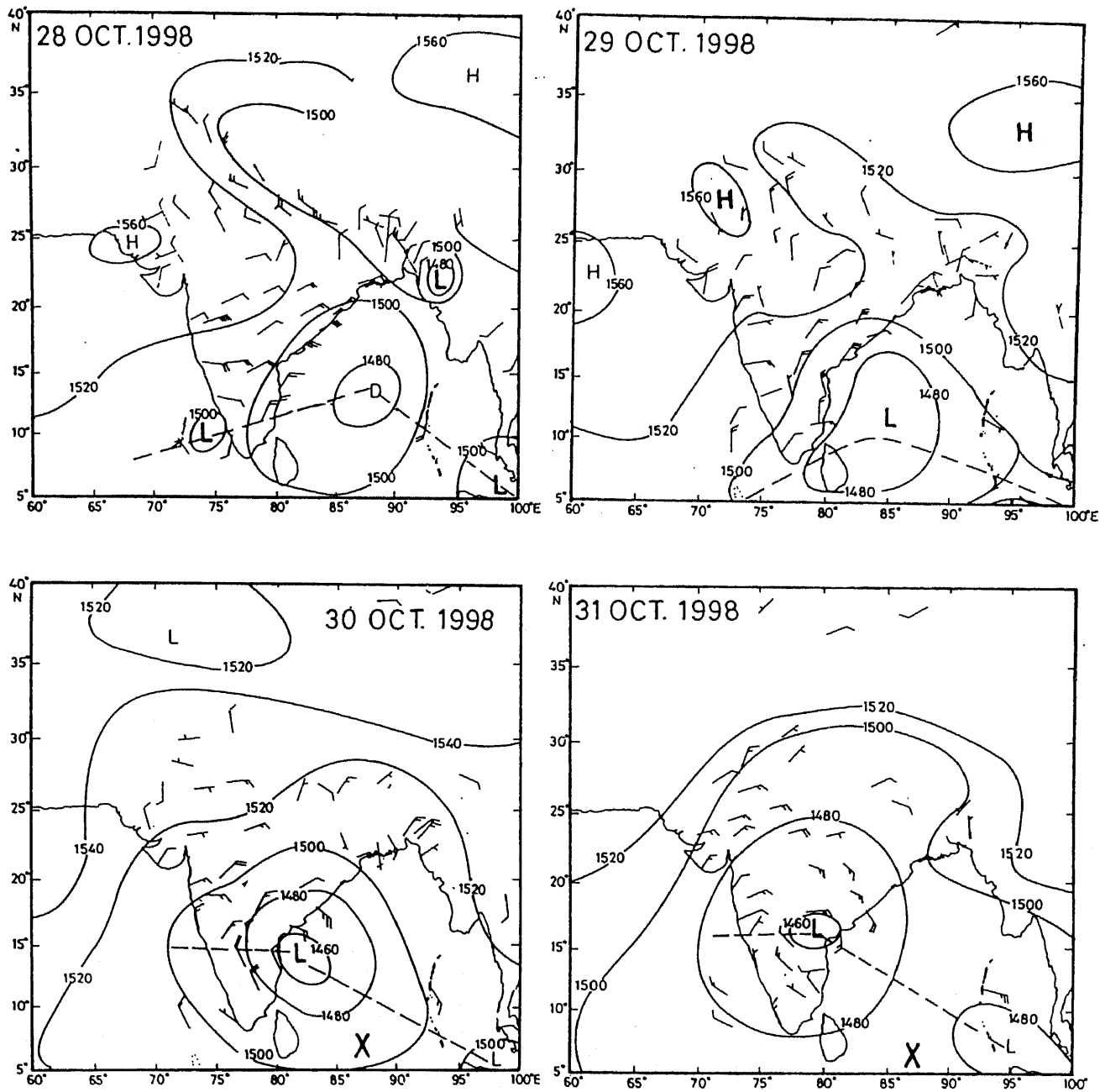
Figure 8. 850 hPa analysis at 0000 UTC of 28th October to 31st October 1998. X – Position of Sagar Kanya.

## 4. Low pressure area in the southwest Bay of Bengal

The shear zone continued over southwest Bay even after weakening of the depression. Figure 8 shows a set of satellite images for the period 1st – 4th November 1998 whereas the corresponding analysis is given in figure 9. A satellite observed cloud disturbance is seen throughout this period that moved westward from 1st November and lay over coastal Tamilnadu and its neighbourhood on 4th November. A low pressure developed off south Tamilnadu and east Sri Lanka on

circular and intense on 2nd November in which OLR as low as 160 watts per sq. meter was observed on this day (figure 10). The low pressure persisted over the southwest Bay until 6th November and became less marked on 7th November. It was more marked on 2nd November when the associated upper air circulation at 850 hPa level was seen positioned vertically above the surface low. This circulation split up into two parts on 3rd November and again became flat on 4th November in which the shear line was still visible. This weak scenario continued for the next two weeks. A simulation

*S R Kalsi*
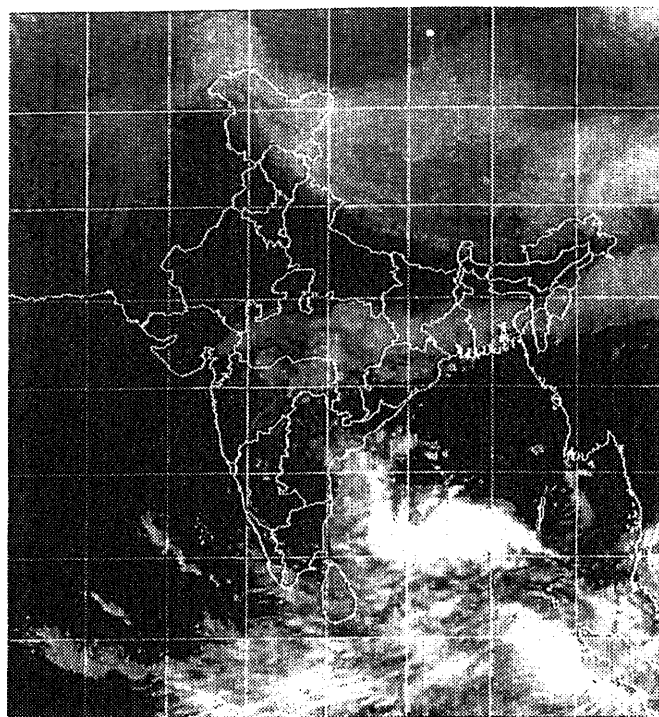
## 1 NOV. 1998

## 2 NOV. 1998
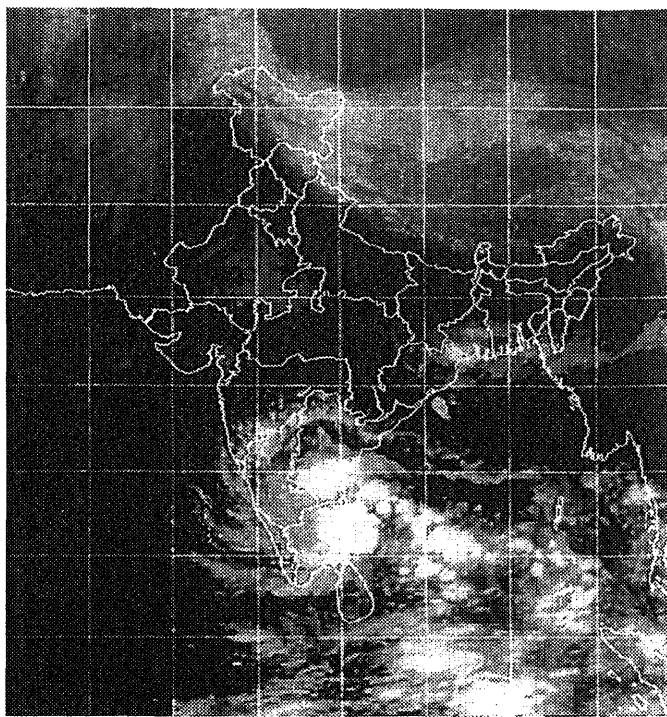
## 3 NOV. 1998
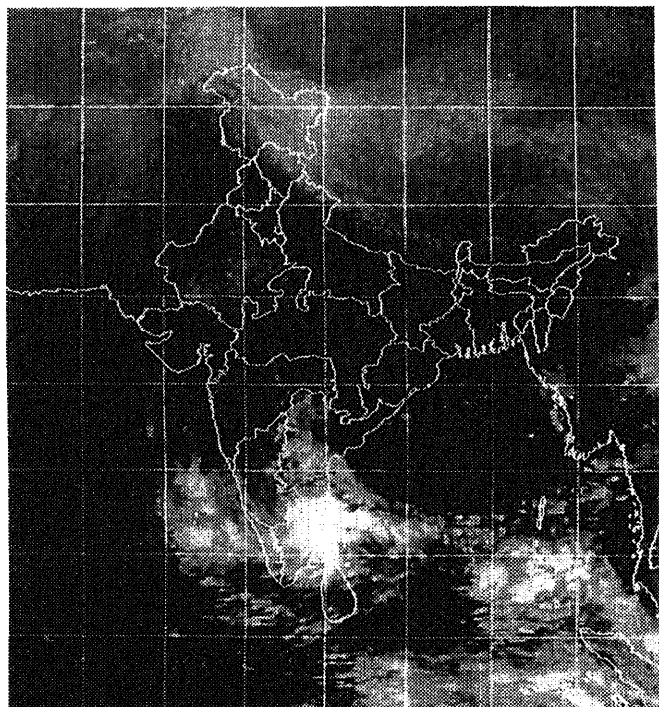
## 4 NOV. 1998
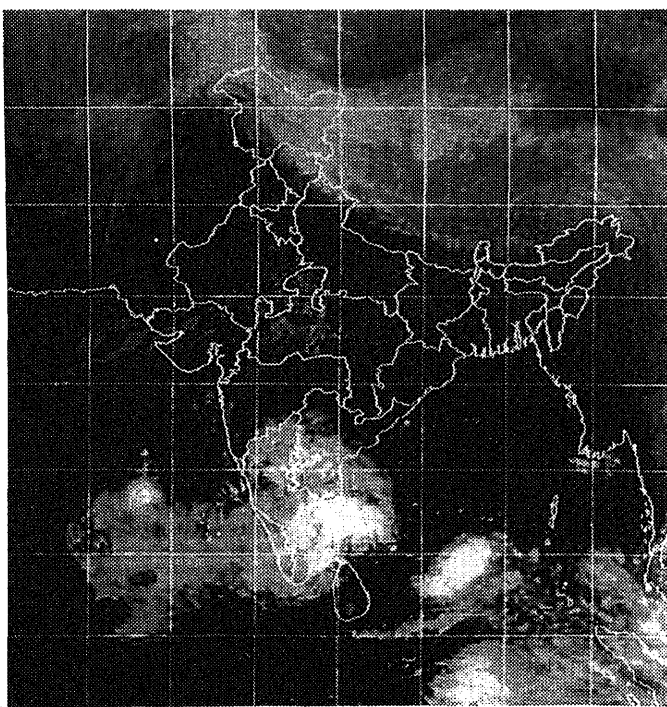
Figure 9.  Sequence of INSAT pictures (1st — 4th November 1998) showing clouds associated with low pressure area over southwest Bay and neighbourhood.
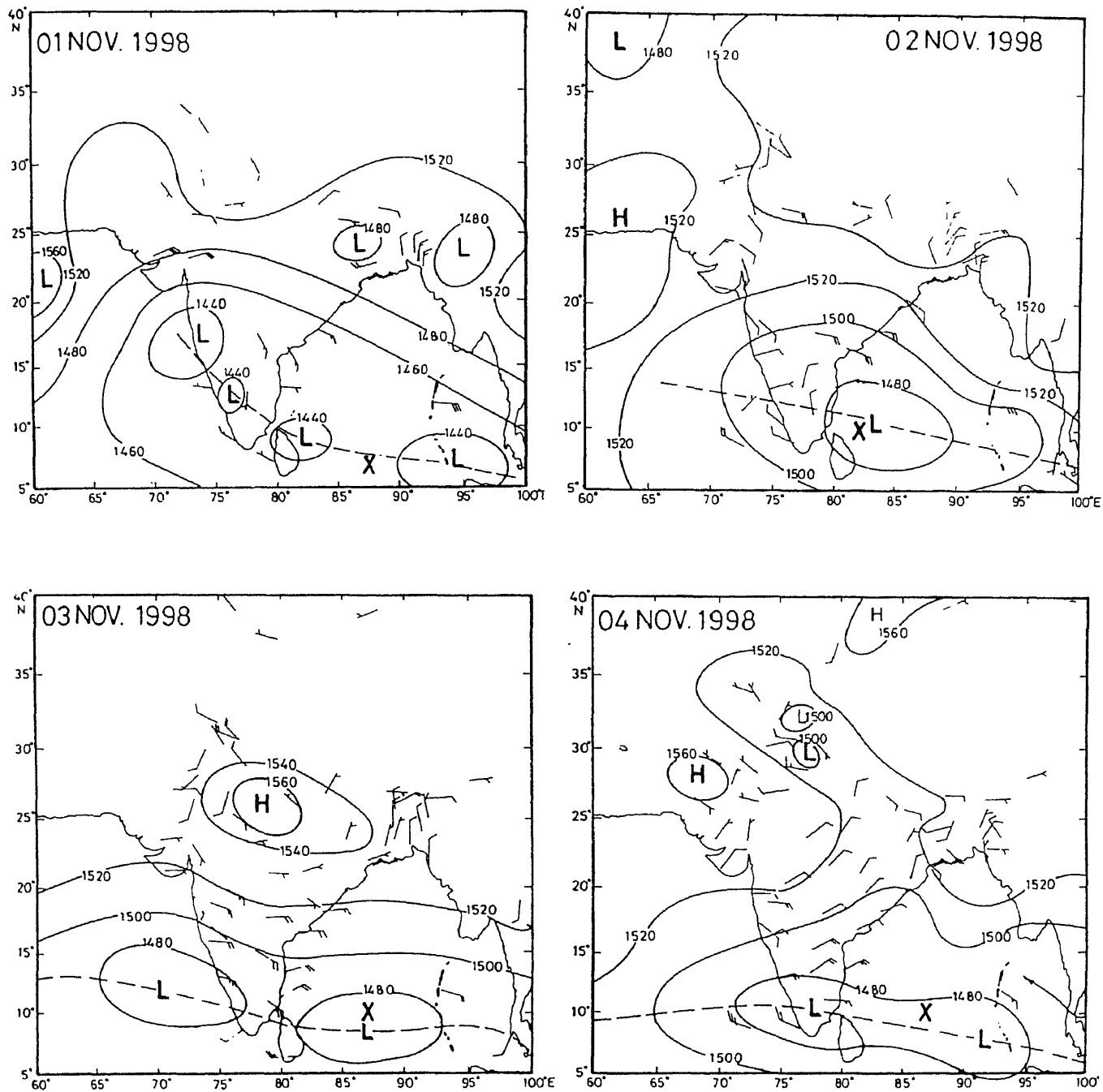
Figure 10. 850 hPa analysis at 0000 UTC from 1st to 4th November 1998 with shear line (-----). X – Position of Sagar Kanya ship.

## 5. Conclusion

The following features of circulation were observed during the pilot study period of BOBMEX:

- A shear line in the south Bay of Bengal and the Nicobar Islands with weak to moderate monsoon

movement towards westnorthwest and eventual dissipation over west central Bay.

- Establishment of northeast monsoon on 28th October.
- Formation of a low pressure area in the southwest Bay off Sri Lanka, south Tamilnadu coast.
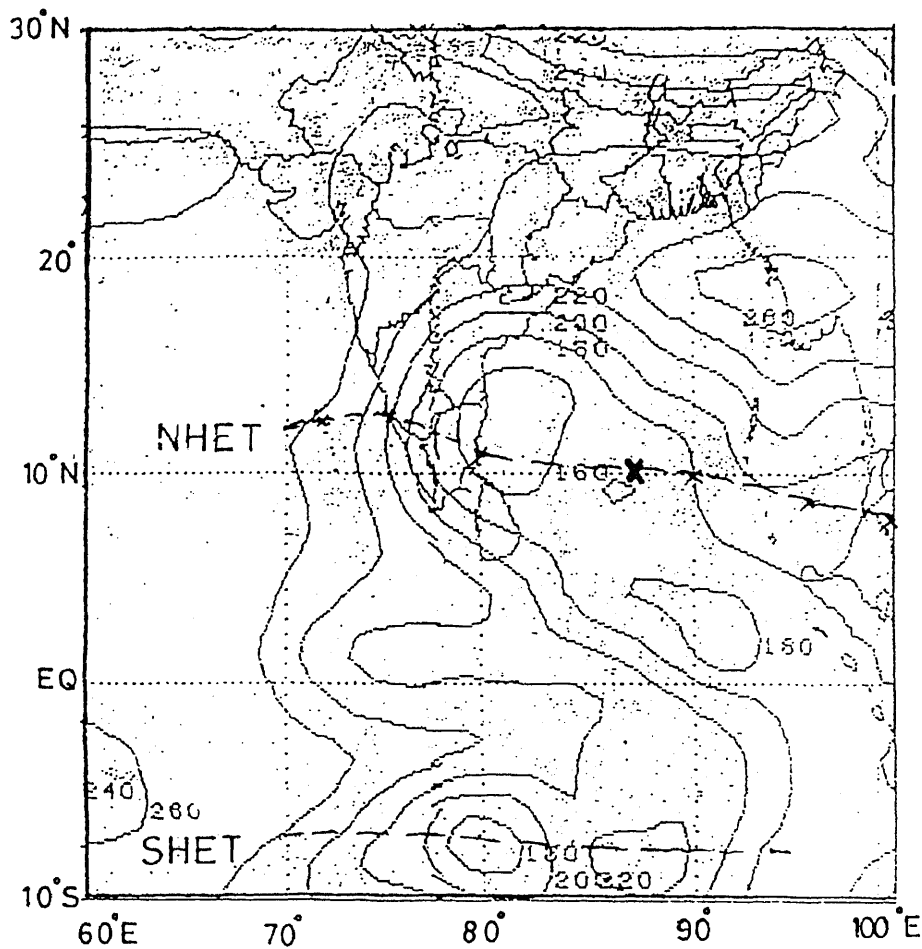
Figure 11.   INSAT derived OLR on 2-11-1998 with 850 hPa shear line (-----) X – Position of Sagar Kanya ship.

## References

Kalsi S R, Rao A V R K, Misra D K, Jain R K and Rao V R, 1995 Structural variability of tropical disturbances in the Bay of Bengal, Advances in Tropical Meteorology; (ed) R K Dutta, (Concept Publishing Company).

Kanti Prasad, Kalsi S R and Dutta R K 1990 Wind and cloud structure of monsoon depressions; *MAUSAM*, **41** 3 365–370.

Srinivasan V, Raman S and Ramakrishnan A R 1971 Monsoon depression as seen in the satellite pictures; *IJMH&G*, **22** 3 337–346.

# Surface meteorological instrumentation for BOBMEX

G S BHAT and S AMEENULLA

*Centre for Atmospheric and Ocean Sciences, Indian Institute of Science, Bangalore 560 012, India*

Although India has a long experience in ship-borne experiments and oceanographic instrumentation, the atmospheric component has not received much attention in the past. In this paper, the basis of the atmospheric instrumentation system assembled for use on board ORV Sagar Kanya for the BOBMEX-Pilot experiment is described along with some representative results. Wherever possible, Woods Hole's IMET recommendations for meteorological sensors for applications in the marine environment have been followed to keep our measurements in par with international standards. The sensors were tested during the BOBMEX-Pilot experiment and all sensors worked well. Velocity, humidity and temperature data have been successfully collected using fast sensors. It is shown that the component due to the ship's pitching motion can be removed from the measured vertical velocity by making use of an accelerometer. This makes it possible to calculate the surface fluxes by direct methods.

## 1. Introduction

One major emphasis of the Indian Climate Research Programme (ICRP) is on the physical processes taking place during the summer monsoon in the atmosphere and the ocean over the warm seas that surround the Indian sub-continent. For this purpose, several ocean-based field experiments of four to six weeks duration have been planned, the Bay of Bengal and Monsoon Experiment (BOBMEX) and the Arabian Sea Monsoon Experiment (ARMEX) being two examples (ICRP Implementation Plan 1998). The main components of these experiments will be carried out on board research ships. The exchange of mass, momentum and energy between the ocean and the atmosphere takes place at the sea surface and accurate measurement of near surface meteorological parameters is necessary to calculate the interface fluxes. However, this is a difficult task because of high humidity levels, sea spray and the movement of the platform from where measurements are made. In addition, the sensors and instruments have to work in the harsh marine environment without requiring service support. India has a long experience in ship-borne experiments and oceanographic instrumentation, however, the atmospheric component has not received much attention in the past. Therefore, one important task was to set up an instrumentation system for the measurement of surface meteorological parameters on board research ships. In this paper, the atmospheric instrumentation system assembled for use on board ORV Sagar Kanya for the BOBMEX-Pilot experiment, the first field campaign under ICRP, is described along with some representative results.

## 2. Sensor selection

Important surface meteorological parameters include pressure, wind speed and wind direction, air temperature, humidity, radiation and rainfall. The accuracy requirements on these parameters is dictated by the application such as the acceptable uncertainty on surface fluxes for use in numerical models. The precise accuracy requirements on the above parameters have not been worked out in the Indian context. For the International programs such as WOCE (World Ocean Circulation Experiment) and TOGA (Tropical Ocean Global Atmosphere), the absolute accuracy of various parameters have been arrived at in order to achieve heat flux accuracy of $10 \, \text{W/m}^2$ for each component of energy balance (table 1) (Large 1985; Hosom *et al*

| Variable | Desired accuracy |
|---|---|
| Wind speed | Larger of 2% or 0.2 m/s |
| Wind direction | 2.8° |
| Air temperature | 0.25°C |
| Incoming short wave radiation | Better than 10 W/m² |
| Incoming long wave radiation | Better than 10 W/m² |
| Relative humidity | 1.7% |
| Specific humidity | 0.25 g/kg |
| Precipitation | 1 cm per month |
| Barometric pressure | 1 mb |

1995). The numbers given in table 1 are absolute accuracies, i.e., includes that of sensor, interface electronics, signal transmission and data acquisition. Such accuracies are required for getting the uncertainties in the predictions of climate models within acceptable limits, and by no way mean that all are achievable in practice.

The selection of each component of the measurement system consisting of the sensors, signal cables, interface electronics and data acquisition procedure is very crucial in achieving high levels of accuracy. A survey of the available sensors revealed that, in principle, several makes could meet the above accuracy specifications, and the main question would be their performance and reliability under marine conditions. Considerable time and a lot of resources are needed to make field trials and to decide on the best among the available makes. Given the time frame of our programmes, this is not possible and therefore we considered the experience of others involved in the earlier land and ocean based experiments. A group at Woods Hole Oceanographic Institution (WHOI), USA has developed IMET (Improved Meteorology) system for use on-board in ship and buoy (Hosom *et al* 1995). A series of performance and reliability tests under real marine conditions were carried out by them on meteorological sensors made by well known companies. These tests lasted for a period of about two years. Based on the outcome, IMET system has been configured (Hosom *et al* 1995). In the IMET system, the best performing wind, temperature, humidity, radiation, pressure and precipitation sensors have been integrated into one complete system along with the data acquisition system. The makes recommended by WHOI and used in the IMET system are shown in table 2. It is seen from table 2 that R M Young products are recommended for wind speed, wind direction and precipitation, Eppley Lab for the radiation, and Rotronic for humidity. The IMET system has been extensively used during the TOGA observations. The IMET system is sold by WHOI, however, the entire system is very expensive. The same sensors are directly available from manufacturers at a much cheaper price, and using the

and integrating them into a complete system turned out to be considerably less expensive and was followed while developing the atmospheric instrumentation for the BOBMEX programme.

We would like to stress here that the IMET system developed by WHOI includes only slow sensors, i.e., sensors whose response times are few seconds or more. For meeting certain objectives of BOBMEX, namely the direct estimation of surface heat and momentum fluxes, wind, temperature and humidity sensors need to have a frequency response of at least 5 to 10 Hz (fast sensors). Since a study comparable to IMET has not been carried out for the fast sensors, the decision was based on the experience in our recent national experiments, namely MONTBLEX-90 and land surface processes experiment at Anand (personal communication, Sri. K G Vernekar, IITM) along with the overall sensor design. The basic surface met sensors selected for BOBMEX are shown in table 3. (Surface pressure was manually recorded from the pressure gauge on board the ship). From tables 2 and 3 we see that by and large, the slow sensors selected for BOBMEX are the same as those used in the IMET system except the humidity sensor. In the IMET system, Rotronics humidity sensor is used along with R M Young radiation shield whereas in the BOBMEX set up, R M Young humidity sensor with R M Young radiation shield is used (Rotronics sensor might have required certain modifications in the radiation shield, and on compatibility considerations R M Young humidity sensor was selected). We have used R M Young humidity sensor during INDOEX cruises and found it to be accurate and it worked well in the marine environment.

The measurement of humidity, especially from a fast response sensor, has been a major problem in the previous field experiments in India. In previous experiments, Lyman alpha sensor had been used and was found to have problems when it rained. In the present set up, we have selected the infrared (IR) hygrometer as the fast response humidity sensor. This instrument operates on the principle of electromagnetic radiation absorption characteristics of water vapor. It consists of a light source and a detector enclosed in two sealed housings, that are separated by

Table 2. *Woods Hole Oceanographic Institution recommendations for ship and buoy MET sensors.*

| Variable | Make |
|---|---|
| Wind speed | R M Young |
| Wind direction | R M Young |
| Air temperature | PRT with R M Young shield |
| Incoming short wave radiation | Eppley |
| Incoming long wave radiation | Eppley |
| Relative humidity | Rotronic |
| Specific humidity | – |
| Precipitation | R M Young |

Table 3. *Sensors used in the system developed for ICRP ship based field experiments.*

| Parameter | Accuracy | Make |
|---|---|---|
| **Slow Sensors** | | |
| Air temperature | 0.2°C | PRT, R M Young radiation shield |
| Humidity | 3% RH | R. M. Young |
| Incoming short wave | $\sim 10\,W/m^2$ | Eppley |
| Incoming long wave | $\sim 10\,W/m^2$ | Eppley |
| Precipitation | 1 mm | R M Young |
| **Fast sensors (10 Hz or better)** | | |
| 3-D wind velocity | 0.1 m/s (Sonic) | METEK Germany |
| 3-D wind velocity | 1% (Gill propeller) | R M Young |
| Temperature | 0.01°C (Sonic) | METEK Germany |
| Humidity | $0.5\,g/m^3$ | Applied Technologies, USA |
| Acceleration | $0.05\,m/s^2$ | Crossbow, USA |
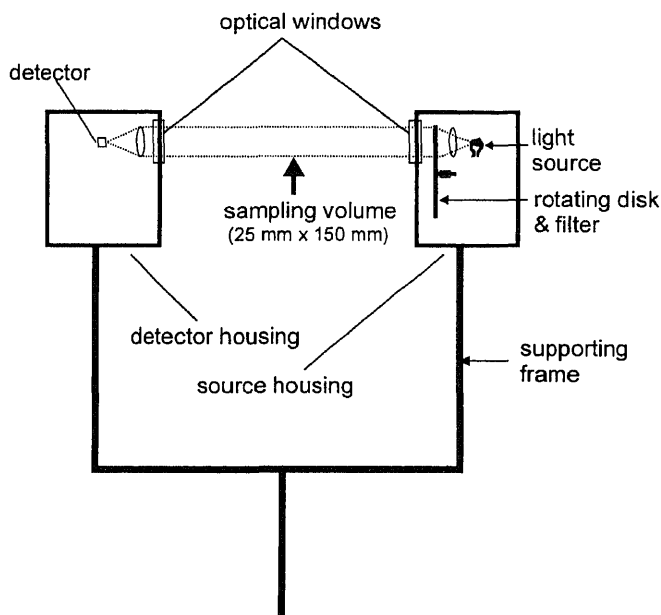


Figure 1. A schematic of the IR hygrometer sensor assembly.

an open space that forms the sampling volume (figure 1). An optical window, in each housing enables the source radiation to pass through the air gap and fall on the detector at the other end. The volume of the air sampled is 25 mm (1") in diameter and 0.15 m long. A rotating (3000 rpm) disk, placed in front of the light source and having two optical filters fixed on it at certain angular positions, alternately makes the water vapor absorbing and water vapor transparent radiation from the same source to pass through the sampling volume. The amount of water vapor present in the air column along the beam path is calculated from the ratio of the intensities of radiation measured by the detector at these two frequencies. The main advantage of this arrangement is that all components are completely sealed (sensor not spoilt by rain or sea spray), and any deposition on the mirror surface or

when their ratio is taken. This design is rugged and suitable for marine applications.

## 3. Signal transmission and interface electronics

The data acquisition system was located in the Met laboratory at a distance of about 80 meters from sensors. Shielded cables have been used to transmit the signals from the sensors to reduce the interference from other sources. The multi-core, shielded nylon cables are very good for such purposes and have been used during BOBMEX-Pilot. The output of some of the sensors were RS232 (IR hygrometer) or RS422 (sonic anemometer) digital signals, whereas, others analogue. The RS422 signal was converted to RS232 signal in the Met laboratory. Digital signals were directly fed to the PC through a multi-serial port add-on PC card. Analogue signals were digitized before being fed to the data acquisition system.

When the cable lengths are long (e.g., 90–100 meters as in the present case), precaution is required in measuring the sensor output voltage because of the loop current. Sensors draw a small current and the voltage drop between the two ends of the connecting cable can become important if the cable lengths are long. In such cases, the calibration constants obtained in the laboratory using short cables (typically few meters) will not be valid. Also, for each parameter, two channels (representing high and low ends of the sensor output) of the A/D converter are required. Thus, if the number of signals are large (as in the present case), then the demand on the capacity of the data acquisition board becomes severe. A solution to both these problems is an electronics circuitary (interface electronics) based on operational amplifier, whose schematic is shown in figure 2. Outputs (high and low) from each sensor were transmitted to the laboratory using cables independent of that used for
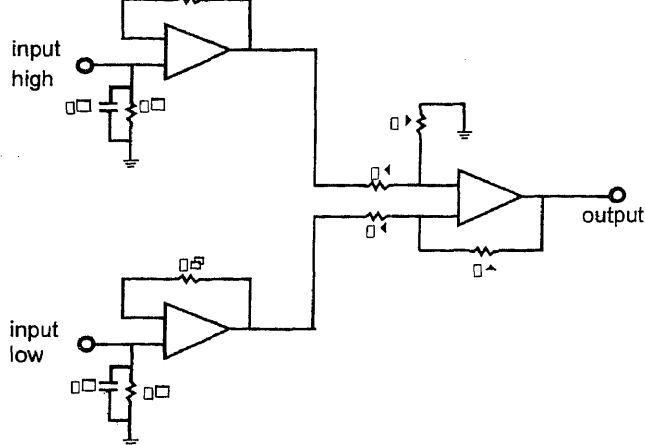
Figure 2. Schematic of the interface electronics for measuring the sensor outputs relative to a common ground.



Figure 3. Comparison of Gill and Sonic anemometer measured wind speeds with the wind tunnel wind speed.

Wherever required, additional signal conditioning facility was incorporated in the circuit to suit individual sensor characteristics. The outputs from the interface electronics were fed to the data acquisition system, a 12 bit system having 16 single ended analogue input channels (DAQbook). A PC working on Windows 95 was used for acquiring and storing the data. Data acquisition and archival were controlled by software. This program handled the data from the DAQbook and RS232 digital inputs coming from sonic anemometer and IR Hygrometer, as well as the display of all the parameters on the screen for visual monitoring in real time.

## 4. Sensor testing

Most of the sensors were new and calibrated at the factory. Since the marine atmosphere is very corrosive and the sensors can get degraded, all sensors have been tested after the field experiment. The radiation instruments have been tested at the Central Radiation Laboratory, IMD Pune and were found to maintain the factory calibrated sensitivity. Wind, temperature and humidity sensors have been tested in the laboratories at Indian Institute of Science, Bangalore. For example, figure 3 shows the performance of Gill and Sonic anemometers tested in the two feet wind tunnel after the Pilot experiment. One component of the sensor was aligned along the mean wind direction, wind speed increased from about 3 m/s to 15 m/s and then decreased back (steady wind speeds below 4 m/s are difficult to maintain and less accurate). The results shown are the averages of two sets for each component. There is good agreement between the wind tunnel, sonic and Gill anemometer wind speeds. The overall error includes that of alignment and wind speed setting, in addition to sensor accuracy. In our opinion, much of the scatter seen in figure 3 is due
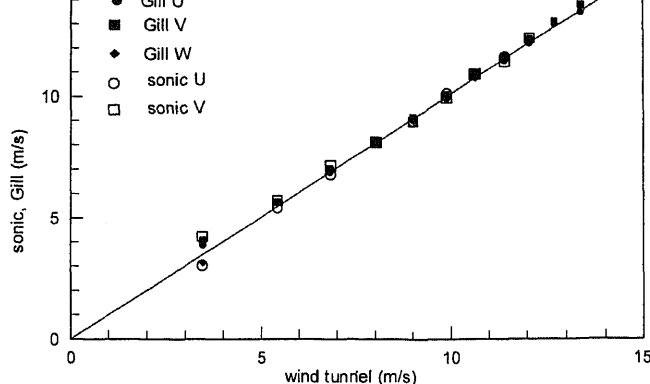
to alignment and wind speed setting problems. The testing confirmed that the performance of Sonic and Gill anemometers have not been degraded after they were used in the Pilot experiment.

Temperature and humidity sensors have been tested in a closed, insulated chamber where the relative humidity is maintained constant using saturated salt solutions and the temperature was controlled by circulating water from a constant temperature bath. These sensors have been tested using connecting cables used in the field experiment. The humidity sensor's response was in good agreement with the original specifications, however a change in the sensitivity of the temperature sensor was observed (from 20°C/V to 21°C/V) and the new values have been used in the preparation of the Pilot data set.

The sonic anemometer measures the virtual temperature of the air, i.e., the temperature corrected for the presence of water vapor. Our calibration confirmed this, however, a constant offset between the reference virtual temperature and sonic temperature was noted. The reason for this is that by an option in the sonic anemometer set up menu, the mean temperature can be set to the dry bulb temperature. This way, the mean temperature corresponds to the air temperature (approximately) and the fluctuating component gives the turbulent component of virtual temperature.

## 5. Results

The sensors were tried in the field during the BOBMEX-Pilot experiment on board ORV Sagar Kanya from 25th October to 12th November 1998. The sensors were mounted on a micrometeorological tower fixed at the end of a seven meter long horizontal boom at the forecastle deck of the ship (figure 4). The sensors on the tower were switched on from October 25th to November 8th, 1998. The data archival was controlled by the DASYLab software. Basically, the
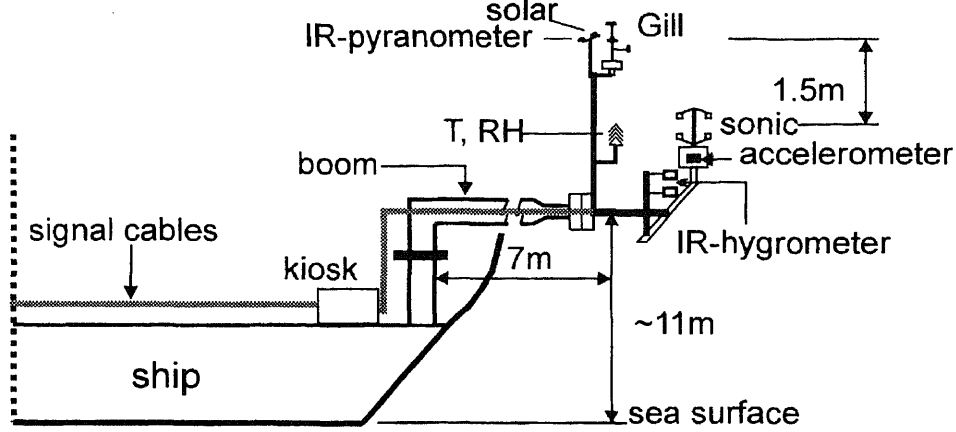
Figure 4. Arrangement of surface meteorological sensors on board ORV Sagar Kanya.
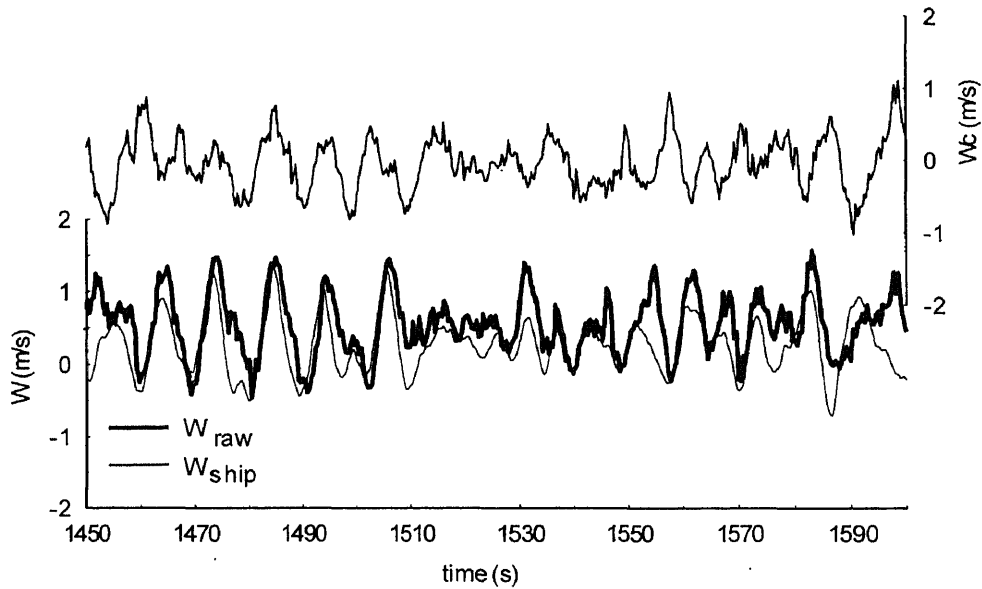


Figure 5. A short time series of the vertical velocity. $W_{\mathrm{raw}}$ is the vertical velocity measured by the sonic anemometer, $W_{\mathrm{ship}}$ is vertical velocity caused by the ship's pitching motion calculated from the accelerometer data and $W_c$ is the corrected vertical velocity.

so called fast data (10Hz sampling rate) was acquired for 65 minutes once in every three hours (00, 03, 06, 09, 12, 15, 18 and 21 hours IST) and stored in separate files. The data from the fast sensors were averaged for 10 seconds and these values were stored continuously. The data from the slow sensors (1 Hz sampling frequency) were averaged for 10 seconds and also archived continuously. In order to limit the size of individual files, one set of files was closed and a new set of files was opened every three hours automatically. All the sensors, interface electronics and the data acquisition system worked continuously without any problem for the entire duration of the Pilot experiment.

Results from the slow sensor data are presented in a companion paper in this volume (Bhat *et al* 2000) wherein we present representative data from fast sensors. One main application of the fast data is in the

estimation of the fluxes by the eddy correlation method. This involves computing $v'w'$, $q'w'$, $T'w'$, etc., where $v$ and $w$ are respectively horizontal and vertical components of wind velocity, and $q$ and $T$ are mixing ratio of water vapor and air temperature respectively; the primes denote the deviations from respective 15 to 20 minutes average values. Accurate measurement of vertical component of velocity is very important in these calculations. However, at the sampling rate of 10 Hz, measured $w$ is strongly influenced by the rolling and pitching motion of the ship. An accelerometer was mounted on the stem of the sonic anemometer to measure the movement of the sensor caused by the ship's motion. Figure 5 shows the vertical velocity measured by the sonic anemometer ($W_{\mathrm{raw}}$), calculated from the accelerometer output ($W_{\mathrm{ship}}$) and the difference between the two, namely the corrected vertical velocity ($W_c$). It is
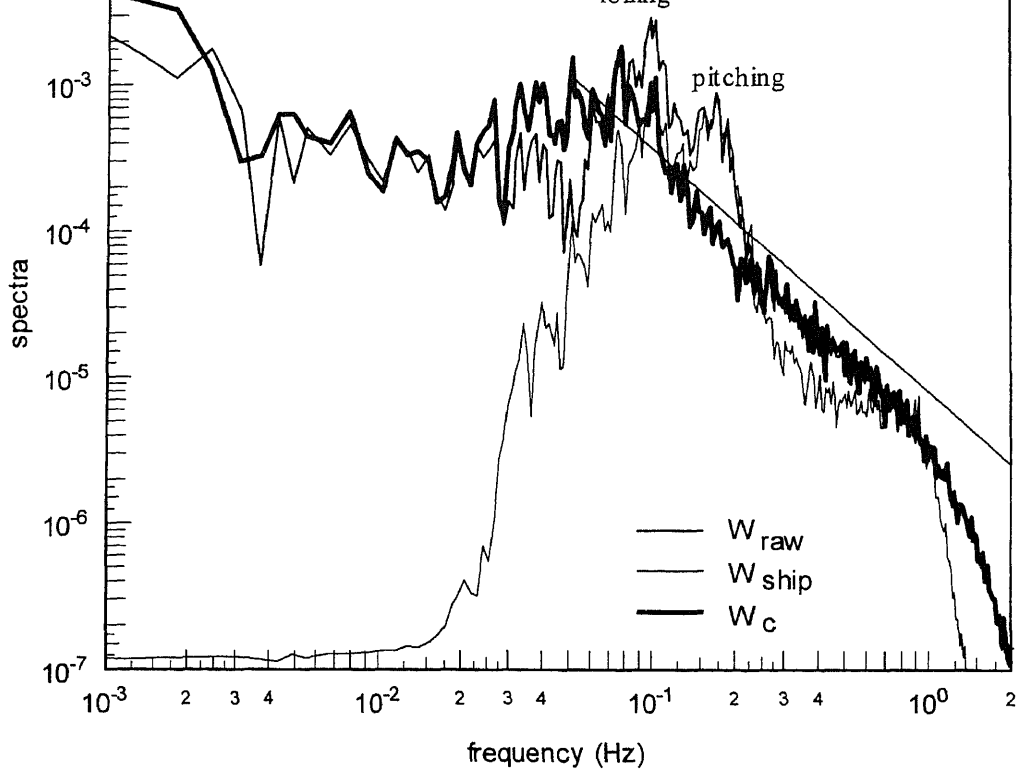
Figure 6. The spectra of vertical velocities. The thin straight line corresponds to $f^{-5/3}$ decay rate.

observed from figure 5 that large fluctuations in the vertical velocity measured by the sonic anemometer are caused by the ship motion itself and the actual vertical velocity of the air ($W_c$) has a different appearance. This is clearly seen in the spectra of three velocities shown in figure 6. The spectrum of $W_{raw}$ has two peaks near $0.1\,Hz$ corresponding to the pitching and rolling motions of the ship. In the spectrum of the corrected vertical velocity, the component due to the pitching motion of the ship has been very successfully removed. The peak at the rolling frequency has been reduced by a factor of about five, but not completely removed. This encourages the hope that it is possible to obtain wind vertical velocity on board the ships with reasonable confidence.

In a fully developed turbulent flow, the spectra of velocity and scalars follow the Kolmogorov's $k^{-5/3}$ decay law over a range of wave number $k$ at high wave numbers (inertial subrange) (Batchelor 1953). The wave number is proportional to the frequency $f$, and therefore the spectrum is proportional to $f^{-5/3}$ in the inertial subrange in figure 6. It is observed from figure that the range of frequencies where the $k^{-5/3}$ decay prevails is enhanced after the correction to the motion. The question is, how important is the tion for $w$ in the estimation of fluxes? Our ations showed that the contamination due to



Figure 7. Time series (bottom) and spectrum (top) of mixing ratio $q$ measured by the IR Hygrometer. The thin straight line in the top frame has a slope of $(-5/3)$.

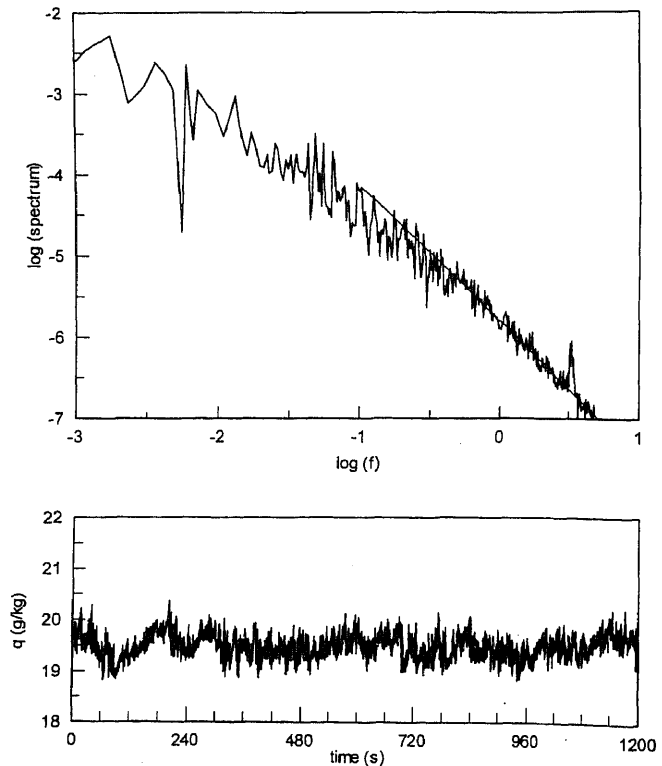the ship's pitching on the estimated fluxes is substantial when swell waves are strong and wind speeds less than 3 m/s. For example, when swell waves were about 2 meters high, the calculated sensible heat fluxes are about $35\,\mathrm{W/m^2}$ and $10\,\mathrm{W/m^2}$ respectively using uncorrected and corrected vertical velocities, the latter looks very reasonable over the oceans (these results will be reported in a separate paper).

Figure 7 shows the data from the IR hygrometer sampled at 10 Hz. According to theory, the spectrum of the scalars should follow the $k^{-5/3}$ decay law at higher frequencies in a turbulent flow, and the data from the hygrometer are in good agreement with the theory suggesting that the frequency response of the hygrometer is pretty good.

## 6. Conclusion

The surface Met instrumentation for measurements on board ship for ICRP has been developed. Wherever possible, Woods Hole's IMET recommendations have been followed. The sensors were tested during the BOBMEX-Pilot experiment and all sensors worked well. Post field experiment testing has confirmed that there was no noticeable degradation in the performance of the sensors. Velocity, humidity and temperature data have been successfully obtained using fast sensors. It is shown that the component due to the ship's pitching motion can be removed from the measured vertical velocity by making use of an accelerometer. The rolling component is not completely removed and additional sensors like tilt sensors that measure the roll angle may help in determining the contamination due to rolling.

## References

Batchelor G K 1953 *Theory of homogenous turbulence* (Cambridge University Press)

Bhat G S, Ameenulla S, Venkataramana M and Sengupta K 2000 *Proc. Indian Acad. Sci.*, (*Earth Planet. Sci.*) (this issue)

Hosom D S, Weller R A, Payne R E and Prada K E 1995 *J. Atmos. and Oceanic Tech.* **12** 527–540

*Indian Climate Research Programme. Implementation Plan* 1998 (New Delhi: Department of Science and Technology)

Large W G (ed.) *World Ocean Circulation Experiment: U.S. WOCE* 1985, Tech. Rep. No.1, WOCE Global Air-Sea Interaction Fields, 36 pp.

# Atmospheric boundary layer characteristics during the BOBMEX-Pilot experiment

G S Bhat[1], S Ameenulla[1], M Venkataramana[2] and K Sengupta[2]

[1] Centre for Atmospheric and Oceanic Sciences, Indian Institute of Science, Bangalore 560 012, India
[2] Space Physics Laboratory, Vikram Sarabhai Space Centre, Trivandrum, India

The atmospheric boundary layer characteristics observed during the BOBMEX-Pilot experiment are reported. Surface meteorological data were acquired continuously through an automatic weather monitoring system and manually every three hours. High resolution radiosondes were launched to obtain the vertical thermal structure of the atmosphere. The study area was convectively active, the SSTs were high, surface air was warm and moist, and the surface air moist static energy was among the highest observed over the tropical oceans. The mean sea air temperature difference was about 1.25°C and the sea skin temperature was cooler than bucket SST by 0.5°C. The atmospheric mixed layer was shallow, fluctuated in response to synoptic conditions from 100 m to 900 m with a mean around 500 m.

## 1. Introduction

Many synoptic systems that produce rainfall over the Indian subcontinent form and intensify over the Bay of Bengal. The frequency of occurrence of convective systems over the Bay of Bengal is among the highest in the world during the summer months. The physical processes responsible for this have not been clearly understood. The Bay of Bengal has many special oceanographic features as well. For example, the variation in the sea surface temperature (SST) of 1°C to 2°C over a period of 2 to 4 weeks (intraseasonal oscillation) is larger than the inter annual variation of 0.5°C (Premkumar *et al* 2000). The head Bay is influenced by the large volume of freshwater discharge from rivers, which is not the case in the central and southern Bay, thus giving rise to strong north-south gradient in salinity. Thus, the Bay of Bengal has certain unique features which make it an exciting place for scientific investigations.

There have been three major summer monsoon experiments in the Bay of Bengal in the past. The first two experiments, called MONSOON-77 and MONEX-79, were carried out more than two decades back and with international collaboration. MONSOON-77 involved four USSR ships forming a polygon over the Bay of Bengal centered at 17°N 89°E during 11th – 19th August 1977. The observations included upper air soundings every six hours (00, 06, 12 and 18 GMT). A trough formed over the head Bay on August 16th which developed into a depression on August 19th. Thus, the experiment provided data that enabled the study of the changes in the horizontal wind fields, vertical velocity and large-scale heat and moisture budgets between disturbed and undisturbed conditions in the Bay (e.g., Mohanty and Das 1986). MONEX-79 measurements over the Bay involved mainly four Russian ships forming a stationary polygon centered at 16.2°N 89.5°E during the period 11th – 24th July 1979. Observations from the ships included upper air soundings two times a day (00 and 12 GMT), surface air temperature, dew point temperature, wind speed and direction, cloud amount and sea surface pressure. This period happened to be the break/weak monsoon period over the region and disturbed conditions could not be observed. In addition to ships, an aircraft equipped with dropwind sonde was used during MONEX-79. The third experiment, MONTBLEX-90, was carried out on board the Indian research vessel ORV Sagar Kanya during August – September 1990 in the head Bay.

**Keywords.** Marine boundary layer; air-sea coupling.

on the changes in the wind fields, surface fluxes and large scale heat and moisture budgets, between disturbed and undisturbed conditions in the Bay (Mohanty and Das 1986; Saha and Saha 1988; Rao et al 1993; Murty et al 1996; Sarma et al 1997; Sanilkumar et al 1994; Moshonkin and Harenduprakash 1991). These experiments had certain limitations too. The dominant signal in the atmosphere and the SST of the Bay is on the intraseasonal scale of two to four weeks and the ocean and the atmosphere are strongly coupled on this time scale (Premkumar et al 2000). The time series in the earlier experiments are either too short ($\sim 10$ days) or the ships were continuously moving to reveal clearly the intraseasonal time scales. Further, the surface fluxes were derived using empirical relations and bulk aerodynamic formulae, and solar and longwave radiation were not directly measured. The soundings had typical vertical resolution of 25–50 mb, which is not sufficient to study the structure of the marine atmospheric boundary layer.

There are several outstanding questions regarding both the atmosphere and the ocean over the BoB, and a field experiment, called the Bay of Bengal Monsoon Experiment (BOBMEX) was proposed under ICRP. The background and objectives of BOBMEX as well as the BOBMEX-Pilot experiment are given in the paper by Sikka and Sanjeeva Rao in this issue.

In this paper, we present the surface meteorological parameters, the atmospheric mixed layer height and the sea surface temperature (SST) observed during the Pilot experiment. The Pilot experiment was carried out on board ORV Sagar Kanya during October – November 1998. The cruise track is shown in figure 1; it started from Marmugao on October 23rd and ended at Tuticorin on November 12th. The first stationary time series station was located at 7°N 87°E for two days on October 30th and 31st. The second time series station was at 10°N 87°E for two days (2nd – 3rd November), and the last time series station for a day was located at 13°N 87°E on November 5th.

## 2. Experimental arrangement: Atmospheric component

The surface micrometeorological sensors were mounted on a tower fixed to a seven meter long (horizontal) boom at the forecastle deck. Figure 2 shows a schematic of the sensor arrangement on the tower. Wind, temperature, humidity, solar and long-wave radiation sensors were installed on the tower and the data from these sensors were continuously acquired. The characteristics of the sensors whose data are reported in this paper are given in table 1. Both fast response (frequency response 10 Hz) and
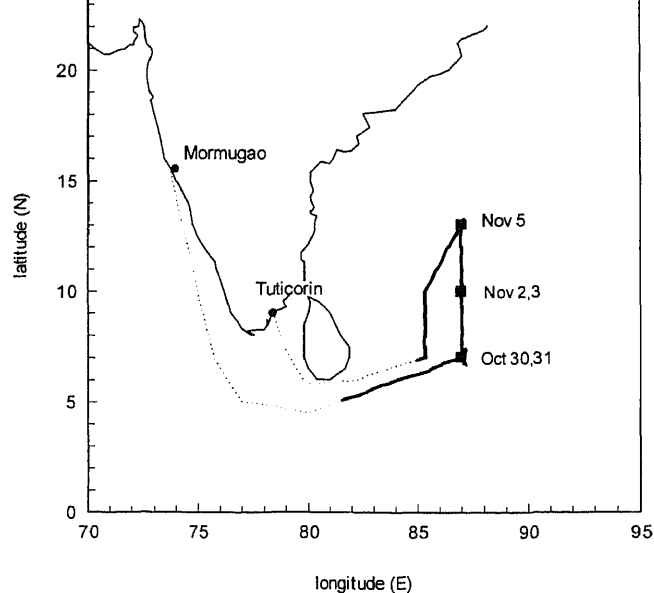


Figure 1. BOBMEX-Pilot cruise track. The solid box symbols refer to the locations of time series stations.

slow response (frequency response slower than 1 Hz) were used. Output of some of the sensors were RS232 digital signals (e.g., sonic anemometer) whereas others were analogue signals. Digital signals were directly fed to the RS232 ports through a multi-serial port add-on PC card. For each analog signal, a variable gain differential input with a small filter facility was provided. The analog voltage signals were routed to the data acquisition system. The Data Acquisition System was a 12 bit system having 16 analogue input channels (DAQbook model 120, manufactured by M/s Iotech Inc., USA). The digitized signals from the DAQbook were fed to the computer through a parallel port connection. A pentium machine working on Windows 95 was used for acquiring and storing the data.

High vertical resolution radiosondes manufactured by AIR (Atmospheric Instrumentation Research Inc., USA) were launched using 300 g balloons. These provided the temperature and humidity values as a function of pressure every 5 seconds (see table 1 for sensor characteristics). The ascent rate was adjusted to 3–4 m/s by controlling the amount of hydrogen gas filled in the balloon to provide a vertical resolution between 15 and 20 meters.

The ship position (latitude, longitude and heading), surface pressure, dry bulb and wet bulb temperatures (psychrometer), and SST (bucket temperature) were recorded every three hours manually. The sea surface skin temperature was measured by an infrared thermometer (henceforth, the infrared thermometer reading is referred to as SKINSST).
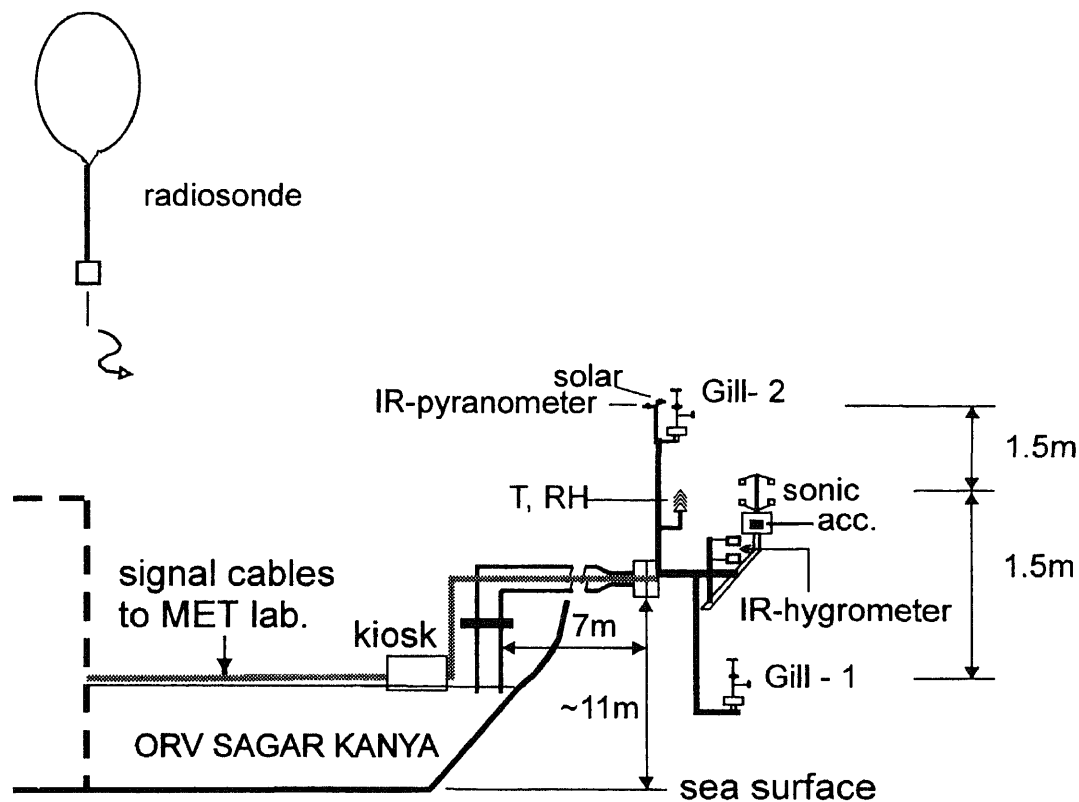
Figure 2. A schematic of the sensor arrangement on board ORV Sagar Kanya during the Pilot experiment.

Table 1. Specifications of the Instruments used during the BOBMEX-Pilot experiment.

| Sensor/Instrument | Parameter | Make | Accuracy | Sampling rate |
|---|---|---|---|---|
| Sonic Anemometer | Wind Component $(u, v, w)$ | METEK, Germany | $\pm 0.1\,\text{m/s}$ | $10\,\text{Hz}$ |
| | Temperature | | $0.01°\text{C}$ | $10\,\text{Hz}$ |
| Pyranometer | Short Wave ($\%3$-$3\mu$) | Eppley Lab, USA | $\sim 10\,\text{W/m}^2$ | $0.1\,\text{Hz}$ |
| | Long Wave ($3$-$50\mu$) | Eppley Lab, USA | $\sim 10\,\text{W/m}^2$ | $0.1\,\text{Hz}$ |
| Humicap | Relative Humidity | R M Young, USA | $3\%$ | $0.1\,\text{Hz}$ |
| Radiosonde | Temperature | AIR Inc. USA | $0.5°\text{C}$ | $5\,\text{sec}$ |
| | Humidity | | $3\%$ | $5\,\text{sec}$ |
| | Pressure | | $1\,\text{mb}$ | $5\,\text{sec}$ |

## 3. Results

### 3.1 *Synoptic conditions*

The southern Bay of Bengal was convectively active during this period. INSAT-1D satellite visible imagery showed a huge cloud band over Andhra and Orissa coasts and south Tamilnadu on October 30th (see paper by Kalsi in this issue). New cloud bands formed between 65°E and 90°E around the latitude 3°N on October 31st, moved northward and passed over ORV Sagar Kanya on November 1st. One system intensified as it approached Tamilnadu coast on November 3rd and the entire south India experienced heavy rains for

observed from the ship. Few isolated cumulonimbus clouds were seen, however they did not develop into any long lasting organized convective system. Within a week after the ship moved away from the last time series station, another synoptic system was seen over the area. We expect that the conditions that prevailed during the Pilot experiment were representative of the cyclone period in the southern Bay of Bengal.

### 3.2 *Surface parameters*

Here, the observations taken for a period of 12 days, starting from October 28th (Julian day 301) to November 8th (Julian day 312) are presented. The
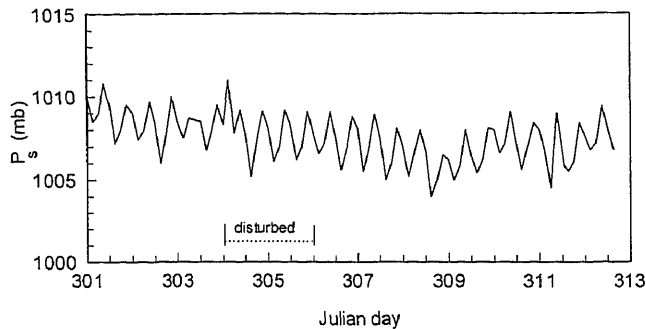
Figure 3. Variation of the surface pressure during BOBMEX-Pilot.



Figure 4. Variation of (a) the surface wind speed, and (b) surface wind direction.

The variation of the surface pressure is shown in figure 3. The prominent feature is the semi-diurnal cycle with an amplitude of about 1.5 mb. The daily mean surface pressure decreased from 1009 mb on day 301 to 1006 mb on day 309 and then gradually increased. On day 305 (November 1), thick deep clouds were seen from the ship and 20 mm rain was recorded on board the ship. Satellite data showed that the convective system that produced this rain belonged to a long cloud band extending from 120°E 8°S to 85°E 13°N. From the surface pressure variation, it cannot be inferred that a big tropical cloud system passed over this area. Further observations are required to understand whether this is a characteristic feature of near equatorial synoptic systems in this region or just that the ship was not at the center of convective activity. (From the satellite picture, it appeared that the ship was towards the periphery of a thick deep cloud system embedded in the synoptic system on day 305.).

The wind velocity measured by the sonic anemometer includes the component due to ship motion. The ship speed and heading were continuously monitored by a GPS system and data stored every ten minutes (facility of ORV Sagar Kanya). From the sonic anemometer and GPS data, true wind speed and true wind direction have been calculated and shown in figure 4. (The data from sensors mounted on the tower and shown in figures 4, 5, 6 and 10 are five minute averages at the start of each hour.) It is observed from figure 4(a) that wind speed ranged from less than a meter per second to more than 12 m/s. Sudden jumps in the wind speed observed in figure 4(a) correspond to the passage of precipitating systems over the ship. Often, convective showers and rains were preceded by a sudden increase in the wind speed (by about 5 m/s) and change in wind direction. On few such occasions, wind speeds larger than 13 m/s have been recorded for short time duration. Winds were mostly westerlies and south westerlies till day 308 and then changed over to easterly (figure 4(b)).

Figure 5(a) shows the variation of air temperature and SST. The SST shown is the bucket SST, i.e.,
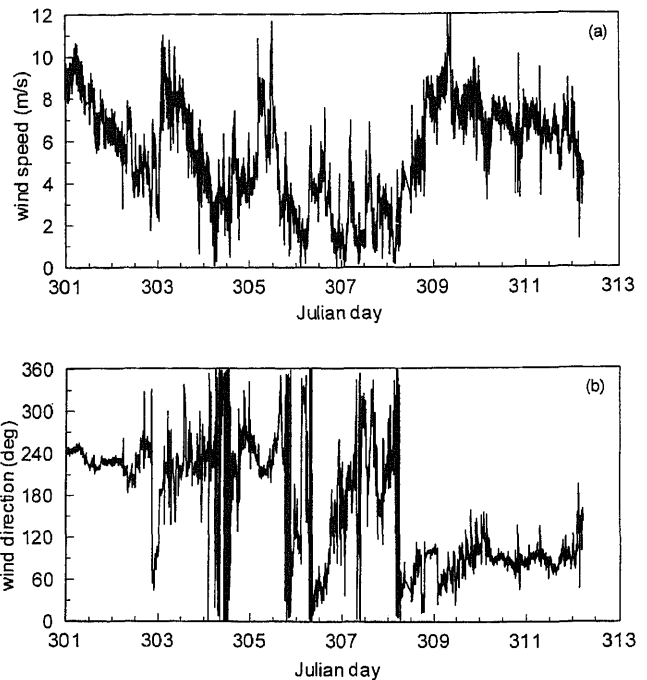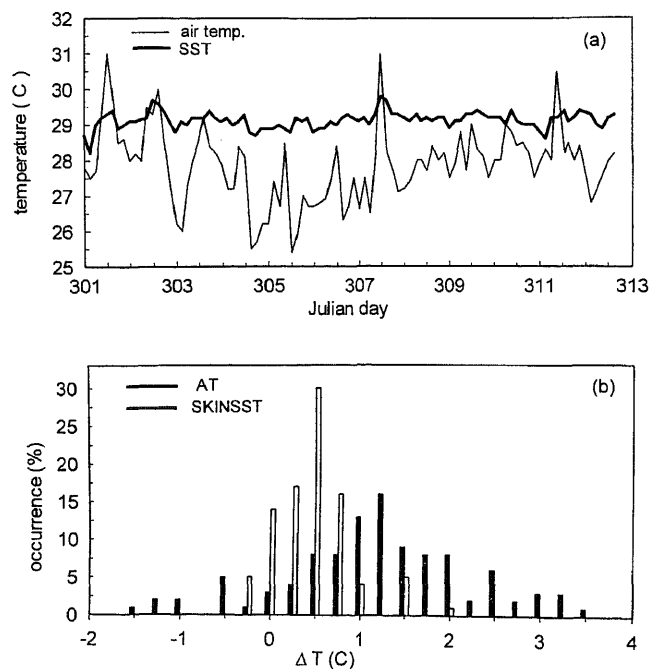


Figure 5. (a) Variation of the air temperature and SST during BOBMEX-Pilot; (b) Frequency of occurrence of the difference between SST and air temperature (AT) and SST and skin temperature (SKINSST).

temperature of the top layer of the sea water taken in a bucket. It is observed from figure 5(a) that SST was warmer than 28°C all the time with an average near 29°C. Warmest SSTs were encountered on days 302 and 307. In general, the air temperature is lower than

it was as warm or slightly warmer than SST (e.g., on days 301 and 302). One important parameter in the estimation of the surface sensible heat flux is the air sea temperature difference. Figure 5(b) shows the frequency distribution of SST and air temperature difference. It is observed from this figure that sea air temperature difference varied in the $-1.5°$ to $3.5°C$ range with a peak at $1.25°C$. Observations over tropical oceans in other parts of the globe also show sea air temperature differences typically in $1°–2°C$ range (Slutz *et al* 1985; Bradley *et al* 1991). The negative values are associated with the measurements taken during noon hours on calm sunny days. Differences greater than $+2$ degree centigrade were observed when it was raining. Just before the arrival of rain and for some time following it, air temperature drops (up to four degree Celsius), whereas, SST remained nearly unaffected, thus giving rise to a larger sea air temperature difference. It may be noted that larger sea air temperature difference in the presence of increased winds enhances the surface heat flux and thus can help in the rapid recovery of the surface temperature following the rain.

Also shown in figure 5(b) is the difference between bucket SST and surface skin temperature (SKINSST). SKINSST was measured by the IR thermometer standing on the forecastle deck at the bow of the ship where the disturbance caused by the ship's body to the sea surface was minimum. SKINSST is important in estimating the longwave radiation emitted by the ocean surface, and also in the evaporation of water. It is observed from figure 5(b) that SKINSST was cooler than the bucket SST about 95% of the time, with a peak at $0.5°C$. SKINSST is expected to be cooler than SST owing to the evaporation of water from the top most layer of the surface. On few days however, SKINSST is observed to be slightly warmer than SST; the (negative) difference is small and not more than $-0.3°C$ and occurred during the day time on sunny days. For the entire period, the mean difference between SST and SKINSST is about $0.5°C$, comparable to the values observed over the Pacific Ocean (Bradley *et al* 1991).

The variation of the relative humidity measured both manually (on ship deck) and automatically (on tower) is shown in figure 6. In general, there is good agreement between the relative humidity measured by the humicap sensor (automatic) and the psychrometer (manual), and except on few occasions when the psychrometer readings were influenced by the warm ship deck, they are within 2% of each other. It is seen from figure 6 that the relative humidity was 80% or more most of the time with an average around 83%, i.e., air was very rich in moisture. Values more than 90% were normally associated with drizzle and rain.

The saturation vapor pressure of water increases by about 6% for every degree centigrade increase in
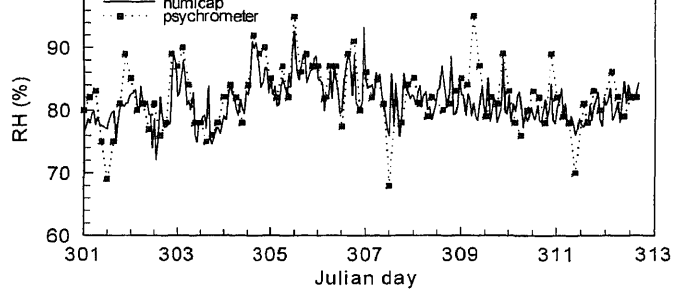


Figure 6. Variation of the surface relative humidity measured by the humicap (tower) and psychrometer (ship deck) during BOBMEX-Pilot.
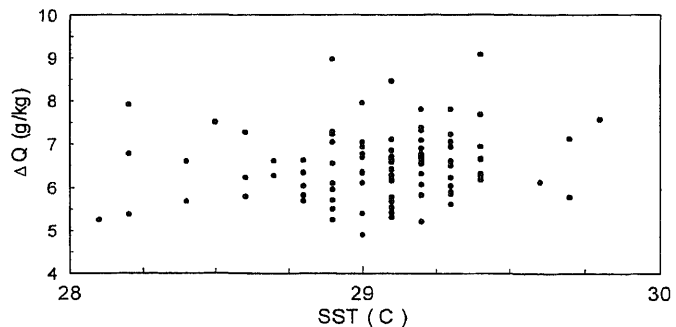


Figure 7. The variation of mixing ratio difference $\Delta Q$ ($Q_s$ (SST)-$Q_a$) with SST.

temperature around $28°C$ (this can be seen from the Clausius-Clapeyron relation). If the surface layer of the atmosphere is strongly coupled to the underlying ocean, we expect the amount of water vapor in the air to increase proportionately as SST increases. One measure of the water vapor in air is the *mixing ratio* defined as the amount of water vapor per unit mass of dry air, normally expressed as g/kg. The difference in the mixing ratios

$$\Delta Q = Q_s - Q_a,$$

where $Q_s$ is the saturation mixing ratio at SST and $Q_a$ is the mixing ratio of the surface air, is shown in figure 7. $\Delta Q$ varies in 5 to 9 g/kg range. There is no clearly discernible dependence of the mixing ratio difference on SST. In the bulk aerodynamic formulae for calculating the surface latent heat flux, $\Delta Q$ is taken as a function of SST. In the SST range encountered during the Pilot experiment, there is no clear evidence for such a dependence and a constant value around 6.5 g/kg describes the variation pretty well.

Moist static energy, usually denoted by $h$, is a measure of the total energy of the air (neglecting the kinetic energy which is a very small fraction of $h$ and is an important thermodynamic parameter in tropics, particularly in problems involving moist convection. Another thermodynamic parameter important in deep convection is the equivalent potential temperature $\theta_e$.
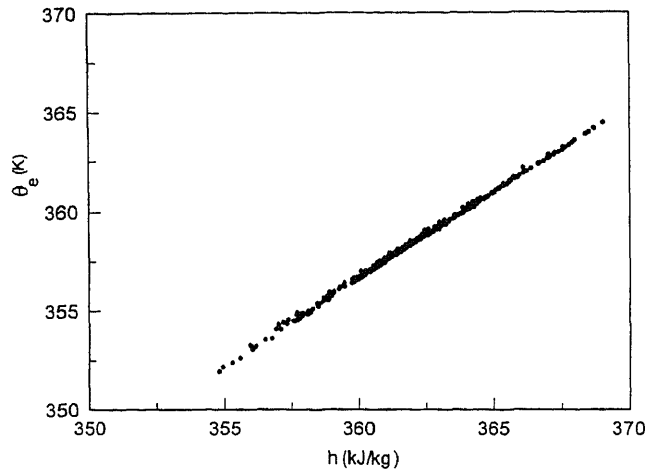
Figure 8. Scatter plot of equivalent potential temperature ($\theta_e$) versus moist static energy $h$.



Figure 9. Global hemispheric incoming radiation.

$\theta_e$ is the potential temperature attained by a parcel of moist air when it is lifted in the atmosphere pseudo-moist adiabatically, condensing all the moisture and then brought back to 1000 mb dry adiabatically. $\theta_e$ is a measure of the total entropy of the moist air. Now, $h$ is defined by

$$h = C_p T + gz + Lq,$$

where $C_p$ is the specific heat of air at constant pressure, $T$ is the air temperature, $L$ is the latent heat of evaporation, $q$ is the water vapor mixing ratio, $g$ is acceleration due to gravity and $z$ is the height above the sea level. Scatter plot of $\theta_e$ versus $h$ (both based on psychrometer data) is shown in figure 8. The moist static energy was more than 350 kJ/kg with a mean around 355 kJ/kg (during rains, the temperature and humidity were not systematically collected and $h$ could have been lower than 350 kJ/kg due to downdrafts). It is observed from figure 8 that $\theta_e$ and $h$ are very strongly (linearly) correlated. $\theta_e$ in the study area mainly varied between 352 K and 365 K. The corresponding range in the warm pool of the Pacific Ocean is 345 K to 362 K (Godfrey *et al* 1998). Thus, SST and surface energies in the Bay of Bengal were among the highest in the tropics during the Pilot experiment. It is said that $\theta_e$ values greater than 345 K are conducive for deep convection in tropics (Betts and Ridgway 1989), and that found in the south Bay of Bengal is larger than this critical value. Therefore, the southern Bay of Bengal provides the ideal breeding ground for the formation and intensification of tropical disturbances.

### 3.3 *Radiation*

Figure 9 shows the incoming global (hemispheric) solar radiation along with its daily mean, and the daily
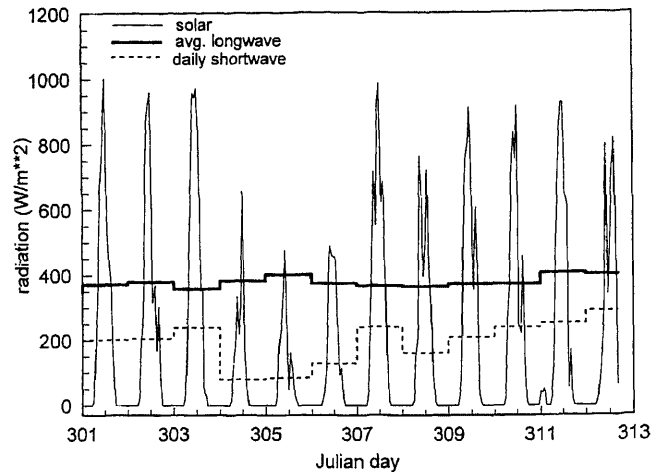
to 250 W/m$^2$. The minimum average value of 80 W/m$^2$ was observed on days 304 and 305 (convective days), and the maximum value of 250 W/m$^2$ on days 307 and 311. The average incoming shortwave radiation for the entire twelve day period is 188 W/m$^2$. The downward longwave radiation fluctuates in a narrower range of 350 to 400 W/m$^2$ with a mean around 375 W/m$^2$. Generally, the downward longwave radiation increased in the presence of deep clouds, reaching as high as 425 W/m$^2$ for short time duration when thick cumulonimbus clouds were overhead. The upward longwave radiation calculated from the SKINSST is between 445 and 450 W/m$^2$, virtually constant compared to the fluctuations in the incoming radiation. Thus, the net longwave radiation at the surface varied from 25 W/m$^2$ to 100 W/m$^2$ (positive upwards) with an average of 75 W/m$^2$.

### 3.4 *Mixed layer height*

The atmospheric mixed layer is that part of the atmosphere which continuously interacts with the underlying surface and its properties are strongly coupled to that of the surface below. The mixed layer height (MLH) is an important parameter because the effects of the surface are not directly felt above this layer unless convective clouds are present. MLH is inferred from the vertical profile of the virtual potential temperature $\theta_v$ defined by,

$$\theta_v = T(1000/p)^\gamma (1. + 0.608^* q),$$

where $T$ is the temperature (K), $p$ is pressure (mb) and $q$ is the water vapor mixing ratio (kg/kg) and $\gamma = 0.28$. A constant value of $\theta_v$ with height implies a neutrally stable atmosphere, whereas, increasing (decreasing) $\theta_v$ with height means that the atmosphere is stable (unstable) for dry adiabatic displacements. In figure 10, we show typical vertical profiles of $\theta_v$ taken
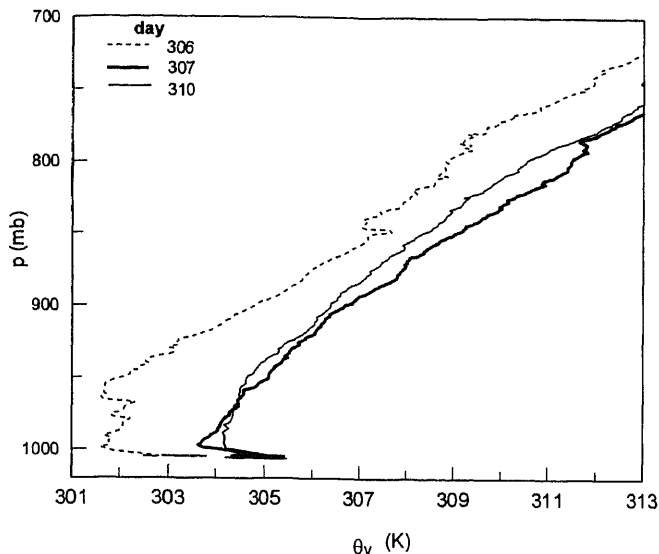
Figure 10. Vertical profiles of the virtual potential temperature $\theta_v$ for three afternoon (09 UTC) soundings.



Figure 11. Variation of the mixed layer and surface layer heights during BOBMEX-Pilot.

decreases with height. This is the convectively unstable super adiabatic layer (called the surface layer), and air parcel will accelerate if displaced vertically. Above the surface layer, the nature of the profiles differ. On day 306, the ship was at 10°N, 87°E and a large deep cloud band had passed over this area the previous day, the area was still cloudy and the average short wave radiation for the day was about 130 W/m$^2$ (figure 9). The atmospheric cooling caused by convection is clearly seen on day 306. On this day, $\theta_v$ decreased sharply immediately above the surface and then there is a region where it remained nearly constant (well mixed layer). This extended up to 950 mb and then $\theta_v$ started increasing almost monotonically with height. The profile of $\theta_v$ for the day 307 is distinctly different where it decreased initially, reached a minimum, and then started increasing. There is no well mixed layer. On day 310, $\theta_v$ was constant in a shallow layer of about 20 mb deep and then gradually started increasing, the slope of $\theta_v$ changed around 950 mb, however, there was no sudden jump/increase in $\theta_v$ (capping inversion) that marks the mixed layer top in tropics. There is no substantial variation in the nature of the profiles above 900 mb.

The height from the surface up to which the well mixed layer extends is taken as the mixed layer height here. The profiles during the Pilot experiment very rarely showed a layer where $\theta_v$ strictly remained constant and some amount of subjectivity is involved in determining the mixed layer height. The uncertainty is 50 meters at most. Figure 11 shows the variation of the mixed layer height during the Pilot experiment along with the height of the surface layer. It is observed from figure 11 that the height of the super adiabatic layer varied from about 20 meters to 100 meters, and that of the mixed layer from 50 meters to 900 meters with a mean between 400 m and 600 m.
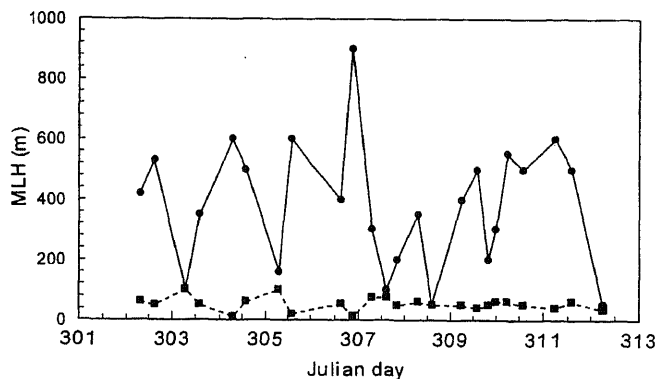
The height of the mixed layer over other tropical oceans is about 500 meters (LeMone 1978) and for the majority of the time, that observed during the Pilot experiment is in good agreement with this.

## 4. Discussion

As stated in the introduction, the frequency of occurrence of deep convective systems over the Bay of Bengal is among the highest in the world. A mean SST of 29°C and high values of $h$ and $\theta_e$, make the surface conditions very favorable for the occurrence of deep convection (Bhat *et al* 1996). High values of $h$ and $\theta_e$ are due to very warm SST. Thus, the basic issue is the physical mechanisms that maintain high SSTs in the Bay of Bengal. SST is the outcome of energy balance, where radiation, sensible and latent heat fluxes and advection are main contributors. Observations carried out during the Pilot experiment suggested that among other factors, the atmospheric and oceanic mixed layers can have an important role in controlling SST. Here we consider one specific case, namely, day 307. For the 12 day period under study, the solar radiation was the highest on this day (figure 9). SST increased by nearly a degree centigrade, air temperature increased by more than a degree centigrade (figure 5(a)) and relative humidity decreased below 80% during the forenoon. Wind speeds were moderate (less than a meter per second to about 4 m/s). A rough estimation of the surface heat fluxes indicated that the sensible heat flux was between 10 and 20 W/m$^2$, and the latent heat flux varied from 30 to 100 W/m$^2$. The observed MLH was less than 100 meters and therefore, the heat and moisture fluxes from the ocean were trapped in a shallow atmospheric layer near the surface. The corresponding afternoon CTD profile (data not shown here) showed the formation of a warm water layer of about 5 m deep due to intense short wave heating. Around noon time, winds were very low (figure 4(a)) and this helped in the formation of a thin, warm and stable

layer in the ocean. Thus, very shallow atmospheric and oceanic mixed layers together restricted the vertical diffusion of heat and led to rapid increases in the air temperature and SST. As the depth of the warm layer of water was small, SST rapidly decreased once the intensity of solar radiation decreased. This example shows that shallow mixed layers can be very effective in trapping the heat energy from shortwave radiation in shallow layers. Further studies are required to understand the precise role and contribution of the mixed layers in controlling the SST evolution.

A related question is, what caused the very shallow mixed layer on day 307. Except in regions of large scale low level convergence, subsidence prevails in the atmosphere and the subsidence tends to decrease the mixed layer depth by 300 to 400 meters per day (Betts and Ridgway 1989). The surface fluxes on the other hand tend to push the mixed layer upwards, and the actual height of the mixed layer is decided by the balance between these two opposing processes. On day 307, the surface fluxes were reasonably high (perhaps that could maintain a mixed layer height around 400 to 500 meters under normal conditions), still we see practically no mixed layer. Therefore, a very strong subsidence must have been prevailing to push down the mixed layer top to almost close to the surface. This subsidence might have been caused by a disturbance that had intensified near the Tamilnadu coast on day 307. Thus, while an intense convective system cools the ocean due to increased surface fluxes and reduced solar radiation directly under it, it can aid the enhancement of SST in the surrounding regions where subsidence induced by it prevails.

We have seen that there is no systematic dependence of $\Delta Q$ on SST (figure 7). Similarly, the sea air temperature difference $\Delta T$ also varies in a wide range (figure 5(b)). $\Delta Q$ or $\Delta T$ depend mainly on SST if some sort of quasi-equilibrium prevails between the ocean and the air in the mixed layer. Such quasi-equilibrium is possible provided the synoptic conditions persist for a sufficiently long time. We have seen that during the Pilot experiment, synoptic conditions changed and both convective and clear sky conditions were present. Following rain, the surface humidity decreased due to drier air being brought down to the surface by the convective downdrafts. Similarly, the air temperature decreased by as much as 4°C whereas SST remained almost unaffected. After the rains stopped, the surface air properties slowly recovered to the pre-rain conditions. Thus, for the same SST, a wide range of $\Delta Q$ and $\Delta T$ are encountered. A clearer picture might emerge if the data are stratified according to the prevailing synoptic conditions.

It is observed that the moist static energy $h$ and the equivalent potential temperature $\theta_e$ are linearly correlated with comparable magnitudes. However, a linear relationship between $h$ and $\theta_e$ is not obvious.

Though both are thermodynamic parameters, $h$ is the measure of total energy and $\theta_e$ is the measure of the total entropy of the air, and are calculated in different fashions. For example, in the calculation of $h$, surface sensible heat, latent heat and potential energy are added together. On the other hand, $\theta_e$ involved integrating the properties of an air parcel along a moist pseudoadiabat with the pressure varying from that corresponding to the surface value to less than 100 mb. Further studies are needed to understand $h$ and $\theta_e$ relationship over other oceans and also over the Bay of Bengal under different synoptic conditions.

## 5. Conclusion

The Pilot experiment for BOBMEX was very successfully conducted and useful data in the southern Bay of Bengal during a cyclone period have been collected. It is observed that the SSTs were high, surface air was warm and moist, and the surface air moist static energy was among the highest observed over the tropical oceans. The mean sea air temperature difference was about 1.25°C and the sea skin temperature was cooler than bucket SST by 0.5°C. The two commonly used thermodynamic parameters, namely the moist static energy and the equivalent potential temperature are linearly correlated. The atmospheric mixed layer was shallow, fluctuated in response to synoptic conditions and sometimes shallower than 100 meters. The mixed layer dynamics can play an important role in controlling SSTs in the Bay of Bengal.

# References

Betts A K and Ridgway W 1989 *J. Atmos Sci.* **46** 2621–2641

Bhat G S, Srinivasan J and Gadgil S 1996 *J. Meteor. Soc. Japan* **74** 155–166

Bradley E F, Coppin P A and Godfrey J S 1991 *J. Geophys. Res.* **96** 3375–3389

Godfrey J S, Houze R A Jr, Johnson R H, Lukas R, Redelsperger J -L, Sumi A and Weller R 1998 *J. Geophys. Res.* **103** 14395–14450

Kalsi S R 2000 *Proc. Indian Acad. Sci. (Earth Planet. Sci.),* (this issue)

LeMone M L, Wyngaard J C (ed.), *Proc. Workshop on the Planetary Boundary Layer*, 14–18 August, 1978 (American Meteorological Society) 182–234

Mohanty U C and Das S 1986 *Proc. Indian Natn. Sci. Acad.* **52** 625–640

Moshonkin S M and Harenduprakash L 1991 *Okeanologiya* **31(3)** 384–394

Murty V S N, Sarma Y V B and Rao D P 1996 *Proc. Ind. Acad. Sci. (Earth Planet. Sci.)* **105** 41–61

Premkumar K, Ravichandran M, Kalsi S R, Sengupta D and Gadgil S 2000 *Curr. Sci.* **78** 323–330

Rao R R, Basil Mathew and Hareeshkumar P V 1993 *Deep-Sea Res.* **40** 1647–1672

Saha K R and Saha S 1988 *Mon. Weather Rev.* **116** 242–255

Sanilkumar K V, Mohankumar N, Joseph M X and Rao R R 1994 *Deep-Sea Res.* **41(10)** 1569–1581

Sarma Y V B, Seetaramayya P, Murty V S N and Rao D P 1997 *Boundary Layer Met.* **82** 517–526

Slutz R J, Lubker S J, Hiscox J D, Woodruff S D, Jenne R L, Joseph D H, Steurer P M and Elms J D 1985 *COADS: Comprehensive Ocean Atmosphere Data Set.* Release 1, 262 pp.

Sikka D R and Sanjeeva Rao P 2000 *Proc. Indian Acad. Sci. (Earth Planet. Sci.)* (this issue).

# Inertial-Dissipation flux measurements over south Bay of Bengal during BOBMEX-Pilot experiment

M Venkataramana[1], K Sengupta[1], G S Bhat[2], S Ameenulla[2] and J V S Raju[2]

[1] Space Physics Laboratory, Vikram Sarabhai Space Centre, Trivandrum 695 022, India

[2] Centre for Atmospheric and Oceanic Sciences, Indian Institute of Science, Bangalore 560 012, India

This paper describes measurement of air-sea parameters and estimation of sensible and latent heat fluxes by the "Inertial-Dissipation" technique over south Bay of Bengal. The data were collected on ORV Sagar Kanya during BOBMEX-Pilot cruise during the period 23rd October 1998 to 12th November 1998 over south Bay of Bengal. The fluxes are estimated using the data collected through fast response sensors namely Gill anemometer, Sonic anemometer and IR Hygrometer. In this paper the analyses carried out for two days, one relatively cloud free day on November 3rd and the other cloudy with rain on November 1st, are presented. Sea surface and air temperatures are higher on November 3rd than on November 1st. Sensible heat flux for both the days does not show any significant variation over the period of estimation, whereas latent heat flux is more for November 3rd than November 1st. An attempt is made to explain the variation of latent heat flux with a parameter called thermal stability on the vapor transfer from the water surface, which depends on wind speed and air to sea surface temperature difference.

## 1. Introduction

The turbulent heat fluxes (sensible and latent) are important components of the total heat budget at the air-sea interface. The momentum flux (surface stress) is the major driver of ocean turbulence and surface currents. The surface sensible and latent heat fluxes represent interfacial inputs of heat and moisture into the boundary layer that influence convection, the formation of clouds and precipitation. There are four standard techniques for calculating these fluxes from atmospheric measurements:

- covariance (eddy correlation),
- inertial subrange dissipation and direct dissipation,
- profiles
- bulk aerodynamical methods.

By definition the fluxes are the ensemble Reynolds averages of the instantaneous vertical air velocity component with horizontal velocity, enthalpy and water vapour density to give the stress, sensible heat flux and latent heat flux respectively. The covariance method is a direct computation from the data and yields a flux which is considered an unbiased estimate of the intrinsic flux at the height of the measurement, but subject to sampling uncertainty i.e., it requires measurements of the vertical and downwind component of air velocity, temperature and humidity over a sufficiently long averaging period and with sufficient frequency response (Wyngaard 1973). The covariance method is used extensively over land, but straightforward application over the ocean is limited to fixed towers. If one wishes to apply this method on a moving platform (ship or aircraft), then the orientation and motion of the platform must be accounted for before computing the correlations. Furthermore, distortion of the flow by the ship superstructure may invalidate the results. The profile method requires precise measurements of the vertical gradient of the mean meteorological variables, which has proven to be a very difficult task from a ship (Blanc 1983). The bulk method requires only mean meteorological information and is the obvious choice for climatological studies and numerical models. The bulk

aerodynamic method (drag coefficients) has and will continue to have a special place in flux estimation method, simply because of its extensive use in numerical models and its applicability to historical data sets from weather ships, buoys and ships of opportunity. For bulk meteorological data of reasonable quality the major source of uncertainty in the long-term mean estimates of stress, sensible heat and latent heat is probably due to uncertainties in the air-sea transfer coefficients. The dissipation method, which relies on measurements at high frequencies is unaffected by ship motion. This method is a good compromise, being insensitive to platform motion (unlike covariance method) and relatively insensitive to platform distortion of the airflow (unlike the covariance and profile methods). The dissipation methods (high frequency turbulence), is more direct than the bulk method simply because it is true turbulence statistics. The dissipation method is also advantageous if the sensors are not situated close enough to each other to correctly measure cross-correlations. Studies using the dissipation methods over the ocean (Pond *et al* 1971, Scharcter *et al* 1981) and over land (Champagne *et al* 1977, Mestayer *et al* 1980) have yielded good results.

### 1.1 *Scope of this paper*

This paper describes the air-sea fluxes using the inertial-dissipation method during BOBMEX-Pilot experiment. The paper is divided into five sections. The instrumentation and data acquisition are described in section 2. In section 3, the theory, methodology and corresponding formula of turbulent flux measurements using Inertial-Dissipation method are described. Weather conditions and results are discussed in section 4. Our conclusions are given in section 5.

## 2. Instrumentation and data acquisition

The pilot experiment was carried out on board ORV Sagar Kanya. The ship left Mormugao on 23rd October 1998 and reached the first stationary time series station located at 7°N 87°E on October 30th where it halted for two days. The second time series station was at 10°N 87°E for two days (2nd–3rd November), and the last time series station for a day was located at 13°N 87°E on November 5th. The ship started sailing back on November 6th and reached Tuticorin on November 12th, 1998. The instrumentation system on board ORV Sagar Kanya Cruise #138C for the estimation of air-sea fluxes consisted of sonic anemometer for measuring the 3-dimensional wind vector and the virtual temperature, IR-hygrometer for the specific humidity, accelerometers for the

determination of the ship motion, Gill $u, v, w$ sensors for measuring triaxial wind vector. The above sensors were having a frequency response of 10 Hz or more. For mean parameters there were slow response sensors (frequency response less than 1 Hz) which included Humicap for measuring relative humidity, platinum resistance thermometer for air temperature, pyranometers for measuring short wave and long wave radiation and rain gauge for measuring the rainfall were used. Specifications of the instruments used and the schematic of the sensors deployed at different levels over the boom are explained in Bhat *et al* (this issue). A pentium PC working on Windows-95 was used for acquiring and storing the data. Data acquisition and archival were controlled by DASYLab software. Apart from acquiring the date, DASYLab was programmed to display all the parameters on the screen in real time for visual monitoring. The signals from the sensors were sampled at 10 Hz. The data from the fast sensors were stored at 10 Hz rate, for a one-hour period every three hours. In addition, data from all the sensors were averaged for 10 seconds and continuously stored.

During the campaign, high-resolution radiosondes manufactured by M/s. Atmospheric Instrumentation Research (AIR) Inc., USA were launched using 300-g balloons. These provided the vertical profiles of temperature and humidity fields of the atmosphere as a function of pressure at 5-second interval. The temperature, humidity and pressure data transmitted by the radiosonde were received through antenna, and the RS232 output from the receiver was sent to a note-book PC for data display and archival. GPS data were also collected by installing a GPS system on board Sagar Kanya.

There were also independent surface meteorological measurements from the ship including ship position (latitude, longitude and heading with respect to north) barometric pressure, dry bulb and wet bulb temperatures, and sea surface temperatures every three hours manually. The sea surface skin temperature was measured by an infrared thermometer. The infrared thermometer was not used during rains.

## 3. Flux determination by the inertial-dissipation method

There are many different scales of motion in meteorology. They extend from the trade winds that exist over the equatorial oceans to the Kolmogorov inertial subrange, and molecular viscosity. Since spectral analysis of meteorological variables is essentially a statistical method of describing fluctuations, it enables us to study the various aspects of boundary layer structure like the predominant scales of motion, the nature of energy containing eddies, the nature of cascading in the inertial-subrange, the intermittent outbreak of

modifications by plume and wave activity and the estimation of the size of eddies that carry maximum energy (Winston *et al* 1993).

The dissipation technique is based on Kolmogorov's theoretical prediction of universality in the inertial subrange. Spectra are measured in the inertial regime, related to the turbulent kinetic energy (TKE) dissipation rate via Kolmogorov's equation. The main attraction of dissipation methods is their use of Monin-Obukhov similarity forms for the high-frequency portion of the spectrum, where platform motions are negligible in relation to turbulence signals. There is a distinction between "direct" measurements of dissipation rates by integrating over the spectrum of the derivative versus the "inertial-dissipation" method, using a fit to the Kolmogorov $f^{-5/3}$ power law in the inertial subrange to determine the appropriate structure function parameter (Fairall *et al* 1990). "Direct" dissipation methods are rarely made over the ocean because fast response sensors that can measure temperature and humidity fluctuations of the order of 5 kHz are difficult to maintain in the marine environment. Henceforth we refer to the "inertial-dissipation" method, which requires frequency response only up to the order of 5–50 Hz. It is based on the assumption that turbulent fluxes of momentum, sensible heat and water vapour are linked to the spectra of velocity $(S_u(f))$, temperature $(S_t(f))$ and absolute humidity $(S_q(f))$ variances through the dissipation of turbulent kinetic energy, temperature and humidity variances (Fairall and Larsen 1986). The spectra of wind, temperature and absolute humidity follow a power law $[S_u(f), S_t(f)$ and $S_q(f) \propto f^{-5/3}]$ over an inertial subrange of frequencies. Fluxes can be estimated from measurements of spectra within this subrange, which is typically found to apply at normalized frequencies $f_n = fz/u \geq 1$ (Phelps and Pond 1971).

The surface latent heat fluxes can be calculated from the expressions of the form (Smith 1989)

$$\langle wq \rangle_{\text{Diss}} = S_E [2\pi kz/U]^{2/3} f^{5/3}$$
$$\times [S_u(f) \cdot S_q(f)/(k' \cdot \beta_q)]^{1/2}. \quad (1)$$

Where $S_E$ is stability dependence coefficient and is given by

$$S_E = [\Phi_q(Z/L)]^{-1/2} [\Phi_m(Z/L) - Z/L]^{-1/6}. \quad (2)$$

Where the one-dimensional Kolmogorov constants are $k' = 0.55$ for velocity and $\beta'_q = 0.80$ for humidity (Paquin and Pond 1971). $U$ is mean wind, $z$ is the height of observations and $k$ is Von Karman constant.

Review of the flux-profile relationships (Dyer 1974, Yaglom 1977) indicates the reasonable forms as If $0 < Z/L < 0.2$

$$\Phi_m(Z/L) = 1 + 7Z/L$$
$$\Phi_t(Z/L) = \Phi_q(Z/L) = 1 + 7Z/L \quad (3)$$

$$\Phi_m(Z/L) = (1 - 16Z/L)^{-1/4}$$
$$\Phi_t(Z/L) = \Phi_q(Z/L) = (1 - 16Z/L)^{-1/2}. \quad (4)$$

Where $L$ is the Monin–Obukhov length with both humidity and temperature effects included and $Z/L$ is given by (Deardroff 1968)

$$\frac{Z}{L} = \frac{-100z}{(Uz)^2 T_0}$$
$$\times [\Delta\theta + 1.7 \times 10^{-6} T_0^2 \Delta q] \Delta\theta > 0 \text{ unstable} \quad (5)$$
$$= \frac{70z}{(Uz)^2 T_0} [\Delta\theta + 2.5 \times 10^{-6} T_0^2 \Delta q] \Delta\theta < 0 \text{ stable}.$$

Where $T_0$ is mean temperature of the layer, $\Delta\theta$ is difference between sea surface temperature and air temperature at 10 m and $\Delta q$ is difference between absolute humidity at the sea surface and 10 m level.

The advantage of the inertial-dissipation method over the eddy correlation method is that the vertical component of the wind is not required, and so constraints on the rigidity and flow-distortion of the supporting structure can be relaxed. Sensible heat flux $\langle wt \rangle_{\text{Diss}}$ calculation is analogues to that of $\langle wq \rangle_{\text{Diss}}$.

## 4. Results

First, let us consider the synoptic conditions during the BOBMEX-Pilot period. Kalsi (1999) reported that the conditions prevailing during the pilot experiment were typical of the cyclone period in this part of the globe. He reported that a weak disturbance on 26th October 1998 was seen to migrate from the Gulf of Thailand westwards across the Andamans into the central part of the Bay of Bengal and became unimportant on 31st October. INSAT-ID satellite visible imagery showed that new cloud bands formed between 65°E and 90°E around 3°N on October 31st, moved northward and passed over ORV Sagar Kanya on November 1st. The system intensified into a tropical storm as it approached Tamilnadu coast on November 3rd, and the entire south of India experienced heavy rains for the next couple of days. As observed from the ship during the period between October 30th – November 2nd the sky was mostly covered with cumulus clouds. As preliminary analyses we have chosen two typical days, one relatively cloud free day (November 3rd) and the other being cloudy with rain or continuous drizzle (November 1st).

The daily mean surface pressure decreased from around 1009 mb on October 28th to around 1006 mb on November 5th and then gradually increased. On November 1st thick deep clouds were seen from the ship and 20 mm rain was recorded on board the ship. It was observed that wind speed varied from less than a meter per second to more than 10 ms$^{-1}$. Winds were
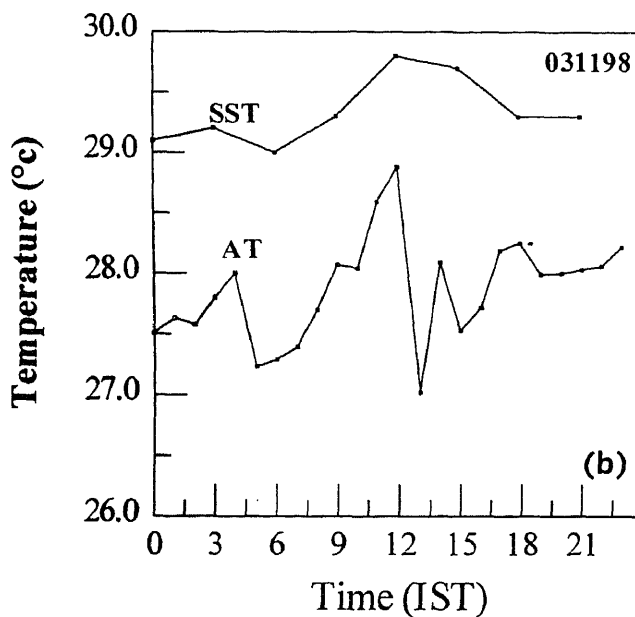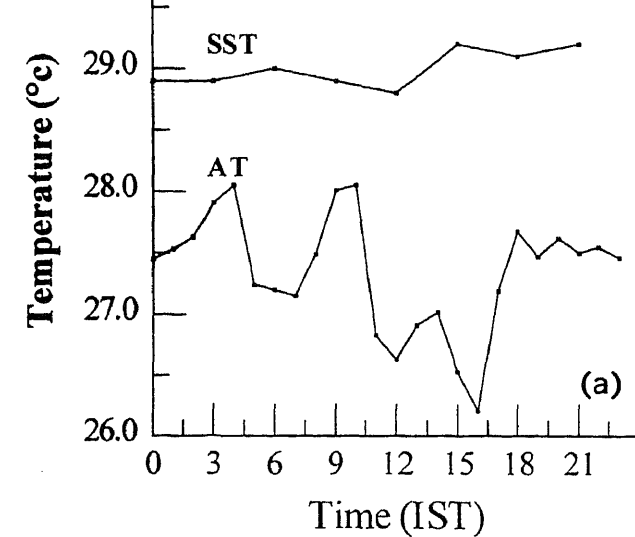
Figure 1. Three hourly values of sea surface temperature (SST) and hourly values of air temperature (AT) at 11 m above the sea surface for (a) November 1st 1998 and (b) November 3rd 1998.

mostly westerlies and south westerlies till November 4th and then became north easterlies. On some occasions, wind speeds larger than $13\,ms^{-1}$ have been observed for short time durations associated with systems. Sea surface temperature was warmer than 28°C with an average near 29°C; and maximum sea surface temperature 29.8°C was observed on November 3rd. The relative humidity was 80% and for most of the time with an average around 83% i.e., the air was very rich in moisture.

air temperature (AT) at 11 m above the sea surface for November 1st and 3rd respectively. For both the days SST was higher than AT indicating unstable condition, in general. SST on November 3rd show more diurnal variation than November 1st, as the la was generally cloudy. On an average the difference between SST and AT was more on November 3rd than on the 1st. As November 1st was associated with
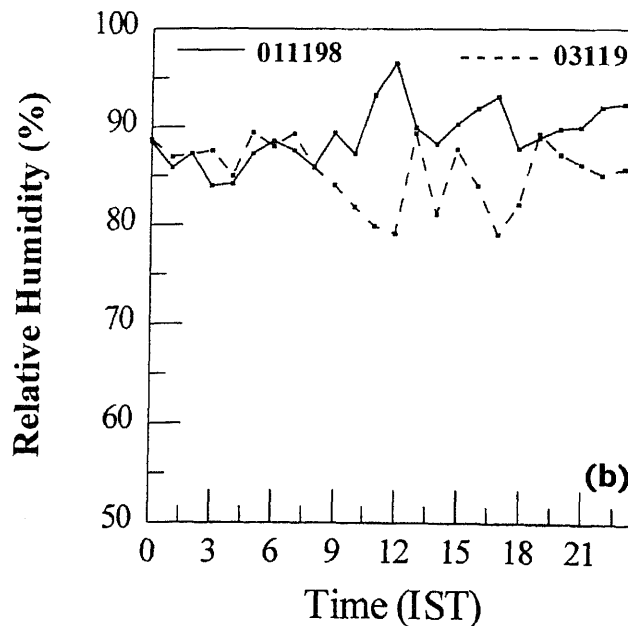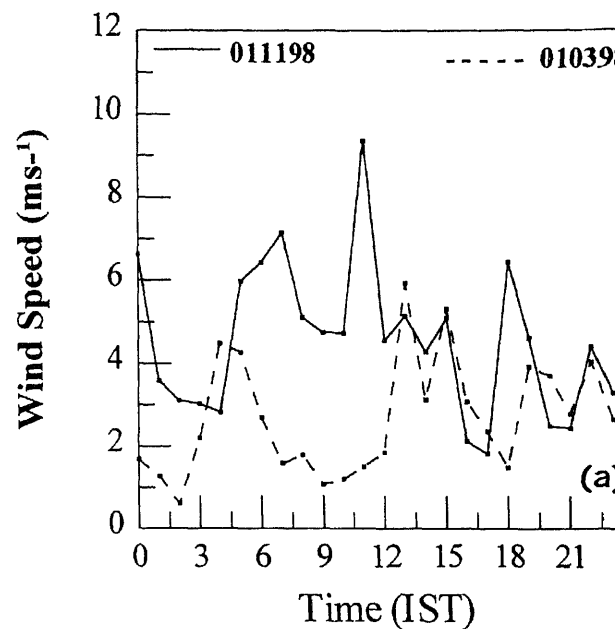


Figure 2. (a) Corrected horizontal wind speed measured b the sonic anemometer. (b) Relative humidity. Data shown a hourly averages.

the system, we observed higher wind speeds on the 1st than on the 3rd as shown in figure 2(a). Figure 2(b) shows hourly values of relative humidity (RH) for November 1st (continuous line) and November 3rd (dashed line) at 11 m height above the sea surface. It shows the gradient of RH between the sea surface and 11 m was more on November 3rd than on the 1st. Figure 3(a) shows incoming solar radiation measured by the pyranometer on November 1st and 3rd. It is seen from figure 3(a) that deep clouds drastically reduced the solar insolation reaching the surface on

November 1st except for some time between 9 am and 10 am. On November 3rd, the morning was sunny and the peak short wave radiation reached $984 \, W.m^{-2}$ around noon. The hemispheric incoming longwave radiation (ILR) measured by the upward facing infrared pyranometer is shown in figure 3(b). Comparison of IR pyranometer data of November 1st and 3rd shows that ILR flux is enhanced by $25$–$60 \, W.m^{-2}$ in the presence of deep clouds, indeed, 20 mm of precipitation was observed on the 1st.

For the computation of sensible heat flux (SHF) and latent heat flux (LHF), one hour data length with 1 Hz sampling rate, amounting to 3600 data points have been subject to a mixed radix Fast Fourier Transform and the spectrum is then smoothed by averaging the spectral information over frequency bands of increasing width. Figures 4 and 5 show sample power spectra of u-component of wind, absolute humidity ($q$) and sonic temperature ($T_s$) obtained for November 1st and 3rd respectively, during 1500 hrs, measured at a height of 11 m above the sea surface. The spectra showed the typical dropoff of energy with increasing frequency that is normally found for meteorological parameters over the frequency band examined. The general characteristic of the unstable spectrum with a '$-5/3$' slope in the inertial-subrange is evident in all the spectra. In figure 5 the power spectral density is high due to high turbulence activity for the convective atmospheric boundary layer on November 3rd. Figure 4 shows the existence of the spectral gap (as marked in the figure) in the gravity wave frequency range of power spectra for November 1st. The classical study of Van Der Hovan (1957) extends over at least seven decades on the frequency scale and represents a variety of flow regimes, governed by widely different mechanisms. The two spectral peaks in Van Der Hovan's spectrum represent the two dominating types of flow: the quasi horizontal motion with their center of gravity in the range $10^{-6}$–$10^{-5}$ Hz, and the genuine turbulence, the maximal energy of which is located roughly at $10^{-2}$ Hz if the measurements are taken at standard anemometer level. In the intermediate spectral region several special "mesoscale" types of flow are known to exist, such as deep convection, large roll vortices, and local circulations (land and sea breeze). As pointed out by Hess and Clarke (1973) the existence of a gap depends on both the strength of the microscale turbulence and the spectral shape in the synoptic-mesoscale region. Kolesnikova and Monin (1965) also try to relate the value of the gap to synoptic situations, but they can only draw the conclusion that these spectral divisions vary with weather conditions. The small peaks in figures 4 and 5 at the frequency of around 0.1–0.2 Hz in the $u$ spectrum are due to contamination by the ship motion (Fujitani 1985). The scalar variables are much less affected.
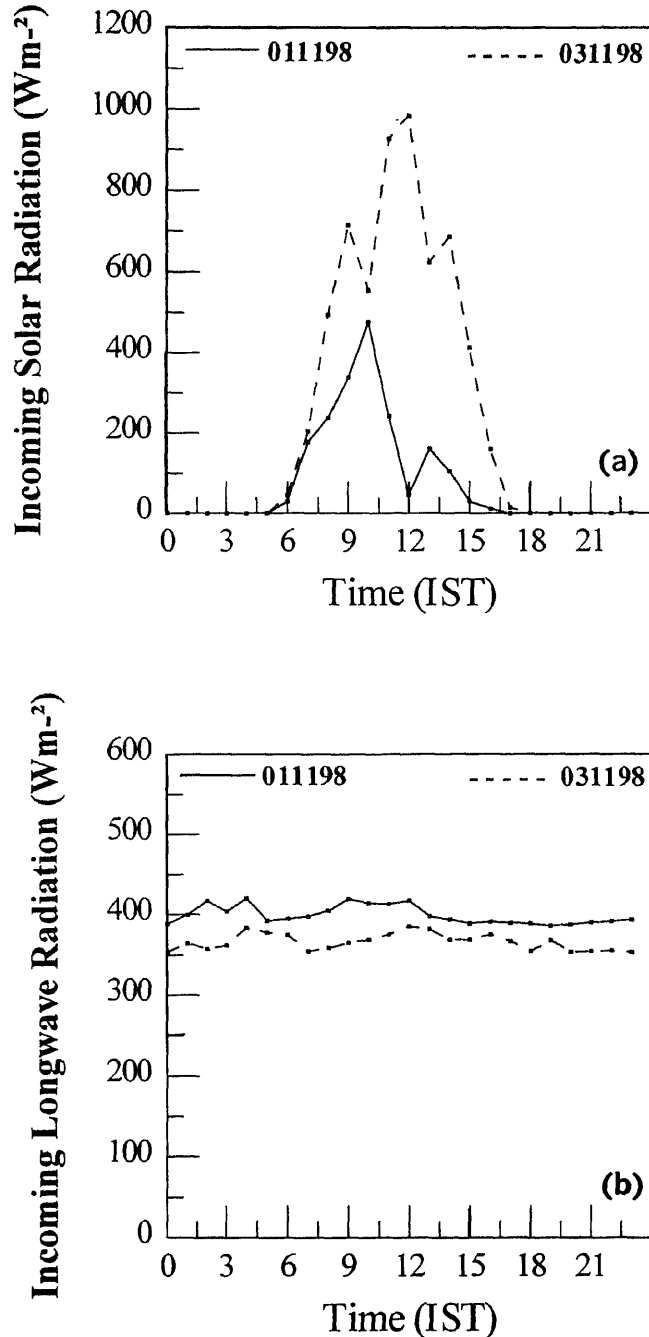


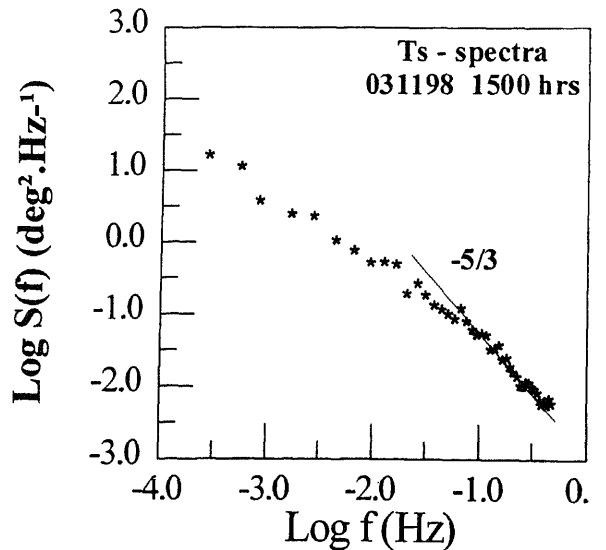Figure 3. Incoming solar radiation (a) and incoming longwave radiation (b) for November 1st and November 3rd, 1998.
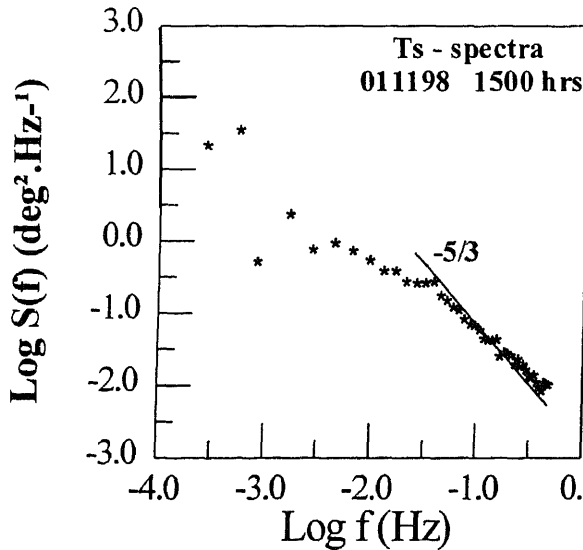
Figure 4. Power spectra of u-component of wind, absolute humidity (q) and sonic temperature (Tₛ) with frequency for November 1st, 1998 during 1500 hrs. The thick line with −5/3 slope indicates inertial sub-range.

Figure 5. Power spectra of u-component of wind, absolute humidity (q) and sonic temperature (Tₛ) with frequency for November 3rd, 1998 during 1500 hrs. The thick line with −5/3 slope indicates inertial sub-range.

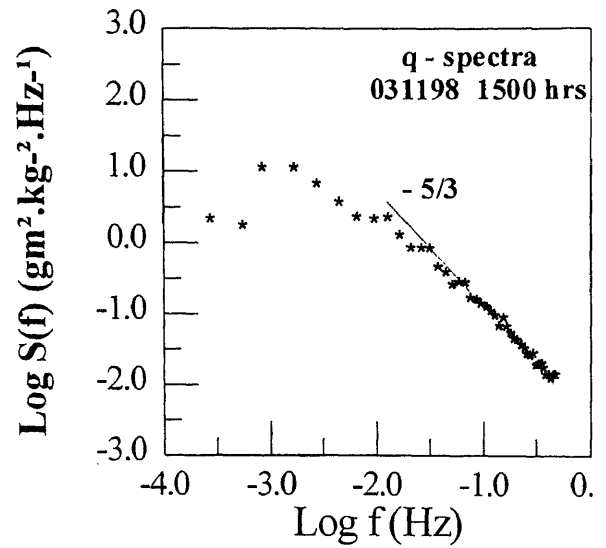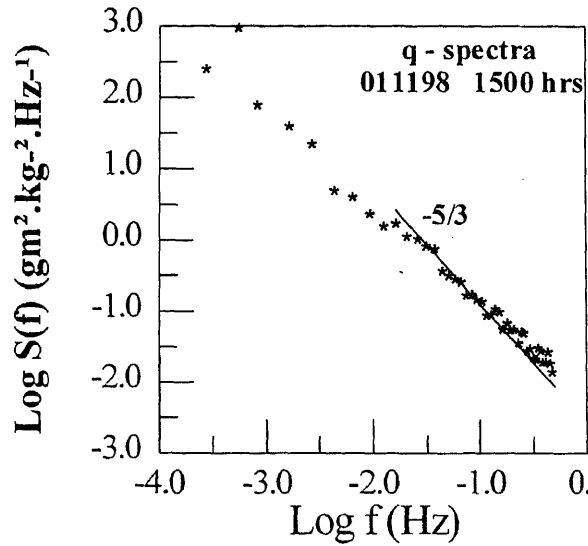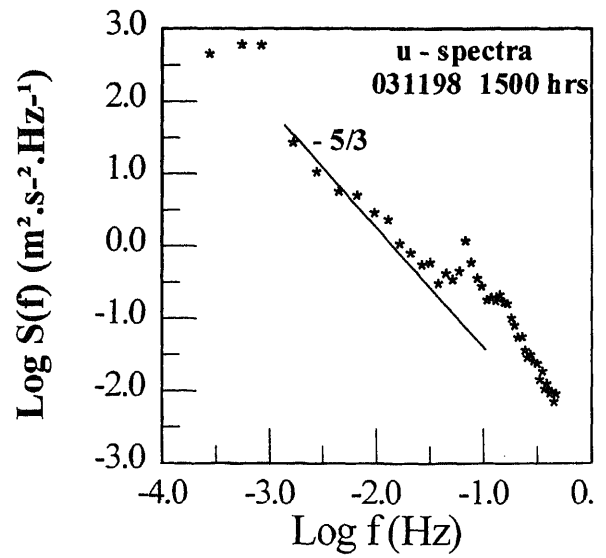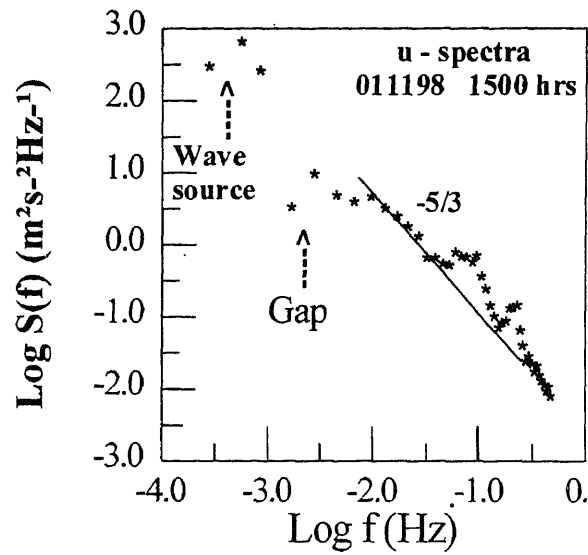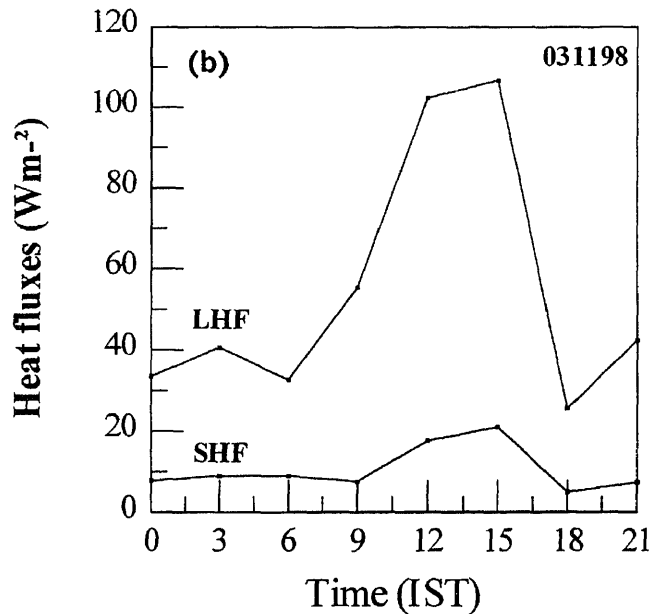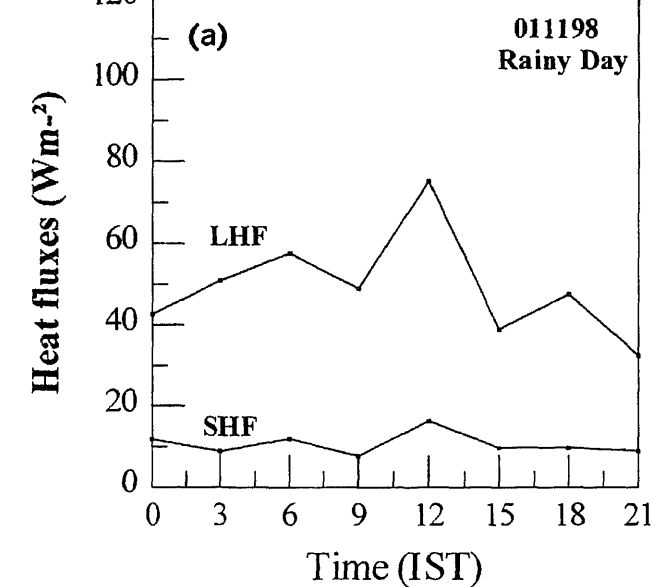Figure 6. Turbulent fluxes of latent heat (LHF) and sensible heat (SHF) estimated using Inertial-Dissipation method for (a) November 1st, 1998 and (b) November 3rd, 1998.

Fluxes are estimated using the inertial dissipation method as described in section 3. The spectral power of velocity $(S_u(f))$, absolute humidity $(S_q(f))$ and temperature $(S_t(f))$ were obtained at non-dimensional frequency $f$; satisfying the condition $fz/U \geq 1$. To obtain the spectral power at $f$ satisfying the condition $fz/U \geq 1$ often the spectral slope of $-5/3$ in the inertial-subrange has been extended and interpolated values of spectral power densities have been taken and used in equation (1). Hence, contamination of spectra,

estimation by this method. Fluxes thus obtained are shown in figures 6(a) and 6(b) for the two days. The SHF is a very small part of the total heat flux and does not seem to vary much for both the days November 1st and 3rd. LHF is more for November 3rd than for the 1st because of more of RH gradient being observed on the 3rd. To examine the variation of LHF, we considered the effect of the thermal stability on the vapor transfer from the water surface. Assouline and Mahrer (1993) concluded that temperature and wind speed are two main factors affecting LHF from the open water surface.

The combined effect of the temperature and wind speed can be examined in terms of stability parameter, $S_R$ (analogous to the Richardson number)

$$S_R = (g/T)(\text{AT} - \text{SST})(z/U^2)$$

where $g$ is acceleration due to gravity, AT is the air temperature at a height $(z)$ of $11\,\text{m}$, SST is the sea surface temperature, $T$ (in K) is the mean temperature of the layer $(T = (\text{AT} + \text{SST})/2)$, and $U$ is the wind speed at a height of $11\,\text{m}$. The diurnal variations of stability parameter $(S_R)$ for the two days are shown in figure 7. A sharp decrease in the magnitude of LHF between 1500 and 1800 hrs is related to value of $S_R$ $(-0.02)$ close to neutral, as shown in figure 7. Bowen's ratio was found to vary from 0.1 to 0.2, which is typical over tropical oceans. Figure 8 shows the RH profiles on October 25th (over the Arabian Sea) and on November 1st and 3rd (over Bay of Bengal). Profiles over the Bay of Bengal showed constant RH up to 500 mb whereas the profile over the Arabian Sea showed a marked decrease in RH above the boundary layer. The general decrease in RH above the mixed
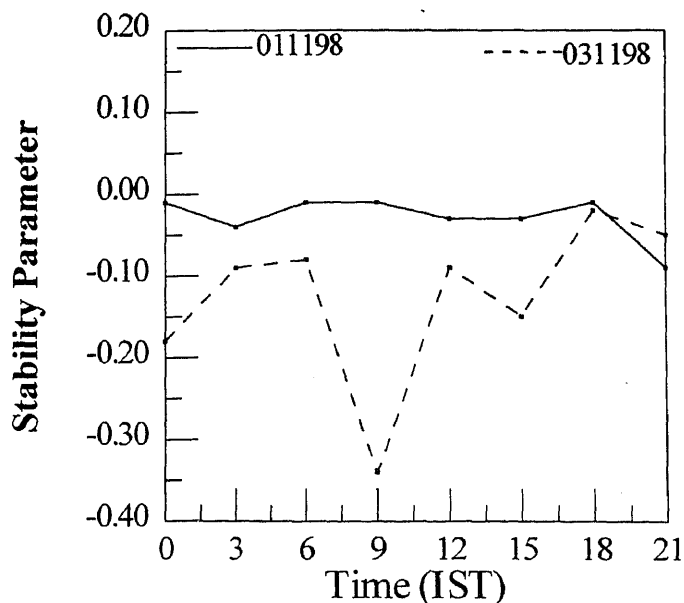


Figure 7. Stability parameter $(S_R)$ measured for (a) November 1st, 1998 and (b) November 3rd, 1998.
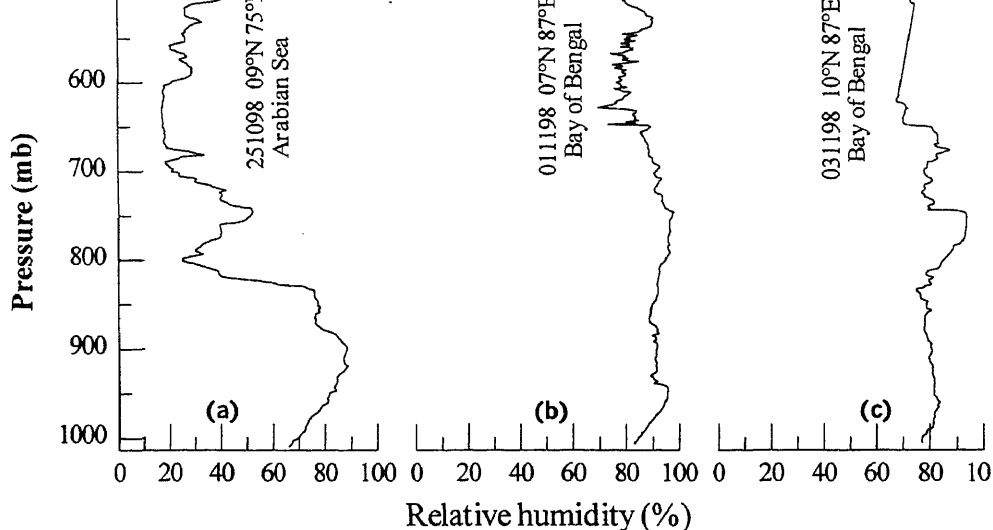
Figure 8. Relative humidity as function of the pressure height for **(a)** October 25th, 1998 over the Arabian Sea and **(b)** November 1st, 1998 **(c)** November 3rd, 1998 over the Bay of Bengal during 1400 hrs.

layer inversion is absent in the profile over the Bay of Bengal, which could be due to the presence of high level clouds and cumulonimbus clouds over the Bay of Bengal. However, in a companion paper, Bhat *et al* (in this issue) present an overview of the variation of the mixed layer height over the Bay of Bengal. They found that the height of the mixed layer varied from 500 m to 900 m with a mean between 400 and 600 m.

## 5. Conclusions

A sea going system capable of complete surface flux and sophisticated boundary layer profile measurement has been demonstrated through this BOBMEX-Pilot trail cruise. Comprehensive, synergistic and high-quality data over the Bay of Bengal have never been available before and are potentially quite useful for analysts and modellers. This field program achieved a high level of success.

Mesoscale atmospheric activity over the ocean appeared to exist during a particular period during the pilot experiment of the Bay of Bengal monsoon experiment in 1998. The existence of a spectral gap is important in the discussion of atmospheric motions because these motions can usually be divided into two categories, synoptic and micro-scale, by the spectral gap. Therefore, in general numerical models, the grid size is chosen in the dimension corresponding to the scale of the spectral gap to filter out turbulent noise. However, if there exist significant mesoscale atmospheric motions, large errors in numerical prediction over a long period will be induced from aliasing.

It has been demonstrated that the turbulent heat fluxes, like SHF and LHF can be estimated, by the inertial-dissipation technique, which relies on measure-

ments at high frequencies unaffected by ship motion. The most attractive feature of the inertial-dissipation technique is that it avoids an explicit measurement of the vertical velocity.

## References

Assouline S and Mahrer Y 1993 Evaporation from Lake Kinneret', Eddy correlation system measurements and energy budget estimates; *Water Resour. Res.* **29** 901–910

Bhat G S, Ameenulla S, Venkataramana M and Sengupta K 2000 Atmospheric boundary layer characteristics during BOBMEX-Pilot experiment (in this issue)

Blanc T V 1983 An error analyses of profile, flux, stability and roughness length measurements made in the marine atmospheric surface layer; *Boundary-Layer Meteorol.*, **26** 234–267

Champagne F H, Friehe C A, La Rue J C and Wyngaard J C 1977 Flux estimation techniques and fine-scale turbulence

measurements in the unstable surface layer over land; *J. Atmos. Sci.* **34** 515–530

Deardroff J W 1968 Dependence of air-sea transfer coefficients on bulk stability; *J. Geophys. Res.* **73** 2549–2557

Dyer, A J 1974 A review of flux-profile relationships; *Boundary-Layer Meteorol.* **7** 363–372

Fairall C W, Edson J B, Larsen S E and Mestayer P G 1990 Inertial-Dissipation air-sea flux measurements: A prototype system using real-time spectral computations; *J. Atmos. Oceanic Technol.* **7** 425–453

Fujitani T 1985 Method of turbulent flux measurement on a ship by using a stable platform system; *J. Meteorol. Soc. Japan.* **63** 157–170

Hess G D and Clarke R H 1973 Time spectra and Cross-spectra of kinetic energy in the planetary boundary layer; *Q. J. R. Meteorol. Soc.* **99** 130–153

Kalsi S R 1999 Synoptic weather conditions during the pilot study of Bay of Bengal and Monsoon Experiment (BOB-MEX), *Workshop on BOBMEX-Pilot Study Results,* held at I.I.T. Delhi, pp 1–2

Kolesnikova V N and Monin A S 1965 Spectra of meteorological field fluctuations; *Izv. Atmos. Oceanic Phys.* **1** 377–386

Mestayer P G, Pages J P, Coantic M and Saissac J 1980 *Joint Symposium Heat and Mass Transfer and the Structure of Turbulence,* Z. Zaric (ed.) (Washington, DC: Hemisphere publ)

Paquin J E and Pond S 1971 The determination of the Kolomogroff constants for velocity, temperature and mois-ture from second and third order structure functions; *J. Fluid Mech.* **50**, part 2, 257–269

Phelps G T and Pond S 1971 Spectra of the temperature and humidity fluctuations and of the fluxes of moisture and sensible heat in the marine boundary layer; *J. Atmos. Sci.,* **28** 918–928

Pond S, Phelps G T, Paquin J E, McBean G A and Stewart R W 1971 Measurements of turbulent fluxes of momentum, moisture and sensible heat over the ocean; *J. Atmos. Sci.* **28** 901–917

Scharcter G E, Davidson K L, Houlihen T and Fairall C W 1981 Measurement of the rate of the dissipation of turbulent kinetic energy, $\varepsilon$ over the ocean; *Boundary-Layer Meteorol.* **20** 321–330

Smith S D 1989 Water vapor flux at the sea surface; *Boundary-Layer Meteorol.* **47** 277–293

Van Der Hovan 1957 Power spectrum of horizontal wind speed in the frequency range from 0.0007 to 900 cycles per hour; *J. Meteorol.* **14** 160–164

Winston J P, Radhika R, Nair K N, Sengupta K and Kunhikrishnan P K 1993 On the spectral behaviour of atmospheric boundary-layer parameters at Thumba, India *Q. J. Meteorol. Soc.* **119** 187–197

Wyngaard J C 1973 On surface-layer turbulence, in *Workshop on micrometeorology,* (ed) D. Haugen (American Meteorological Society: Science press) pp 101–149

Yaglom A M 1977 Comments on wind and temperature flux profile relationships; *Boundary-Layer Meteorol.* **11** 89–102

# BOBMEX-98 Pilot: Measurement and analysis of incoming shortwave radiation data

K GOPALA REDDY and P SREE RAM

*Department of Meteorology and Oceanography, Andhra University, Visakhapatnam 530 003, India*

Empirical formulae for estimation of hourly incoming shortwave radiation over the Indian Ocean under different cloud amounts have been developed by using the pyranometer measurements of the incoming solar radiation and the cloud observations during BOBMEX Pilot (October – November 1998) cruise.

## 1. Introduction

Incoming shortwave radiation at the ocean surface is one of the major components affecting land and ocean surface heating. It plays a vital role in understanding the ocean–atmosphere interactions. Although the incoming shortwave radiation is a very important component in oceanic studies, it is seldom measured over the oceans. This has resulted primarily from the difficulty of making radiation measurements at the ocean surface. Until very recently our only knowledge of the incoming shortwave radiation in large oceanic regions came from sparse cloud observations used in empirical formulae. After the advent of satellite technology, the incoming shortwave radiation at the ocean surface has been estimated using satellite measurements. However, the development of satellite techniques for estimating the incoming shortwave radiation will depend crucially on the capability of calibrating the satellite estimates with *in situ* measurements in the region of study (Gautier 1986, 1988).

Empirical formulae for estimating the incoming shortwave radiation are developed in terms of the atmospheric transmission factor, defined as the ratio of the incoming shortwave radiation at the sea surface to the radiation incident on a horizontal surface at the top of the atmosphere. The most commonly used empirical formulae for estimating the incoming short-wave radiation over the Indian Ocean are those developed by Wyrtki (1971); Seckel and Beaudry (1973); Budyko (1974); Reed (1977); Simpson and Paulson (1979); Atwater and Ball (1981) and

Mohanty and Mohan Kumar (1998). Most of these widely used formulae were developed using the data over the Atlantic and Pacific Oceans in the extra tropics. A problem with such empirical coefficients is that they may not be suitable for other climatic regimes and latitudes. Their validity and accuracy remain undemonstrated for the tropics in general, and for the Indian Ocean in particular.

Even though there have been numerous formulae, significant disagreement exists currently between the standard measurements and estimates from the formulae even for clear sky conditions (Reed 1977; Simpson and Paulson 1979; Dobson et al 1982). For example, Reed (1977) found that his measurements of clear-sky insolation differed by an average of −10% with that of the 'Berliand' formulae used by Budyko (1974). The use of a single cloudiness (without cloud type) parameter is not sufficient in general, since, low, middle and high clouds have very different effects on radiation. However, no systematic validations are available between empirical estimates and *in situ* measurements of this region. Weare (1989) has considered all sources of error associated with empirical formulae and concluded the random and systematic uncertainties to be around $\pm 72\,\mathrm{Wm^{-2}}$ and $\pm 5\,\mathrm{Wm^{-2}}$ respectively. Further, Bradley *et al.* (1990) have found the RMS difference of $30\,\mathrm{Wm^{-2}}$ between empirical estimates and *in situ* data.

The empirical formulae will be helpful to estimate the incoming shortwave radiation simply by knowing the cloud factor. IMD, IITM have developed empirical formulae for estimating the incoming shortwave

**Keywords.** Radiation; cloud; empirical formulae.

surface generates cloud regimes different from those generated over land (Dobson and Smith 1988). Secondly, the aerosols in the atmosphere reduce the total radiation on land when compared with that at sea in the same latitude. Also, there is a great need to develop parameterization on shorter time scales for the marine conditions, since the estimates of daily averages are of greater necessity as air-sea interaction studies focus more on diurnal time scales. In the hourly formulae (Lumb 1964; Lind *et al.* 1984; Gopala Reddy 1987; Dobson and Smith 1988) the cloud factor is directly incorporated. However, similar studies for the Indian Ocean are missing. Therefore, in the present study an attempt has been made for developing empirical formulae to estimate hourly incoming

## 2. Data and methodology

Hourly incoming shortwave radiation over Bay of Bengal and Arabian Sea has been measured by using a pyranometer on board INS Sagar Kanya for 17 days (161 samples) during the BOBMEX Pilot cruise (October – November, 1998). Along with the incoming shortwave radiation, the hourly cloud amount has also been observed during the same period.

Lumb (1964) developed regression equations for estimating solar radiation from hourly cloud observations, which can be fitted into one of nine categories, based on cloud amount and type. This method cannot be directly applied since it does not specify for the
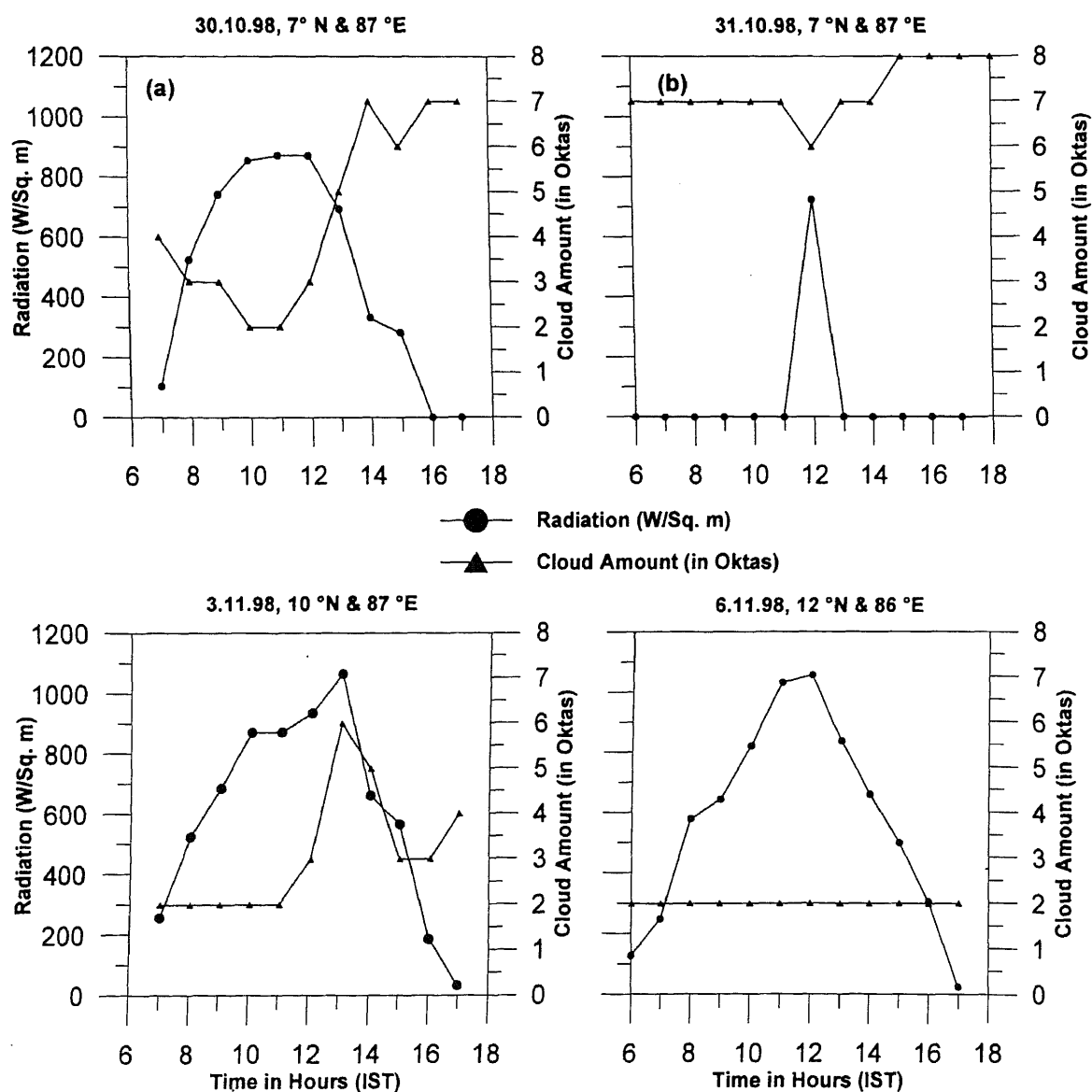


Figure 1. (a) to (d) Graph showing the relation between solar radiation and the cloud amount for four selected days.

cloud observations which do not fit into one of the nine categories. Lind (1981) and Lind and Katsaros (1982) have extended Lumb's approach to include all cloud observations. Gopala Reddy (1987) and Dobson and Smith (1988) have revised the Lind model by incorporating the distance correction for calculating the solar radiation at the top of the atmosphere as follows:

$$Q_T = (\bar{d}/d)^2 \times S_0 \times \sin h \tag{1}$$

where $(\bar{d}/d)^2$ is distance correction for revolution of earth, which accounts for a variation of about ±3.3% in the incoming shortwave radiation at the top of the atmosphere, $S_0$ is solar constant (Wm$^{-2}$) and $\sin h$ is sine of the solar altitude.

Empirical formulae are developed for determining the incoming shortwave radiation at the ocean surface on hourly basis from a knowledge of total cloud amount reported, in terms of the atmospheric transmission factor (TF), the incoming shortwave radiation observed at the ocean surface ($Q_{SW\downarrow}$) and the radiation incident at the top of the atmosphere ($Q_T$) as:

$$T.F. = Q_{SW\downarrow}(\text{observed})/Q_T \tag{2}$$

where $Q_T$ is calculated from equation (1). Gopala Reddy (1987) and Dobson and Smith (1988) have found a relation between T.F. and sine of the solar altitude as:

$$T.F. = A_i + B_i \sin h \tag{3}$$

with $i = 0$ to 8 oktas, $A_i$ and $B_i$ are regression coefficients for different total cloud amounts.

Using different values of T.F. and $\sin h$, the regression coefficients $A$ and $B$ of equation (3) were found for different amounts of cloud.

## 3. Results and discussion

It is well known that cloud feedback strongly regulates the solar radiation. The graphs between the observed hourly incoming shortwave radiation and cloud amount on four selected days, presented in figure 1 show a clear inverse relationship between the two. Figure 1(c) shows a maximum radiation of 1065 Wm$^{-2}$ on 3.11.98 and figure 1(d) shows a secondary maximum of 1057 Wm$^{-2}$ on 6.11.98 at noon under nearly clear sky conditions. On 31.10.98 (figure 1b) it can be seen that under overcast sky with cloud amount 7 to 8 oktas, the solar radiation is almost negligible.

The relationship between the Transmission Factor (T.F.) and sine of the solar altitude for different cloud amounts has been presented in figure 2. This shows that T.F. increases linearly with the sine of the solar
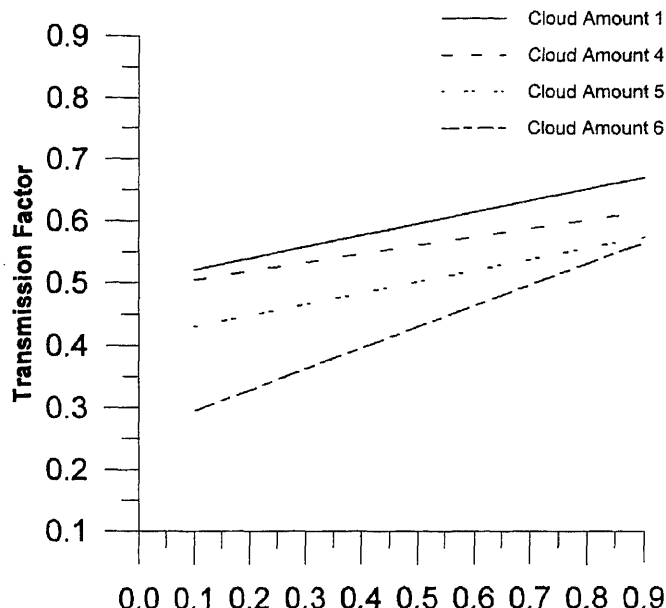


Figure 2. The relation between T.F. and $\sin h$ for different cloud amounts.
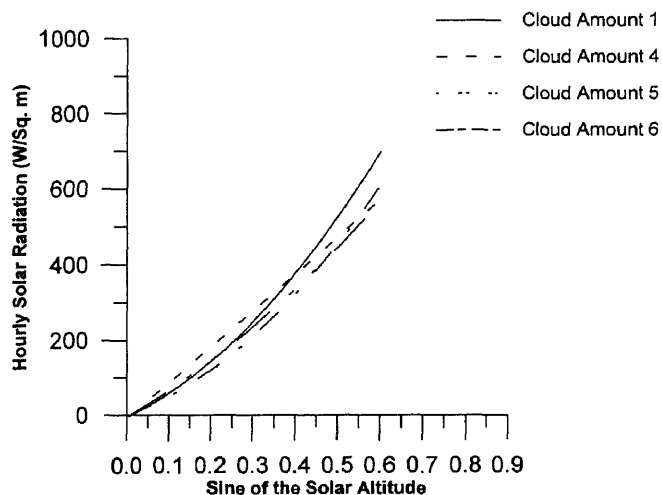


Figure 3. Graph showing the relation between hourly solar radiation and $\sin h$ for different cloud amounts.

the sine of the solar altitude. The relationship between the measured values and those estimated by using other models (Lind *et al* 1984; Gopala Reddy 1987; Dobson and Smith 1988) of T.F. and the sine of the solar altitude are given in figure 4 for comparison. Similar graphs showing the estimated incoming radiation and $\sin h$ are given in figure 5.

In the present study, the distance correction is also incorporated while calculating the T.F. The distance correction accounts for about ±3.3% of variation in the solar radiation at the top of the atmosphere. Thus, the present model is a slightly improved model than that of Lumb (1964). Due to data limitations, 4 categories of regression coefficients are obtained for

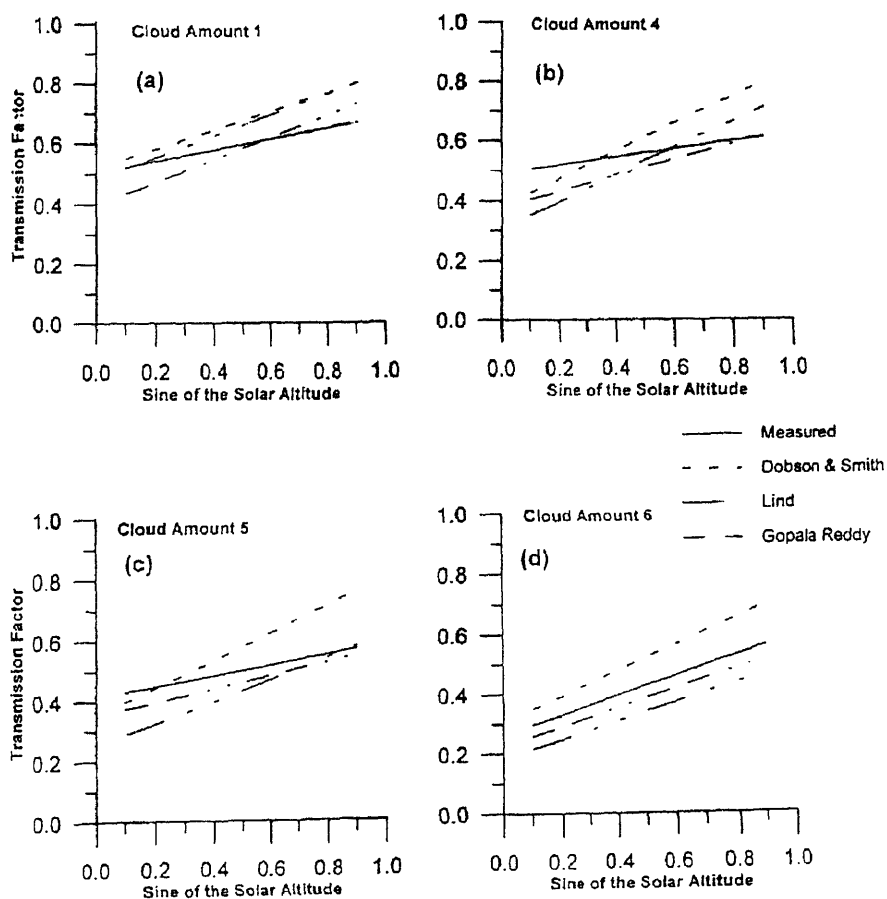Figure 4.  (a) to (d) Graph showing the relation between T.F. and sin$h$ for different cloud amounts using different methods.
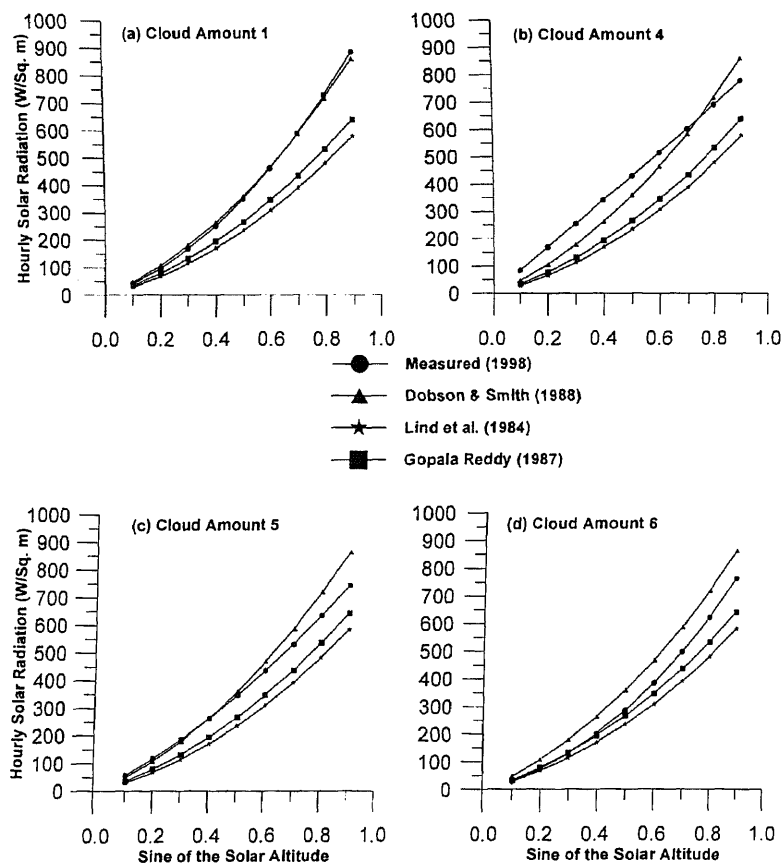
Table 1. *Regression coefficients for estimation of T.F.*

| Cloud amount in oktas | Regression Coefficient | | | |
|---|---|---|---|---|
| | A | B | SD | RMS |
| 1 | 0.502 | 0.187 | 0.048 | 0.038 |
| 4 | 0.491 | 0.138 | 0.082 | 0.507 |
| 5 | 0.412 | 0.179 | 0.093 | 0.492 |
| 6 | 0.261 | 0.336 | 0.096 | 0.393 |

Table 2. *Comparison of the present model with other okta models.*

| Cloud amount in oktas | Present model (1998) | | Lind *et al.* (1984) | | Gopala Reddy (1987) | | Dobson and Smith (1988) | |
|---|---|---|---|---|---|---|---|---|
| | SD | RMS | SD | RMS | SD | RMS | SD | RMS |
| 1 | 0.048 | 0.038 | 0.046 | 0.272 | 0.087 | 0.222 | 0.036 | 0.331 |
| 4 | 0.082 | 0.507 | 0.118 | 0.404 | 0.113 | 0.334 | 0.121 | 0.451 |
| 5 | 0.093 | 0.492 | 0.095 | 0.229 | 0.083 | 0.146 | 0.117 | 0.350 |
| 6 | 0.096 | 0.393 | 0.057 | 0.237 | 0.085 | 0.184 | 0.068 | 0.296 |

Similar formulae were obtained by Lind *et al.* (1984) from JASIN data set, Gopala Reddy (1987) from Kiel Bay (lat. 54.5°) data set and Dobson and Smith (1988) from Pacific Ocean data set between 44° N and 62° N. The SD and RMS errors of these formulae are given in table 2 along with those of the formulae obtained in the present study for comparison. It can be seen that the RMS error for cloud amount 4 is higher, which is higher in the other models too. Further it can be seen from the table that the accuracy of the present formulae is in good agreement with those of the others.

## 4. Summary and conclusion

Empirical formulae for estimating hourly incoming shortwave radiation over the Indian Ocean under different cloud amounts (1, 4, 5, 6 oktas) were obtained by using the pyranometer measurements of the incoming shortwave radiation and the observed cloud amounts. These formulae have been developed by using the *in situ* observations taken over the Indian Ocean and can be used for estimating the hourly incoming shortwave radiation from cloud observations. The RMS error of these formulae varies between 0.038 and 0.507.

## Acknowledgements

## References

Atwater M A and Ball J T 1981 A surface solar radiation model for cloudy atmospheres, *Mon. Weather Rev.* **109**, 878–888.

Bradley E F, Godfrey J S, Nunez M, Coppin P A, 1990 Estimating the total heat flux into the tropical oceans; *WCRP-43*, Oct. 1990, 121–128

Budyko M I 1974 *Climate and Life* (London): Academic Press Inc. Ltd., 508 pp.

Das H P and Pujari, A D 1993 A simple approach towards estimating solar irradiance; *Mausam* **44**, 3, 239–242

Dobson F W, Bretherton F P, Burridge D M, Crease J, Kraus E B and Von der Haar T H, 1982 The 'CAGE' experiment: A feasibility study. Report WCP- 22; *World Meteorological Organization*, Geneva 95 pp.

Dobson, F W and Smith D S 1988 Bulk models of solar radiation at sea.; *Q.J.R. Meteorol Soc.* **114** 165–182

Ganesan, H R 1970, Estimates of solar radiance over India; *India. J. Met. Geophys.*, **21** 629–636

Gautier C 1986 Evaluation of the net short-wave radiation over the Indian Ocean during summer MONEX 1979; *Mon. Weather Rev.* **114** 525–533

Gautier C 1988 Surface solar irradiance in the central Pacific during tropical heat. Comparisons between *in situ* measurements and satellite estimates; *J. Climate* **1** 600–608

Gopala Reddy K 1987 Parameterization of short-wave radiation in the Marine Atmosphere; (Canada: IUGG General Assembly, Vancouver)

Lind R J 1981 Models of long and short wave irradiance with radiation estimates from JASIN 1978; M.Sc. Thesis, Dept. of Atmos. Sci., U. of Washington, Seattle, 129 pp.

Lind R J and Katsaros K B 1982 Tests of radiation parameterizations for clear and cloudy conditions, *JASIN News* **22** 6–9.

Lind R J, Katsaros K B and Gube M 1984 Radiation budget components and their parameterization in JASIN; *Q.J.R. Meteorol. Soc.* **110** 1061–1071

Lumb F E, 1964 The influence of cloud on hourly amounts of

Mohanty U C and Mohan Kumar N 1998 A method for estimation of net surface short-wave radiation over the Bay of Bengal; *Indian J. Marine Sci.*, **27**, 60–65

Reed R K 1977 On estimating insolation over the ocean; *J. Phys. Oceanogr.*, **7** 482–485

Seckel G R and Beaudry F H 1973 The radiation from the sun and sky over the Pacific Ocean. (Abstract); *Trans. Am. Geophys. Union* **54** 1114

Simpson J J and Paulson C 1979 Mid-ocean observation atmosphere radiation; *Q.J.R. Meteorol. Soc.* **105** 487–5

Weare B C 1989 Uncertainties in estimates of surface fluxes derived from marine reports over the tropical subtropical oceans; *Tellus* **41A**, 357–370

Wyrtki K 1971 Oceanographic Atlas of the Internati Indian Ocean Expedition; (Washington, D.C.: Nat Science Foundation), 531

# Thermohaline structure and circulation in the upper layers of the southern Bay of Bengal during BOBMEX-Pilot (October – November 1998)

V RAMESH BABU, V S N MURTY, L V G RAO, C V PRABHU and V TILVI

*National Institute of Oceanography, Dona Paula, Goa 403 004, India*

Hydrographic data collected on board ORV Sagar Kanya in the southern Bay of Bengal during the BOBMEX-Pilot programme (October – November 1998) have been used to describe the thermohaline structure and circulation in the upper 200 m water column of the study region. The presence of seasonal Inter-Tropical Convergence Zone (ITCZ) over the study area, typically characterized with enhanced cloudiness and flanked by the respective east/northeast winds on its northern part and west/southwest winds on its southern part, has led to net surface heat loss of about 55 W/m². The sea surface dynamic topography relative to 500 db shows that the upper layer circulation is characterised by a cyclonic gyre encompassing the study area. The eastward flowing Indian Monsoon Current (IMC) between 5°N and 7°N in the south and its northward branching along 87°E up to 13°N appear to feed the cyclonic gyre. The Vessel-Mounted Acoustic Doppler Current Profiler (VM-ADCP) measured currents confirm the presence of the cyclonic gyre in the southern Bay of Bengal during the withdrawing phase of the southwest monsoon from the northern/central parts of the Bay of Bengal.

## 1. Introduction

The Bay of Bengal and Monsoon Experiment (BOBMEX) is a national scientific activity under the Indian Climate Research Programme (ICRP) designed for the summer monsoon season of 1999 in order to improve the understanding of intra-seasonal ocean-atmosphere coupling over the energetically active Bay of Bengal through multi-ship surveys. However, a pilot experiment called the BOBMEX-Pilot was conducted during October – November, 1998 over the southern Bay of Bengal to test the sophisticated equipment meant for use in the main BOBMEX field observations. During the BOBMEX-Pilot period the southwest monsoon conditions still prevailed with the presence of strong westerly/southwesterly winds and inclement weather with active ITCZ and intense convection. Temperature and salinity observations using CTD and the Vessel-Mounted Acoustic Doppler Current Profiler (VM-ADCP) measured direct currents

during BOBMEX-Pilot have given us a good opportunity to describe the thermohaline fields, currents and circulation in the southern Bay of Bengal during October – November 1998. This study has an added advantage of direct current measurements by VM-ADCP to compare with the derived geostrophic currents as was hitherto practiced by earlier investigators (Murty *et al* 1992, 1993, 1996; Suryanarayana *et al* 1993; Varkey *et al* 1996; Gopalkrishna *et al* 1996; Sarma *et al* 1999). Their studies mainly deal with the hydrography and circulation based on dynamic topography fields in the northern and central parts of the Bay of Bengal during southwest and post-southwest monsoon seasons. Some of these studies address the intra-seasonal variability of volume transports across selected sections. In this paper, we present the thermohaline structure and circulation in the upper layers of southern Bay of Bengal at the time of the southwest monsoon receding from the Bay of Bengal.
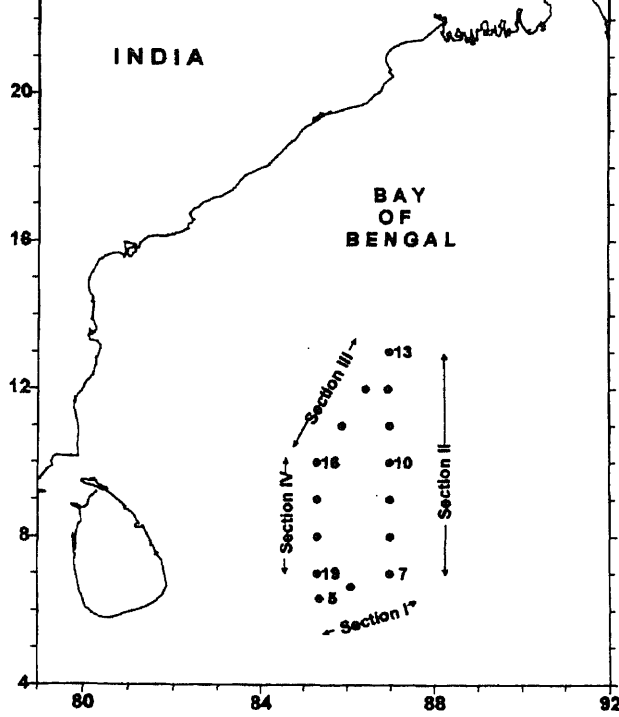
Figure 1. Study area showing CTD station locations during October – November, 1998 (BOBMEX-Pilot).

The locations of hydrographic stations occupied during BOBMEX-Pilot are shown in figure 1. The Sea-Bird CTD (conductivity-temperature-depth) probe was operated at these locations to obtain temperature and salinity profiles. CTD rosette was used to collect water samples from various depths for salinity and chemical analysis. On board AUTOSAL (Guildline, USA), calibrated with standard sea water, was used to obtain the salinity. At three locations (#7, #10 and #11) representing the southern, central and northern parts of the study area, 1–2 day time-series CTD observations were also carried out at 3-hour intervals. The CTD data were processed using SEASOFT (version 4.0) software and the CTD salinity values were corrected with the help of regression equations developed after comparing the CTD salinity values with the AUTO-SAL (accuracy: ±0.001 psu) salinity values. Routine surface meteorological observations (wind speed and direction, atmospheric pressure, air temperature and relative humidity) were recorded at 10-minute intervals by the on board Automatic Weather Station (AWS). The treatment of AWS data together with the sea surface temperature (SST) is outlined by Murty et al. (2000). The bulk-aerodynamic formulae
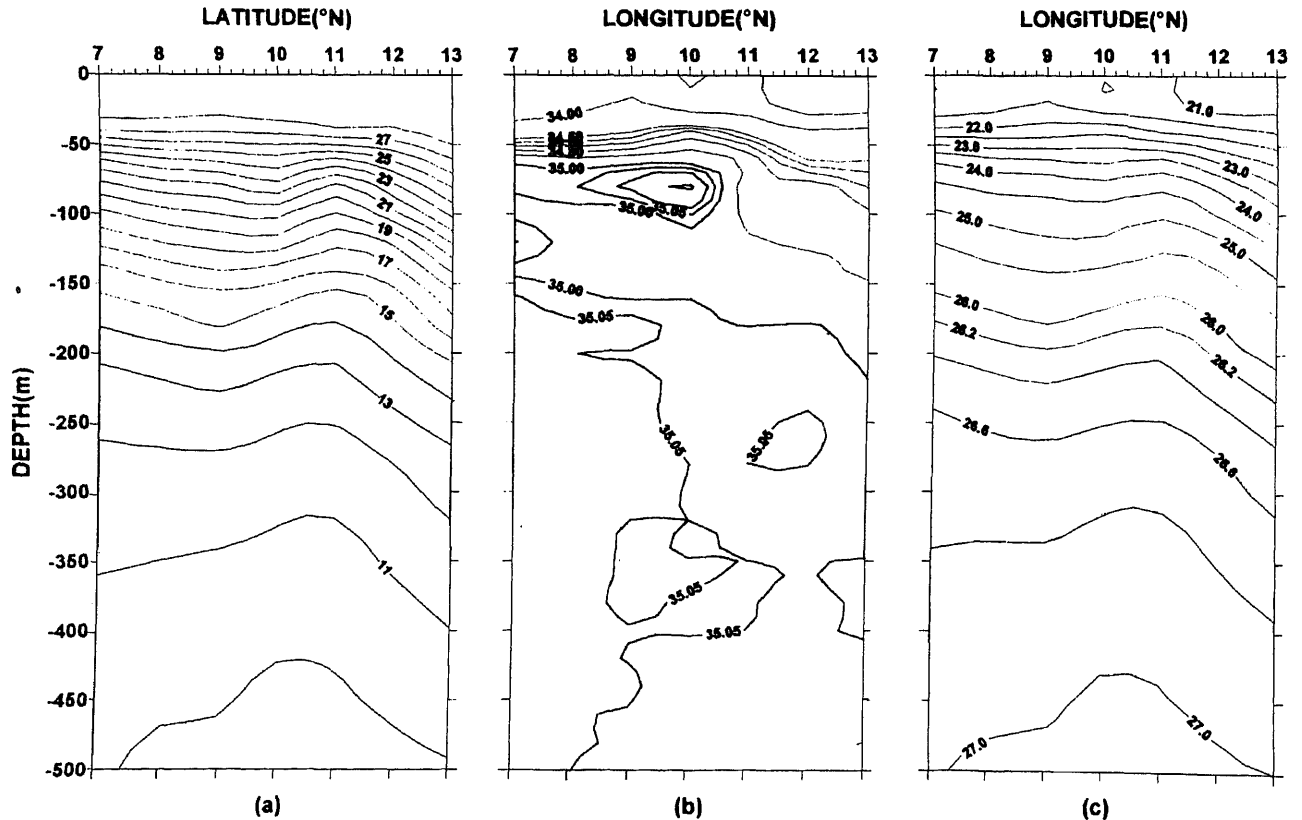


Figure 2. (a) Upper layer thermal structure, (b) salinity and (c) potential density along section II (87°E longitude) during BOBMEX-Pilot.

heat, sensible heat and effective back radiation) following the methodology of Stevenson (1982) and Sarma *et al.* (1997). The AWS measured global solar radiation data were used to estimate the net heat flux at the sea surface during the observational period in the study area.

### 3.1 *Upper ocean thermal structure*

Figure 2(a) presents the upper ocean thermal structure along 87°E between 7°N and 13°N. The surface mixed layer is around 30 m and deepens to 50 m at



Figure 3.   Distribution of temperature at various depths: (a) sea surface, (b) 50 m, (c) 100 m and (d) 200 m during BOBMEX Pilot.

13°N. Doming of isotherms is the conspicuous feature from a 500 m depth to the base of the surface mixed layer. The vertical temperature gradients are relatively stronger on the northern part of the dome suggesting an intense westward flow between 11°N and 13°N.

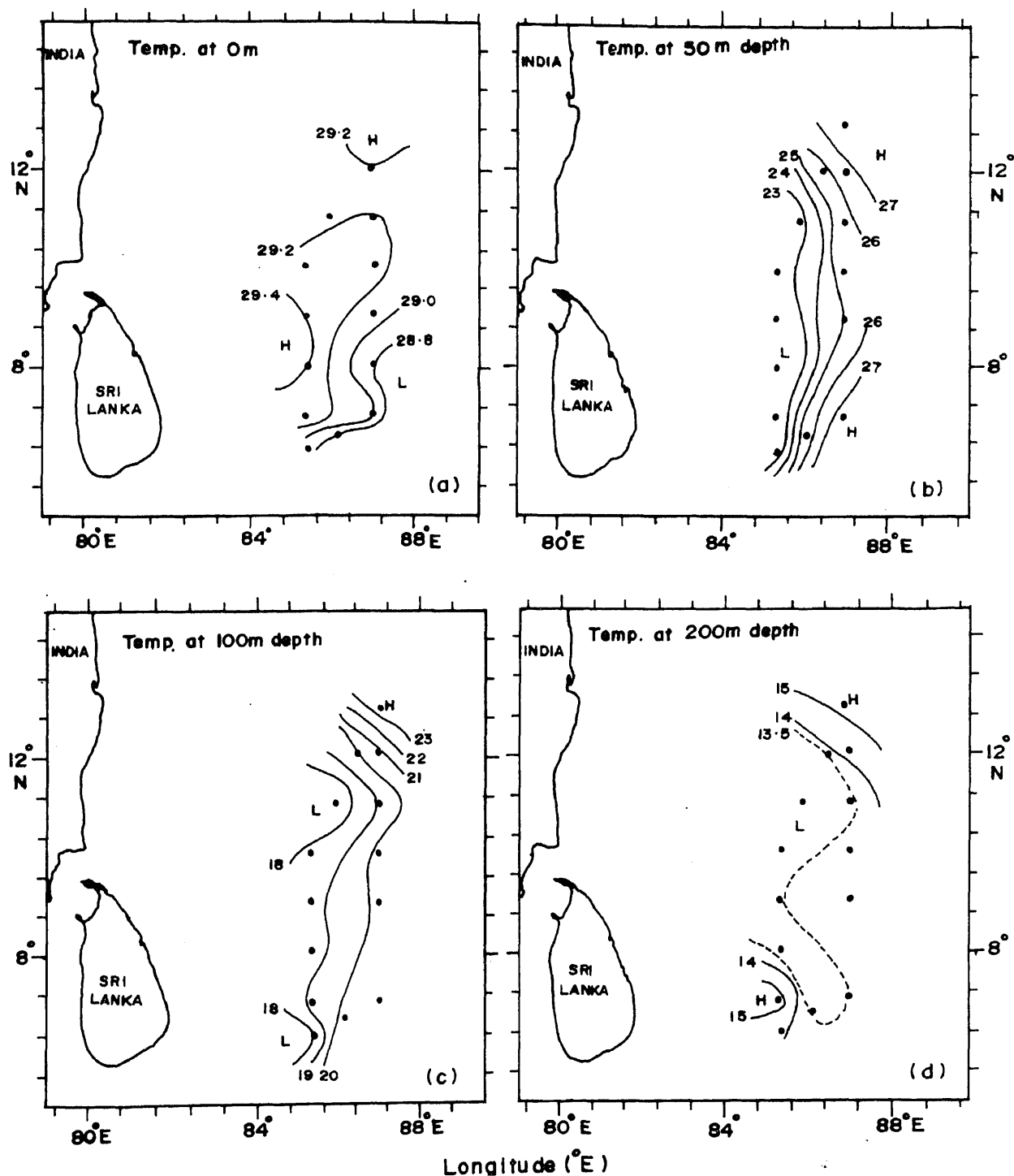Figures 3(a–d) show the temperature distribution at sea surface at a depth of 50 m, 100 m, and 200 m. Sea surface temperature (SST) varies from 28.8°C to 29.4°C with cold waters to the east of 86°E and warmer (> 29.2°C) to the west of 86°E. The spatial variation in SST is of the same order as its diurnal range at three time series locations (Murty *et al.* 2000). At 50 m, temperature varies between 23°C and 27°C and the isotherms exhibited near-meridional orientation with strong westward directed zonal temperature gradient which is opposite to that at the sea surface. At 100 m, the temperature variation is about 5°C between 11°N and 13°N and the zonal temperature gradient weakens from that at 50 m south of 11°N. At 200 m depth, the temperature variation is marginal (1.5°C) from 13.5°C to 15°C and over a larger part of study area, the temperature is around 13.5°C.

### 3.2  *Upper ocean salinity structure*

Near-surface salinity is less on the northern part of the section and the isohalines follow the pattern of isotherms in the upper 75 m (figure 2b). However a cell of high salinity (35.0–35.10) occupies 75–100 m depth interval between 8°N and 10°N. This high salinity cell lies along 24.5 $\sigma_\theta$ isopycnal (figure 2c) and can be identified as the Arabian Sea High Salinity Watermass (ASHSW). A portion of Bay of Bengal high salinity layer of salinity greater than 35.05 psu is present in the depth interval 150–500 m in the south and the layer thickness decreases northward followed by a decrease in the salinity of this layer.

Figures 4(a–d) present the spatial variation of salinity in the upper 200 m. The sea surface salinity varies from 32.0 to 34.0 psu and the zonal gradient of salinity is directed westward (figure 4a) which is opposite to the zonal gradient of SST (figure 3a). The
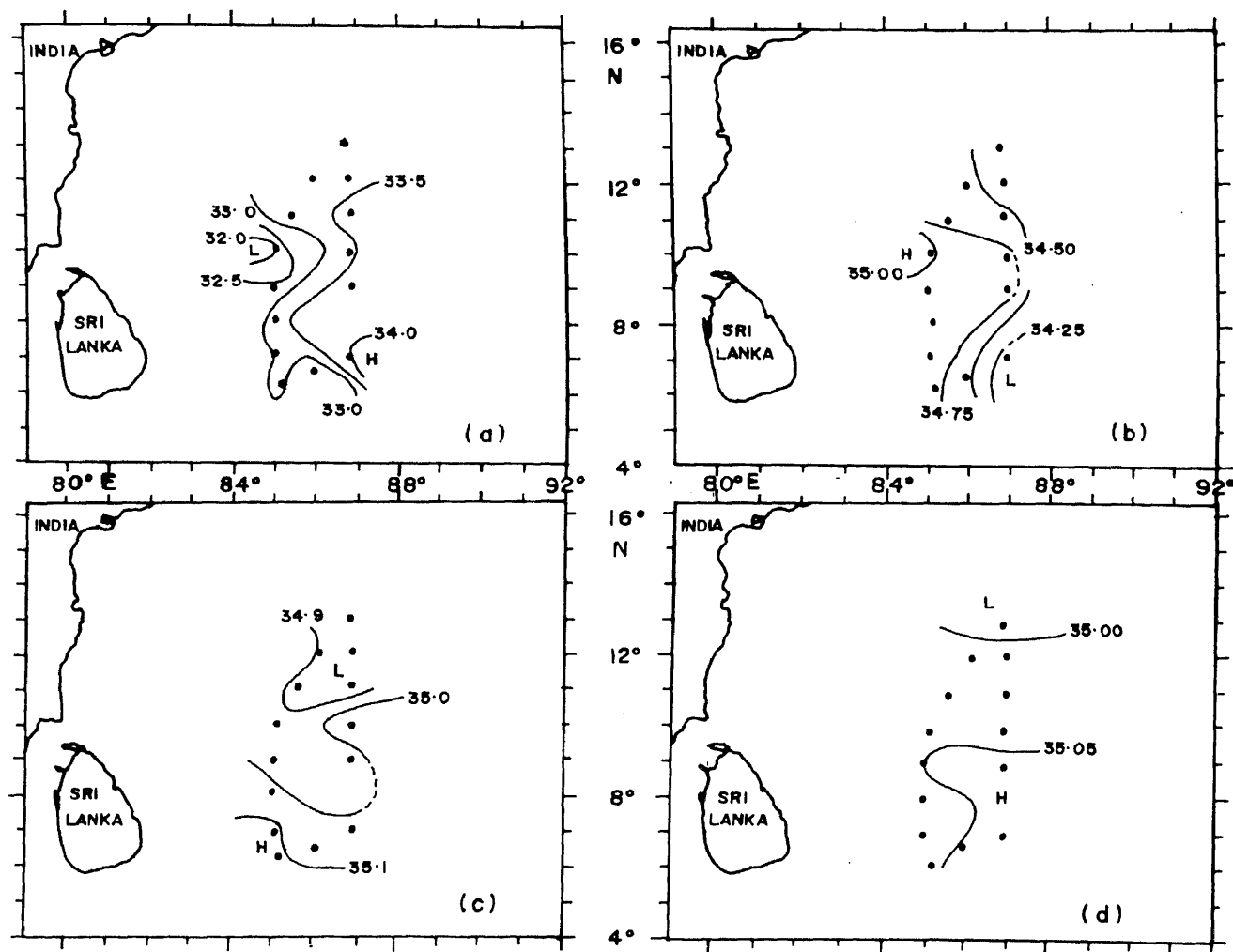


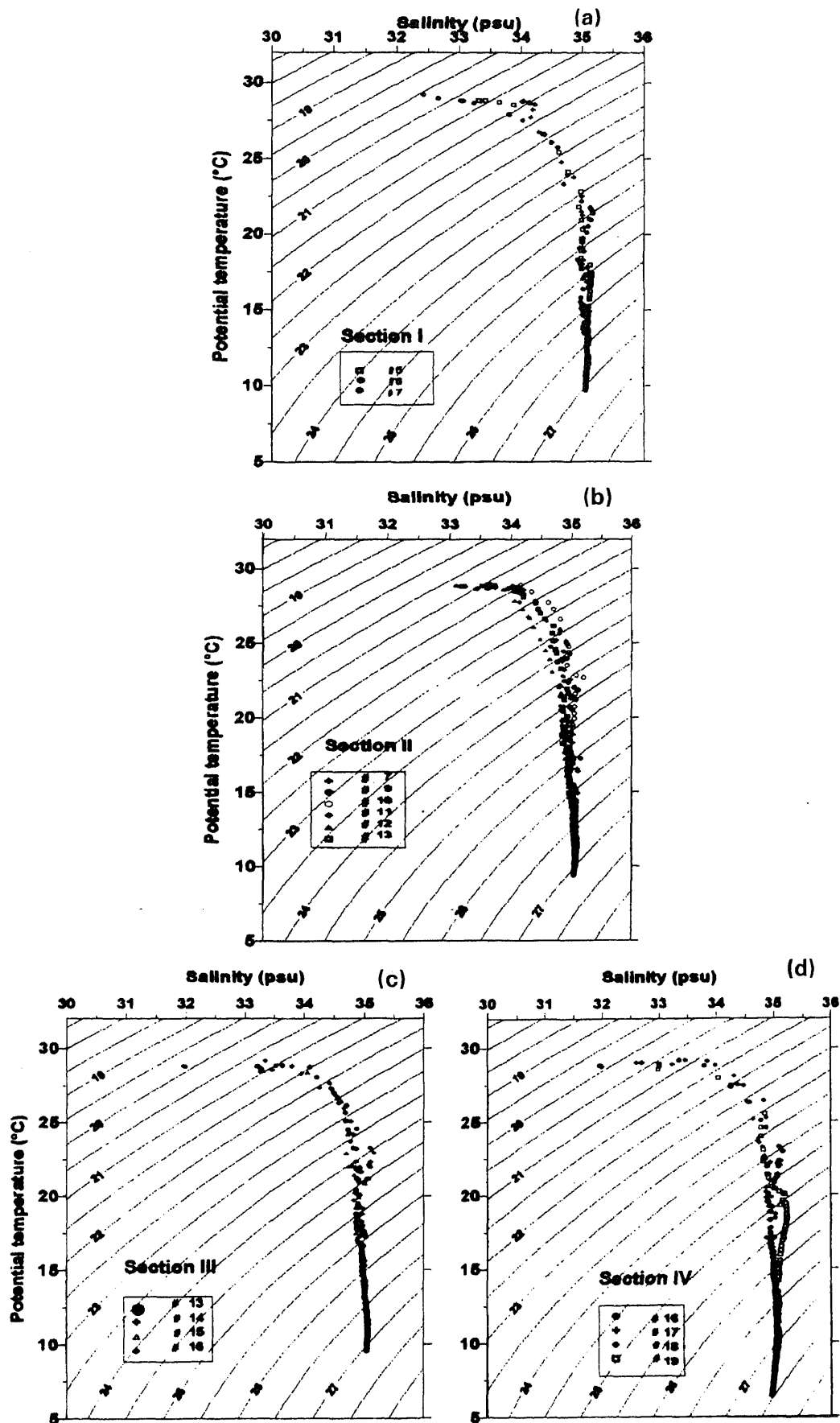Figure 4.  Same as at figure 3, but for salinity during BOBMEX Pilot.

Figure 5. Watermass structure at the CTD stations along section I (a), section II (b), section III (c) and section IV (d) during
BOBMEX-Pilot.

surface waters thus exhibit different T-S relations; warmer, saline waters in the east and cold, less saline waters in the west. At and below 50 m, the salinity variations are both reduced and reversed, and the waters are characterised by different T-S relationship (warm and less saline in the east and cold and saline in the west) from that at the surface (figure 4b). However, at 100 m and 200 m depth, the salinity gradient is directed northward with higher salinity waters in the south (figure 4c and d).

### 3.3 *Watermass structure*

The watermass structure of the study area during the study period is represented by T-S diagrams drawn using the CTD data at the stations along the 4 sections (figures 5a–d). The near surface layer is characterised by warm and halocline and a salinity maximum is encountered between the 24.0 and 24.5 isopycnals at subsurface depths. This high salinity water is identified as the Arabian Sea High Salinity

Watermass (ASHSW) advecting into the Bay under the influence of the Indian Monsoon Current (IMC). In the south, the ASHSW is located between 24.5 and 25.0 $\sigma_\theta$ isopycnals with reduced salinity towards the north.

### 3.4 *Upper ocean currents and circulation*

Figures 6(a–d) represent the dynamic topography maps at various depths relative to 500 db. The near surface circulation at 15 m (figure 6a) shows a northward flow encompassing the study area up to 11°N where it turns northwestward between 11°N and 13°N. The associated geostrophic velocity is doubled in its magnitude between 11°N and 13°N when compared to its magnitude in the south as seen from the crowding of isolines of dynamic topography. The geostrophic circulation weakens with depth, though the presence of strong currents associated with the northwestward flow is consistent with depth. At 200 m depth, (figure 6d) the circulation shows a nearly closed cyclonic gyre encompassing the study area.
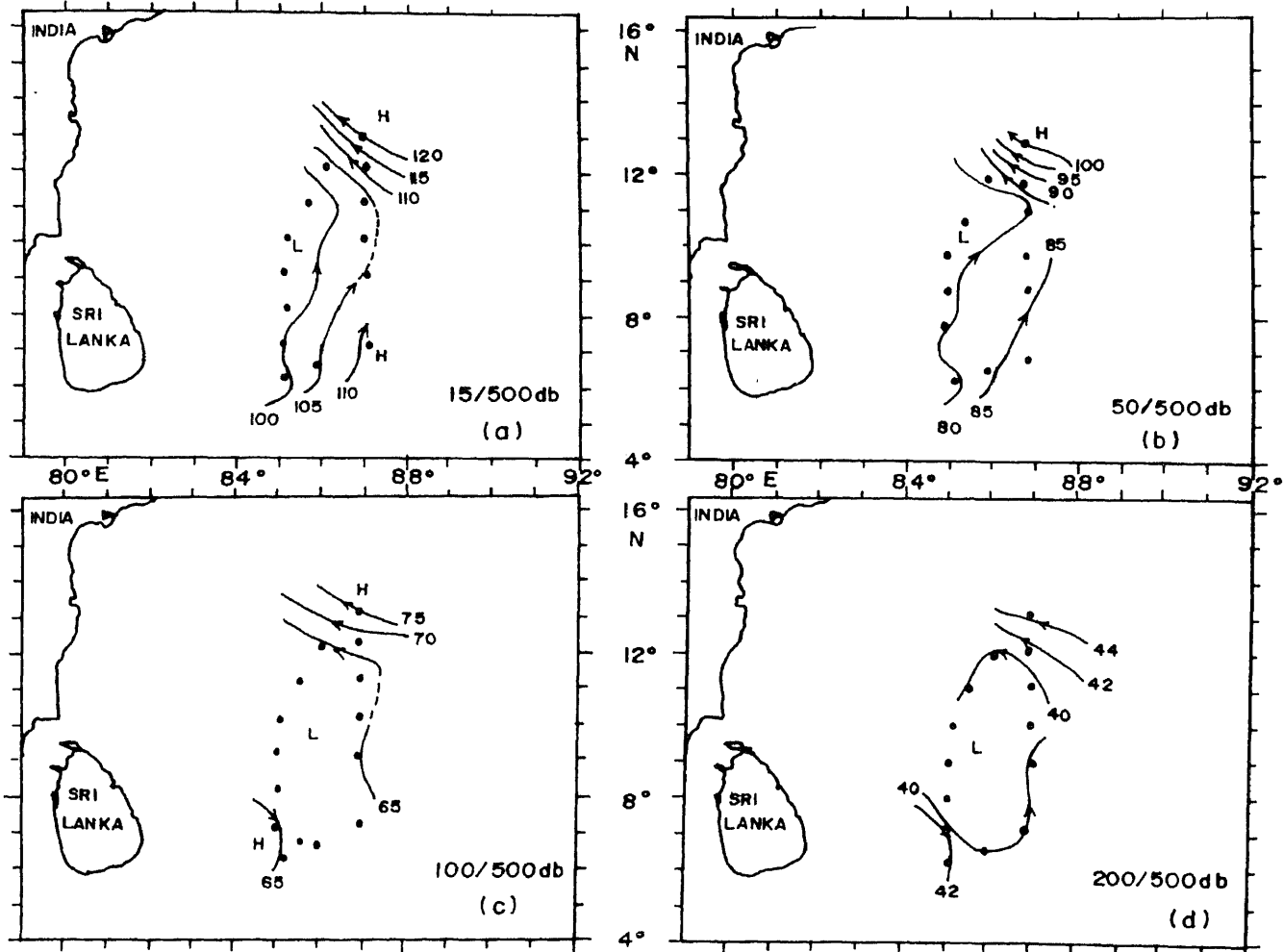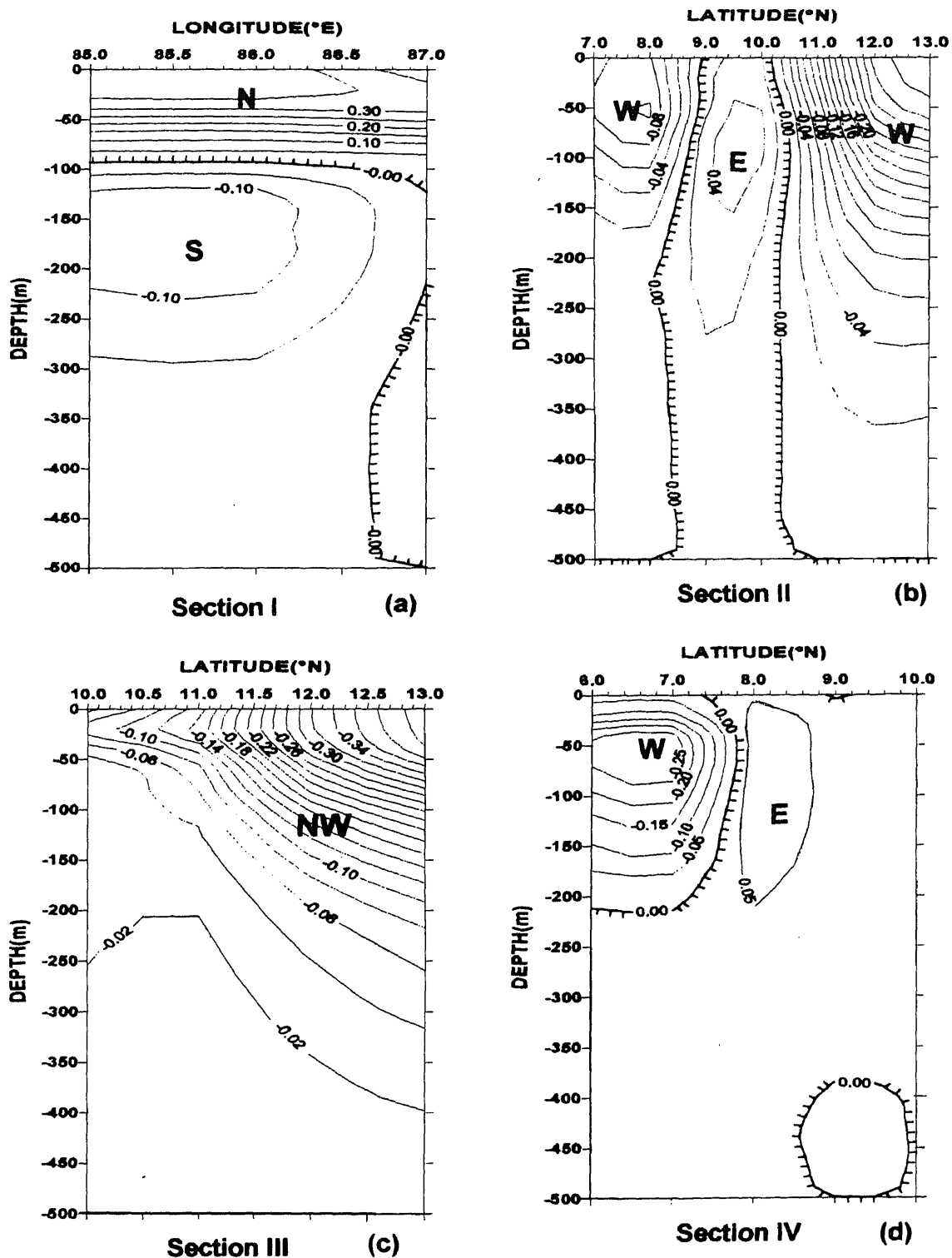
Figure 7. Upper layer geostrophic current (m/s) structure along sections I (a), section II (b), section III (c) and section IV (d) during BOBMEX Pilot. In (a) letter N(S) stands for northward (southward) flow. In (b) and (d) letter w (E) stands for westward (eastward) flows. In (c), NW stands for northwestward flows.

The above flow pattern in the upper 200 m water column suggests that the divergence of the waters is more intense below 100 m depth and weakens upward to the surface. This indicates that horizontal conver-

face across the study area and the near-meridional orientation of the thermohaline fields and the northward flow in the upper 100 m layer.

The geostrophic velocity structure in the upper
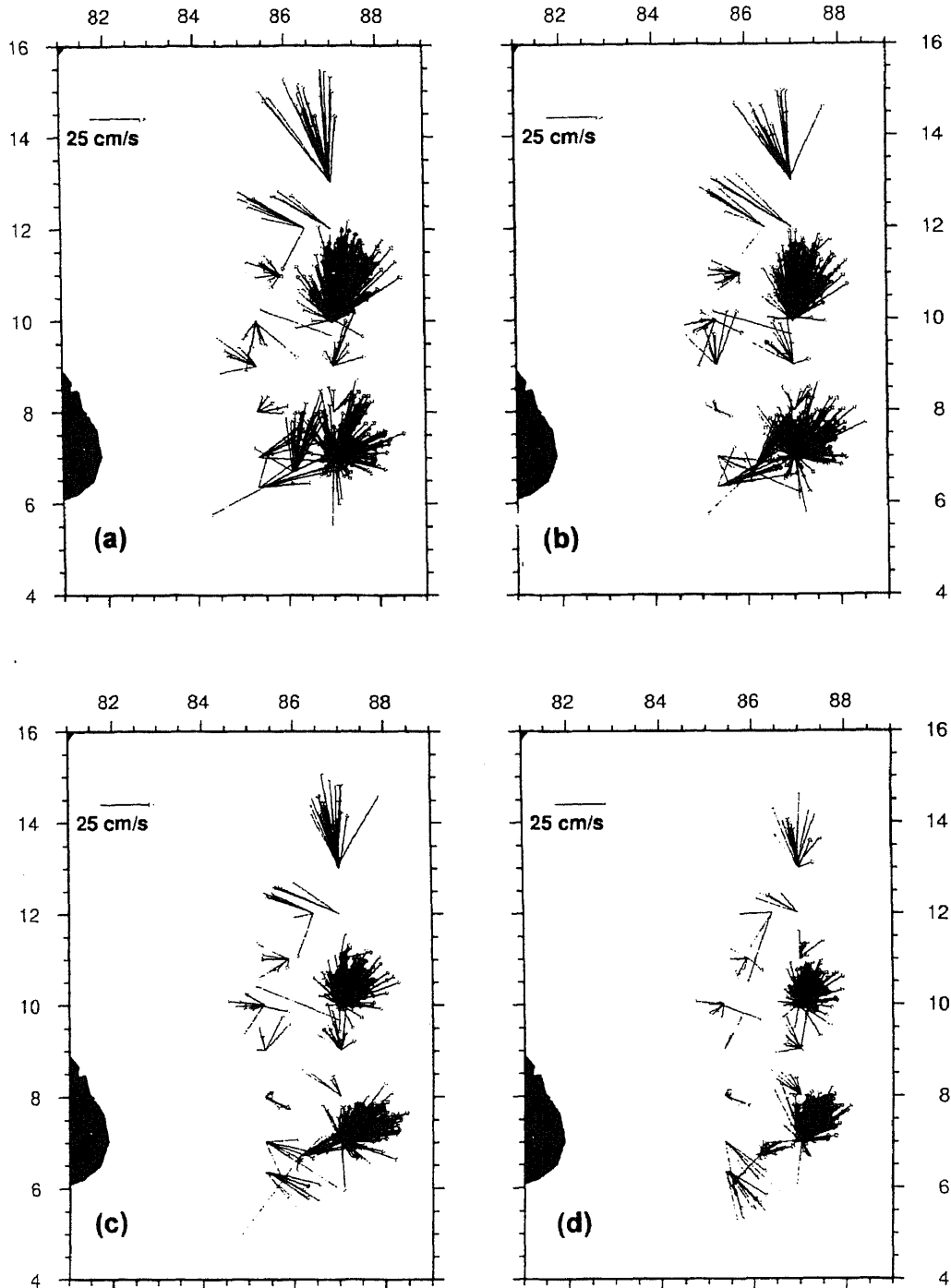
Figure 8. VM-ADCP measured ocean current vectors at the CTD stations at various depths: (a) 31 m, (b) 51 m, (c) 100 m and (d) 200 m during BOBMEX-Pilot. Note the cluster of vectors at 7°N, 10°N and 13°N represent the time-series observations over a period of 48 hr, 48 hr and 24 hr respectively.

current structure-predominant northward flow with higher velocity (35 cm/s) at the surface in the upper 100 m and weaker (10 cm/s) southward flow between 150 and 200 m depth is present. This change in the flow pattern with depth is also evident from the change in the direction of Indian Monsoon Current (IMC) with depth (current shear) as seen in the VM-ADCP currents–NE vectors in the upper 100 m and

section II, between 7°N and 13°N, the flow is predominantly westward and embedded in it is a weak (4 cm/s) eastward flow between 9°N and 10°N. The westward flow attains higher velocity (40 cm/s) near the surface in the north between 12° and 13°N. Along section III, between 10°N and 13°N only northwestward flow is present throughout the section. However, it is interesting to note that this north-
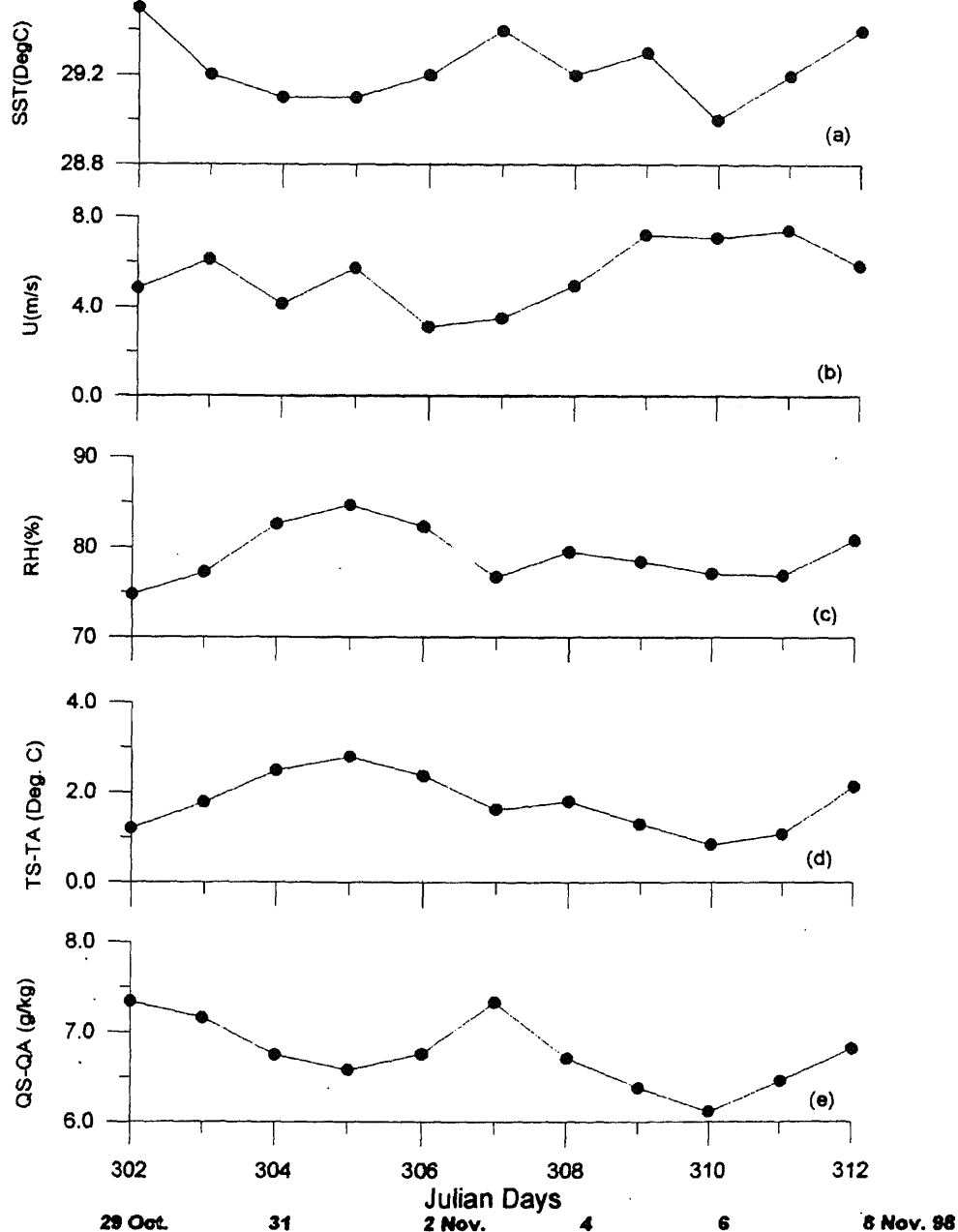
Figure 9. Along the track daily variation of (a) sea surface temperature, (b) wind speed, (c) relative humidity, (d) sea minus air temperature at 10 m height above the surface and (e) sea minus air specific humidity difference at 10 m height above surface during BOBMEX-Pilot.

(40 cm/s) at the northern part of the section and extends to greater depth. (~ 400 m). Its velocity weakens towards southeast. The VM-ADCP currents also confirm this pattern of currents. Along section IV, (figures 8 a–d) strong westward flow with its core (~ 25 cm/s) at subsurface depths (~ 50 m) is noticed between 6°N and 8°N while weaker eastward flow occurs north of 8°N.

The VM-ADCP measured currents at the CTD station locations are presented for four depths (31, 51, 100 & 200 m) in the upper 200 m layer (figures 8 a–d). Details of VM-ADCP data processing are given in

Murty et al. (2000). The depth bin of measured currents is 31 m. The monthly mean as well as 10 day mean ship drift currents during the month of October reveal eastward currents in the south (5°N − 7°N) and northward currents along 87°E (Cutler and Swallow 1984). The VM-ADCP currents at 31 m also indicate eastward currents in the southern bay including at the time series locations (figure 8a). These eastward currents represent the Indian Monsoon Current (IMC) with velocity between 25 and 50 cm/s. The turning of the IMC towards north along 87°E is also evident in the VM-ADCP currents.

Figure 10. Along track daily variation of (a) heat budget components ($Q_e$, $Q_h$, and $Q_b$) and (b) net surface heat flux ($Q_n$). Incoming solar radiation ($Q_i$) and total heat loss ($Q_e + Q_h + Q_b$) during BOBMEX-Pilot.

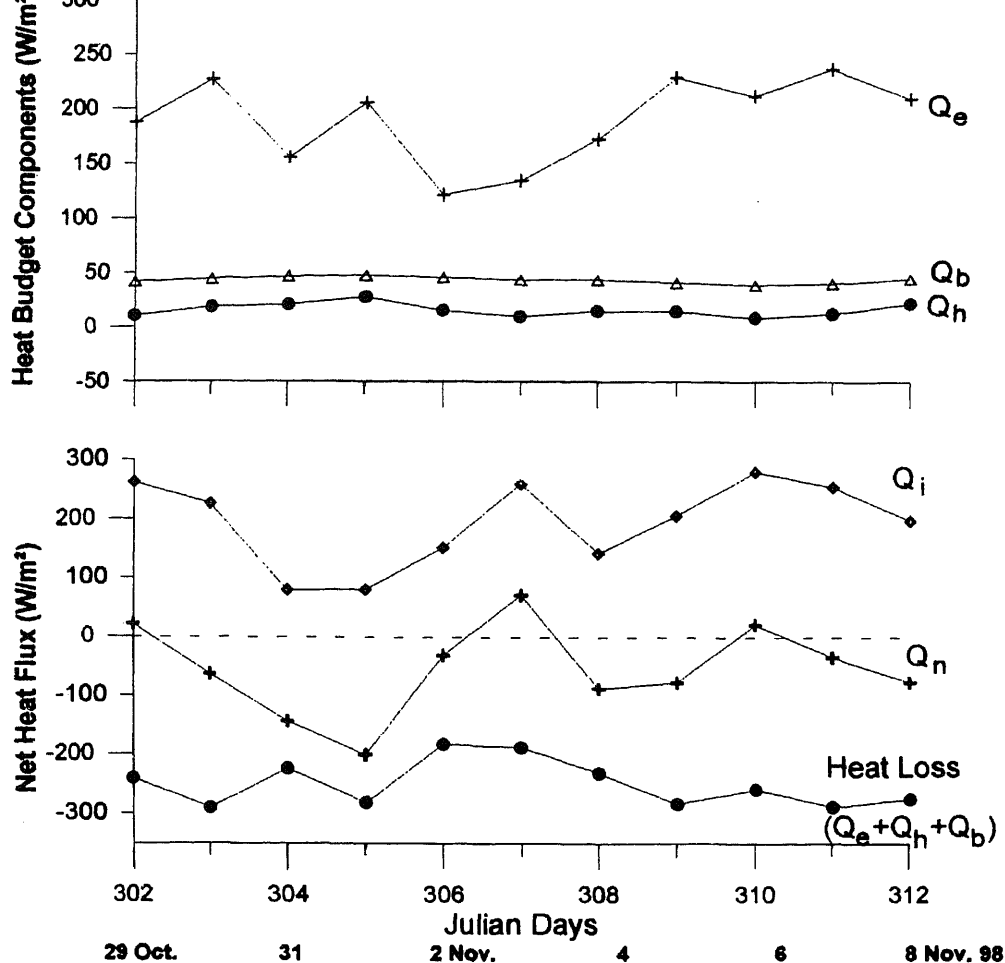The mean velocity of the northward flow is increased gradually towards north. At 200 m depth, (figure 8d) the measured currents describe the cyclonic flow as noticed in the geostrophic flow pattern at 200 m depth (figure 7d). The measured current vectors at the other locations to the west of 87°E indicate that the circulation becomes more cyclonic gyral with the depth but with the reduced speeds in upper 200 m. The monthly diagnostic bulletins of climate (1998) for October and November, 1988 months show that this study area is witnessed with the incidence of low fluxes of Outgoing Longwave Radiation (OLR) which can be attributed as a result of increased cloudiness in ITCZ. However, the current vectors exhibited a rightward shift in direction with depth. Baroclinic current shear is noticed between 50 and 100 m depths. Recent results of ocean circulation modelling studies (Vinayachandran et al 1998, 1999) of the Bay of Bengal have shown the northward turning of IMC along 87°E in July itself and its axis of northward turning is found shifting progressively westward with the advancement of summer monsoon.

### 3.5 Heat budget of the study area

Surface meteorological observations (wind speed, relative humidity) obtained at 10 min. interval are averaged daily and are shown in figure 9 along with daily average of Sea Surface Temperature (SST). On three days, the SST has reached higher values ($\sim 29.4° - 29.6°$). Relatively weaker wind speeds are encountered around 2nd November when the ship has been in the central part of the study area (figure 9b). The RH and sea-air temperature interface (TS-TA) shows trends similarly with a maximum value on 305 Julian day (1st November) (figures 9c and d). The specific humidity difference ($Q_s - Q_a$) between the sea surface and air (figure 9e) varies between 6.0 and 7.5 g/kg while the relative humidity changes between 75% and 85%. The sea surface minus air temperature ($T_s - T_a$) values vary between 1°C and 3°C indicating the instability in the atmospheric boundary layer over the study area. The dependence of SST on $Q_s - Q_a$ is quite evident.

The computed sensible heat flux ($Q_h$) and effective back radiation ($Q_b$) are nearly constant at $10 - 15$ W/

m$^2$ and $45-50\,\mathrm{W/m}^2$ respectively (figure 10a). The daily variation of the latent heat flux ($Q_e$) follows the daily variation of wind speed (figure 9b) and attains a minimum value of $125\,\mathrm{W/m}^2$ on 306 Julian day. The latent heat flux dominates the total heat loss in the study area (figure 10b). The AWS global solar radiation ($Q_i$) varies from a minimum value of $80\,\mathrm{W/m}^2$ to a maximum of $300\,\mathrm{W/m}^2$ during study period. The low values of $Q_i$ on 304 and 305 Julian days are associated with overcast skies. The net heat flux ($Q_n$), a residual of insolation and total heat loss, is negative during most of the study period and the mean net heat flux is about $-55\,\mathrm{W/m}^2$. This suggests that the southern Bay of Bengal, on an average, loses heat energy across the sea surface during October–November when the study area is under the influence of southward moving Intra- Tropical Convergence Zone (ITCZ).

## Conclusions

- Southern Bay of Bengal where the summer monsoon is quite active during October – November, 1998 is generally seen as a region of net heat loss from the sea surface to the atmosphere promoting convective activity in the latter.

- The upper ocean circulation (0–200 m layer) in the study area shows a northward turning of IMC along 87°E under the influence of the depth-increased cyclonic motion and this cyclonic gyre could be attributed to the wind shear associated with ITCZ which is present in the study area during the observational period.

## Acknowledgements

## References

Climate Diagnostic Bulletin of India – Seasonal Postmonsoon (October – November), 1998, (Special Issue No. 11) India Meteorological Dept., India, pp 19.

Cutler A N and Swallow J C 1984 Surface currents of the Indian Ocean (to 25°S, 100°E). Surrey: Institute of Oceanographic Scienices (United Kingdom).

Gopalakrishna V V, Pednekar S M and Murty V S N 1996 *Indian J. Mar. Sci.*, **25** 50–55

Murty V S N, Ramesh Babu V, Rao L V G, Charuta V Prabhu and Tilvi V, 2000 *Proc. Indian Acad. Sci. (Earth Planet Sci.)*, (this issue)

Murty V S N, Sarma Y V, Rao D P and Murty C S 1992 *J. Mar. Res.* **50** 207–228

Murty V S N, Suryanarayana A and Rao D P 1993 *Indian J. Mar. Sci.* **22** 12–16

Murty V S N, Sarma Y V B and Rao D P 1996 *Proc. Indian Acad. Sci. (Earth and Planet. Sci.)* **105** 41–61

Sarma Y V B, Murty V S N and Rao D P Thermodynamics of the oceanic and atmospheric boundary layers over head of the Bay of Bengal during the southwest monsoon of 1990; *NIO Technical Report No. NIO/Tr-3/97*, 1997, pp. 35.

Sarma Y V B, Ramarao E P, Saji P K and Sarma V V S S 1999 *Oceanologica Acta*. **22** 453–471

Stevenson J W 1982, *Computation of heat and momentum fluxes at the sea surface during the Hawaii to Tahiti shuttle experiment; Univ. Hawaii, Honolulu, Hawaii.*

Suryanarayana A, Murty V S N and Rao D P 1993 *Deep-Sea Res.*, **40** 205–217

Varkey M J, Murty V S N and Suryanarayana A 1996 *Oceanography and Marine Biology: An Annual Review.*, (eds.) A D Ansell, R N Gibson and Margaret Barnes, (UCL Press) **34** 1–70

Vinayachandran P N, Masumota Y, Mikawa T and Yamagata T 1999 *J. Geophys. Res.* **104** 11077–11085

Vinayachandran P N and Yamagata T 1998 *J. Phys. Oceanography.* **28** 1946–1960

# Diurnal variability of upper ocean temperature and heat budget in the southern Bay of Bengal during October – November, 1998 (BOBMEX-Pilot)

V S N Murty, V Ramesh Babu, L V G Rao, Charuta V Prabhu and V Tilvi

*National Institute of Oceanography, Dona Paula, Goa 403 004, India.*

Time-series data on upper-ocean temperature, Vessel-Mounted Acoustic Doppler Current Profiler (VM-ADCP) measured currents and surface meteorological parameters have been obtained for the first time in the southern Bay of Bengal at 7°N, 10°N, and 13°N locations along 87°E during October – November, 1998 under BOBMEX-Pilot programme. These data have been analysed to examine the diurnal variability of upper oceanic heat budget and to estimate the eddy diffusivity coefficient of heat in the upper layer. Diurnal variation of near-surface temperature is typical at northern location (13°N) with a range of 0.5°C while the diurnal range of temperature is enhanced to 0.8°C at the central location (10°N) due to intense solar radiation (1050 W/m$^2$), clear skies and low wind speeds. At the southern location (7°N), the diurnal variation of temperature is atypical with the minimum temperature occurring at 2000 hrs instead of at early morning hours. In general, the diurnal curve of temperature penetrated up to 15 to 20 m with decreasing diurnal range with depth. The VM-ADCP measured horizontal currents in the upper ocean were predominantly easterly/northeasterly at southern location, north/northerly at central location and northwesterly at northern location, thus describing a large-scale cyclonic gyre with the northward meridional flow along 87°E. The magnitudes of heat loss at the surface due to air-sea heat exchanges and in the upper 50 m layer due to vertical diffusion of heat are highest at the southern location where intense convective activity followed by overcast skies and synoptic disturbance prevailed in the lower atmosphere. This and the estimated higher value (0.0235 m$^2$/s) of eddy diffusivity coefficient of heat in the upper ocean (0–50 m depth) suggest that 1-D processes controlled the upper layer heat budget at the southern location. On the other hand, during the fair weather conditions, at the central and northern locations, the upper layer gained heat energy, while the sea surface lost (gained) heat energy at northern (central) location. This and lower values of eddy diffusivity coefficient of heat (0.0045 and 0.0150 m$^2$/s) and the northward intensification of horizontal currents at these locations suggest the greater role of horizontal heat advection over the 1-D processes in the upper ocean heat budget at these two locations.

## 1. Introduction

Under the earlier Monsoon Experiment programmes (MONEX-77, MONEX-79 and MONTBLEX-90) in the Bay of Bengal, time-series measurements were conducted in the northern and central Bay and the results of the data analysis were published in various scientific journals (Rao *et al* 1985, Rao and Rao 1986, Rao 1987, Rao *et al* 1991,1993, Sanilkumar *et al* 1994,

Murty *et al* 1996, Sarma *et al* 1997). Under the recent Bay of Bengal and Monsoon Experiment-Pilot (BOB-MEX-Pilot) programme, time-series measurements of temperature, salinity and VM-ADCP currents in the upper 500 m were carried out at 7°N, 10°N and 13°N locations along 87°E in the southern Bay during 29th October – 8th November 1998. The period of time-series measurements varied from 48 hours at the southern and central locations to 25 hours at the

Table 1.  *Details of the time-series locations occupied during BOBMEX-Pilot.*

| Location | Latitude | Longitude | Period | Julian Day |
|---|---|---|---|---|
| 1 | 7° N | 87°E | 0245 IST of 30.10.98 to 0135 IST of 01.11.98 | 303–304 |
| 2 | 10° N | 87° E | 0240 IST of 02.11.98 to 0255 IST of 04.11.98 | 306–308 |
| 3 | 13° N | 87°E | 0150 IST of 05.11.98 to 0340 IST of 06.11.98 | 309 |

northern location (table 1). A detailed description of the prevailing synoptic conditions in the southern Bay of Bengal during BOBMEX-Pilot programme has been provided by Bhat et al (2000). These authors expect that the synoptic conditions that prevailed were representative of the cyclone period or persistence of active southwest monsoon in the southern Bay of Bengal. Large-scale convective activity followed by overcast skies and synoptic weather depressions associated with the Inter-Tropical Convergence Zone (ITCZ) characterise the meteorological forcing at the southern location (7°N, 87°E) during 30th – 31st October, 1998. Clear sky and shallow cumulus clouds were mainly observed from 2nd to 6th November, 1998 during the period of measurements at the central (10°N, 87°E) and southern (13°N, 87°E) locations. In this paper, the authors discuss the diurnal variability of the upper ocean heat budget in relation to the observed differential synoptic weather conditions over the southern Bay of Bengal during BOBMEX-Pilot period (October – November, 1998).

## 2. Materials and methods

Profiles of temperature and salinity in the upper 500 m were obtained using a Seabird CTD (SBE plus 9/11) at 3 hourly interval at three stationary locations (7°N, 10°N and 13°N) along 87°E (figure 1). At the southern (7°N, 87°E) and the central (10°N, 87°E) locations, CTD measurements were taken for 48 hours while at the northern location (13°N, 87°E) these measurements were taken for 25 hours. Bucket thermometer was used to measure the sea surface temperature (SST). Surface meteorological parameters such as air temperature, relative humidity, wind speed and direction, atmospheric pressure and global solar radiation were recorded at 10 minute interval through on board Automatic Weather Station (AWS). The wind data were obtained from two similar sets of sensors located at 22.6 m height above the sea surface on the port and starboard sides of the vessel. The true wind speed and direction referred to True North were estimated using the ship's heading and speed at each time interval for both the sets of sensors. The correct wind data set was carefully chosen for the analysis. The atmospheric pressure recorded by AWS was compared and corrected with the simultaneously recorded aneroid barometric pressure data. Data processing details along with the data are provided in the BOBMEX-Pilot
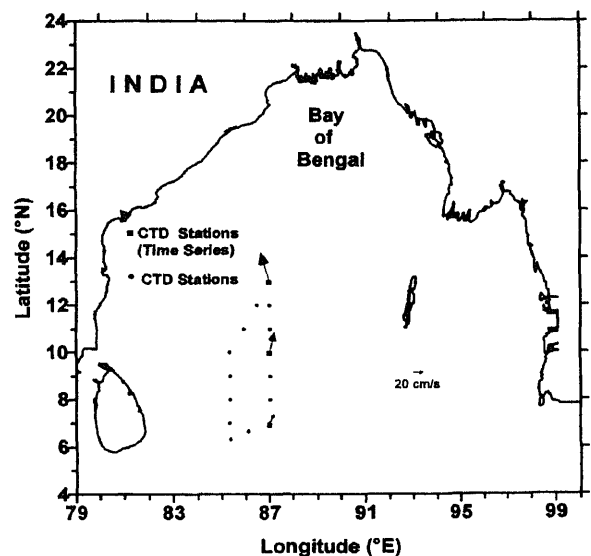


Figure 1.  Study area showing the time-series locations during BOBMEX-Pilot observational period (29th October-8th November 1998). VM-ADCP measured mean currents vectors in the 30–50 m layer (at the time-series locations) are also depicted. Northward increase of the mean current speed is evident.

SST data was supplemented with the 1 hour interval AWS surface meteorological data to make a comprehensive data set to estimate the heat fluxes across the air-sea interface. Bulk aerodynamic formulae are used to estimate the net long wave radiation ($Q_b$), latent heat flux ($Q_e$) and sensible heat flux ($Q_h$). The hourly-mean incoming solar radiation, $Q_i$, as obtained through AWS is considered as heat input to the upper layer. The net heat flux ($Q_n$) at the sea surface is estimated as a residual of the following heat balance equation (Stevenson 1982, Zavialov and Murty 1995):

$$Q_n = Q_i - Q_b - Q_h - Q_e. \tag{1}$$

The computational scheme for obtaining the coefficients of bulk formulae for $Q_b$, $Q_h$ and $Q_e$, and the procedure for computing each of the heat flux parameters are adopted from Sarma et al (1997).

The heat content in the upper 50 m (H) layer is estimated from the temperature profiles at the time-series locations using the equation (Murty et al 1996):

$$H = \rho C_p \int_0^{50} T \, dz \tag{2}$$

where $\rho$ is the water density, $C_p$ is the specific heat at constant pressure and $T$ is the temperature, $z$ is the

## 3. Results and discussion

### 3.1 *Diurnal variation of temperature and upper layer heat content*

For the present study, we have used the time series CTD data covering a day from midnight to midnight of 24 hours duration at the southern and central locations though data are available for 48 hours of duration. However, the variations in the weather and oceanic parameters during the omitted days at the southern and central locations have been discussed as when required. Figures 2(a–c) show the vertical profiles of temperature in the upper 100 m at southern, central and northern locations plotted for the Julian days 304 (31st October), 307 (3rd November) and 309 (5th November) respectively. These profiles indicate considerable vertical and horizontal variability. At all the locations, the temperature of the mixed layer is about 28.5°C, but at 100 m depth the waters are cooler (19°–21°C) at the southern location and warmer (23°–24°C) at the northern location. Vertical excursions in the thermocline are large at the southern location and minimum at the northern location. The temporal variations in temperature in the upper 100 m water column are minimum at the northern location when compared to that at the southern and central locations. At southern location, the surface mixed layer is deep (70 m) at 0355 hrs and shoaled to 25 m at 0030 hrs of the following day (figure 2a). At central location, the surface mixed layer is about 20 m thick and among the profiles, the minimum temperature difference is noticed at 50 m (figure 2b). At the northern location, surface mixed layer is homogenous up to 40 m and among the profiles, the minimum temperature difference can be found at 25 m (within the mixed layer) and at 90 m (within thermocline).

Thermosalinograph measured continuous near-surface (∼3 m depth) temperature data (corrected with the bucket SST data) is used to examine the diurnal variation of near-surface temperature and its deviation over the daily mean value is presented in figures 3(a–c) at the southern, central and northern locations. At southern location, diurnal range is about 0.5°C with a maximum positive deviation value occurring at 1300 hrs and minimum value at 2000 hrs (figure 3(a)). At the central location, the diurnal range is large (0.8°C) with the minimum deviation at 0200 hrs and maximum deviation (0.55°C) occurring at 1500 hrs (figure 3(b)) due to intense insolation on this day under cloud free and low wind speed conditions. The temperature curve sharply drops to 0.1°C by 1600 hrs. At northern location, the temperature curve shows a range of 0.47°C with minimum deviation (−0.25°C) around 0500 hrs and maximum deviation (0.22°C) at 1300 hrs and after 1300 hrs the
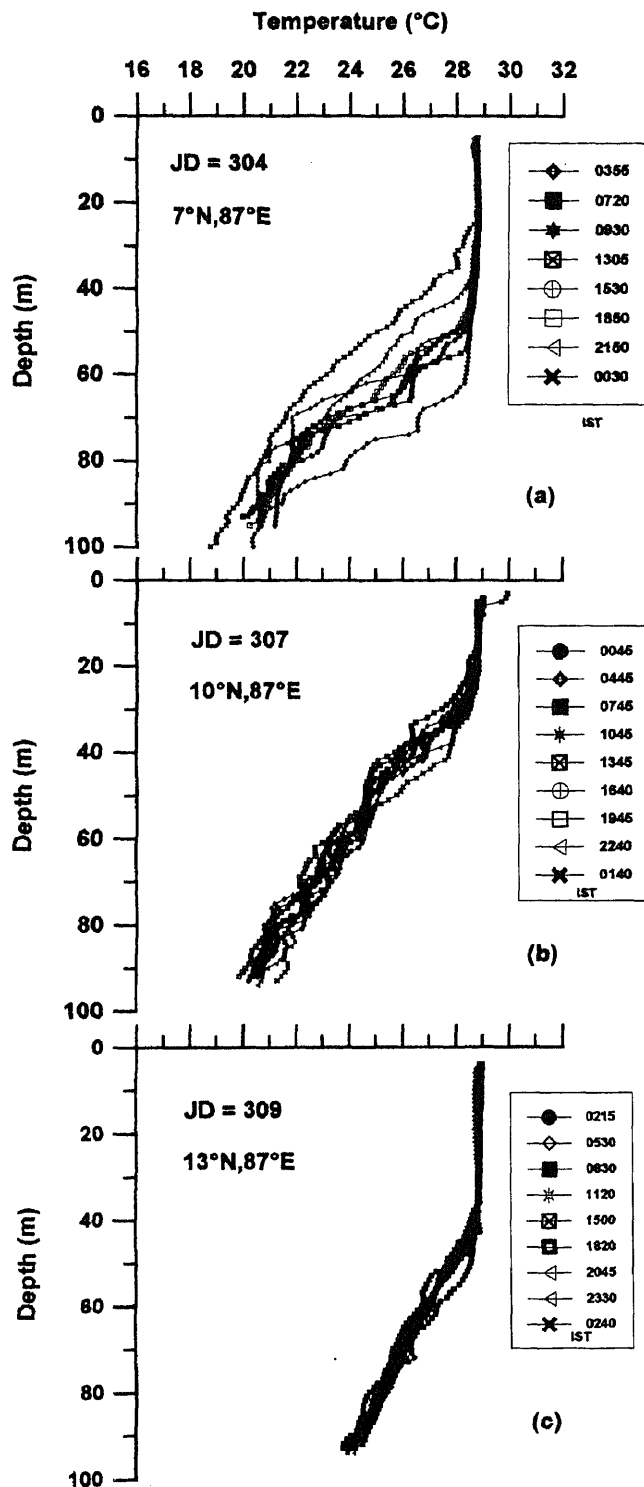


Figure 2. Profiles of temperature in the upper 100 m at the time-series locations: (a) 7°N, 87°E, (b) 10°N, 87°E and (c) 13°N, 87°E for the Julian days 304 (31st October), 307 (3rd November) and 309 (5th November) respectively.

(figure 3(c)). From the above, it can be seen that the diurnal temperature curve at southern location is atypical with the occurrence of minimum temperature at night hours, when compared to that at central and
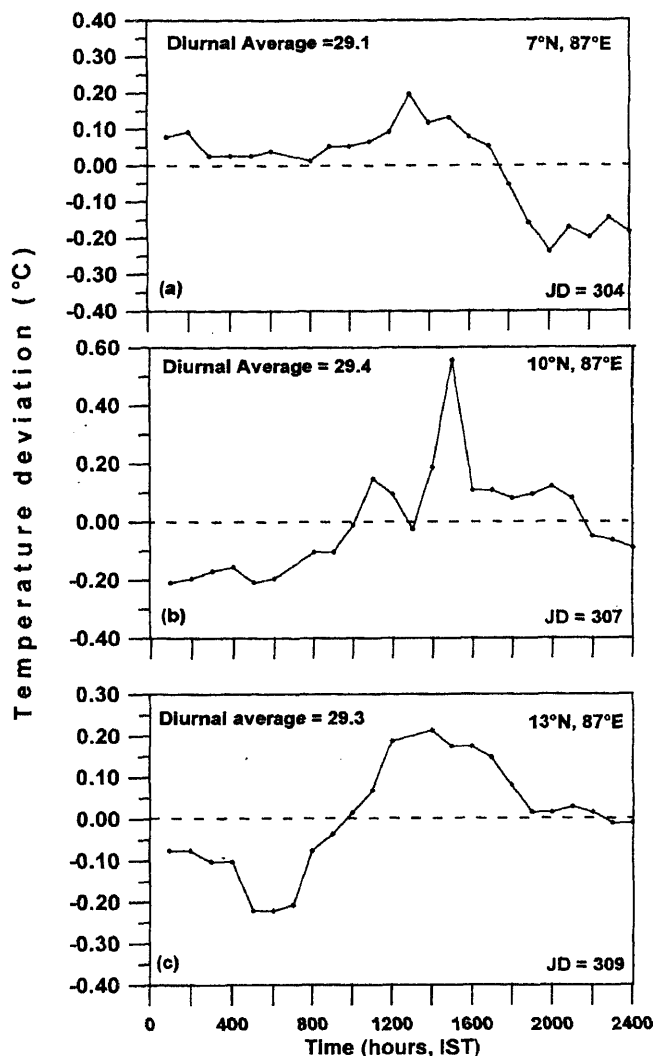
Figure 3. Diurnal variation of deviation of near-surface temperature (∼ 3 m below surface) from the daily mean value at the time-series locations: (a) 7°N, 87°E, (b) 10°N, 87°E and (c) 13°N, 87°E for Julian days 304, 307 and 309 respectively, based on thermosalinograph measurements. Please note the change in the upper limit of ordinate scales.

Utilising the CTD data, the diurnal variation of temperature at subsurface depths (below 3 m) is examined as deviations over the daily mean value at three depths, viz., 5, 10, 20 m at all the three locations (figures 4(I)a–c, 4(II)a–c and 4(III)a–c). The diurnal temperature curves at southern location at these depths also are atypical with large minimum occurring at night hours (2000–2100 hrs). At the central and northern locations, the diurnal curves of temperature are typical with a minimum value at early hours and maximum value around noon at the depths of 5 and 10 m. The trend of diurnal variation is reversed at 20 m depth at all the locations. In general, the diurnal range of temperature decreased with depth. At southern location, the diurnal range of temperature at 5 m is the same as that at surface (figure 4(I)a and figure 3a). The diurnal range dropped to as low as 0.1°C at 10 m. At 20 m, the trend of diurnal variation

is reversed and the temperature deviation is close to zero, suggesting that the diurnal temperature curve is affected by the vertical excursions in the thermocline (figure 2(a)). At central station, the daily mean temperature decreases from 5 m to 20 m (figure 4(IIb)). The diurnal range of temperature deviation is exceptionally large i.e., 0.9°C at 5 m (figure 4(IIb)) and shows a typical diurnal cycle as that at near-surface (figure 3(b)). This indicates the penetration of intense solar radiation up to this depth under fair weather conditions with low wind speeds. At northern location, the diurnal range of temperature is considerably small (0.26°C) at both 5 m and 10 m and further decreased to 0.2°C at 20 m (figure 4(IIIc)).

The upper layer heat content (H) is computed up to 50 m depth wherein the diurnal temperature curve penetrates close to 20 m depth. The diurnal variation of deviation of H from the daily mean value at the three locations (figures 5(a–c)) is large during night and is negative at southern location and positive at the other two stations. This indicates that the trend of heat storage over the diurnal cycle is heat loss from the upper layer at southern location and heat gain to this layer at central and northern locations and the heat gain is relatively more at central location (figure 5(b)). The heat loss from the upper layer at southern location results from the upward shift of the thermocline in association with the intense convective activity followed by overcast skies and synoptic weather disturbance. The lesser (0.5°C) diurnal range of temperature at the southern location is due to the prevailing synoptic weather conditions, as against the larger diurnal range of 0.8°C at the central location where fair weather conditions with intense solar radiation prevailed.

### 3.2 Diurnal variation of surface meteorological parameters and surface heat budget components

The diurnal variability of the meteorological forcing at the sea surface at the three locations is presented in figures 6(a–j). For this purpose, we used the AWS recorded meteorological parameters. The wind speed and direction over the diurnal period at the three locations exhibited wide variations both in the direction and speed (figures 6(a–b)). At southern location, on 31st October, the wind speeds were low (< 5 m/s) and changed from west to northwest/north from 0000 hrs to 1200 hrs (figure 6(a)). Moderate (> 5 m/s) southwesterly winds prevailed from 1200 hrs to 2400 hrs. On the previous day, 30th October, 1998, the winds were from southwest with relatively strong speeds (10 m/s) in the early morning and weaker wind speeds (2.5 m/s) around noon. At central location, on 3rd November, winds were variable (southerly/northwesterly) with speeds between 2 and 9 m/s during the first half of the day. The winds became weak (< 4 m/s) southwesterlies during the second half of the day. As
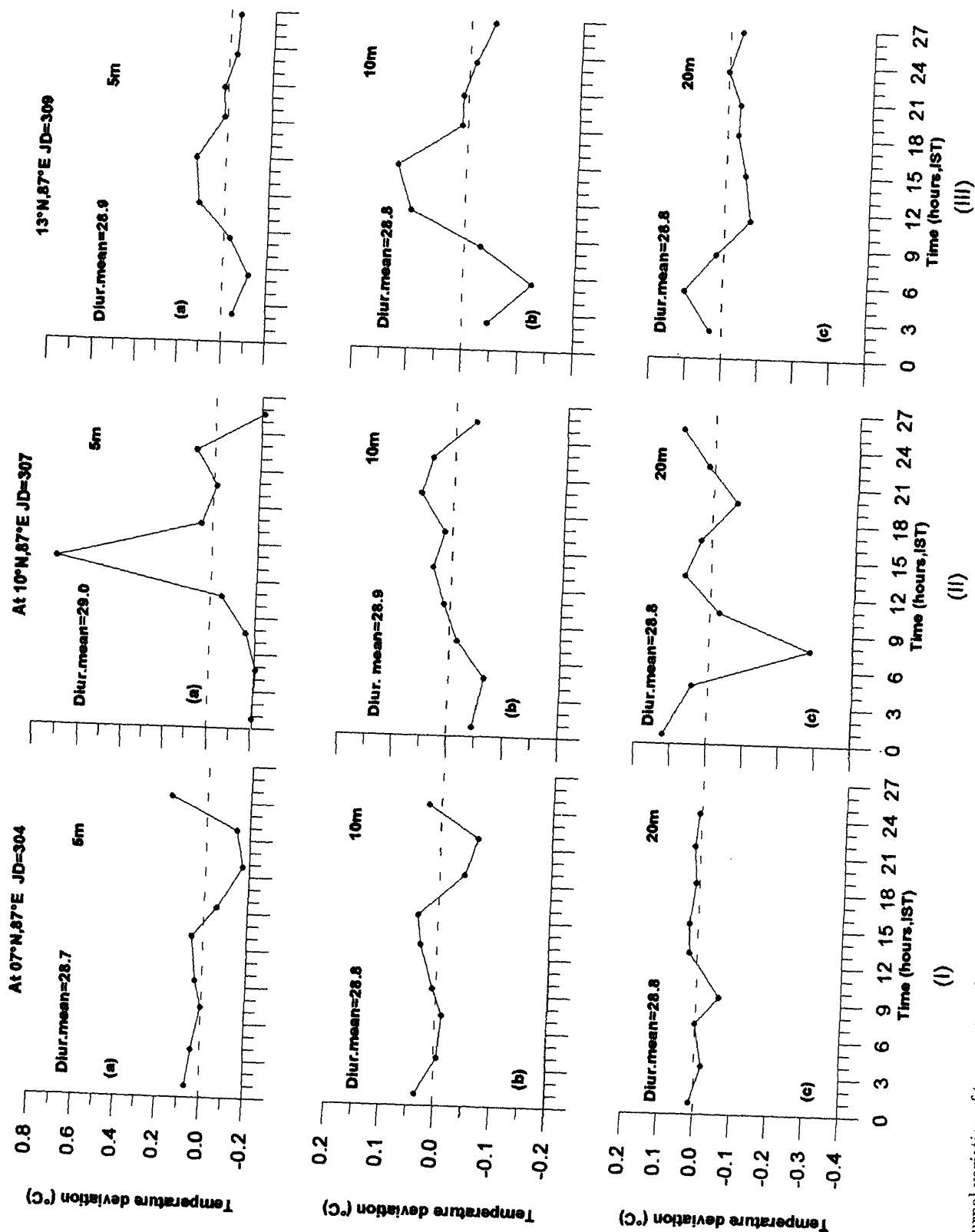
Diurnal variation of temperature deviation from the daily mean value at (a) 5 m, (b) 10 m and (c) 20 m depths for the time-series locations: (I) 7°N, 87°E, (II) 10°N, 87°E, (III) 13°N, 87°E on Julian days 304, 307 and 309 respectively. Please note the change in the scales of ordinate in (a) to (c).
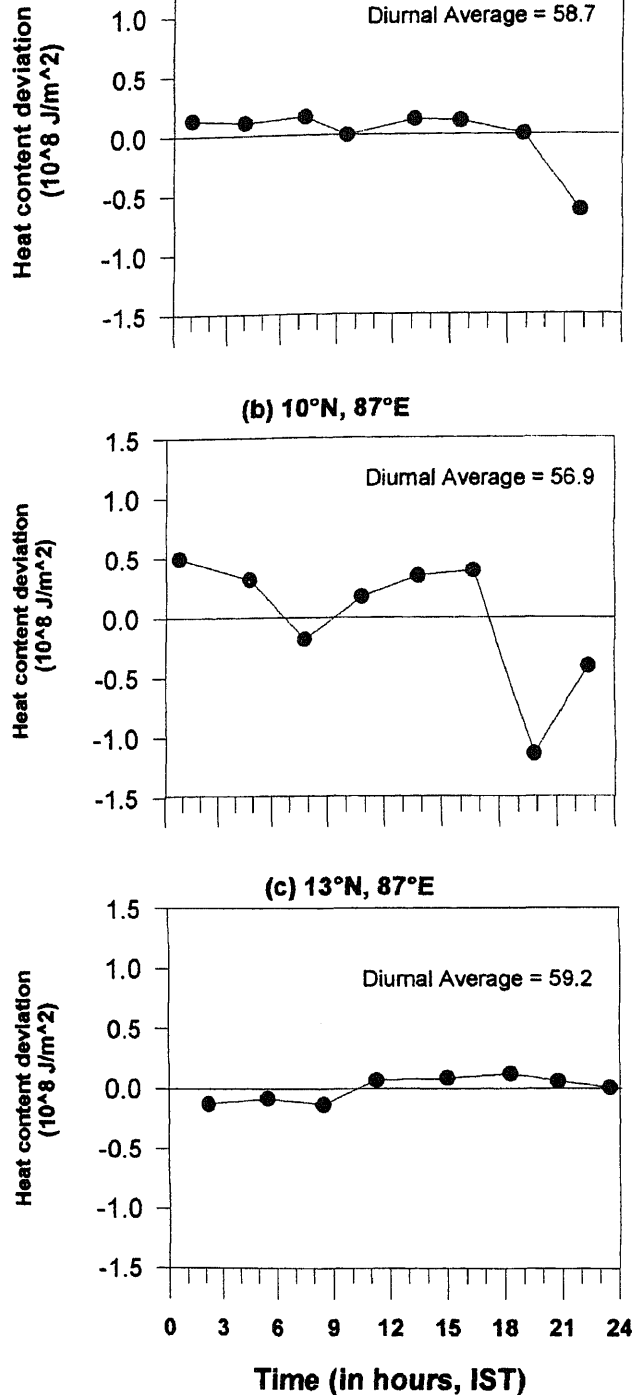
Figure 5. Diurnal variation of upper ocean (0–50 m) heat content deviation from its daily mean value at the time-series locations: (a) 7°N, 87°E, (b) 10°N, 87°E and (c) 13°N, 87°E for the Julian days 304, 307 and 309 respectively.

noticed above, these weak winds help enhancing the diurnal range of temperature at this location with higher SSTs around noon. On the previous day, i.e., on 2nd November, the weather parameters indicate prevalence of fair weather conditions. At northern

The atmospheric pressure at the sea surface showed a typical diurnal variation at all the locations (figure 6(c)) with two maxima (at 0900 and 2100 hrs) and two minima (0300 and 1400 hrs). However, typically lower pressures occurred at the central and northern stations between 1200 and 2400 hrs depicting the influence of warmer SSTs under fair weather conditions. Air temperature exhibited wide variations at southern and central locations; a drastic decrease of 4°C at afternoon hours at southern location and a significant increase of 6°C from 0700 to 1000 hrs at central location (figure 6(d)). On the previous day (30th October) also, the air temperature at southern location showed a drastic decrease by 4°C from noon to evening hours. This decrease in air temperature is in association with the change of northerly wind to southwesterly winds followed by decrease in SST and increase of R.H. by 10% (not shown here), indicating the northward passage of synoptic disturbance (cloud bands). At northern location, diurnal variation of air temperature is comparatively less. Associated with the significant changes in air temperature, the relative humidity exhibited wide variation; lower R.H. (50–70%) at the southern location and higher R.H. (80–90%) at the northern location (figure 6(e)). At the southern location, the drastic decrease of SST and air temperature followed by 20% increase in R.H. (figure 3(a) and figure 6(e)) may be related to the downdraft associated with the synoptic disturbance. Similarly, at the central location, the increase of SST and air temperature followed by a decrease in R.H. by about 15% from 0000 hrs to 1200 hrs could be related to the intense solar radiation due to fair weather conditions and clear skies.

The diurnal variation of global solar radiation reaching the sea surface at the three locations (figure 6(f)) shows a day-maximum at noon at southern and northern locations; the maximum is only 400 W/m$^2$ at southern location while it is large (1000 W/m$^2$) at northern location. The overall low magnitudes of solar radiation at southern location reflect the significant influence of synoptic weather system and the associated overcast skies. It is to be noted that at the same location the magnitude of maximum radiation is large (1000 W/m$^2$) on the previous day, i.e., 30th October (not shown).

The computed effective back radiation ($Q_b$) and the sensible heat flux ($Q_h$) curves (figures 6(g–h)) exhibited similar diurnal patterns. These variations correspond largely on the prevailing weather events of clear skies and intense convection. At southern location, the higher magnitudes of $Q_b$ and $Q_s$ during 1200–1700 hrs are associated with the downdraft event (lower air temperature and higher relative humidity) and the resulting large sea-air temperature
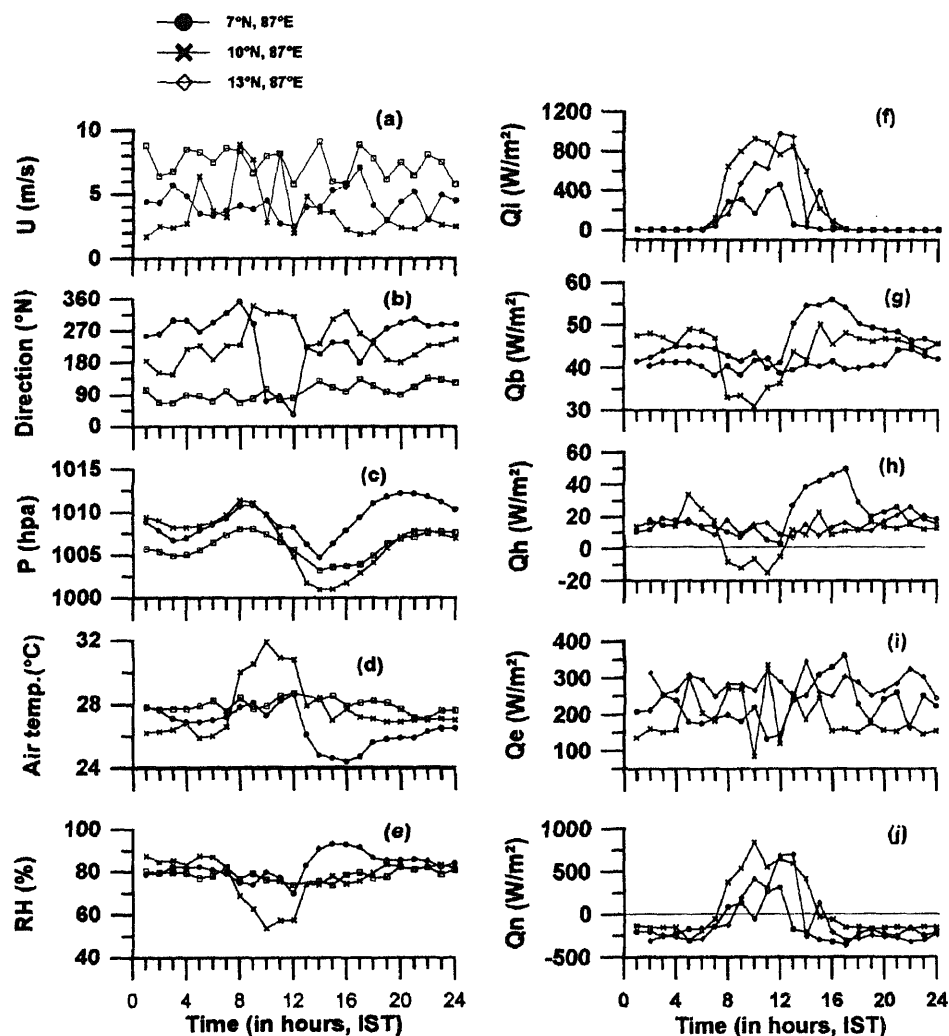
Figure 6. Diurnal variation of various surface meteorological parameters and surface heat budget components at the time-series locations: (a) 7°N, 87°E, (b) 10°N, 87°E and (c) 13°N, 87°E for the Julian days 304, 307 and 309 respectively.

difference (2.5°C). Similarly, at central location, the lowest values of $Q_b$ and negative $Q_h$ during 0800–1200 hrs correspond to the intense radiation event (warmer air temperature and lower relative humidity). At northern location, both $Q_b$ and $Q_s$ varied around $40\,W/m^2$ and $10\,W/m^2$ respectively. The latent heat flux $(Q_e)$ is the most important component of the surface heat budget of the tropical ocean and compensates the effect of sea surface heating due to solar radiation. The magnitudes of $Q_e$ are between 100 and $350\,W/m^2$ (figure 6(i)). The latent heat flux increased rapidly from $125\,W/m^2$ to $350\,W/m^2$ during the period of downdraft at southern location and reached a peak minimum $(80\,W/m^2)$ at the time of (1000 hrs) intense radiation at central location. It is, in general, high (above $200\,W/m^2$) at northern location where higher wind speeds occurred.

The pattern of net heat flux $(Q_n)$ which is estimated as the residual of the surface heat budget is similar to

sea surface gained heat during this part of the day (figure 6(j)). Over the diurnal cycle, the sea surface loses heat energy to a tune of $144\,W/m^2$ at southern location and nearly half of this amount at northern location (table 2). However, at central location, the sea surface gained heat energy (table 2), mainly due to intense solar radiation under relatively low cloudiness and wind speeds, contributing to higher daily mean SST at 10°N (table 2).

The large net heat loss at the sea surface and the northward passage of synoptic disturbance (cloud band) from 3°N during 30th – 31st October 1998 at southern location have led to the shoaling mixed layer depth (MLD) and isotherms (28°, 27°, 26° and 20°C) in the thermocline (figure 7(a)). At central location, deepening of MLD and the isotherms by the end of the day (3rd November, 1998) is evident in figure 7(b). At northern location, the diurnal variation of MLD and the depth of chosen isotherms is minimum (figure 7(c))

Table 2. *Diurnal averages of SST, wind speed (U), relative humidity (R.H.), heat input through solar radiation (Q_i), heat loss components due to sensible heat flux (Q_h), latent heat flux (Q_e), effective back radiation (Q_b) and net surface heat flux (Q_n) at the time-series locations. Positive (negative) value of $Q_n$ indicates heat gain (loss) at sea surface.*

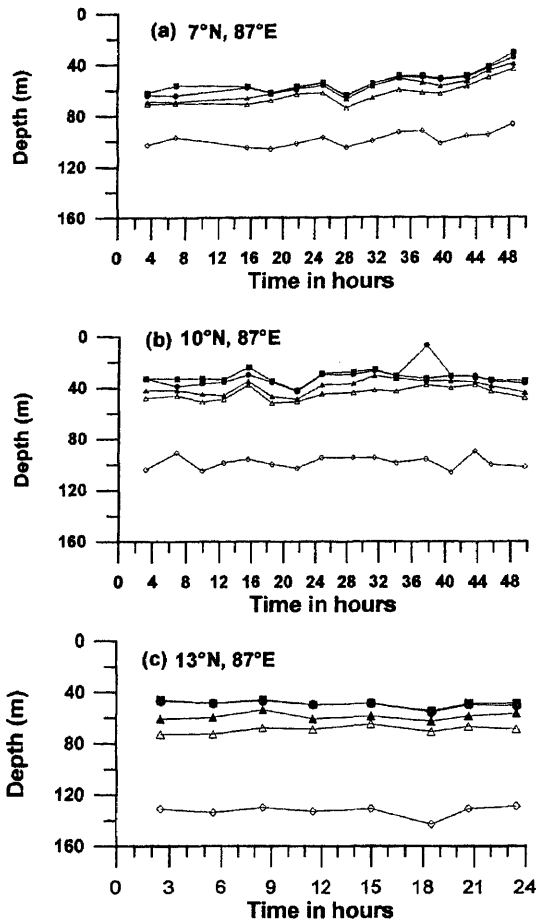| Location/Julian day | SST (°C) | $U$ (m/s) | R.H. (%) | $Q_i$ (W/m²) | $Q_h$ (W/m²) | $Q_e$ (W/m²) | $Q_b$ (W/m²) | $Q_n$ (W/m²) |
|---|---|---|---|---|---|---|---|---|
| 07°N,87°E/304 | 29.1 | 4.1 | 83 | 79 | −28 | −206 | −48 | −144 |
| 10°N, 87°E/307 | 29.4 | 3.5 | 77 | 260 | −10 | −134 | −44 | 72 |
| 13°N, 87°E/309 | 29.3 | 7.2 | 78 | 206 | −15 | −228 | −41 | −78 |



Figure 7. Diurnal variation of mixed layer depth and depths of selected isotherms (28°, 27°, 26° and 20°C) at the time-series locations: (a) 7°N, 87°E, (b) 10°N, 87°E and (c) 13°N, 87°E for the Julian days 303–304, 306–308 and 309 respectively.

## 3.3 *Diurnal variation of VM-ADCP measured currents in the upper layer*

The VM-ADCP (150 kHz, RD Instruments, USA) measured currents at 31 m and 51 m at the three locations are shown in figures 8 and 9 respectively. The current vectors represent the 10 minute averaged velocities, considered only when the ship's speed was below 2 knots. This explains the gaps between the current vectors and is more evident at the northern location where the observed winds were strong and the vessel drifted northwestward with speeds exceed-

southern and central locations, the current vectors are shown for the 2-day period of time-series observations (figures 8(a–b), 9(a–b)). The direction of flow at 31 m and 51 m depths is almost similar at all the three locations. At southern location, the eastward current is predominant on the first day (00–24 hrs; 30th October, Julian day = 303) and changed to north-eastward on the 2nd day (24–48 hours; 31st October, Julian day = 304 in figures 8(a), 9(a)). This change in the current direction is in agreement with the change of winds to southwesterly under the influence of the northward passage of the synoptic disturbance (as discussed above). At central location, there appears a change in the flow from the first day (2nd November, Julian day = 306, 00–24 hours) to the second day (3rd November, Julian Day = 307, 24–48 hours). On the first day, the currents at 31 m and 51 m depths are directed north-north-east and northwestward. On the second day, the flow is changed between north and northeast (figures 8(b), 9(b)). The current vectors at northern location show strong flow with a predominant northwestward current at 31 m and 51 m depths (figures 8(c), 9(c)). The diurnal and tidal variations in the measured currents on the Julian days 304, 307 and 309 at southern, central and northern locations respectively are nearly absent. The mean current in the layer 31–51 m on each day at the locations is shown in table 3. At the southern and central locations, the mean current in the layer intensified from the 1st day to the 2nd day. The mean current in the layer also intensifies from 21 cm/s in the south to 71 cm/s in the north (table 3). This strong current speed at the northern location agrees well with the gesotrophic velocity computed between 12°N and 13°N from the hydrographic data (Rameshbabu *et al* 2000). The mean current vectors on the Julian days 304, 306 and 307 are depicted in figure 1. The northward flow of mean currents in the 31–51 m layer (depicted in figure 1 and shown in table 3) is consistent with the cyclonic circulation with a meridional flow towards north along 87°E as derived from the thermohaline fields (Rameshbabu *et al* 2000).

## 3.4 *Upper ocean heat budget*

The rate of change of heat storage in the oceanic upper layer is obtained as the difference between the

**Currents at 31m depth**

25 cm/s

(c) 13°N, 87°E

(b)10°N, 87°E

(a) 7°N, 87°E

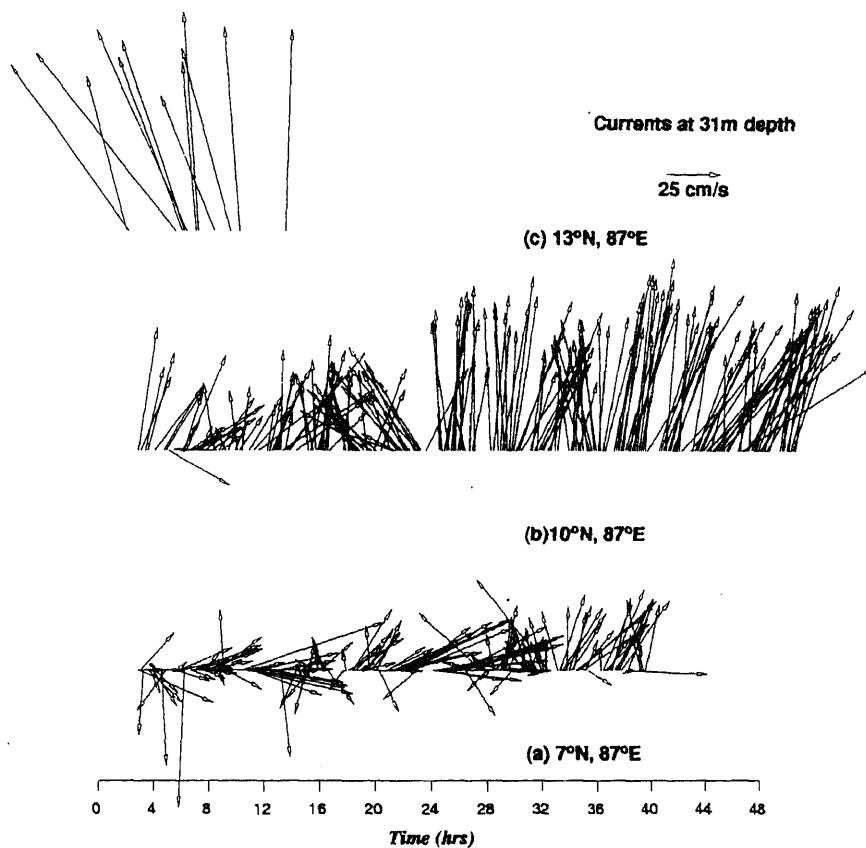| 0 | 4 | 8 | 12 | 16 | 20 | 24 | 28 | 32 | 36 | 40 | 44 | 48 |

*Time (hrs)*

Figure 8.   Temporal variation of VM-ADCP measured currents vectors at 31 m depth at the time-series locations: (a) 7°N, 87°E, (b) 10°N, 87°E and (c) 13°N, 87°E for the Julian days 303–304, 306–307 and 309 respectively.
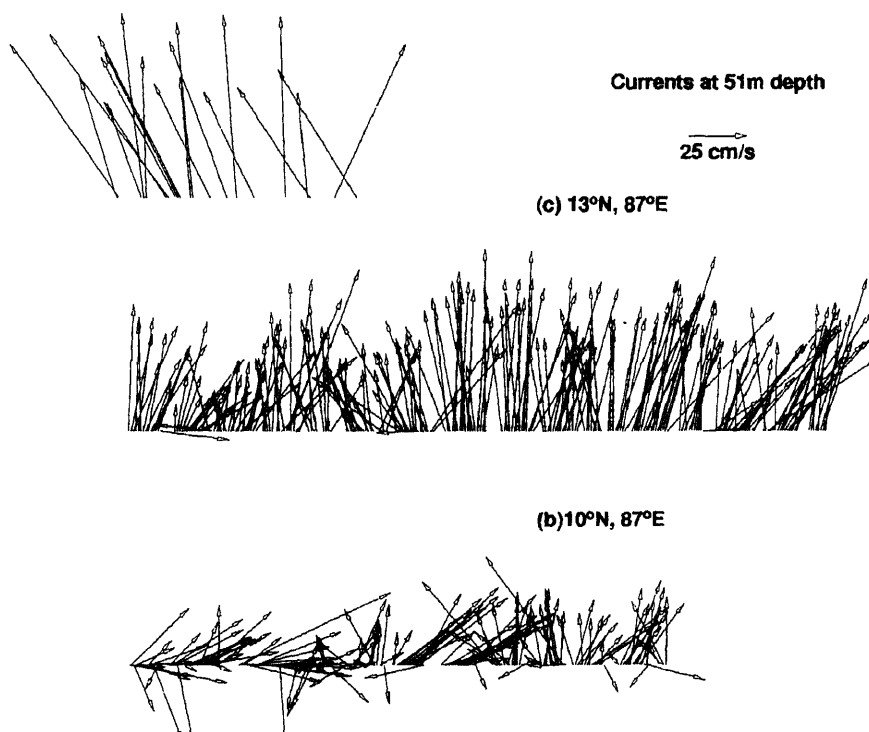


**Currents at 51m depth**

25 cm/s

(c) 13°N, 87°E

(b)10°N, 87°E

Table 3. *Diurnal averages of currents in the layer 31–51 m at the three time-series locations during BOBMEX-Pilot.*

| Location/Julian day | $U$ Zonal comp. (cm/s) | $V$ Meridional comp. (cm/s) | Vectoral current speed (cm/s) | Vectoral direction of current |
|---|---|---|---|---|
| 07°N,87°E/303 | 14.42 | 6.27 | 16.0 | 67° |
| 304 | 9.19 | 18.86 | 21.0 | 26° |
| 10°N, 87°E/306 | 1.21 | 29.39 | 29.4 | 2° |
| 307 | 11.17 | 52.18 | 53.3 | 12° |
| 13°N, 87°E/309 | −19.30 | 68.45 | 71.0 | 344° |

heat across the bottom surface of this layer (Zavialov and Murty 1995, Delnore 1972). At the time-series locations, the upper ocean heat budget is studied considering the 1-D upper layer heat balance equation of Zavialov and Murty (1995) wherein the horizontal advection of heat is not considered. An examination of the time-series temperature profiles at each location (figures 2(a–c)) suggests that the lower boundary of the upper layer can be chosen at 50 m depth where minimum temperature difference is evident (with slight exception of two profiles at southern location). Further, the diurnal variability of temperature is very much confined to the upper 15–20 m layer, well within the chosen 50 m water column. The net heat flux at the sea surface at the three locations is given in table 2. The rate of net heat gain in the upper 50 m water column over the diurnal cycle ($\Delta H = H_{24} - H_{00}$) is estimated as the difference of heat content at 0000 hrs from that at 2400 hrs (Zavialov and Murty 1995).

The net heat gain in the oceanic upper layer may be written as:

$$\Delta H = (Q_n - Q_{bott})\Gamma \tag{3}$$

where $Q_{bott}$ is the heat flux at the lower boundary (50 m depth) of the upper layer and $\Gamma = 24$ hours ($= 86400$ s). The heat storage in the oceanic upper layer over the diurnal cycle ($Q_t$) can be obtained from ($Q_t = \Delta H/\Gamma$).

The heat flux across the lower boundary ($Q_{bott}$) of the upper layer can be estimated from the equation (Zavialov and Murty 1995):

$$Q_{bott} = -K_h \cdot \rho \cdot C_p(dT/dz) \tag{4}$$

where $K_h$ is the depth-averaged eddy diffusivity coefficient of heat, $\rho$ is the water density and $C_p$ is the specific heat at constant pressure and $dT/dz = $ temperature gradient of mean temperatures at surface

and 50 m depth. The negative sign on the R.H.S. indicates that the $Q_{bott}$ is downward (from the layer).

Firstly, the value of $Q_{bott}$ is estimated from the values of $Q_t$ and $Q_n$ (table 4). Then the values of $Q_{bott}$ are substituted in (4) along with $dT/dz$ values (table 4) to estimate the depth averaged $K_h$ (table 4). The variation of $K_h$ from south to north is more closely related to the daily mean $Q_i$ values (table 2) rather than the daily mean wind speed (Hoeber 1972); the large value of $K_h$ is associated with lower value of $Q_i$ and vice versa (table 2 and table 4). The order of magnitudes of $K_h$ are in agreement with that reported by Zavialov and Murty (1995) for the upper layers of the equatorial Arabian Sea.

While the upper layer loses heat at southern location, it gains heat at the central and northern locations (values of $Q_t$ in table 4). It is more interesting to note that the upper layer loses heat across both the upper and lower boundaries at southern location, where intense convection and passage of cloud bands characterise the synoptic weather and the thermocline shoals up (figure 7(a)). This emphasises the response of the upper ocean to the passage of large cloud band followed by intense convection and overcast skies. The computed eddy diffusivity coefficient of heat is extremely large (0.0235 m²/s) at the southern location (table 4), suggesting that the upper ocean heat budget at this location (7°N, 87°E) is controlled by 1-D processes under the given synoptic weather conditions. On the contrary, at central and northern locations, the upper ocean gained heat mainly across the lower boundary, as the net surface heat flux is small (positive at the central location and negative at northern location). This upper ocean gain can be realised as the manifestation of thermocline deepening (evident from the profiles of temperature in figures 2(a–c) and depths of 20°C isotherm in figures 7(a–c))

Table 4. *Diurnal averages of oceanic upper layer heat budget parameters at the three time-series locations during BOBMEX-Pilot. [$Q_n$ = net heat flux at sea surface (upper boundary of the layer), $Q_t$ = rate of heat storage in the upper layer, $Q_{bott}$ = heat flux across the lower boundary (at 50 m depth) of the layer, $dT/dz$ = mean temperature gradient of the layer (0–50 m) and $K_h$ = the depth-averaged eddy diffusivity coefficient of heat. Positive (negative) values of $Q_n$ and $Q_t$ denote heat gain (loss) in (from) the layer. Positive (negative) value of $Q_{bott}$ indicates heat loss (gain) from (into) the layer.]*

| Location/Julian day | $Q_n$ (W/m²) | $Q_t$ (W/m²) | $Q_{bott}$ (W/m²) | $dT/dz$ (°C/m) | $K_h$ (m²/s) |
|---|---|---|---|---|---|

which in turn takes place due to mass convergence in the upper layer. The northward intensification of upper layer mean currents (figure 1 and table 3) supports the thermocline deepening. At these locations, the prevailing synoptic weather was fair with almost clear skies and sea surface gains heat at central location and sea surface loses heat at northern location. Further, the computed diffusivity coefficient of heat shows extremely lower value ($0.0045\,\mathrm{m^2/s}$) at southern location and relatively higher value ($0.0150\,\mathrm{m^2/s}$) at northern location. These smaller values of $K_h$ (compared to that at southern location), higher mean currents and heat gain in the upper layer suggest that the horizontal advective processes dominate over the 1-D processes in the upper layer heat budget, when synoptic weather is fair. It appears that the air-sea coupling is of complex nature during fair weather conditions when compared to that during intense convective activity followed by synoptic disturbances and overcast skies.

## 4. Conclusions

Upper ocean time-series data from three locations ($7°$N, $10°$N and $13°$N along $87°$E) in the southern Bay of Bengal have been analysed. The diurnal variation of temperature varied between $0.5°$C and $0.8°$C and the diurnal temperature curve penetrated up to 15–20 m depth. The incoming solar radiation reduced significantly at southern location ($7°$N) under the influence of synoptic weather system and the associated overcast skies. The downdrafts associated with the weather depression enhanced the air-sea heat fluxes at the southern location. The study area experienced net surface heat loss both at southern and northern ($13°$N) locations and net heat gain at central location ($10°$N). The upper ocean lost heat energy at southern location and gained heat at central and northern locations. The estimated eddy diffusivity coefficient of heat is large ($0.0235\,\mathrm{m^2/s}$) at $7°$N and low ($0.0045\,\mathrm{m^2/s}$) at $10°$N. The upper layer heat budget suggests that the air-sea coupling at southern location is relatively simple through 1-D processes, during intense convective activity associated with the passage of cloud band followed by synoptic weather disturbance and overcast skies. On the other hand, the air-sea coupling is of a complex nature with the horizontal advective processes dominating over the 1-D processes during the fair weather with clear skies, as at central and northern locations.

## Acknowledgements

## References

Anon 2000 BOBMEX-Pilot CD-ROM; National Institute of Oceanography Goa

Bhat G S, Ameenulla S, Venkataramana M and Sengupta K 2000 Atmospheric boundary layer characteristics during BOBMEX-Pilot experiment; *Proc. Indian Acad. Sci. (Earth Planet. Sci.)*, (this issue)

Delnore V E 1972 Diurnal variation of temperature and energy budget for the oceanic mixed layer during BOBMEX; *J. Phys. Oceanogr.* **2** 239–247

Hoeber H 1972 Eddy thermal conductivity in the upper 12 m of the tropical Atlantic; *J. Phys. Oceanogr.* **2** 303–304

Murty V S N, Sarma Y V B and Rao D P 1996 Variability of the oceanic boundary layer characteristics in the head of the Bay of Bengal during MONTBLEX-90; *Proc. Indian Acad. Sci. (Earth Planet. Sci.)* **105** 41–61

Rameshbabu V, Murty V S N, Rao L V G, Prabhu C V and Tilvi V 2000 Thermohaline structure and circulation in the upper layers of the southern Bay of Bengal during BOBMEX-Pilot (October – November 1998); *Proc. Indian Acad. Sci. (Earth Planet. Sc.)* (this issue)

Rao R R, Ramam K V S, Rao D S and Joseph M X 1985 Surface heat budget estimates at selected areas of north Indian Ocean during MONEX-77; *Mausam* **36** 21–32

Rao D S and Rao R R 1986 A case study of the genesis of a monsoon low and the thermal structure of the upper north Bay of Bengal during MONEX-79; *Mahasagar* **19** 1–9

Rao R R 1987 On the thermal response of the upper central Arabian Sea to the summer monsoonal forcing during MONSOON-77; *Mausam* **38** 293–302

Rao R R and Kumar K V S 1991 Evolution of salinity fields in the upper layers of the east central Arabian Sea and northern Bay of Bengal during summer monsoon experiments; *Proc. Indian Acad. Sci. (Earth Planet. Sci.)* **100** 69–78

Rao R R, Mathew B and Hareesh Kumar P V 1993 A summary of results on thermocline variability in the upper layers of the east central Arabian Sea and Bay of Bengal during summer monsoon experiment; *Deep-Sea Res.* I **40** 1647–1672

Sanilkumar K V, Mohankumar N, Joseph M X and Rao R R 1994 Genesis of meteorological disturbances and thermocline variability of the upper layers in the head of the Bay of Bengal during Monsoon Trough Boundary Layer Experiment (MONTBLEX-90); *Deep-Sea Res.* **41** 1569–1581

Sarma Y V B, Seetaramayya P, Murty V S N and Rao D P 1997 Influence of the monsoon trough on air-sea interaction in the head of the Bay of Bengal during the southwest monsoon of 1990 (Monsoon Trough Boundary Layer Experiment-90); *Boundary-layer Meteor.* **82** 517–526

Sarma Y V B, Murty V S N and Rao D P 1997 *Themodynamics of the oceanic and atmospheric boundary layers over head of the Bay of Bengal during the southwest monsoon of 1990.* NIO Technical Report No. NIO/TR-3/97, pp. 35

Stevenson J W 1982 *Computation of heat and momentum fluxes at the sea surface during the Hawaii to Tahiti Shuttle Experiment*; Tech. Rep. JIMAR No. 82-0044, University of Hawaii Press, Hawaii, Honolulu, pp. 42

Zavialov P O and Murty V S N 1995 Estimation of eddy diffusivity coefficient of heat in the upper layers of equatorial Arabian Sea; *Indian J. Mar. Sci.* **24** 177–185

# Controls of dimethyl sulphide in the Bay of Bengal during BOBMEX-Pilot cruise 1998

D M SHENOY*, M DILEEP KUMAR* and V V S S SARMA**

*National Institute of Oceanography, Dona Paula, Goa 403 004, India.
**CEREGE, Université d'Aix-Marseille III, Europole de l'Arbois, BP 80, Cedex 4 13545
Aix En Provence, France.

The air-sea exchange is one of the main mechanisms maintaining the abundances of trace gases in the atmosphere. Some of these, such as carbon dioxide and dimethyl sulphide (DMS), will have a bearing on the atmospheric heat budget. While the former facilitates the trapping of radiation (greenhouse effect) the latter works in the opposite direction through reflectance of radiation back into space by sulphate aerosols that form from oxidation of DMS in atmosphere. Here we report on the first measurements made on DMS in the Bay of Bengal and the factors regulating its abundance in seawater. Phytoplankton alone does not seem to control the extent of DMS concentrations. We find that changes in salinity could effectively regulate the extent of DMSP production by marine phytoplankton. In addition, we provide the first ever evidence to the occurrence of DMS precursor, DMSP, in marine aerosols collected in the boundary layer. This suggests that the marine aerosol transport of DMSP will supplement DMS gaseous evasion in maintaining the atmospheric non-sea salt sulphur budget.

## 1. Introduction

The oceans emit 20% of sulphur to the marine boundary layer in the form of DMS (Rodhe 1999), which is a non-sea salt sulphate compound. Marine phytoplankton produces DMSP for the maintenance of osmotic pressure between the cell fluid and the surrounding seawater (Liss *et al* 1993). Once released into seawater, through cell lysis or zooplankton grazing, DMSP is decomposed to DMS and acrylic acid. The DMS thus produced, being less soluble, escapes to the atmosphere where it is susceptible to photochemical degradation. The importance of DMS and its climatological implications invited the attention of those studying the boundary layer. The Indian Ocean is the least studied in this respect (Kettle *et al* 1999). The surface mixed layer in the bay of Bengal is maintained through the combined effects of wind forcing and fresh water run-off (Shetye and Gouveia 1998). The rivers from the Indian subcontinent drain about $1.6 \times 10^3$ km$^3$ of water into the bay annually. The strong vertical stratification, resulting from the low salinity lens at the surface, reduces effective upward transport of nutrients across the pycnocline (Rao *et al* 1994). Consequently, the column primary production is less in the Bay of Bengal than in the Arabian Sea (Qasim 1977). In addition, the bay is well known to be a highly turbulent region, particularly during monsoons. Therefore, it is important to understand the dynamics of gases of climatic importance in this region and their air-sea fluxes. For instance, atmospheric carbon dioxide is stated to find a sink in the Bay of Bengal (Kumar *et al* 1996) while the Arabian Sea is a perennial source (Sarma *et al* 1998). In the present attempt we try to understand the factors regulating DMS production in the bay.

## 2. Material and methods

### 2.1 *Measurements of water column parameters*

Data were collected during the Bay of Bengal Monsoon Experiment (BOBMEX) Pilot Cruise,
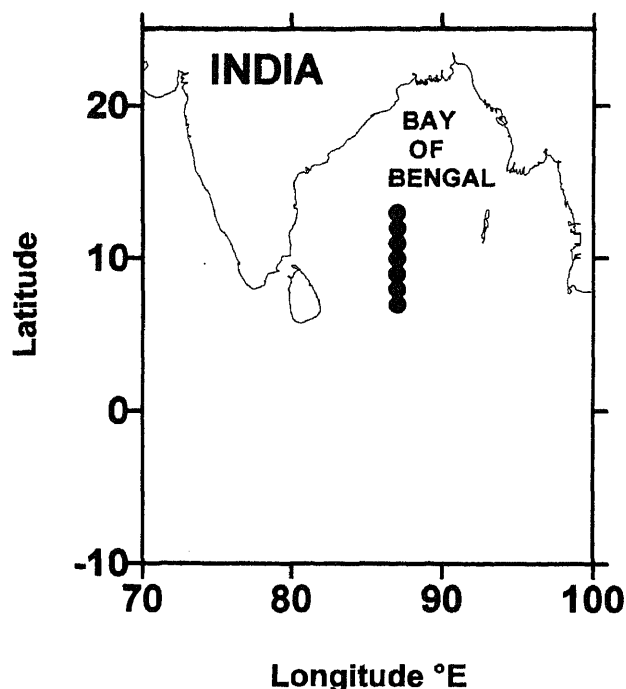
Figure 1. Locations of stations occupied during the BOB-MEX-Pilot cruise in the Bay of Bengal.

October – November 1998, on board ORV Sagar Kanya. Station locations are shown in figure 1. A Sea-Bird CTD system was used along with a rosette to collect water samples from the upper 250 m of the water column. Temperature, salinity and chlorophyll data were obtained through the use of respective sensors. Water samples were analyzed for oxygen, nitrate, chlorophyll, DMS and DMSP. Oxygen and

nitrate were analyzed by photometry. A SKALAR Autoanalyser was used in nitrate analysis. Chlorophyll samples, collected at selected stations, were processed on board and analyzed in the shore-based laboratory. These chlorophyll results were used to calibrate those obtained from the fluorescence sensor attached to the CTD system. DMS analysis was done through purging and cryogenic trapping technique (Turner et al 1990). Immediately upon sampling DMS samples were preserved at 4°C in dark glass bottles. Samples were analyzed within 24 hrs after sampling. The eluted DMS, under warm ($\sim 80°C$) conditions, was detected on a HP Gas Chromatograph equipped with Chromosil 330 separator column and Flame Photometric Detector. The precision of DMS analysis was found to be 8–10%. Samples for DMSP were immediately subjected to alkali hydrolysis (Turner et al 1990) during which it decomposed to DMS. Since the samples were not filtered our DMSP values represent total (dissolved + particulate) concentrations in water. Subsequently, DMSP was quantified in terms of DMS. Sea-to-air fluxes of DMS were calculated based on the formulations given by Turner et al (1996). Wind speeds were measured on board. For the purpose of sea-to-air flux calculations, DMS in the atmosphere was assumed to be zero since its concentration in air is about three orders of magnitude lower than that in seawater (Turner et al 1996; Andreae and Crutzen 1997).

### 2.2 Aerosol measurements

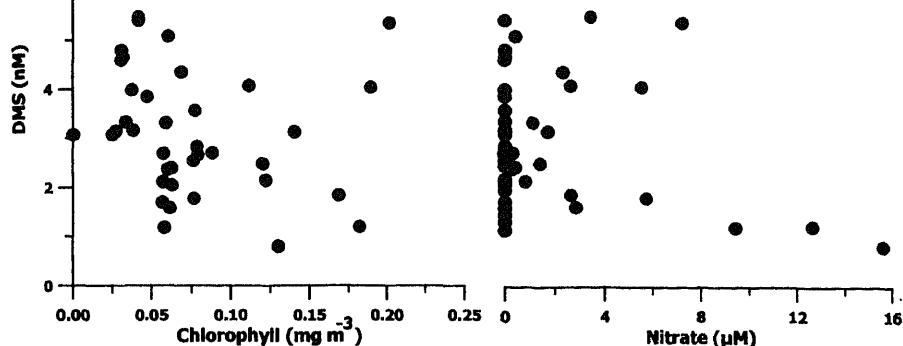Aerosol samples were collected at variable heights above the sea level on board the ship. Polycarbonate
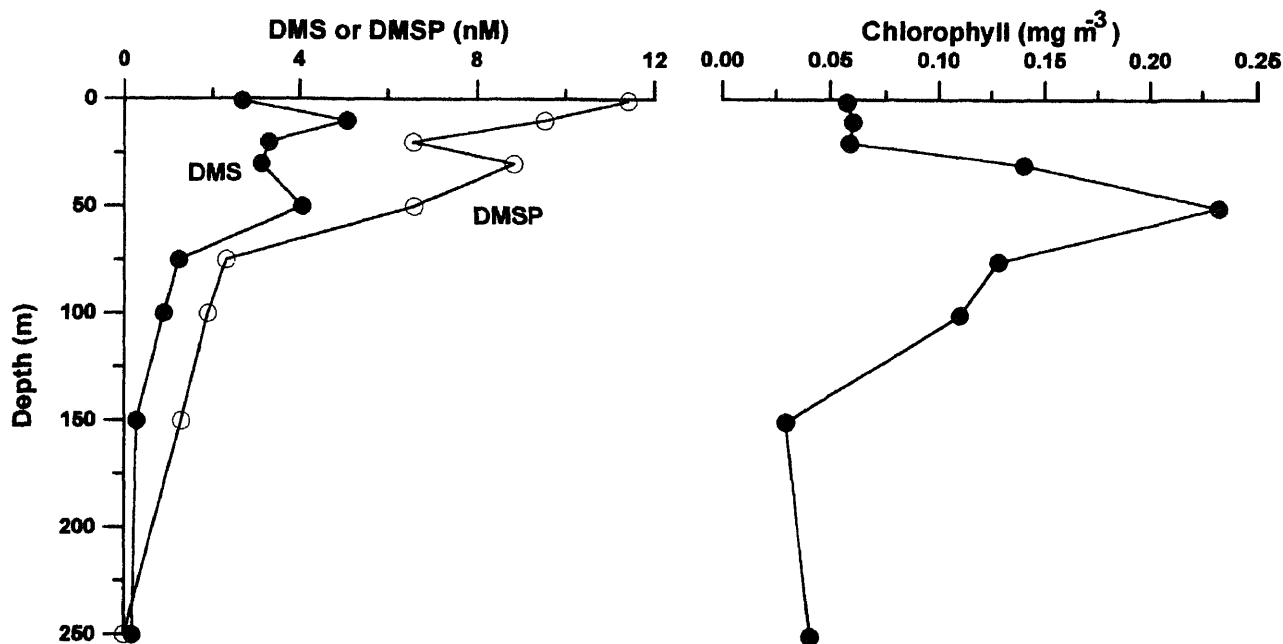
Figure 3. Relationships for DMS with chlorophyll and nitrate in the upper 30 m of the study region.

membrane filter papers of 0.4 μm pore size and 47 mm diameter were used to collect aerosols under vacuum. A Millipore pump with constant vacuum was used and the volume of air filtered was calculated. Immediately upon sampling the filter paper was transferred to the purging unit where it was first subjected to DMS analysis. Upon completion of DMS analysis, alkali was added to the filter paper and purging continued during which DMSP, on the filter, was quantitatively converted to DMS. Thus produced DMS was analysed as detailed above.

## 3. Results and discussion

### 3.1 Controls of DMS in water column

The concentrations of DMS and DMSP were higher in the upper 50 m and decreased to near zero levels at 250 m (figure 2). DMS and DMSP vertical profiles resembled mirror images in surface layers (upper 50 m) but are not necessarily so always. This is because of the fact that DMSP can be decomposed by phytoplankton and bacterial lyases in addition to photolysis (Andreae and Crutzen 1997). Moreover, DMS not only undergoes photolytic and bacterial decomposition but can also escape to atmosphere. The relations between vertical profiles of these reduced sulphur compounds and chlorophyll were not complementary (figure 2). For instance, although the chlorophyll was lower at the surface both DMS and DMSP were higher. When chlorophyll reached maximum the abundance of DMSP began to decrease. Figure 3 depicts relationships for DMS with chlorophyll and nitrate. In concurrence with the vertical trends there was no specific quantitative relation between DMS and chlorophyll. Similarly, nitrate also did not exhibit any clear relation with DMS. The extent of production of DMSP is proposed to decrease under nitrogen available conditions (Liss et al 1993). However, recent laboratory experiments revealed non-dependence of DMSP levels on nitrate availability (Keller et al 1999). Relation between nitrate and DMSP in the Bay of Bengal was poor. Our present observations (figure 3) concur well with the laboratory results of Keller et al (1999).

As chlorophyll and nutrients did not exhibit any control on DMS we attempted to find if physicochemical properties have any role to play. For this purpose we used salinity since this property shows large horizontal gradients in the surface layer of the Bay of Bengal than temperature. Salinity was positively related to chlorophyll but negatively to DMSP (figure 4). These contrasting relations could be explained by vertical variations in these parameters. While salinity and chlorophyll usually increase from surface to the base of the mixed layer the DMSP maximum occurs closer to the surface in the Bay of Bengal.
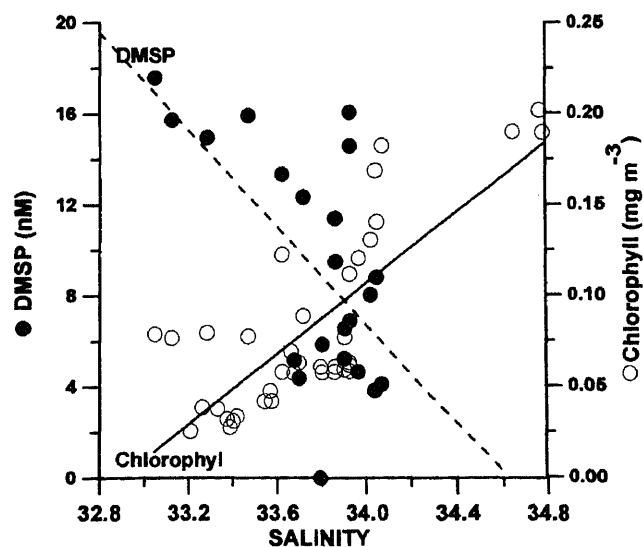


Figure 4. Relationships for salinity with DMSP and chlorophyll in the upper 30 m of the study region. Solid line is the least square regression for chlorophyll and the dashed one for DMSP.
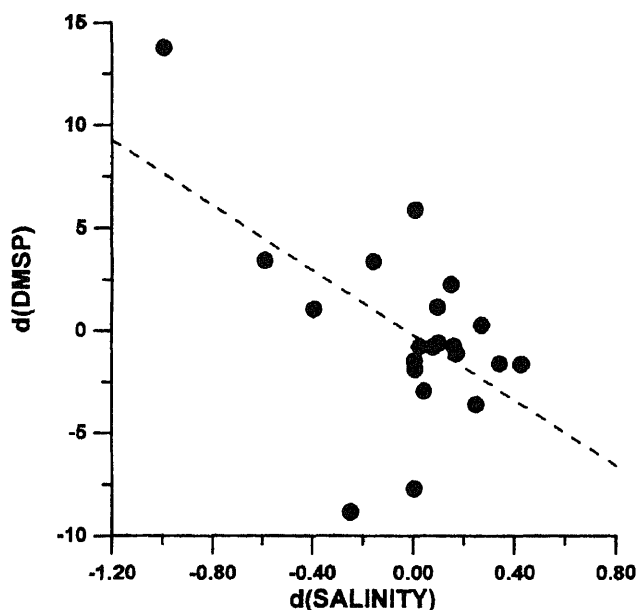
Figure 5. Relation between differences, horizontally or vertically between two depths or locations, in salinity and DMSP.



Figure 6. Latitudinal variations in sea-to-air fluxes of DMS in the Bay of Bengal.

### 3.2 Hypothesis

Here, besides the above, we offer an alternative explanation. In spite of the low chlorophyll at lower salinities the higher abundance of DMSP could imply that this osmolyte production is favoured by higher osmotic pressure imbalance between phytoplankton cell fluid and the surrounding seawater medium. This may be justified from the fact that the phytoplankton acclimatized to a salinity of 35 will undergo physiological changes when salinity drops thus producing more osmolyte, DMSP. If this alternative explanation is valid we should find an inverse relation between differences in salinity and DMSP. Figure 5 reveals a negative linear relation between the two proving the fact that a drop in salinity indeed leads to higher production of DMSP. The salinity, therefore, appears to have a control on the production of DMSP, which in turn controls the DMS abundance in the bay.

### 3.3 Sea-to-air transport of DMS and DMSP

Sea-to-air exchange of DMS will depend on the intensity of wind and DMS concentration in surface seawater. In the present study surface DMS concentrations ranged between 1.4 and 4.65 nM with an average of 2.82 nM. The evaluated DMS fluxes varied from 0.16 to 10.93 $\mu$mol S m$^{-2}$ d$^{-1}$ The highest DMS flux occurred at 8°N (figure 6) where the wind speed was the strongest (8.6 m s$^{-1}$). The average gaseous efflux during the study period is found to be 1.6 $\mu$mol S m$^{-2}$ d$^{-1}$. Table 1 presents the results of DMS and DMSP in marine aerosols. The results clearly indicate

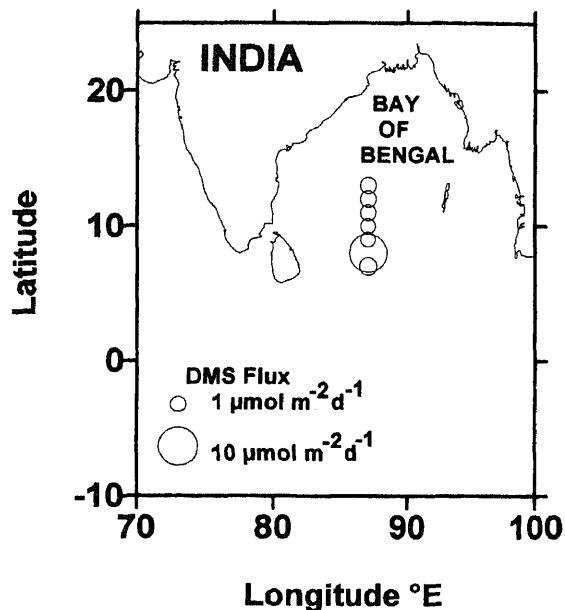Table 1. Concentrations of DMSP and DMS in marine aerosols.

| S. No. | Height above sea level (m) | Aerosol DMS pmol m$^{-3}$ | Aerosol DMSP pmol m$^{-3}$ |
|---|---|---|---|
| 1 | 1–2[a] | 0 | 0.795 |
| 2 | 2.6[b] | 0.504 | 0 |
| 3 | 6.85[b] | 0.796 | 1.066 |
| 4 | 2.6[c] | 0 | 0 |
| 5 | 6.85[c] | 0 | 0 |
| 6 | 2.6[d] | 0 | 4.042 |
| 7 | 2.6[e] | 0 | 0.455 |
| 8 | 4.7[e] | 1.441 | 0 |
| 9 | 6.85[e] | 0 | 0 |
| 10 | 1–2[f] | 0 | 0 |
| 11 | 6.85[g] | 0 | 0.418 |
| 12 | 6.85[h] | 0.597 | 0.836 |

Superscripts in col. 2 indicate the heights of sampling at a given location.

tration levels are comparable to DMS concentrations in marine air. Non-detectable levels in table 1 imply that the ejected DMSP and DMS might have been lost from aerosols to air or at least converted to a different and undetectable form. Given the fact that these compounds are susceptible to bacterial decomposition and photolytic oxidation these will be short lived in the atmosphere. The effect of wind speed on DMSP in aerosols cannot be assessed at present. This mechanism, however, could be very important for non-sea salt sulphate budget in the atmosphere. This transport mechanism could be all the more important in the North Indian Ocean since this region experiences strong winds during southwest monsoon and

# 4. Conclusions

Results obtained in this study suggest that the changes in salinity play a major role in the production of DMSP by phytoplankton, which in turn controls the abundance of DMS in seawater. In addition to the diffusive DMS evasion, DMSP (along with DMS) is shown to be ejected to the atmosphere through aerosols thereby forming a new transport pathway.

# References

Andreae M O and Crutzen P J 1997 Atmospheric aerosols: biogeochemical sources and role in atmospheric chemistry; *Science* **276** 1052–1058

Keller M D, Kiene R P, Matrai P A and Bellows W K 1999 Production of glycine betaine and dimethylsulphoniopropionate in marine phytoplankton. I. Batch cultures; *Mar. Biol.* **135** 237–248

Kettle A J, Andreae M O, Amouroux D, Andreae T W, Bates T S, Beresheim H, Bingemer H, Boniforti R, Curran M A J, Di Tullio G K, Helas G, Jones G B, Keller M D, Kiene R P, Leck C, Levasseur M, Malin G, Maspero M, Matrai P, Metaggart A R, Mihalopoulos N, Nguyen B C, Novo A, Putaud J P, Rapsomanikis S, Roberst G, Schebeske G, Sharma S, Simo R, Strobes R, Turner S and Uher G 1999 A global database of sea surface dimethylsulfide (DMS) measurements and a procedure to predict sea surface DMS as a function of latitude, longitude, and month; *Global Biogeochem. Cycles* **13** 399–444

Kumar M D, Naqvi S W A, George M D and Jayakumar D A 1996 A sink for atmospheric carbon dioxide in the north east Indian Ocean; *J. Geophys. Res.* **101C** 18,121–18,125

Liss P S, Malin G and Turner S M 1993 Production of DMS by marine phytoplankton In: *Dimethyl Sulphide: Oceans, Atmosphere and Climate* (eds.) G Restelli and G Angeletti (Kluwer Academic) 1–14

Qasim S Z 1977 Biological productivity of the Indian Ocean; *Indian J. Mar. Sci.* **6** 122–137

Rao C K, Naqvi S W A, Kumar M D, Varaprasad S J D, Jayakumar D A, George M D and Singbal S Y S 1994 Hydrochemistry of the Bay of Bengal: Possible reasons for a different water-column cycling of carbon and nitrogen from the Arabian Sea; *Mar. Chem.* **47** 279–290

Rodhe H 1999 Human impact on the atmospheric sulphur balance; *Tellus* **51A-B** 110–122

Sarma V V S S, Kumar M D, and George M D 1998 The central and eastern Arabian Sea as a perennial source of atmospheric carbon dioxide; *Tellus,* **50B** 179–184

Shetye S R and Gouveia A D 1998 Coastal circulation in the north Indian Ocean. In: *The Sea* (eds.) A R Robinson and K H Brink (John Wiley) **11** 523–556

Turner S M, Malin G, Bagander L E and Leck C 1990 Inter-laboratory calibration and sample analysis of dimethyl sulphide in water; *Mar. Chem.* **29** 47–62

Turner S M, Malin G, Nightingale G D and Liss P S 1996 Seasonal variation of dimethyl sulphide in the North Sea and an assessment of fluxes to the atmosphere; *Mar. Chem.* **54** 243–262

# Marine boundary layer simulation and verification during BOBMEX-Pilot using NCMRWF model

SWATI BASU

*National Centre for Medium Range Weather Forecasting, INSAT Building, Mausam Bhavan Complex, Lodi Road, New Delhi, India*
*email: swati@ncmrwf.gov.in*

A global spectral model (T80L18) that is operational at NCMRWF is utilized to study the structure of the marine boundary layer over the Bay of Bengal during the BOBMEX-Pilot period. The vertical profiles of various meteorological parameters within the boundary layer are studied and verified against the available observations. The diurnal variation of various surface fields are also studied. The impact of non-local closure scheme for the boundary layer parameterisation is seen in simulation of the flow pattern as well as on the boundary layer structure over the oceanic region.

## 1. Introduction

Analysis of the marine boundary layer structure and the air sea interaction processes are crucial and very important in understanding the general flow pattern over the Indian subcontinent including the genesis of lows and depressions. It remains then essential that the boundary layer structure as simulated by the numerical models should be reproduced in the most realistic manner. The marine boundary layer plays a key role in the atmospheric energy exchange processes. As distinguished from most land surfaces, open sea and ocean surfaces are characterized by a remarkable temporal and spatial homogeneity of temperature. This is primarily due to the large heat capacity and efficient mixing processes in the upper oceanic mixed layer. Thus, over much of the ocean, the surface heat flux does not play a large role in determining the boundary layer structure. Observational validation of boundary layer theory, details of boundary layer structure rely heavily on data which is relatively sparse and especially rare in the case of marine boundary layer. Few observational studies are available on the marine boundary layer over the Indian Ocean. BOBMEX offered an opportunity to explore the structure of the marine boundary layer and its evolution over the Bay of Bengal.

## 2. Synoptic conditions

The Pilot experiment was carried out on board ORV Sagar Kanya. The ship left Mormugao on 23rd October 1998, moved towards south almost parallel to the west coast of India up to 5°N, and then turned eastwards. The first stationary (drifting) time series station was at 7°N 87°E for two days (October 30th, 31st), the second time series station was at 10°N 87°E for two days (2nd – 3rd November). During the period for which the Pilot data was obtained (1st and 3rd November 1998), a shear zone was seen over south Bay of Bengal on 1st November in which a low pressure formed on 2nd November in southwest Bay off Srilanka-south Tamilnadu coast. This low pressure persisted over the same area till 6th November and became less marked on 7th November. The operational model at NCMRWF (OPER) was run with the initial condition of 1st November 1998 and the forecasts of three days were obtained. Similar forecasts were also obtained with the NCMRWF model having a different parameterisation scheme for the boundary layer viz. non-local closure scheme (NLC). The flow pattern as well as the precipitation pattern were obtained and compared with the observational analysis using both the schemes. The profiles of temperature and humidity as obtained from Sagar Kanya

were also compared with those obtained from both the models. Since the difference between both the models lies in the parameterisation scheme of the boundary layer only, the impact of the different schemes for the boundary layer could readily be identified.

## 3. Description of the schemes

### 3.1 *PBL parameterisation scheme of NCMRWF model*

A short description of the model, which is run on an operational basis at NCMRWF, is given in Basu *et al* (1999). The standard PBL parameterisation uses a first-order closure approximation whereby the turbulent fluxes are correlated to the mean vertical gradients through the eddy diffusivities. These eddy diffusivities are stability dependent (depending upon the bulk Richardson number) and are determined through mixing length considerations. It is assumed that the mixing length $l$ varies as $kz$ ($k$ being the von karman constant and $z$ the height above the ground) close to the ground, but approaches constant value $\lambda(= 250\,\text{m})$ at greater heights. Thus, the eddy diffusivities are determined through: $K = l^2 S|\partial v/\partial z|$; where $l$ is the mixing length given by

$$l = kz/(1 + kz/\lambda).$$

Here, $S$ is a set of semi-empirical stability functions dependent upon the bulk Richardson number $R$, and $\lambda$ is the limiting mixing length.

### 3.2 *Parameterisation using the non local closure scheme*

There are certain limitations of the mixing length theory (Stull 1984) the most important being its inability to represent realistically mixing in the convective boundary layer involving the "counter gradient fluxes" ( Troen and Mahrt 1986; Hong and Pan 1989). One of the alternatives is to go to higher order closure approaches but they were computationally more expensive. Moreover, Ayotte (1996) showed that these schemes were in the strictest sense local diffusion schemes and had a strong tendency to underentrain in the presence of a strong capping inversion. Recently an alternative approach has been suggested, the so called non-local $K$ closure which is computationally efficient and has the capability to represent large eddy turbulence within a well mixed boundary layer. This scheme (Hong and Pan 1989; Troen and Mahrt 1986) has been widely tested for general circulation models as well as numerical prediction models with further

equations for prognostic variables $(C; u, v, q, q)$ are expressed by

$$\delta_c/\delta_t = \delta/\delta_z[K_c(\delta_c/\delta_z - \gamma_c)]$$

where $K_c$ is the eddy diffusivity coefficient and $\gamma_c$ is a correction to the local gradient that incorporates the contribution of the large scale eddies to the total flux. The diffusivity coefficient in the mixed layer is given by

$$K_m = kw_s z(1 - z/h)_p$$

where $p$ is the profile shape exponent, $w_s$ is the mixed layer velocity scale, $h$ is the PBL height and $k$ is the von karman constant. The PBL height is given by

$$h = R_{ib}\frac{\theta_{va}|U(h)|^2}{g(\theta_v(h) - \theta_s)}$$

where $R_{ib}$ is the critical bulk Richardson number, $U(h)$ is the horizontal wind speed at $h$, $\theta_{va}$ is the virtual potential temperature at the lowest model level $\theta_v(h)$ is the virtual potential temperature at $h$ and $\theta_s$ is the appropriate surface temperature. For the free atmosphere, however, the local $K$ approach is utilized.

## 4. Results

Figures 1(a), (b) and (c) show the flow pattern as seen in the analysis and day 2 forecasts from OPER and NLC respectively valid for 3rd November 1998. As mentioned in the previous section a low pressure area had formed around 87°E 10°N on 2nd November which persisted till 6th November. As seen both OPER and NLC were able to predict the circulation over Bay of Bengal (around 87°E 10°N) although OPER showed intense circulation compared to analysis which shows only a sheared zone. Both the models show two closed circulations over the Bay as well as over the Arabian Sea unlike the analysis which showed an extended shear zone over the Arabian Sea. In general both the models show similar flow patterns for all the forecast days. Figure 2 (a)–(c) shows the observed analysed rainfall (Mitra *et al* 1997) and 24–48 hour accumulated precipitation valid for 3rd November 1998 with OPER and NLC respectively. In general it is seen that OPER shows more rainfall over southeast Bay which is not observed. This may be due to the fact that OPER enhances the flow pattern over the Bay as was seen in figure 1. NLC on the other hand shows a reasonable amount of rainfall over the Bay. The rainfall over southern peninsula is however better simulated in OPER compared to NLC although the observed rainfall is higher (about three times). The rainfall patch in the adjoining part of north Sri Lanka has not been shown by either models.
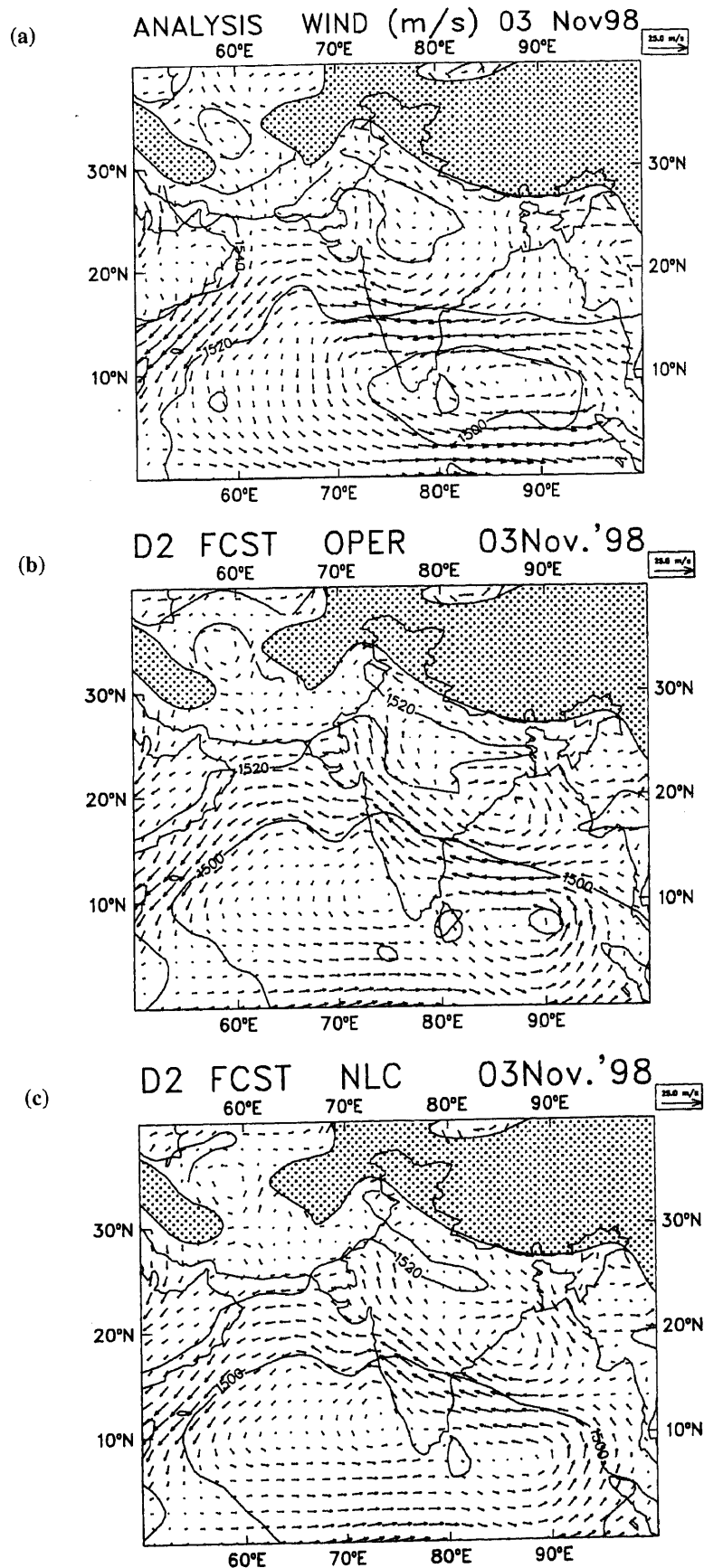
Figure 1. Geographical distribution of 850 hPa wind vectors (ms$^{-1}$) and geopotential heights (m) over the monsoon region for 3rd November 1998 (a) Verifying analysis; (b) 48 hr forecast by OPER; (c) 48 hr forecast by NLC.
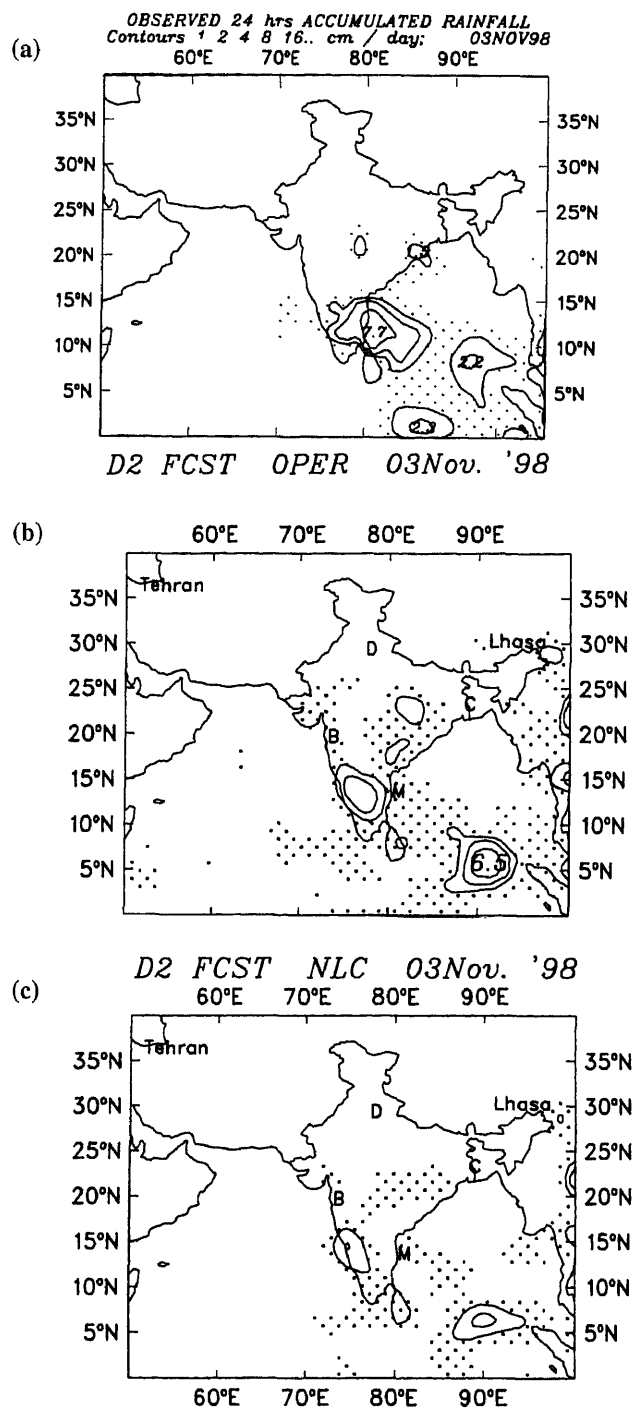
Figure 2. Geographical distribution of accumulated 48–72 hr, precipitation in cm/day for 3rd November 1998 over the Indian region and adjoining areas (min. contour 1 cm) shaded areas represent precipitation < 1 cm. (a) Analysed rainfall from INSAT and rain gauge; (b) 48 hr forecast by OPER; (c) 48 hr forecast by NLC.

The profiles of humidity and temperatures as simulated by the model with the initial condition of 1st November 1998 valid for different forecast hours are compared with the observations. During the period of comparison, it was noted that 1st November was cloudy and rainy compared to 3rd November which was a relatively clear day. The temperature profile in

shallower and extends up to 1000 m. The maximum wind speed is around $10 \, \mathrm{ms^{-1}}$ and the humidity is quite high. It is seen that although the profiles of the humidity are comparing well with the observations till about 890 hPa, the magnitudes are smaller by both the models. Both the models are unable to simulate the higher values of humidity above 890 hPa. The
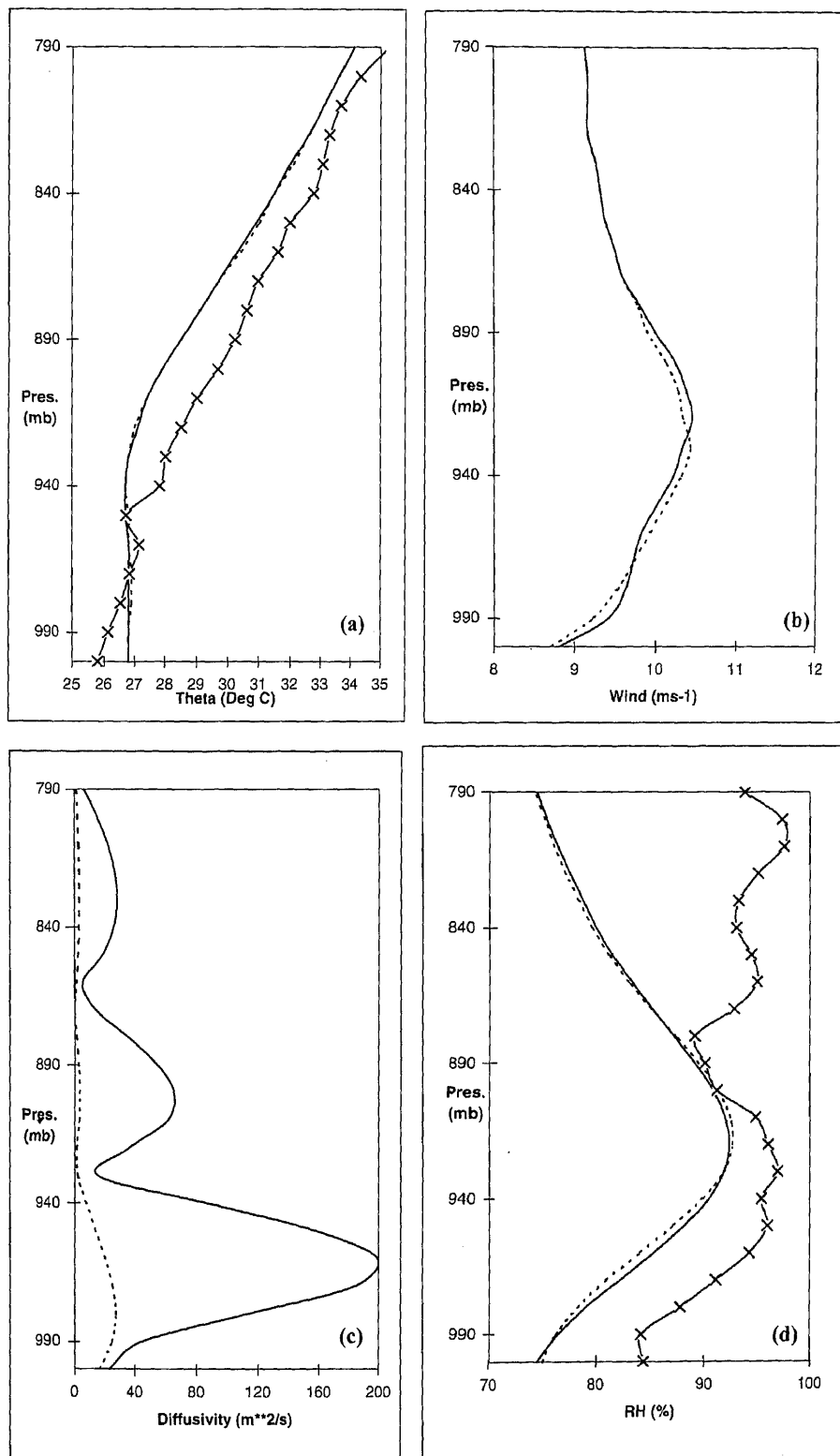
Figure 3. Vertical profiles valid for 0700 hrs of 1st November 1998. Profiles till 790 hPa at 87°E 10°N. Comparison with model forecast with IC: 1st November 1998 00 hrs. (a) Theta profile; (b) wind profile; (c) Diffusivity profile; (d) Relative humidity profile; — OPER; - - - - NLC; - -x---x---x---x Observations.

profile which shows higher values for OPER at the lower levels. Figure 4 shows similar profiles valid for 3rd November 0700 hrs. This day was a clear day which are reflected in the temperature profile that

also higher. However, the wind speed simulated by NLC is lower compared to OPER. The magnitude of the humidity simulated by both the models are higher compared to the observations when a 400 meters. The
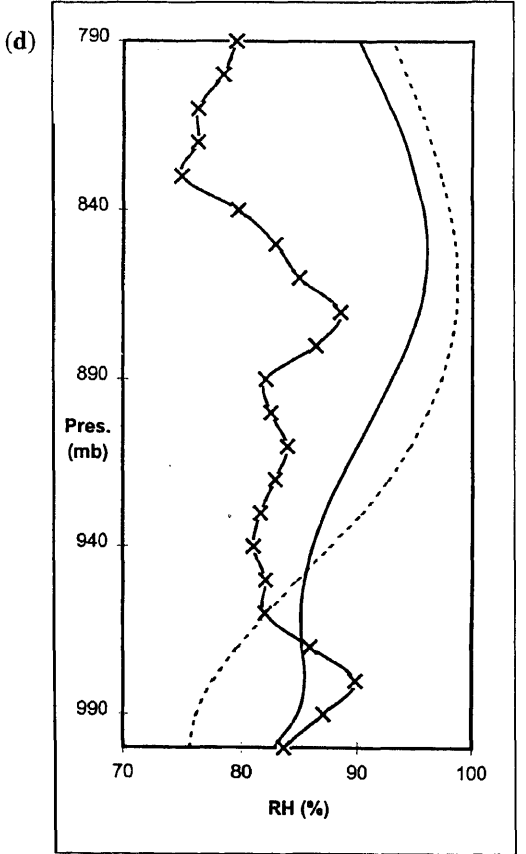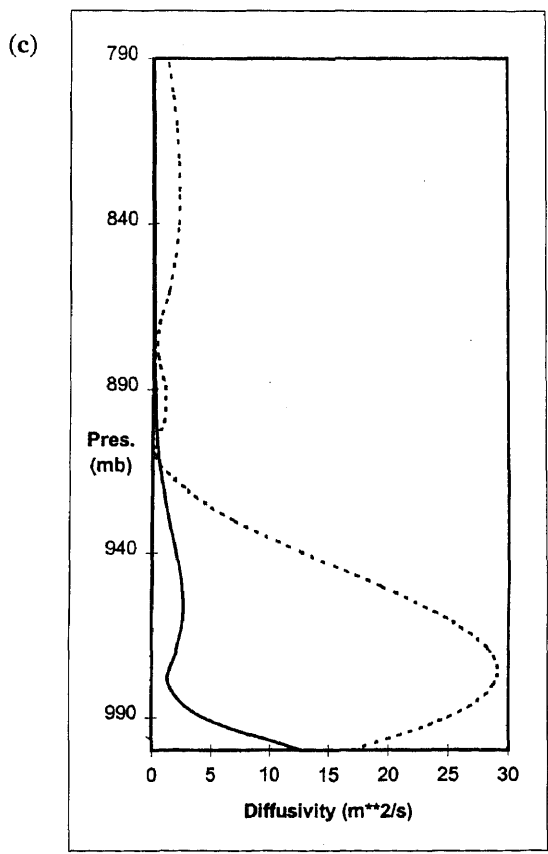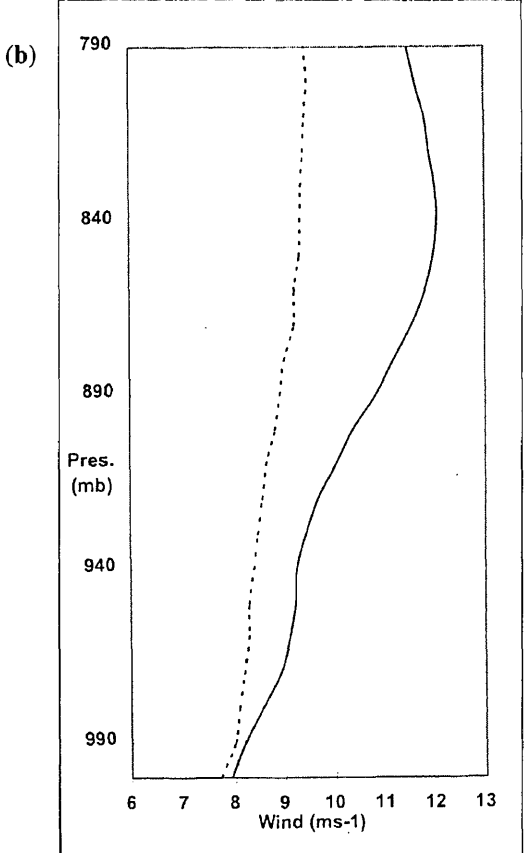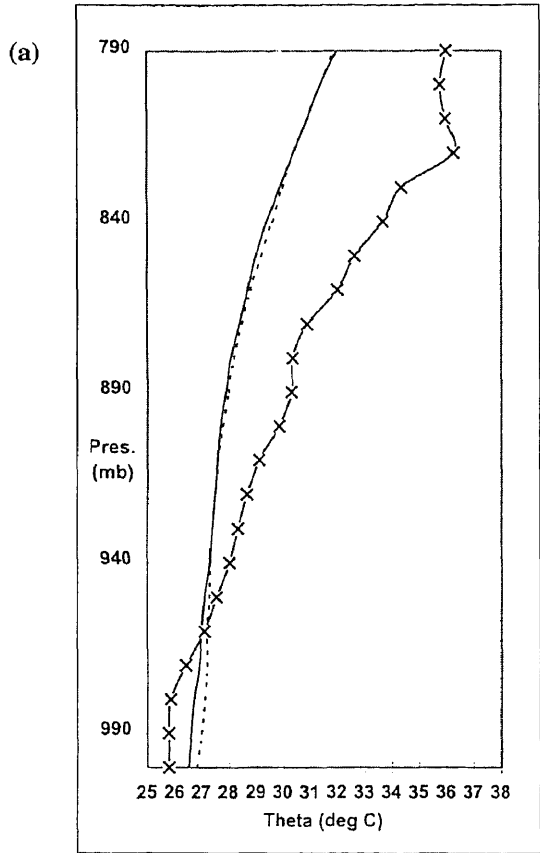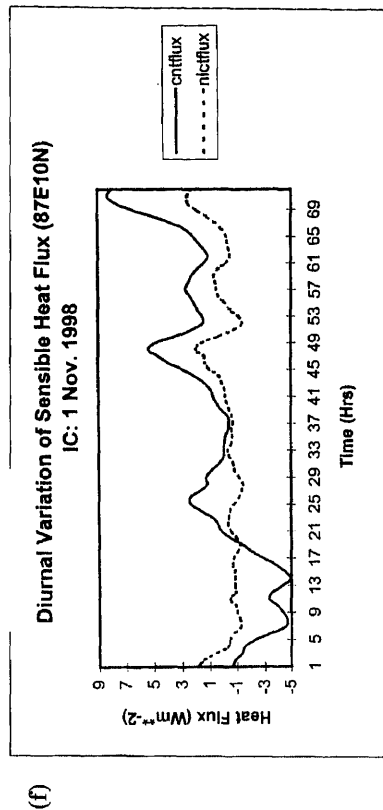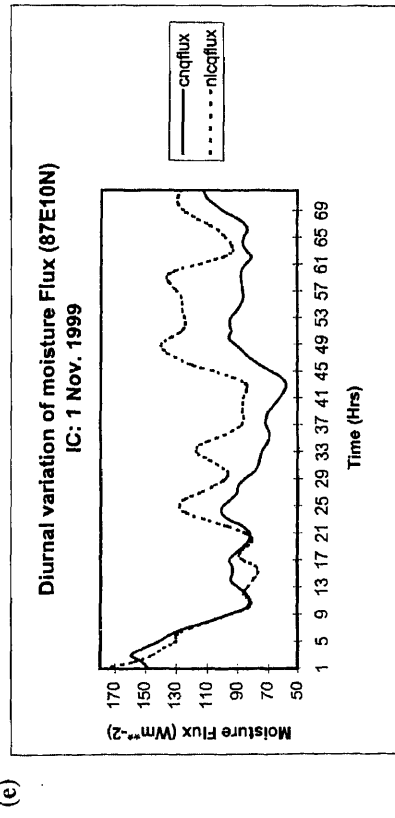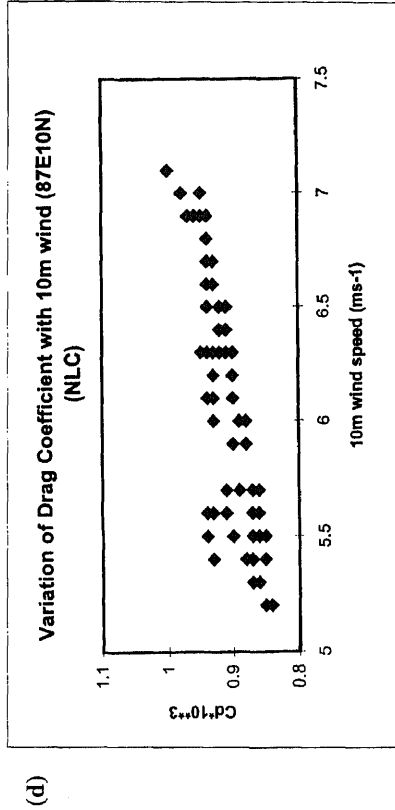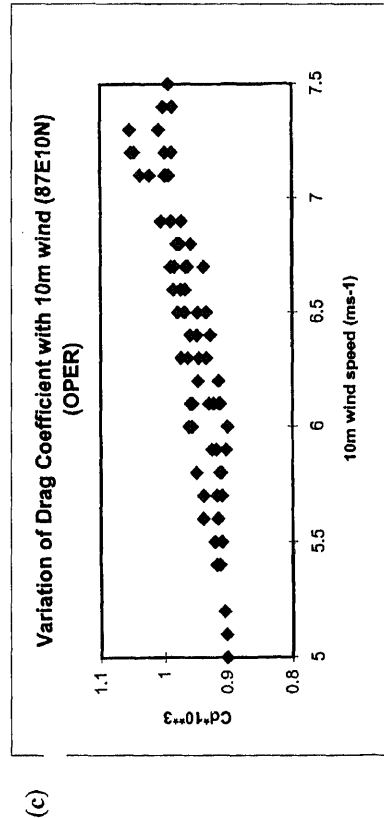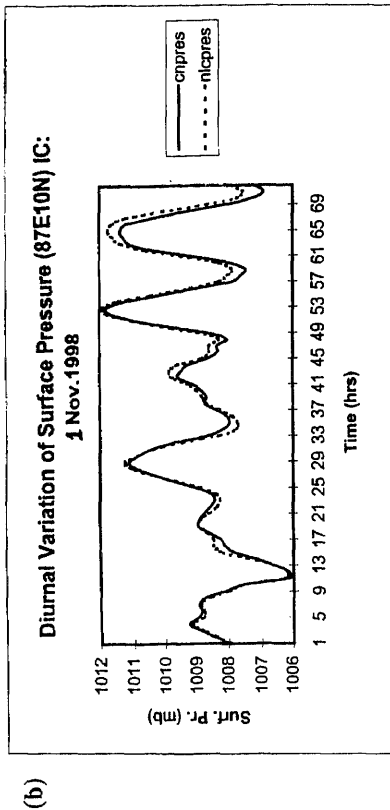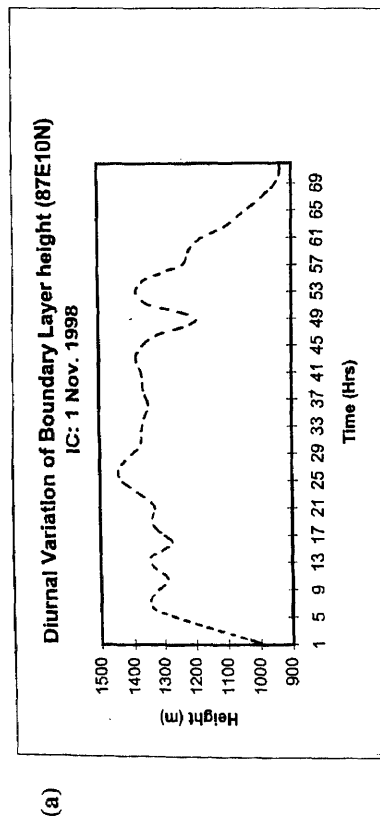
Figure 5.   Diurnal variation of various parameters at 87°E 10°N with IC: 1st November 1998 00 hrs. (a) 72 hr forecast of boundary layer height; (b) 72 hr forecast of surface pressure; (c) Variation of drag coefficient with 10 m wind by OPER; (d) Variation of drag coefficient with 10 m wind by NLC; (e) 72 hr forecast of moisture flux; (f) 72 hr forecast of sensible heat flux; — OPER; ---- NLC.

compared to OPER till about 500 meters, above which the reverse is true. This is apparent from the profiles of diffusivity which shows higher values at lower levels by NLC indicating efficient transport of humidity from the lower levels to the higher levels. Figure 5 (a)–(f) shows the diurnal variation of boundary layer height, surface pressure, heat and moisture fluxes along with variation of drag coefficients with 10 m winds using both NLC and OPER. Since OPER does not explicitly resolve the boundary layer height, the same is produced only by NLC. It is seen that the boundary layer height varies between 950 m and 1400 m. Figure 5(b) shows the surface pressure by OPER and NLC which shows a drop in the same around 1300 hrs of 1st November. This may be attributed to the rainfall that occurred around that time. The variation by OPER and NLC is almost the same in magnitude. Figures 5(c) and (d) show the variation of drag coefficients with the winds at 10 m by OPER and NLC. Both the models show similar variation as well as similar values. As pointed out by Arya (1988) the dependence of the drag coefficients on $U_{10}$ is weak in the transition regime of wind speeds less than $7.5\,\mathrm{ms}^{-1}$ $2.5 < U_{10} < 7.5$. As seen from the figures, the wind speed at 10 m never exceed $7.5\,\mathrm{ms}^{-1}$. It is also seen that there is weaker dependence of the drag coefficients on $U_{10}$. The values are also comparable to those obtained in the moderate range of wind speeds (Kraus 1972) which is nearly constant and is around $1.2 \times 10^{-3}$. Garratt (1994) also shows similar variations as well as values within this wind speed range. Figures 5(e)–(f) show the diurnal variation of moisture and heat flux respectively by both the models. In general, both the models show high values of moisture flux $(150 - 170\,\mathrm{Wm}^{-2})$ which eventually is reduced after the rainfall. By and large NLC shows higher values of the flux compared to OPER. The sensible heat fluxes as expected are very small and the variations by both the models are similar and comparable.

## 5. Conclusions

Simulation of the marine boundary layer is obtained over the Bay of Bengal using two different schemes of the boundary layer for the BOBMEX-Pilot period. During the said period, both the flow pattern as well as the precipitation pattern were simulated reasonably well by both the models. OPER however had a tendency to enhance the circulation over the Bay and the corresponding precipitation patch. The flow patterns by and large compared reasonably with the verifying analysis. As far as the profiles in the boundary layer were concerned, the two situations of atmospheric conditions viz. cloudy during 1st November and the clear day for 3rd November were brought out by the models from the temperature profiles. Although the temperature profiles compared reasonably well with the observed one, the humidity profiles were under predicted for 1st November and over predicted for 3rd November which was a clear day. Winds simulated by the NLC for the clear day are almost constant with height and are less by about $2\,\mathrm{ms}^{-1}$ compared to OPER. The diffusivity profiles by both the models show differences in the lower levels. The differences in the simulation by the two models could be attributed to these differences in the diffusivity profiles which are mainly responsible for the distribution of the parameters in the vertical. Variation of surface parameters by both the models shows similar characteristics. The moisture flux in general is higher and sensible heat flux is lower as simulated by NLC compared to OPER. The boundary layer depth which varies between 900 and 1400 m is simulated by NLC which seemed to be in general agreement with observations (Bhat, personal communication). The variation of drag coefficients is also at par with general observations and both the models simulated similar features. Overall, based on the simulation of 1st November 1998, it was seen that by and large, both NLC and OPER performed in a similar manner. However, OPER had overestimated the circulation as well as the precipitation pattern compared to NLC as well as the verifying analysis and observations. In this respect, NLC had a slight edge over OPER. The surface parameter simulations did not show much variation using OPER and NLC except for the fluxes. The moisture fluxes simulated by NLC were more realistic. Further studies are on to assess the impact of two different schemes for PBL on the simulation of the marine boundary layer structure.

## References

Arya S P S 1988 *Int. Geophys. Series*, **42**, pp. 307
Ayotte K W 1996 *Boundary-Layer Meteorol.* 131–175
Basu Swati, Raman S, Mohanty U C and Rajagopal E N, 1999 *PAGEOPH* 33–55
Bhat G S, personal communication
Garratt J R 1994 *The atmospheric boundary layer*, pp. 316
Holtslag A A M, Boville B A, Bruijn J F and Pan H L 1990 *Mon. Weather Rev.* 1561–1575
Hong S Y and Pan H L 1989 *Mon. Weather Rev.* 1726–1750
Kraus E B 1972 *Atmosphere-Ocean Interaction* (Oxford University Press)
Mitra A K, Bohra A K and Rajan D, 1997 *Int. J. Climatol.* 1083–1092
Stull R B, 1984 *J. Atmos. Sci.* 3351–3367
Troen I and Mahrt L 1986 *Boundary-Layer Meteorol.* 129–148

# Numerical simulation of the marine boundary layer characteristics over the Bay of Bengal as revealed by BOBMEX-98 Pilot experiment

A N V Satyanarayana[1], U C Mohanty[1], N V Sam[1], Swati Basu[2] and V N Lykossov[3]

[1]Centre for Atmospheric Sciences, Indian Institute of Technology Delhi, New Delhi, India
[2]National Centre for Medium Range Weather Forecasting, New.Delhi, India
[3]Institute of Numerical Mathematics, Moscow, Russia

An attempt has been made to study the marine boundary layer characteristics over Bay of Bengal using BOBMEX (Bay of Bengal and Monsoon Experiment) pilot experiment data sets, which was conducted between 23rd October and 12th November 1998 on board ORV Sagar Kanya. A one-dimensional multi-level atmospheric boundary layer with TKE-$\varepsilon$ closure scheme is employed to study the marine boundary layer characteristics. In this study two synoptic situations are chosen: one represents an active convection case and the other a suppressed convection. In the present article the marine boundary layer characteristics such as temporal evolution of turbulent kinetic energy, height of the boundary layer and the air-sea exchange processes such as sensible and latent heat fluxes, drag coefficient for momentum are simulated during both active and suppressed convection. Marine boundary layer height is estimated from the vertical profiles of potential temperature using the stability criterion. The model simulations are compared with the available observations.

## 1. Introduction

Marine Boundary Layer (MBL) plays an important role in the atmospheric energy studies. The vertical structure of the MBL in the tropics depends on the interaction cycle of the air-sea exchange, vertical transport mechanism and the large-scale flow. The energy for driving the atmospheric disturbances is provided by the underlying ocean through sensible and latent heat fluxes and thus the ocean-atmosphere coupling takes place. It is important to study the MBL characteristics to understand the air-sea exchange processes and the transport mechanism in the context of large-scale synoptic features such as the monsoon. Very few studies have been conducted on MBL due to paucity of data. Holt and Raman (1988) have simulated the turbulent characteristics of the marine boundary layer. Satyanarayana *et al* (1999) studied some aspects of MBL over the Indian Ocean using INDOEX Cruise #120 data sets. A pilot experiment acronym as BOBMEX (Bay of Bengal and Monsoon Experiment) was conducted on board ORV Sagar Kanya during 23rd October to 12th November 1998 to understand the air-sea interaction processes and marine boundary layer characteristics over the Bay of Bengal. The main aim of the present study is to understand the marine boundary layer characteristics in different synoptic situations that are observed during the pilot experimental phase. In the present article the MBL characteristics such as temporal evolution of turbulent kinetic energy (TKE), MBL height and surface layer parameters such as sensible and latent heat fluxes, drag coefficient are simulated during active and suppressed convective conditions. The model has also generated the vertical profiles of zonal and meridional wind components, potential temperature and specific humidity. The simulated MBL features are compared with available observations.

PILOT BOBMEX CRUISE TRACK
SAGAR KANYA CRUISE NO: SK 138 C
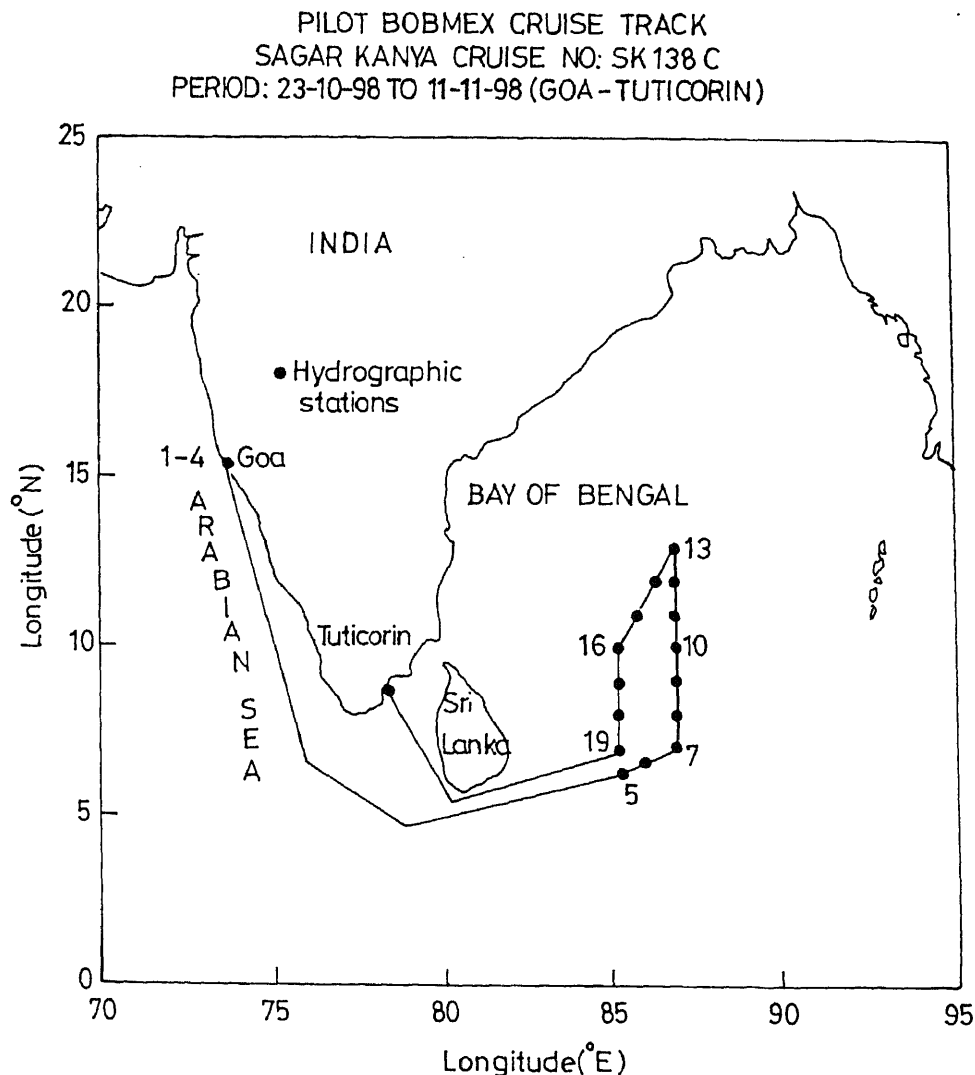PERIOD: 23-10-98 TO 11-11-98 (GOA – TUTICORIN)



Figure 1.    Cruise track of ORV Sagar Kanya during BOBMEX-98 pilot experiment.

## 2. Data

The BOBMEX-Pilot experiment was carried out on board ORV Sagar Kanya. The ship left Mormugao on 23rd October 1998, moving parallel to the West Coast up to 5°N and then turned towards the Bay of Bengal. The first time series observation station (7°N, 87°E) was on 30th October where the ship was stationed for two days, and then it moved towards north (10°N, 87°E) to the second stationary position for two days (2nd – 3rd November). The ship reached the last stationary observation point (13°N, 7°E) on 5th November and was positioned there for that day. The ship sailed back on 6th November and reached Tuticorin on 12th November 1998. The track of the

from satellite pictures (Kalsi 1999) and on board surface synoptic observations (not presented). In this study, these two distinctly different synoptic scenarios representing active and suppressed convection are considered.

Vertical profiles of temperature and moisture at different pressure levels, observed by launching radiosonde, low-level sonde and mini-sonde on board ORV Sagar Kanya, are used for the study. The surface synoptic observations viz. sea surface temperature, wind speed, wind direction, surface pressure, air temperature and dew point temperature are also considered for the study. Due to the absence of wind profile observations, the vertical profiles of wind that are obtained from the National Centre for Medium Range

For two days i.e. 1st and 3rd November, sonic anemometer (three-dimensional fast response wind components and temperature) and Lyman-alpha (fast response humidity) observations are available and the same are used for verification of simulated fluxes by the MBL model.

## 3. Methodology

A multi-level one-dimensional model with TKE-$\varepsilon$ closure scheme is used to simulate the MBL characteristics (Mellor and Yamada 1974; Lykossov and Platov 1992). The model has 40 levels in the vertical and layer thickness of 50 m from the surface to 2000 m. The model adopts TKE-$\varepsilon$ parameterisation scheme for the mixed layer, while the surface layer similarity approach is used for the constant flux layer close to the ocean surface. More details regarding the model are given in Lykossov and Platov (1992), and Satyanarayana *et al* (1999). The model equations are

$$\frac{\partial u}{\partial t} = -\frac{\partial \overline{u'w'}}{\partial z} + fv + \tilde{p}_x/\tilde{\rho}, \tag{1}$$

$$\frac{\partial v}{\partial t} = -\frac{\partial \overline{v'w'}}{\partial z} - fu - \tilde{p}_y/\tilde{\rho}, \tag{2}$$

$$\frac{\partial \theta}{\partial t} + u\tilde{\theta}_x + v\tilde{\theta}_y = -\frac{\partial \overline{\theta'w'}}{\partial z} + Q_r + Q_f, \tag{3}$$

$$\frac{\partial q}{\partial t} + u\tilde{q}_x + v\tilde{q}_y = -\frac{\partial \overline{q'w'}}{\partial z} + E_p - C, \tag{4}$$

$$\frac{\partial q_w}{\partial t} + u\tilde{q}_{wx} + v\tilde{q}_{wy} = -\frac{\partial \overline{q_w'w'}}{\partial z} - E_p + C - P, \tag{5}$$

$$\frac{\partial E}{\partial t} = \left( -\overline{u'w'}\frac{\partial u}{\partial z} + \overline{v'w'}\frac{\partial v}{\partial z} + \frac{g}{\rho}\overline{\rho'w'} + \varepsilon \right) - \frac{\partial \overline{w'E'}}{\partial z}, \tag{6}$$

$$\frac{\partial \varepsilon}{\partial t} = -C_1 \frac{\varepsilon}{b} \left( -\overline{u'w'}\frac{\partial u}{\partial z} + \overline{v'w'}\frac{\partial v}{\partial z} + \frac{g}{\rho}\overline{\rho'w'} + \varepsilon \right) - \frac{\partial \overline{w'\varepsilon'}}{\partial z}, \tag{7}$$

where $u, v,$ and $w$ are $x$-, $y$- and $z$-components of the wind velocity, $\theta$ is the potential temperature, $q$ is the specific humidity, $q_w$ is the specific liquid–water content, $E$ is turbulent kinetic energy and $\varepsilon$ is dissipation, $\rho$ is the density of the air-water-water vapor mixture, $(\tilde{p}_x \tilde{p}_y)(\tilde{\theta}_x \tilde{\theta}_y)(\tilde{q}_x \tilde{q}_y)$ are components of horizontal gradients of the pressure, potential temperature, specific humidity and specific liquid–water content in the free atmosphere, $Q_r$ and $Q_f$ are rates of the heat change due to radiation and phase transitions of the water, $C$ and $E_p$ are rates of phase changes: water vapor to liquid water and water to water vapor, $P$ is the precipitation rate, $\rho\overline{u'w'}, \rho\overline{v'w'}, \rho\overline{\theta'w'}, \rho\overline{q'w'}$ and $\rho\overline{q_w'w'}$ are the vertical turbulent fluxes of momentum, heat, water vapor and liquid water, $f$ is coriolis

parameter, $g$ is acceleration due to gravity, $C_1$ and $b$ are constants.

Marine boundary layer height is estimated from the vertical profiles of potential temperature using stability analysis for comparing the model simulations. Eddy correlation method (Stull 1988) is employed to compute the fluxes of sensible heat and latent heat using sonic anemometer and Lyman-alpha data for comparison purposes.

## 4. Initial and boundary conditions

For the model initial and boundary conditions, data comprising of vertical profiles of winds, temperature and humidity at different pressure levels are utilized. Using linear interpolation technique the data sets of vertical profiles of above cited parameters are prepared at every 50 m in vertical from sea level to the top of model domain. The maximum height of the turbulent boundary layer (top of the PBL) is chosen as the upper boundary. At the top of the boundary layer, the wind speeds, the potential temperature and the moisture attain the observed values at that height. The TKE and energy dissipation is assumed to vanish at that height. The top of the model domain was kept at 2000 m. These data sets served as an input to the PBL model as well as time-varying lateral boundary conditions to study the MBL characteristics.

The boundary conditions are prepared using the surface synoptic observations such as surface pressure, sea surface temperature and surface relative humidity that are collected on board ORV Sagar Kanya.

The active convection case (from 31st October – 2nd November) hereafter referred as Case-1 and the suppressed convection case (3rd – 5th November) referred as Case-2. For Case-1, the model initial conditions are prepared using the vertical profiles of zonal and meridional wind, potential temperature and specific humidity of 0530 IST on 31st October and the model is integrated for 48 hours. Similarly, the initial conditions of Case-2 are prepared using the data of 0700 IST on 3rd November and the model is integrated for 48 hours. The hourly simulations are stored for the purpose of comparison.

## 5. Results and discussion

The model simulations consist of the vertical profiles of zonal and meridional wind components, potential temperature and specific humidity, MBL height, sensible and latent heat fluxes, drag coefficient along with the temporal variation of TKE. The simulated profiles are compared with the available observations. The observed profiles of zonal and meridional wind, potential temperature and specific humidity are linearly

interpolated in the vertical (at every 50 m interval up to 2000 m) and the resultant values are used.

The vertical profiles of zonal and meridional wind after 24 and 48 hours simulations along with the observations of Case-1 and Case-2 are presented in figures 2 and 3, respectively. The vertical profiles of potential temperature and specific humidity after 24 and 48 hours simulations along with the observations of Case-1 and Case-2 are depicted in figures 4 and 5, respectively. For Case-1, 24 hour and 48 hour simulation represent 1st November 1998, 0530 IST and 2nd November 1998, 0530 IST respectively. Similarly for Case-2, the 24 hour and 48 hour simulation represent 4th November 1998, 0530 IST and 5th November 1998, 0530 IST, respectively.

In general, the model simulations of zonal and meridional components are found to be in good agreement with the observations with some differences, as one can see in figures 2(c) and 3(c), which represent the meridional component of the wind. The model simulations of potential temperature and specific humidity are in fairly good agreement with the observations, although there are differences between the simulated and observed values, as can be seen in figures 4 and 5.

In figure 4(a), the nature of the simulated potential temperature profile is similar to that of the observed profile except in the first 250 m of the layer. Neutral conditions are present in the lower layers of the simulated profile whereas stable conditions are noticed in
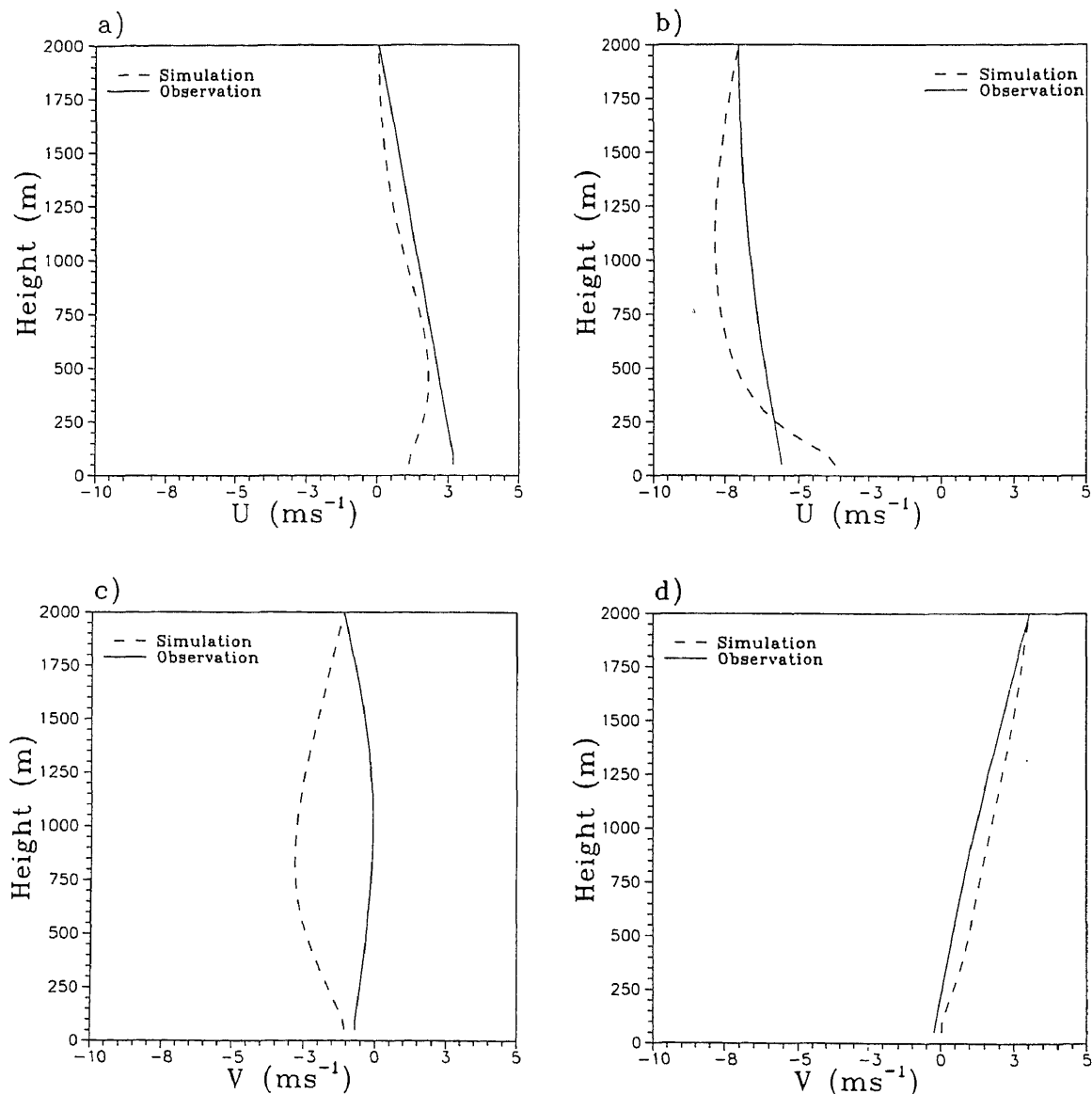


Figure 2. Vertical profiles of (a) zonal wind (ms$^{-1}$) at 00 UTC on 1st November 1998; (b) same as (a) but at 00 UTC on 2nd November 1998; (c) meridional wind (ms$^{-1}$) at 00 UTC on 1st November 1998 and; (d) same as (b) but at 00 UTC on 2nd November 1998 along with the observations of Case-1.
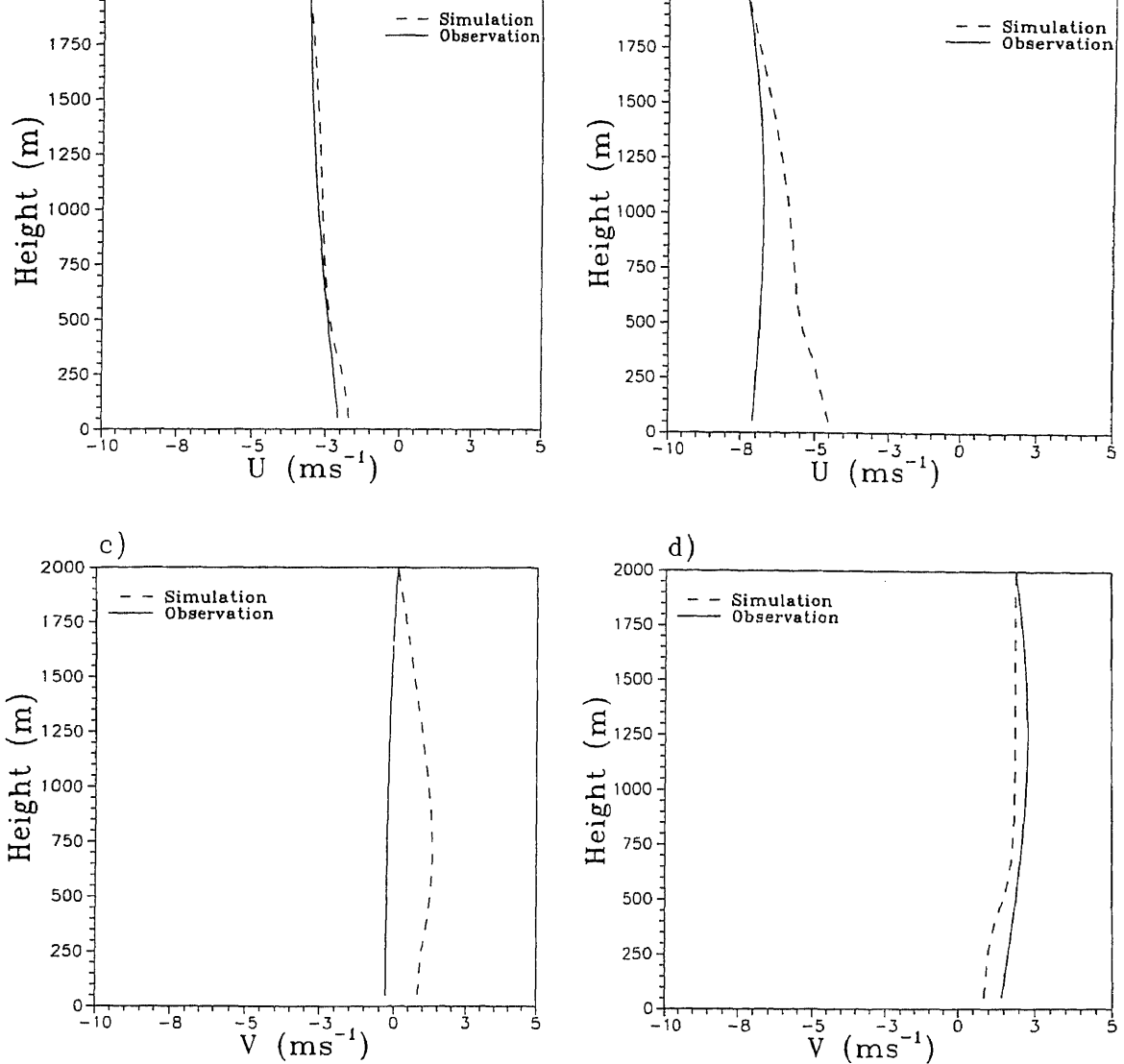
Figure 3.    Vertical profiles of **(a)** zonal wind (ms$^{-1}$) at 00 UTC on 4th November 1998; **(b)** same as (a) but for 00 UTC on 5th November 1998; **(c)** meridional wind (ms$^{-1}$) at 00 UTC on 4th November 1998 and; **(d)** same as (b) but for 5th November 1998 along with the observations of Case-2.

the observations. A similar situation is noticed in figure 4(b). In figures 5(a) and 5(b), one can see the good agreement of simulated potential temperature profile with the observations. The model could simulate the neutral conditions that are noticed in the observations reasonably well. A maximum difference of ∼ 1.2 K is found between simulations and observations (figure 5(a)) and it⸱is ∼ 1.6 K as noticed in figure 5(b).

The vertical variation of the simulated specific humidity is comparable with the observations as shown in figures 4(c) and 4(d). An increase of ∼ 3 g Kg$^{-1}$ in the lower 250 m layer is noticed in the observations and no such variation is noticed in the simulations (figure 4(d)). Nearly constant specific humidity layer of the thickness ∼ 850 m from the surface is seen in the

observations (figure 4(c)). A maximum difference of ∼ 3 g Kg$^{-1}$ (figure 4(c)) and ∼ 4 g Kg$^{-1}$ (figure 4(d)) in the lower layers of the atmosphere is found between simulations and observations. In contrast, there is an initial decrease of specific humidity of ∼ 5g Kg$^{-1}$ (figure 5(c)) and ∼ 4 g Kg$^{-1}$ (figure 5(d)) is noticed in the lower 250 m layer.

There are limitations of one-dimensional model to simulate the boundary layer processes due to non-homogeneity and advection. On overall evaluation of the results, the model could be able to simulate MBL processes reasonably well.

Figures 6 and 7 represent the diurnal variation of fluxes of sensible heat and latent heat, MBL height and drag coefficient for Case-1 and Case-2, respectively. The diurnal variation of these parameters is
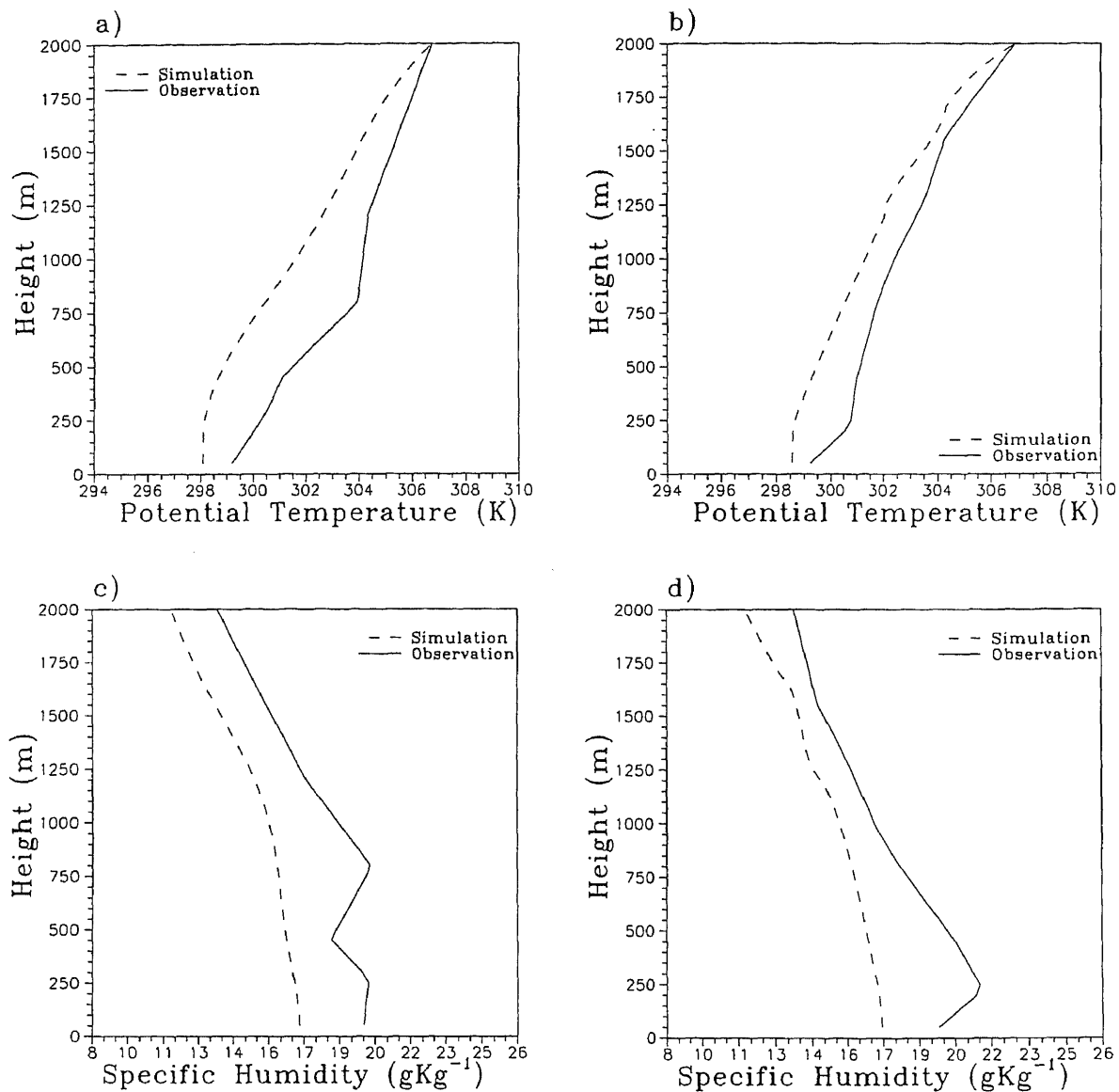
Figure 4.   Vertical profiles of (**a**) potential temperature (K) at 00 UTC on 1st November 1998; (**b**) same as (a) but at 00 UTC on 2nd November 1998; (**c**) specific humidity (g Kg$^{-1}$) at 00 UTC on 1st November 1998 and; (**d**) same as (c) but at 00 UTC on 2nd November 1998 along with the observations of Case-1.

plotted with respect to UTC timings on the abscissa. For example, for Case-1, 0 hours can be read as 0530 IST of 31st October 1998, 24 hours as 0530 IST of 1st November 1998 and 48 hours as 0530 IST of 2nd November 1998. Similarly for Case-2, 0 hours can be read as 0530 IST of 3rd November 1998, 24 hours as 0530 IST of 4th November 1998 and 48 hours as 0530 IST of 5th November 1998.

In Case-1, the model simulated sensible heat and latent heat fluxes values are higher than in Case-2. A maximum sensible heat flux value of 47.7 Wm$^{-2}$ is noticed in Case-1 (figure 6(a)) while 13.8 Wm$^{-2}$ in Case-2 (figure 7(a)) in the model simulations. Similarly, a maximum magnitude of simulated latent heat flux of 414 Wm$^{-2}$ is seen in figure 6(b) while

sensible heat and latent heat are overlaid on the simulation curve in figures 6(a), 7(a), 6(b) and 7(b). A maximum observed sensible heat flux of $\sim$ 33 Wm$^{-2}$ is noticed in Case-1 while $\sim$ 15 Wm$^{-2}$ in Case-2. A higher observed latent heat flux of 196 Wm$^{-2}$ is seen in Case-1 where as 176 Wm$^{-2}$ in Case-2. But for most of the time the values of latent heat flux in Case-1 are on a higher range when compared with the values of Case-2. The under-estimation of simulated fluxes of sensible heat and latent heat with respect to the observations can be probably due to the extracted and vertically interpolated and hence smooth wind profiles that are used in the model as obtained from the coarse resolution NCMRWF analyses. Due to the non-availability of sufficient observations of these fluxes
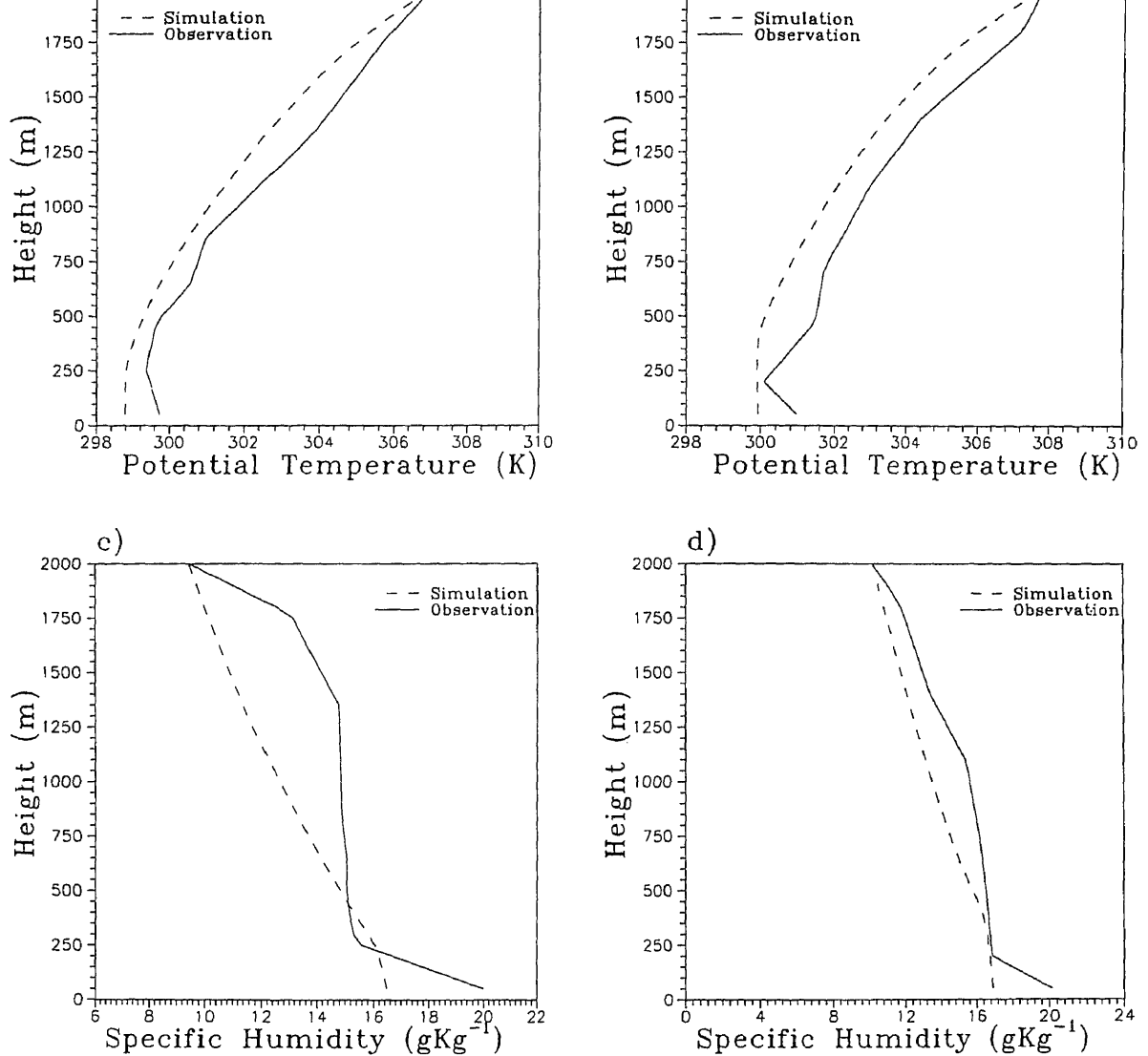
Figure 5. Vertical profiles of (a) potential temperature (K) at 00 UTC on 4th November 1998; (b) same as (a) but at 00 UTC on 5th November 1998; (c) specific humidity (g Kg$^{-1}$) at 00 UTC on 4th November 1998 and; (d) same as (c) but at 00 UTC on 5th November 1998 along with the observations of Case-2.

compare with the simulated diurnal variation. But on comparing the magnitudes of the fluxes of sensible and latent heat, one can see, as cited above, higher values in Case-1 than in Case-2. The reason could be due to the overcast conditions that are prevalent in Case-1.This may lead to thorough mixing due to both mechanical and buoyancy generated turbulence which results in more vertical transportation of the energy for the ocean surface into the boundary layer. In such a scenario, more loss of energy in the form of sensible heat flux, latent heat flux (incoming solar radiation cutoff due to overcast conditions) from the ocean leads to net-oceanic loss (Mohanty and Mohan Kumar 1990). In this process, there may be a regular supply of heat and moisture from the ocean surface into the

atmosphere above for the maintenance of deep convection and cyclogenesis leading to depression.

From the simulations, a maximum MBL height of ~ 640 m above is found during Case-1 (figure 6(c)) while a maximum of 400 m is noticed during Case-2 (figure 7(c)). The estimated MBL height values from the available observations are also plotted against the simulations. The overall variation of the model simulations of MBL height and the observations are fairly in good agreement. This could be attributed to the fact that the more the vertical transportation sensible heat flux, the more the height of the boundary layer height.

No specific variation of the drag coefficient is noticed in the model simulations in both Case-1 (figure 6(d))
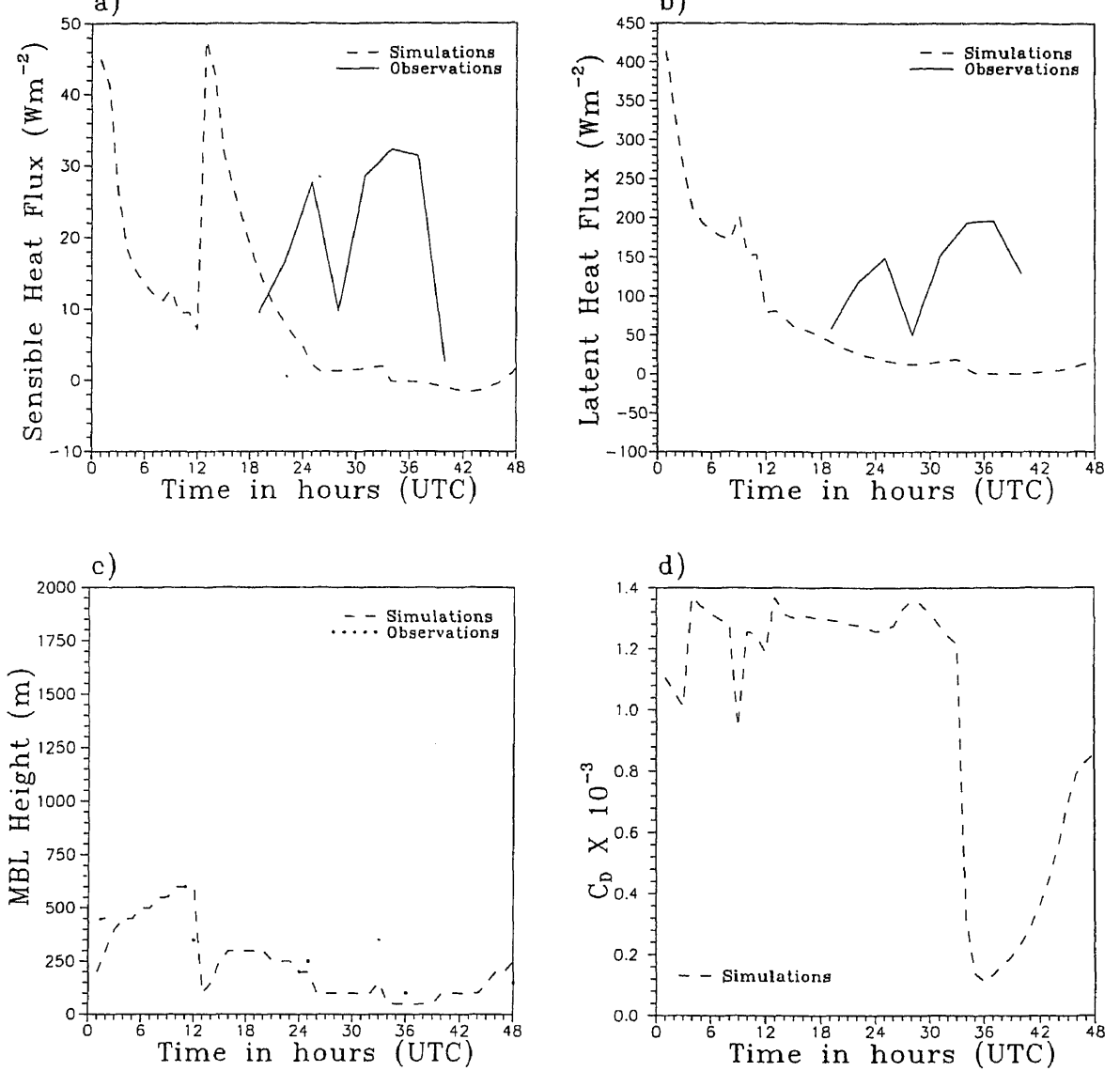
Figure 6. Diurnal variation of (a) sensible heat flux ($Wm^{-2}$); (b) latent heat flux ($Wm^{-2}$); (c) marine boundary layer height (m) and; (d) drag coefficient ($ms^{-2}$) of Case-1.

and Case-2 (figure 7(d)). Most of the time the drag coefficient in Case-1 is higher than in Case-2. A maximum value of $1.37 \times 10^{-3}$ is noticed in Case-1 while a higher magnitude of $1.29 \times 10^{-3}$ is found in Case-2. The higher values in Case-1 might be due to relatively higher winds since drag coefficient is a function of horizontal wind speed. The magnitude of the drag coefficient is well within the limits as noticed elsewhere (Stull 1988).

From the simulations of temporal variation of TKE, it is noticed that the TKE generation is more with a maximum magnitude of $0.34\,m^2s^{-2}$ in Case-1 (figure 8(a) where as it is less in Case-2 (figure 8(b)). It may be due to relatively strong winds in Case-1 and more generation of sensible heat flux. In Case-2, TKE generation is less and a magnitude of $0.18\,m^2s^{-2}$ is noticed. The extent of TKE in vertical defines the

MBL height. On comparing temporal variation of TKE with MBL height, one can see the synonymous variation.

RMS error and correlation coefficient are computed to evaluate the performance of the model simulations with respect to the observations for both Case-1 and Case-2 and shown in table 1. A maximum RMS error of $1.71\,K$ is noticed in potential temperature profiles (Case-1) whereas in the case of specific humidity (Case-1) a maximum error of $2.36\,g\,Kg^{-1}$ is seen. In Case-2, a higher RMS error of $1.16\,K$ is seen in potential temperature profiles, whereas it is $1.89\,g\,Kg^{-1}$ in specific humidity profiles. In both the cases the simulated profiles of potential temperature and specific humidity are fairly correlated with the observations, whereas zonal and meridional profiles are reasonably correlated.
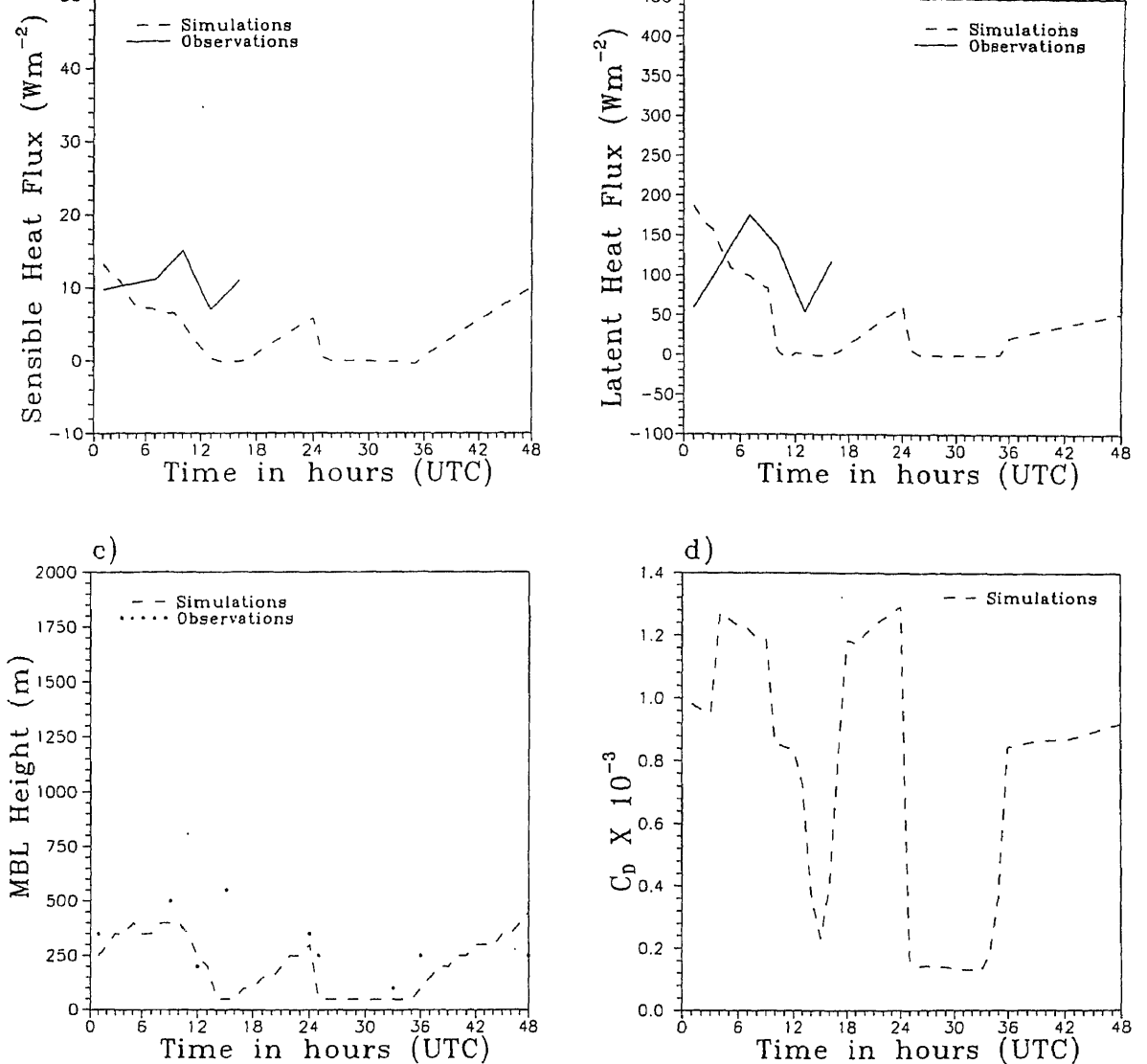
Figure 7. Diurnal variation of **(a)** sensible heat flux $(Wm^{-2})$; **(b)** latent heat flux $(Wm^{-2})$; **(c)** marine boundary layer height (m) and; **(d)** drag coefficient $(ms^{-2})$ of Case-2.

## 6. Conclusions

A multi-level one-dimensional boundary layer model was successfully employed to simulate marine boundary layer processes over the Bay of Bengal during BOBMEX-98 pilot campaign. The MBL characteristics were simulated for two distinctly different observational scenarios: one during active convection and the other during suppressed convection. The model was able to capture the main characteristic features of these two synoptic situations.

From the results of the numerical simulations carried out in this study, the following broad conclusions are drawn.

The model simulations of vertical profiles of potential temperature and specific humidity are found

to be in fair agreement with the observations. The model simulation of zonal and meridional wind components does show some deviations with the observations due to the limitations of the one-dimensional model. In general the model could capture the thermodynamic and dynamical fields reasonably well.

The model was able to simulate fairly well the temporal variation of fluxes of sensible heat and latent heat when compared with the observations to bring out the different transportation in different synoptic scenarios. Higher fluxes of sensible heat and latent heat are noticed in the active convection case than that in clear weather situation. The simulated MBL in the active convection case is higher than in the suppressed convection case. The simulated MBL height is in good agreement with the estimated values. The
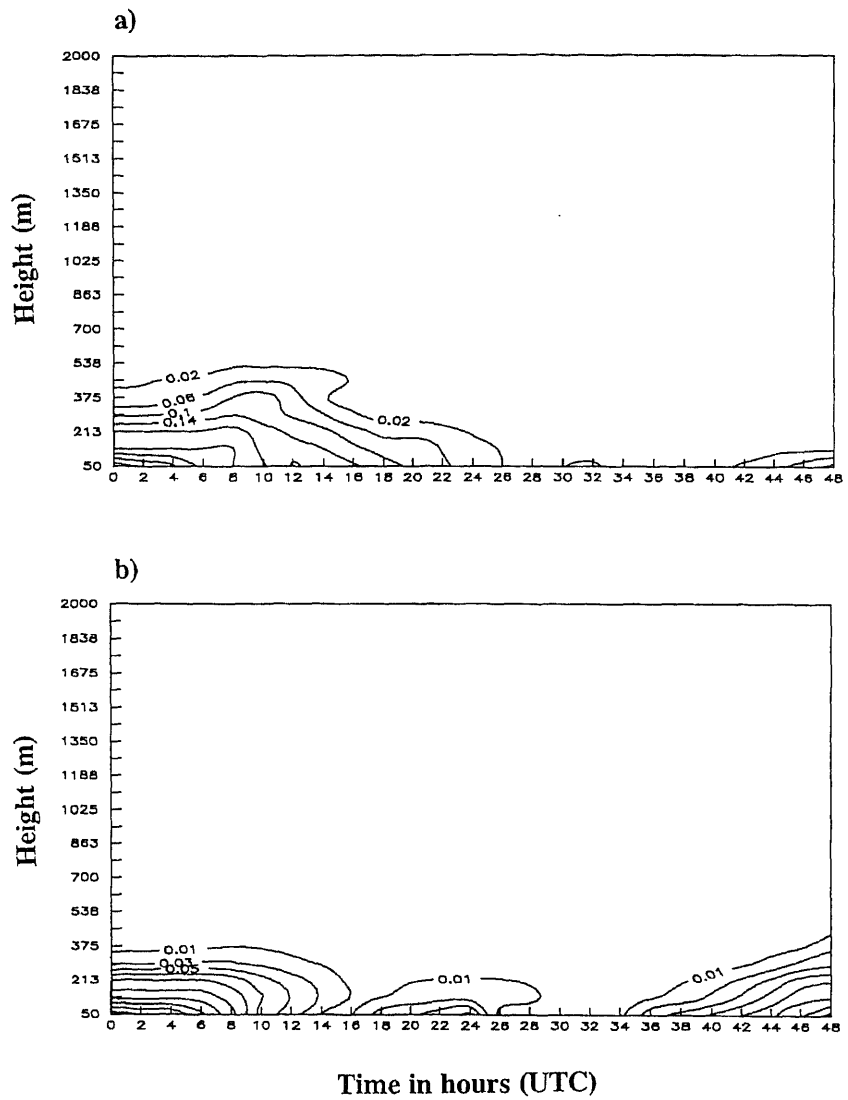
a)



b)



**Time in hours (UTC)**

Figure 8.   Time evolution of turbulent kinetic energy ($m^2 s^{-2}$) of (**a**) Case-1 and (**b**) Case-2.

Table 1.   Statistical evaluation of the performance of the model in the simulation of zonal wind ($ms^{-1}$), meridional win potential temperature (K) and specific humidity ($g Kg^{-1}$).

| Simulation hours for Case-1/Case-2 | Parameter | Case-1 | | Case-2 | |
|---|---|---|---|---|---|
| | | RMS error | Corr. coeff. | RMS error | Co |
| 12/12 | U | 0.69 | 0.85 | 0.59 | |
| | V | 0.82 | 0.30 | 0.65 | |
| | $\theta$ | 1.64 | 0.95 | 0.00 | |
| | q | 2.12 | 0.91 | 0.52 | |
| 24/24 | U | 0.32 | 0.94 | 0.00 | |
| | V | 1.41 | 0.95 | 0.82 | |
| | $\theta$ | 1.71 | 0.96 | 0.47 | |
| | q | 2.20 | 0.98 | 1.89 | |
| 36/36 | U | 0.82 | 0.78 | 0.35 | |
| | V | 0.59 | 0.62 | 0.00 | |
| | $\theta$ | 0.27 | 0.98 | 1.16 | |
| | q | 2.36 | 0.91 | 1.00 | |
| 48/48 | U | 0.67 | 0.72 | 0.89 | |
| | V | 0.00 | 0.99 | 0.00 | |
| | $\theta$ | 0.91 | 0.99 | 0.65 | |

model simulated drag coefficient values in the present study compare reasonably with the values quoted in the literature. The TKE evolution does not show any specific temporal variation. But in the active convection case TKE is found to be higher. On the statistical evaluation of the simulations, it is noticed that the RMS error and correlation coefficient are fairly reasonable in the case of vertical profiles of potential temperature and specific humidity whereas they are reasonable in the case of zonal and meridional wind profiles.

## References

Holt T and Raman S 1988 *Rev. Geophys.* **26** 4 761–780.
Kalsi S R Workshop on *Bay of Bengal and Monsoon Experiment (BOBMEX) Pilot Study Results*, 19 April 1999, IIT Delhi, India
Lykossov V N and Platov G A 1992 *Russ. J. Numer. Anal. Math. Modelling* **7** 419–440.
Mellor G L and Yamada T 1974 *J. Atmos. Sci.* **31**, 1791–1806.
Mohanty U C and Mohan Kumar 1990 *Atmospheric Environment*, **24A**, 823–828
Satyanarayana A N V, Mohanty U C and Sam N V 1999 *Curr. Sci.* **76** 890–897.
Stull R 1988 *An Introduction to Planetary Boundary Layer*, (Dordrecht, The Netherlands: Kluwer Academic Publishers) 666 pp

# Conserved variable analysis of the marine boundary layer and air-sea exchange processes using BOBMEX-Pilot data sets

N V Sam, U C Mohanty and A N V Satyanarayana

*Centre for Atmospheric Sciences, Indian Institute of Technology, Delhi, New Delhi, India*

The present study is based on the observed features of the MBL (Marine Boundary Layer) during the Bay of Bengal and Monsoon Experiment (BOBMEX) - Pilot phase. Conserved Variable Analysis (CVA) of the conserved variables such as potential temperature, virtual potential temperature, equivalent potential temperature, saturation equivalent potential temperature and specific humidity were carried out at every point of upper air observation obtained on board ORV Sagar Kanya. The values are estimated up to a maximum of 4 km to cover the boundary layer. The Marine Boundary Layer Height is estimated from the conserved thermodynamic profiles. During the disturbed period when the convective activity is observed, the deeper boundary layers show double mixing line structures. An attempt is also made to study the oceanic heat budget using empirical models. The estimated short-wave radiation flux compared well with the observations.

## 1. Introduction

The Bay of Bengal and Monsoon Experiment (BOB-MEX) is a cooperative field experiment under the Indian Climate Research Program (ICRP). The main objective of BOBMEX is to study the air-sea interaction and the associated characteristics of the Marine Boundary Layer (MBL) in the Bay of Bengal during the monsoon. This regional scale phenomenon along with the low-level temperature inversion and cross-equatorial fluxes play a significant role in the maintenance of the monsoon activity.

In an effort to understand the MBL over the oceans and its role in regulating the transport of energy and moisture upward into the atmosphere from the surface and its influence on the atmospheric convection, various field experiments were carried out in the past. The International Indian Ocean Expedition (IIOE), during 1963–65, paved the way to study the thermal and kinematic features of the monsoon flow over the Arabian Sea and the adjoining west Indian Ocean. During this expedition, Bunker (1965), made few boundary layer measurements and discussed the characteristics of MBL. After the IIOE, Indo-Soviet Monsoon experiment (ISMEX), 1973, the Monsoon experiment (MONEX), 1979 were carried out. Jambunathan and Ramamurty (1975), studied the air-sea temperature distribution over the west Indian Ocean. Ramanathan (1978), assessed the bulk layer variation over the Arabian Sea along 10°N and along the equator. Pant (1978) discussed the vertical structure of the MBL in the west Indian Ocean using ISMEX data sets. Mohanty and Dube (1981), studied the statistical structure of the meteorological parameters over the Bay of Bengal. Kondo and Mirua (1985), presented the computation of surface MBL fluxes at the air-sea interface over the western Pacific during MONEX-79. All these studies illustrate, that the air-sea exchange processes play a dominant role in the energy transport from ocean surface to the atmosphere, which in turn, act as a feed back mechanism for convection and circulation in the tropics.

It is known that the global climate depends on the transport mentioned earlier and increasing attention is given to the parameterization of the Convective Boundary Layer (CBL) in global forecast models (Betts and Miller 1986; Betts 1986; Albrecht *et al* 1986). The aim of this paper is to study the thermal structure of the MBL, especially the CBL using the Conserved Variable Analysis (CVA), an approach suggested by Betts
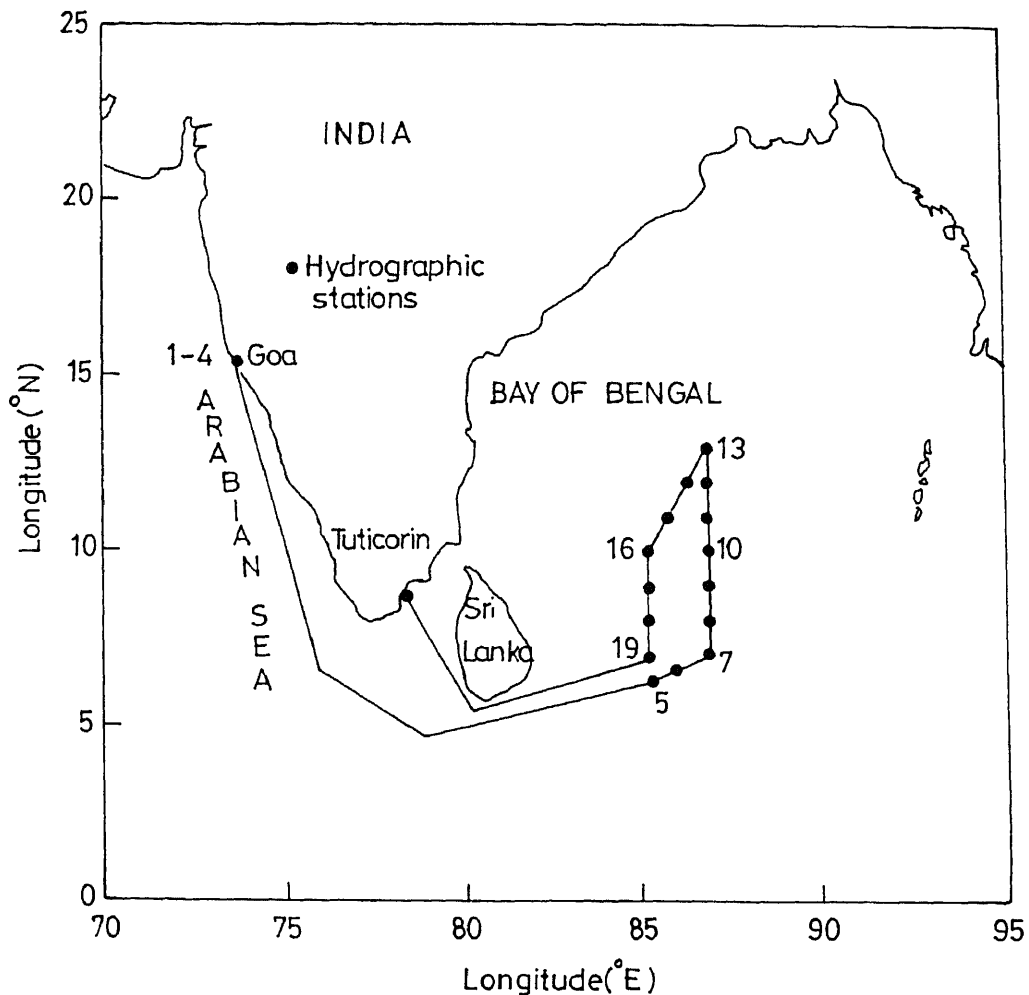
Figure 1. Cruise track of ORV Sagar Kanya during BOBMEX Pilot experiment.

(1985). An attempt is also made to study the oceanic heat budget using the surface synoptic meteorological observations obtained during the experiment, in order to examine the possible linkage between the net oceanic heat budget and the CBL structure.

## 2. Data

Surface meteorological parameters such as wind speed, wind direction, sea surface temperature (SST), dry-bulb and wet-bulb temperature and cloud cover, collected at every 3-hour interval, on board ORV Sagar Kanya from 23rd October – 8th November 1998 are used for the present study. During the cruise three stationary locations were identified for time series observations

- at $(7°N, 87°E)$, 30th – 31st October 1998,
- at $(10°N, 87°E)$, 2nd – 3rd November 1998 and
- at $(13°N, 87°E)$ on 5th November 1998.

The three sites were chosen anticipating specific synoptic activity such as convectively active and convectively suppressed conditions. The ship sailed back thereafter and reached Tuticorin on 12th November 1998. The time series observations were used to compute the oceanic heat budget parameters. In addition to the observed surface parameters, upper air observations of temperature and relative humidity, obtained by launching radiosonde and low-level sonde (India Meteorological Department) and minisonde (Indian Institute of Science and Space Physical Laboratory) are used for the CVA. The cruise track is shown in figure 1.

## 3. Synoptic conditions in the Bay of Bengal

An initial disturbance, which is seen to be innocuous in the satellite imagery on 23rd October $(8°N, 101.5°E)$

that this circulation moved westwards and was more marked on 26th October 1998, with wind speeds in the lower tropospheric levels, of the order of 15–20 knots. Later the low level structure got deformed and was found to be oriented in the northeast direction apparently in response to the trough in the mid and upper tropospheric westerlies over Pakistan/Afghanistan region on 29th October 1998.

of Bengal and throughout the day it had rained. From 3rd – 5th November 1998, the weather is noticed to be relatively calm. Two specific periods were classified for the CVA viz.

- the disturbed period, 30th – 31st October (7°N, 87°E) and 2nd November (10°N, 87°E) 1998
- the undisturbed period, 3rd November (10°N, 87°E) and 5th November (13°N, 87°E).
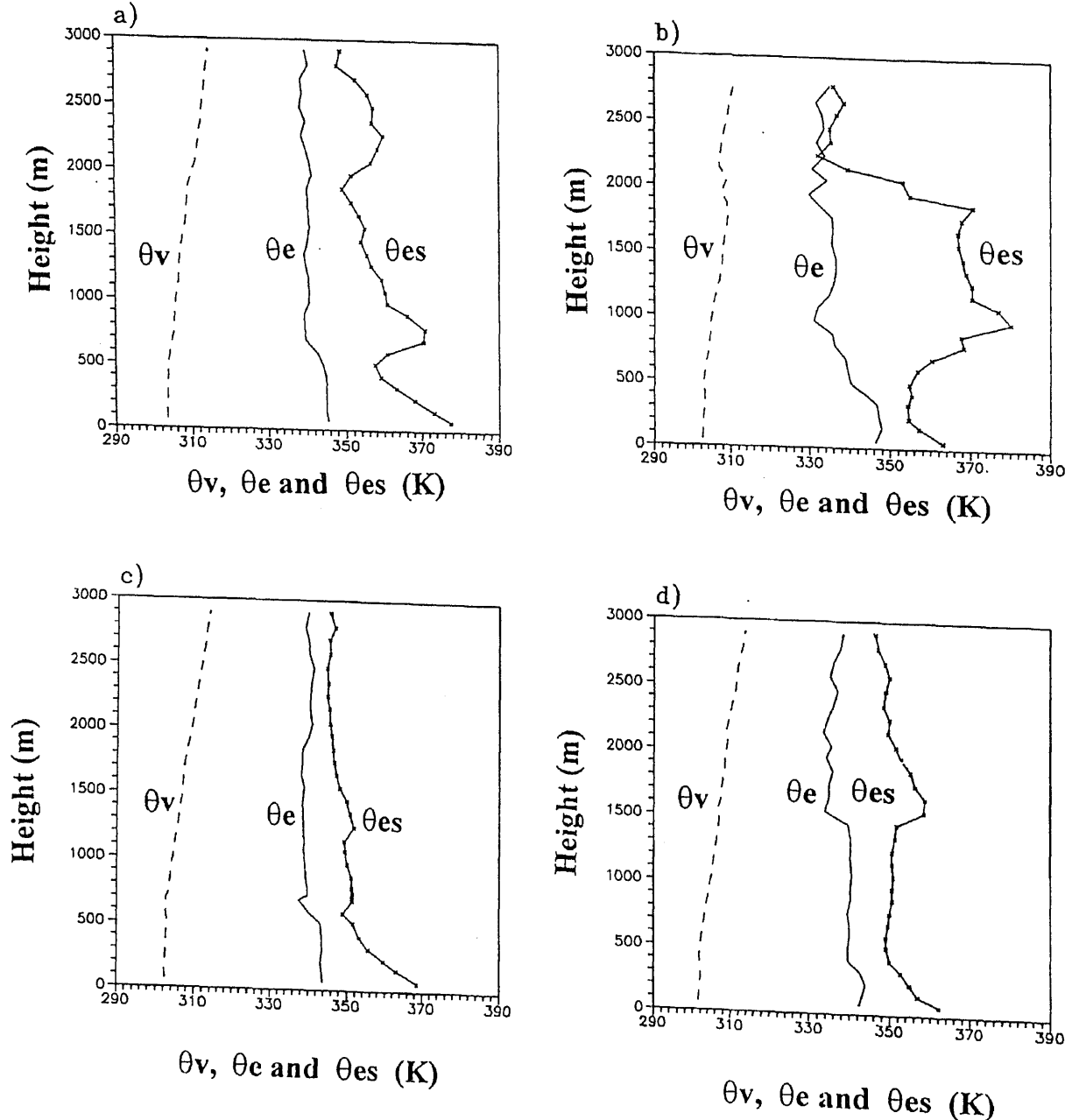


Figure 2. $\theta_v$, $\theta_e$ and $\theta_{es}$ during the disturbed period (a) 31-10-1998, 0700 IST; (b) 31-10-1998, 1545 IST; (c) 01-11-1998, 1430 IST; (d) 02-11-1998, 2100 IST.

# 4. Methodology and analysis procedure

## 4.1  *Conserved Variable Analysis*

Betts and Albrecht (1987) gave an idealized illustration of CVA depicting the importance of the Conserved Variable Diagrams. A schematic mixing line (Betts 1982) is shown between Saturation Points (SPs) of the mixed sub-cloud layer and the CBL top on a $(\theta_e, q_T)$ diagram. The $q_T$ (specific humidity) axis for the unsaturated air has been reversed so that a sounding data plotted on this diagram resembles the more familiar $(\theta_e, p)$ plot. In the absence of irreversible diabatic processes, conserved variables are represented on both the axes. $\theta_e$ (equivalent potential temperature) or $q_T$ is not changed during condensation process, whereas, the precipitating process moves the parcel points to lower $q_T$ at constant $\theta_e$ (and the reverse for the evaporation of falling precipitation). The radiative process does not change $q_T$, but radiative cooling moves SPs to lower $\theta_e$ at constant $q_T$. Mixing lines are straight lines and advective processes do not move the parcel points at all. The thermodynamic changes represented by the triangular path
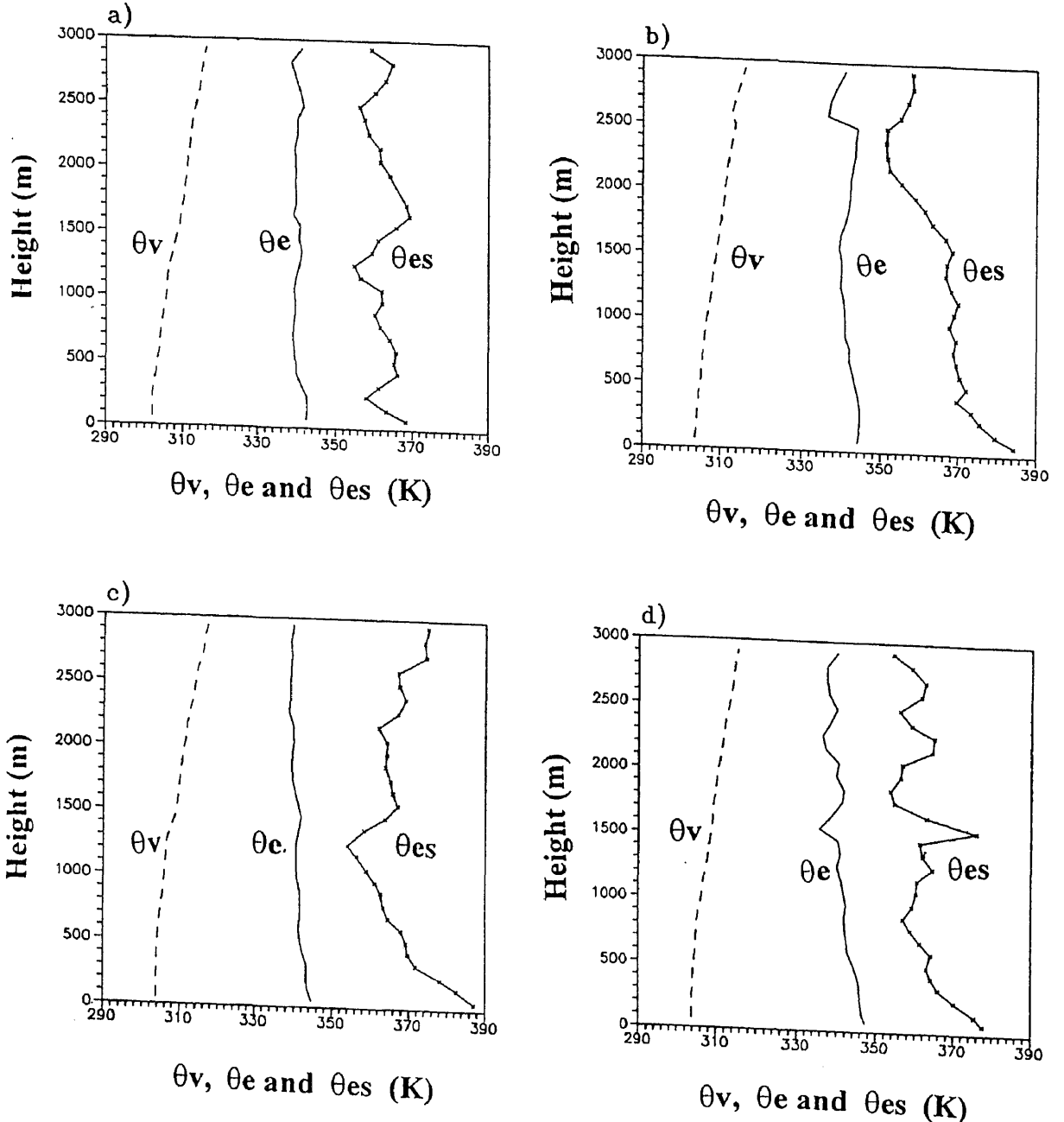


Figure 3.   $\theta_v$, $\theta_e$ and $\theta_{es}$ during the undisturbed period (a) 03-11-1998, 0700 IST; (b) 03-11-1998, 1445 IST; (c) 05-11-1998, 0615 IST; (d) 05-11-1998, 2000 IST.

constant $\theta_e$. Radiative cooling in the subsiding branch lowers $\theta_e$ at constant $q_T$. The air with the lowest $\theta_e$ sinks into the CBL and its SPs move down the mixing line as it is mixed with air from below on its final mean descent back into the sub-cloud layer.

## 4.2 Marine Boundary Layer Height (MBLH)

Vertical profiles of virtual potential temperature ($\theta_v$), equivalent potential temperature ($\theta_e$) and saturation equivalent potential temperature ($\theta_{es}$) are drawn to estimate the MBLH. The MBLH is marked by minimum $\theta_e$ and maximum $\theta_{es}$. This criterion (usage of $\theta_e$ and $\theta_{es}$) was used, because variables such as potential temperature and water-vapour mixing ratio are not conserved in a cloud, because of latent heat release/ absorption and condensation/evaporation processes. MBL and CBL are synonymously used as the cases considered were differentiated on the basis of convection (active or suppressed convection). MBLH is therefore considered to be a mixed layer dominated by buoyant turbulence, which is also the Convective Boundary Layer Height (CBLH). Plots of $p^*$ (saturation level pressure) and $P(= p^* - p)$ against pressure ($p$) were drawn, where the negative values of $P$ are related to the layer of sub-saturation. This MBL height can also be estimated by marking the minimum of $P$ at the inversion top.

### 4.3 Static stability analysis

In the tropical atmosphere, condensation processes are very important. Therefore, it is not enough, to consider only dry adiabatic vertical displacements, as in the process of vertical displacement the parcel is likely to reach the condensation level. Above this level, the parcel cools at the saturation adiabatic lapse rate. The Saturation Static Energy ($S_{es}$), is calculated using the expression:

$$S_{es} = C_p T + gz + Lq_{\text{sat}}, \qquad (1)$$

where, $C_p$ is the specific heat for moisture air, $T$ is the temperature, $g$ is the acceleration due to gravity, $z$ is the height above m.s.l., $L$ is the latent heat of vaporization and $q_{\text{sat}}$ is the saturation specific humidity. The partial change in $S_{es}$ with respect to $z$, i.e. $\partial S_{es}/\partial z$ determines the moist static stability. Stable atmosphere is characterised by the positive gradient of $\partial S_{es}/\partial z$.

### 4.4 Oceanic heat budget

To study air-sea exchange processes over the Indian Ocean, the radiative fluxes (short and long-wave ra-

The oceanic heat budget equation (in Wm$^{-2}$) can be written as:

$$Q_N = Q_S - Q_B - Q_H - Q_E, \qquad (2)$$

where $Q_N$ is the net heat loss/gain, $Q_S$ is the short-wave radiative flux, $Q_B$ is the long-wave radiative flux, $Q_H$ is the sensible heat flux and $Q_E$ is the latent heat flux. Here, the heat transported by ocean currents (advection of heat) is neglected because in short time scales, it is not appreciable. The detail of the estimation of the parameters on the right-hand side of the equation is computed by the methods suggested by Mohanty and Mohan Kumar (1990).

The short-wave radiation flux reaching the ocean surface is obtained using semi-empirical expression given by Atwater and Ball (1981), whereas the effective long-wave radiation flux is computed using the expression given by Girduk and Malevaski-Holekyich (1973). The transfer coefficients were computed as a function of both atmospheric stability and wind speed as suggested by Mohanty and Mohan Kumar (1998).

## 5. Results and discussion

Figure 2(a–d) represents the $\theta_v$, $\theta_e$, and $\theta_{es}$ profiles during the disturbed period. From these profiles the MBLH is estimated, which is characterised by a maximum in $\theta_{es}$ and a minimum in $\theta_e$. The typical three-layer structure (sub-cloud, cloud and inversion layers) of the CBL (Betts and Albrecht 1987) is quite apparent in the present data sets too. The relative high humidity inside in the cloud layer (distinctly moist) is unstable in $\theta_{es}$. Figures 2(a), 2(b) and 2(d) give a distinct estimate of the MBLH as the $\theta_{es}$ and $\theta_e$ profiles show marked increase and decrease respectively at the inversion top. $\theta_v$ profiles are not used to estimate the MBLH as $\theta_{es}$ and $\theta_e$ profiles are more

Table 1. Marine boundary layer height during disturbed and undisturbed period.

| Date | Time (IST) | MBLH (disturbed period) (m) |
|---|---|---|
| 31-10-1998 | 0700 | 800 |
| 31-10-1998 | 1545 | 1000 |
| 01-11-1998 | 1430 | 1300 |
| 02-11-1998 | 2100 | 1700 |

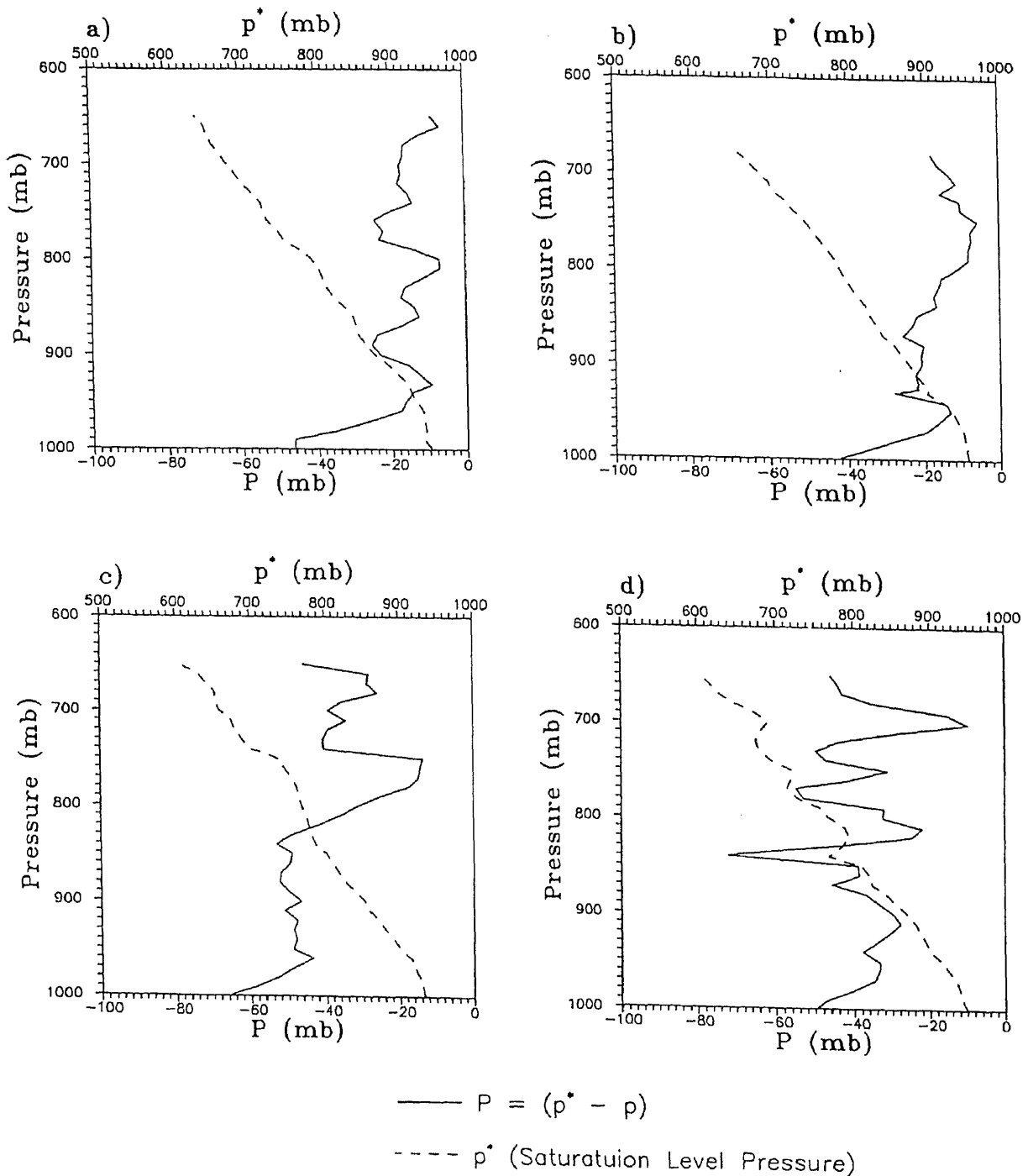| Date | Time (IST) | MBLH (undisturbed period) (m) |
|---|---|---|
| 03-11-1998 | 0700 | 425 |
| 03-11-1998 | 1445 | 507 |
| 05-11-1998 | 0615 | 1250 |
| 05-11-1998 | 2000 | 1555 |

Figure 4. Plot of $p^*$ and $P = (p^* - p)$ against pressure. During disturbed period (a) 01-11-98, 0700 IST; (b) 01-11-98, 1430 IST. During undisturbed period (c) 03-11-98. 1445 IST; (d) 05-11-98, 2000 IST.

distinct and representative. On 2nd November 1998, (figure 2d) the MBLH is observed to attain a maximum of 1700 m. This is due to active convection when deeper boundary layers are formed. Continuous rain is also observed during this period. During the undisturbed period, figure 3(a–d), the estimated MBLH is found to be less, when compared to the disturbed period. In figure 3(d), marked maximum and mini-

while such distinct features are not observed in figure 3(a–c). The estimated MBLH is given in table 1. The average MBLH during the disturbed and undisturbed period is found to be 1200 m and 934 m respectively. Figure 4(a–d) shows $p^*$ and $P = (p^* - p)$ against pressure, where $p^*$ is saturation level pressure. In the absence of radiation and mixing processes, the $p^*$ of a parcel is unchanged by vertical (dry or moist
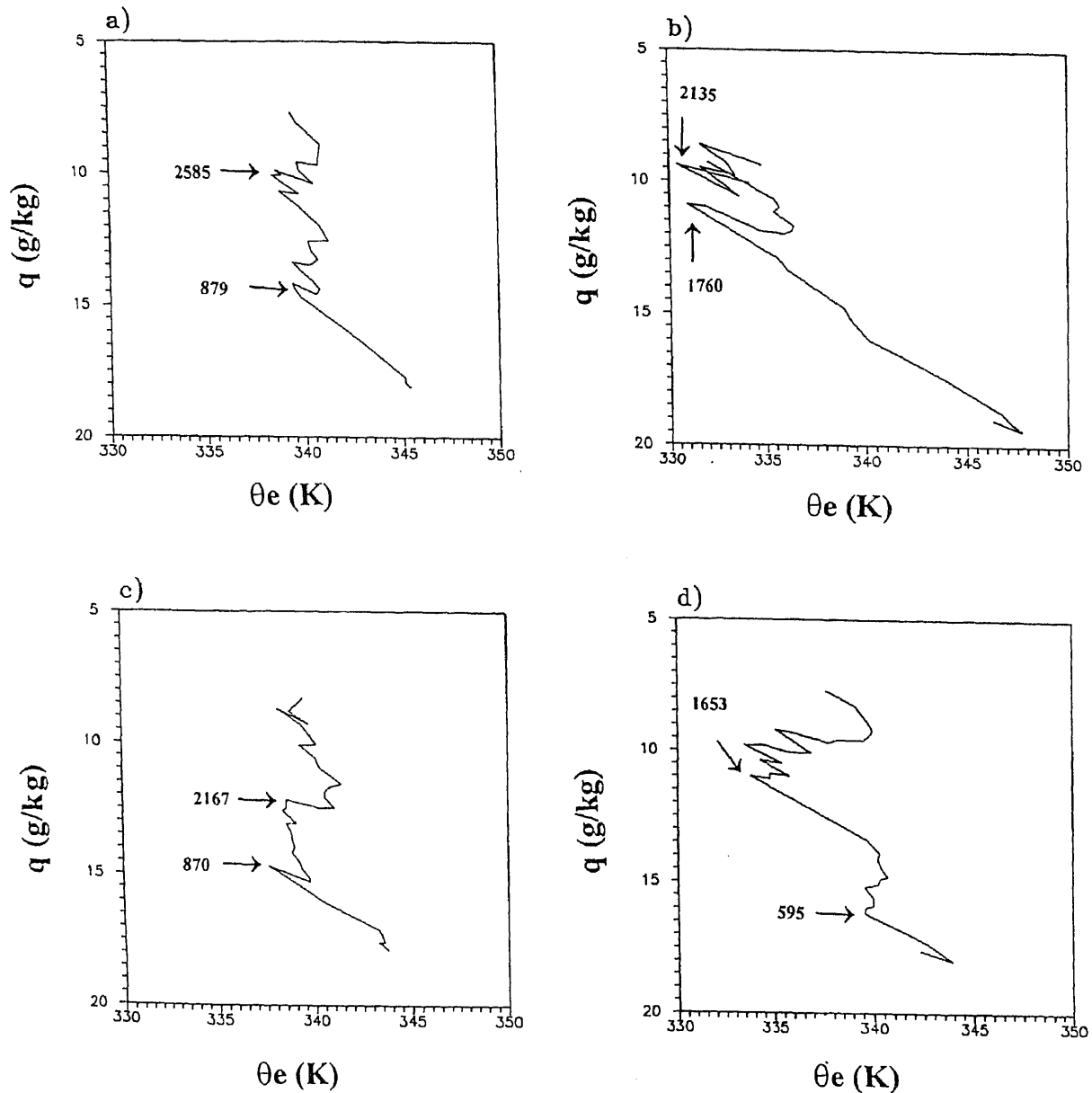
Figure 5. Plot of $\theta_e$ against $q$. During disturbed period (**a**) 31-10-1998, 0700 IST; (**b**) 31-10-1998, 1545 IST; (**c**) 01-11-1998. 1430 ST; (**d**) 02-11-98, 1500 IST. ($\rightarrow$ indicates double mixing).

bsides faster than the radiative increase of $p^*$, then can reach relatively large negative values (figure 4c, d). Figure 4(a, b) which is representative of the isturbed period shows smaller negative values of $P$ s convective mixing dominates during this period. he inversion top can also be characterised by the inimum $P$.

The $(\theta_e, q)$ plots given in figure 5(a–d) show double ixing line structures with a small $q$ reversal at round 879 m, 1660 m, 870 m and 512 m (represented figure) respectively and similarly at the top of the BL at 2585 m, 1761 m, 2167 m and 3256 m (repre-nted in figure) respectively during the disturbed

culated that differential horizontal advection of boundary layers could be the possibility. At the top of the CBL $q$ minimum is observed. Such well mixed layer where convective mixing plays a dominant role is not observed during the undisturbed period (figure 6(a–d)). As suggested by Betts and Albrecht (1987), the precipitation–evaporation processes are respon-sible for this double mixed layer structure, once the CBL reaches a sufficient depth.

The instability in the atmosphere during the dis-turbed period can also be viewed from the $\partial S_{es}/\partial z$ profile figure 7(a, b). It is noticed that during the dis-turbed period when convective activity is prominent
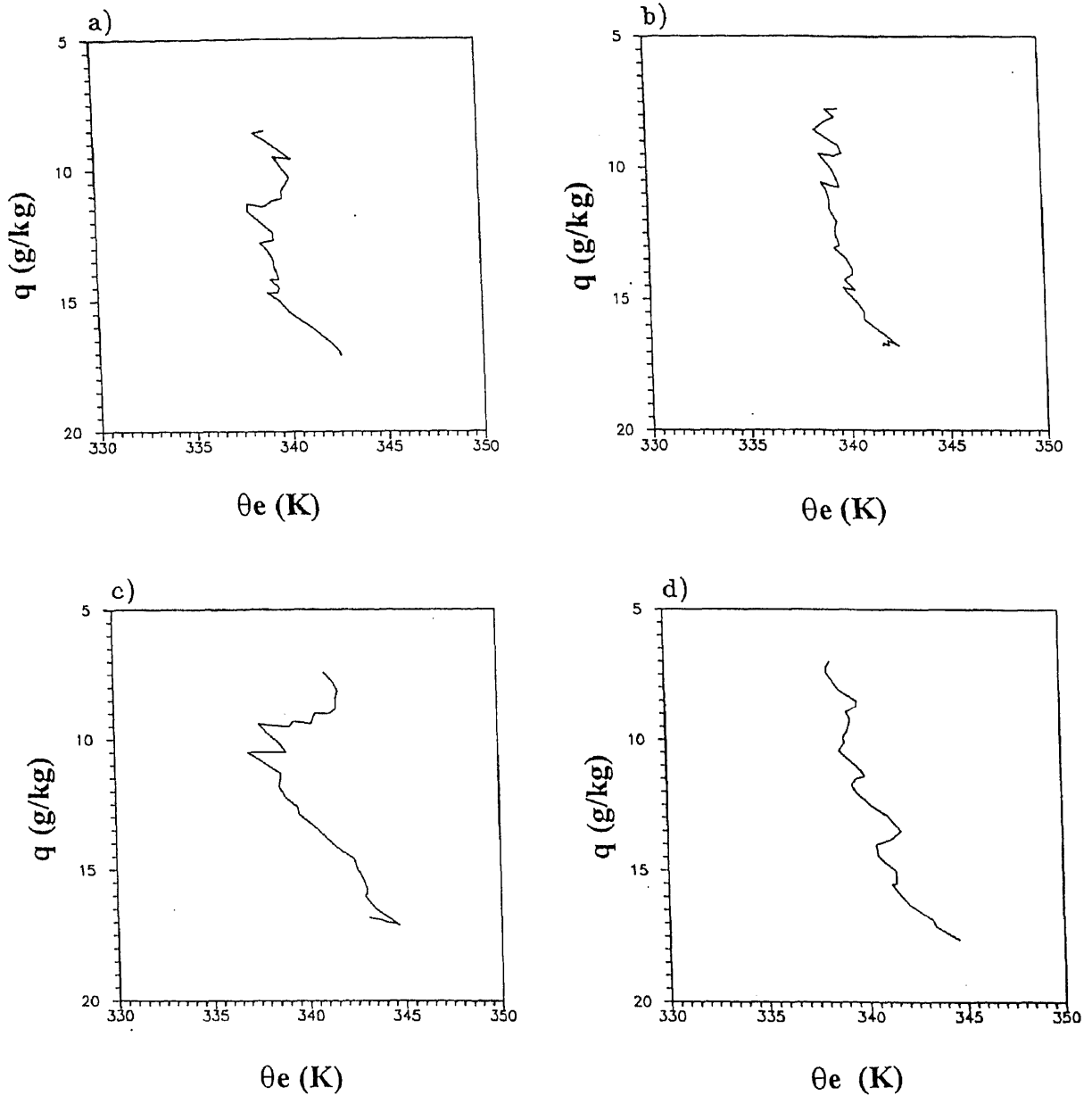
Figure 6. Plot of $\theta_e$ against $q$. During undisturbed period (a) 03-11-1998, 2030 IST; (b) 04-11-1998. 0700 IST; (c) 04-11-1998, 1400 IST; (d) 05-11-1998, 0615 IST.

period (figure 7c, d), this gradient tends to be positive characterizing stable atmosphere.

The daily mean of the components of the Oceanic Heat Budget such as $Q_S$, $Q_B$, $Q_H$, $Q_E$ and $Q_N$, the total cloud amount, wind speed, and sea minus air temperature is given in table 2. On 30th October 1998, the average surface winds observed, are found to be of the order of $8.5\,\mathrm{ms}^{-1}$. On this day, the mean latent heat flux is found to be equal to $222\,\mathrm{Wm}^{-2}$, which is higher than that computed during the undisturbed period. This could also be one of the reasons for higher MBLH during this period. The synoptic observation

disturbed period, when it rained. This observation was confirmed by the analysis of the satellite pictures (Kalsi 1999). While, during the undisturbed period such cloudy conditions were not observed to bring about any significant weather phenomenon. The sea minus air temperature is always positive indicating that throughout the cruise the sea is found to be warmer than the overlying atmosphere. A maximum difference of 2.0°C is observed on 31st October 1998 and a minimum of 0.86°C is seen on 5th November 1998. It is also observed that the short-wave flux obtained from the aforementioned empirical is in good
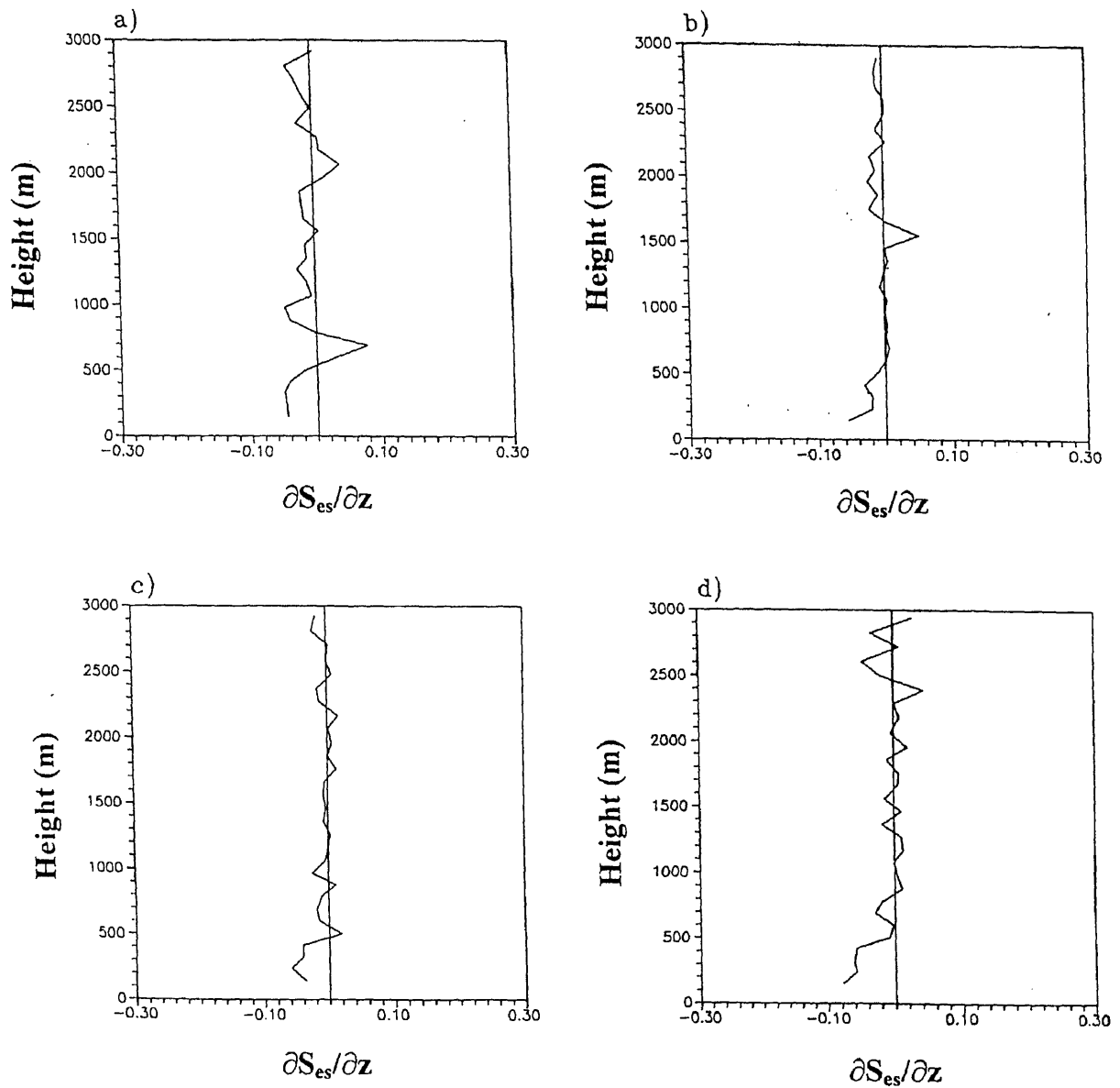
Figure 7. Plot of $\partial S_{es}/\partial z$ against height. During disturbed period (a) 31-10-1998, 0700 IST; (b) 01-11-1998, 1430 IST. During undisturbed period (c) 04-11-1998, 0700 IST; (d) 05-11-1998, 1400 IST.

Table 2. Daily mean of the surface meteorological parameters and the oceanic heat budget components.

| Date | Total cloud amount (Octa) | Wind speed (ms$^1$) | Sea minus air temp. (°C) | $Q_S$ | $Q_B$ | $Q_H$ | $Q_E$ | $Q_N$ |
|------|---------------------------|---------------------|--------------------------|-------|-------|-------|-------|-------|
| 30-10-98 | 6.3 | 8.5 | 1.1 | 204 | 35 | 18 | 222 | −71 |
| 31-10-98 | 6.8 | 3.8 | 2.0 | 179 | 35 | 14 | 95 | 35 |
| 02-11-98 | 6.9 | 3.9 | 1.8 | 205 | 35 | 13 | 99 | 58 |
| 03-11-98 | 5.6 | 2.8 | . 1.8 | 207 | 39 | 11 | 74 | 83 |
| 05-11-98 | 5.7 | 8.1 | 0.8 | 268 | 37 | 13 | 136 | 82 |

## 6. Conclusions

The conserved variable analysis is found to be useful in the study of the thermodynamic structure of the convective boundary layer. For shallow CBLs during the undisturbed period, a single mixing line is seen through the cloud and inversion layers. However, deeper CBLs, all of them show double mixing lines. This could be due to the precipitation–evaporation processes, which are responsible for the double mixed

layer structure once the CBL (and the deepest clouds in it) reaches a sufficient depth. As suggested by Betts and Albrecht (1987), it can be speculated that a $q$ and $\theta_e$ reversal within the CBL could be maintained by penetrative downdrafts driven by evaporation of precipitation.

The soundings show a $\theta_e$ and $P$ minimum, $\theta_{es}$ maximum and local $q$ minimum at the CBL top. The CBL top thus appears on a $\theta_e - q$ diagram as a marked kink, which marks the top of the layer that is thermodynamically coupled to the surface.

The net oceanic heat budget is found to be lower during the disturbed period than that in the undisturbed period. This is due to the reduction in the solar radiation flux because of the overcast condition. Also during this period the latent heat flux is higher due to the high surface wind speeds and the related instability in the surface marine boundary layer.

## Acknowledgement

## References

Albrecht B A, Ramanathan V and Boville B A 1986 Meteorology over the Tropical Oceans, (ed) D. B. Shaw *Roy. Meteorol Soc.* 73–104.

Atwater M A and Ball J T 1981 *Mon. Weather Rev.* **109** 878–888.

Betts A K 1982 *J. Atmos. Sciences* **39** 1484–1505.

Betts A K and Albrecht Bruce A 1987 *J. Atmos. Sciences* **44**, 83–99.

Betts A K 1986 *Q. J. Roy. Meteorol. Soc.* **112** 677–691.

Betts A K 1985 *J. Atmos. Sciences* **42**, 2751–2763.

Betts A K and Miller M J 1986 *Q. J. Roy. Meteorol. Soc.* **112** 693–701.

Bunker A F 1965 Interaction of the summer monsoon air with the Arabian Sea; *Proc. Symp. on Met. Results*, IIOE, Bombay, 3–16.

Girduk G V and Malevaski-Holekyich S P 1973 *Trudi Main Geophysical Observations*, Leningrad **297** 124–132

Jambunathan R and Ramamurty K 1975 *Indian J. Met. Geophys.* **25** 377–410.

Kalsi S R Workshop on *Bay of Bengal and Monsoon Experiment (BOBMEX) Pilot Study Results*, 19 April 1999, IIT Delhi, India

Kondo J and Mirua A 1985 Surface heat budget of the SouthWestern Pacific for May 1979; *J. Meteorol. Soc. Japan.* **63** 633–646.

Mohanty U C and Mohan Kumar 1990 *Atmospheric Environment* **24A** No. 4 823–828.

Mohanty U C and Dube S K 1981 *Mausam* **32** 315–320.

Mohanty U C and Mohan Kumar 1998 *Indian J. Marine Sciences* **27** 60–65.

Pant M C 1978 *Indian J. Hydrol. Geophys.* **29** p 88.

Ramanathan Y 1978 *Indian J. Meteor. Geophys.* **29**, 643–654.

Sam N V, Satyanarayana A N V and Mohanty U C A Study on Certain Characteristic Features of Air-Sea Exchange Processes and Marine Boundary Layer with BOBMEX-98 Pilot Experiment Data Sets, *Report*, DST, January 1999.

*Proceedings of the Indian Academy of Sciences*

# Earth and Planetary Sciences

Vol. 109, No. 2, June 2000

## CONTENTS

**Special issue on: Bay of Bengal Monsoon Experiment**

Indexed in CURRENT CONTENTS